A UNIFORMLY SAMPLED GENETIC ALGORITHM WITH GRADIENT SEARCH FOR SYSTEM IDENTIFICATION

Zhang Zhen

NATIONAL UNIVERSITY OF SINGAPORE
2009

A UNIFORMLY SAMPLED GENETIC ALGORITHM WITH GRADIENT SEARCH FOR SYSTEM IDENTIFICATION

Zhang Zhen

(*B.Eng., HUST, M.Eng., WHUT*)

A THESIS SUBMITTED
FOR THE DEGREE OF DOCTOR OF PHILOSOPHY
DEPARTMENT OF CIVIL ENGINEERING
NATIONAL UNIVERSITY OF SINGAPORE
2009

Acknowledgements

I would like to thank my PhD advisor, Professor Koh Chan Ghee for his warm encouragement, in-depth advice and thoughtful guidance throughout this study. I am particularly appreciative of his kindness to interrupt his work whenever I needed a discussion on my research. In addition, I would like to express my deepest appreciation for sharing with me his serious attitude in publication, precious experience in research and inspiring stories in life.

I would like to thank and share my joy of completing the thesis with the staff in the Structural and Concrete Laboratory, especially Mdm Annie Tan, Mr Koh Yian Kheng, Mr Kamsan Bin Rasman. Their patience and invaluable assistance contributed a lot to the success of the experiment. Great thanks to Mr Lim Huay Bak, for arranging the test in the way that I can finish it within my schedule. Many thanks to Mr Sit Beng Chiat, Mr Ang Beng Oon, Mr Ishak Bin A Rahman, Mr Ow Weng Moon, Mr Yip Kwok Keong, and Mr Yong Tat Fah for their readiness and sincere help to me.

I greatly acknowledge my friends for "sending charcoal to me when I most need it in snowy days" (to quote a Chinese proverb), especially Dr Duan Wenhui and Dr Li Yali for their endless help in my research and life. I wish to thank and extend my heartfelt gratitude to Dr Chen Xi, Dr Hua Jun, Dr Michael J. Perry, Mr Shen Wei, Dr Song Jianhong, Mr Tay Zhiyung, Mr Teng Mingqing, Dr Zhang Jian and other fellow researchers Mr Du Hongjian, Mr Li Ya, Ms Gao Mimi, Ms Wang Xiaojuan, Ms Wang Xiaomei, Mr Xiong Dexin, and Mr Zhang Mingqiang. It is their sincere support and useful tea breaks that helped me to relax and have good laughs throughout this tough

but fulfilling journey.

I wish to thank my elder brother who takes the responsibilities to take care of the entire family. Most importantly, I owe my loving thanks to my parents for their understanding, warm care and love.

Last but not least, I am grateful to the research scholarship generously granted by the National University of Singapore, without which my PhD study in Singapore would not have been possible.

Nothing in Nature is random. ... A thing appears random only through the incompleteness of our knowledge.

Benedict Spinoza, (1632-1677), Dutch philosopher

Summary

Advances in sensor technologies have generated increasing research and development interests in structural health monitoring. An important branch of this field is system identification, which inherently falls into the categories of inverse problem. The focus of this study is to characterize a structural system in physical domain using the measurements of input and output. Under the assumption of unique mapping between the known measurement and unknown system parameters, the system is regarded as identified if the candidate parameters generate the same output as measurements within the convergence criterion. The identification can be interpreted as an optimization process, incorporating a forward analysis of evaluating the fitness function and a backward analysis of searching in the solution domain. The major difficulties in extending the research towards more complex and large systems include: (1) substantial computational effort is involved in the forward analysis, and (2) efficient convergence is not easy to achieve in the backward analysis. The objective of this study is to develop a system identification procedure that will make significant improvements in both the forward and backward analysis.

The identification strategy proposed in the thesis is based on a good understanding of system identification in an optimization perspective. It is observed that the global peak shifts with decrease in amplitude as a result of measurement noise, and new local optima are seldom produced. This phenomenon is referred to as the "peak shifting". This useful observation helps to understand the improvements made in the past literatures. More importantly, it leads to a more advanced optimization strategy, i.e., improved search space reduction method (iSSRM) via uniform samples plus gradient search. The iSSRM

aims to overcome the local optima far away from the global peak while the gradient search is to fine tuning for the global peak. It is a two-layer method with the outer layer to define search range by Hammersley sequence samples and the inner layer to implement population-to-population search via a modified GA based on migration and artificial selection (MGAMAS). Besides, perturbation and jump-back procedures are proposed if any deviation away from the real solution domain is detected. Followed by the iSSRM exploration, the gradient search is conducted by the Broyden-Fletcher-Goldfarb-Shanno (BFGS) method due to the efficient backtracking line search and super linear convergence.

In addition to contribution to more efficient backward analysis, improvement is made on the forward analysis by substructural method in frequency domain and time domain. The frequency domain substructural method, i.e., F-Sub, is extended to application under random excitation, by incorporating the exponential window method. By virtue of imposing exponential window to the input signals and the system, the influence of initial conditions to the output response can be damped out within arbitrarily chosen data length. Therefore the periodic requirement by discrete Fourier transform is maintained without lengthy zero padding. The frequency domain substructural method originally formulated for harmonic excitation is extended to random excitation. The proposed optimization method is also verified in the time domain substurcural method, i.e., T-Sub. The strength in identifying unknown mass system makes the method outstanding in substructural identification.

The performance of the proposed identification strategy is illustrated by not only numerical simulation study but also experimental model tests of a 7-storey steel frame. The identified results are generally excellent in terms of accuracy and efficiency. Compared to SSRM in recent research, computer time is reduced to 50% or less by iSSRM method, 10% by iSSRM with gradient search, and an impressive 4% by applying in substructural identification. Small damage by cutting, strengthening by welding as well as multiple stiffness changes in different magnitudes are successfully identified on the 7-storey steel

frame in the experimental study. Engineering implications in applying the substructural method are also discussed with reference to incomplete measurement and substructure size selection.

Contents

Acknowledgements i

Summary v

Table of Contents viii

List of Tables xii

List of Figures xviii

List of Symbols xxii

1 Introduction **1**

1.1 Mathematical Models on Structural Dynamics 2

1.1.1 Second-Order Model 2

1.1.2 First-Order Model 3

1.2 Overview of Structural Identification Methods 6

1.2.1 Classical Methods 6

1.2.1.1 Eigensystem Realization Algorithm (ERA) 6

1.2.1.2 Natural Excitation Technique (NExT) 7

1.2.1.3 Random Decrement Technique (RDT) 8

1.2.1.4 Ibrahim Time Domain (ITD) Method 9

1.2.1.5 Stochastic Subspace Identification 9

1.2.1.6 Time-Frequency Methods 10

1.2.1.7 Filtering Methods 13

1.2.1.8 Least Squares Method 15

1.2.1.9 Bayesian Method 16

1.2.1.10 Gradient Search Method 17

1.2.2 Non-classical Methods 17
1.2.2.1 Artificial Neural Network 18
1.2.2.2 Genetic Algorithm 19
1.3 Objective and Scope 22
1.4 Organization of Thesis 24

2 Uniformly Sampled Genetic Algorithms: An Improved SSRM 27

2.1 System Identification Using Genetic Algorithms 28
2.2 Simple GA 30
2.2.1 Reproduction 31
2.2.2 Crossover 33
2.2.3 Mutation 33
2.3 Search Space Reduction for Genetic Algorithm 36
2.4 Improved SSRM by Sampling Test 37
2.4.1 Sampling Methods 38
2.4.1.1 Random Uniform Distribution 39
2.4.1.2 Latin Hypercube 39
2.4.1.3 Orthogonal Array (OA) 39
2.4.1.4 Hammerley Sequence 41
2.4.2 Relaxation, Perturbation and Jump-back: Treatment after Sampling 42
2.5 Numerical Examples 45
2.6 Parametric Study 48
2.6.1 Known Mass System 49
2.6.2 Unknown Mass System 50
2.6.3 Recommended GA Parameters 50
2.7 Conclusions 52

3 Improved SSRM with Gradient Search **69**

3.1 Characteristics of Structural Identification as an Optimization Problem . 70

3.1.1 Effect of Measurement Noise 72

3.1.2 Effect of Data Length and Number of Load Cases 74

3.2 Gradient and Non-Gradient Local Search 75

3.2.1 Simulated Annealing 76

3.2.2 Conjugate Gradient Method 80

3.2.3 BFGS Method 82

3.3 Formulation of Objective Function, Gradient, and Convergence Criteria . 85

3.4 Parametric Study for Balanced Global and Local Search 87

3.5 Numerical Examples 90

3.5.1 Lumped Mass System of 10 DOFs 91

3.5.2 Cantilever Plate of 16 Elements and 168 DOFs 92

3.5.3 Truss of 29 Elements and 28 DOFs 93

3.6 Conclusions 94

4 Frequency Domain Substructural Identification under Random Excitation **119**

4.1 Frequency Response Function 121

4.2 Frequency Domain Substructural Method under Harmonic Excitation . . 124

4.3 Frequency Domain Substructural Method under Random Excitation . . . 126

4.3.1 Exponential Window Method 128

4.3.2 Frequency Domain Substructural Identification Using Steady State Formulation 130

4.4 Substructural Efficiency: A Measure of Divide-and-Conquer Methods . . . 131

4.5 Numerical Examples 132

4.5.1 Stiffness Identification of A 12-DOF System 132

4.5.2 Damage Detection of A 12-DOF System 134

4.5.3 Stiffness Identification of A 50-DOF System 134

4.5.4 Damage Detection of A 50-DOF System 136

4.6 Conclusions 137

5 Time Domain Substructual Identification **151**

5.1 Substructural Method in Time Domain 153

5.2 Numerical Examples 155

5.2.1 A Two-Span Truss Structure 156

5.2.2 A 50-DOF System with Known Mass 156

5.2.3 A 50-DOF System with Unknown Mass 157

5.3 Conclusions 159

6 Identification of Structural Changes: Experiment Study **167**

6.1 Static Testing for Baseline Quantification 168

6.2 Dynamic Testing 169

6.2.1 Vibration Testing Setup 170

6.2.2 Data Processing 171

6.3 Baseline Identification 171

6.4 Scenarios of Structural Change Identification 173

6.5 Analysis of Experimental Data 174

6.5.1 Effect of Incomplete Measurement 176

6.5.2 Effect of Substructure Size 178

6.6 Conclusions 178

7 Conclusions and Recommendations **199**

7.1 Conclusions 200

7.2 Recommendations for Further Study 203

References **207**

A Sampling Test and Parametric Study on iSSRM Method **221**

B Identification of Structural Change via Experimental Data **231**

List of Tables

2.1 GA parameters for iSSRM with sampling test: 10-DOF system 62

2.2 GA parameters for iSSRM with sampling test: 20-DOF system 62

2.3 Comparison of sampling methods: 10-DOF lumped mass system with 0% noise 63

2.4 Comparison of sampling methods: 20-DOF lumped mass system with 0% noise 63

2.5 GA parameter test values for known mass system: fixed parameters . . . 64

2.6 GA parameter test values for known mass system: investigated parameters 64

2.7 GA parameter test values for unknown mass system: fixed parameter . . . 65

2.8 GA parameter test values for unknown mass system: investigated parameters 65

2.9 Performance comparison for SSRM and iSSRM methods 66

2.10 Identification of lumped mass systems via iSSRM method 66

2.11 Recommended GA parameters for iSSRM method 67

3.1 Allocations of total evaluation to iSSRM and local search in the enhanced optimization strategy: based on a 20-DOF known mass system 114

3.2 Recommended parameters for iSSRM in the enhanced optimization strategy 114

3.3 GA parameters for numerical example 1: 10-DOF lumped mass system . . 115

3.4 Results for numerical example 1: 10-DOF lumped mass system 115

3.5 GA parameters for numerical example 2: 16-element plate 116

3.6 Results for numerical example 2: 16-element plate 116

3.7 GA parameters for numerical example 3: 29-element truss 117

3.8 Results for numerical example 3: 29-element truss 117

4.1 GA parameters for system identification and damage detection in numerical studies 148

4.2 Structural identification of 12-DOF lumped mass system 149

4.3 Structural identification of 50-DOF lumped mass system 150

5.1 GA parameters for system identification in numerical examples 164

5.2 Identification of truss substructure by SSI without overlap 164

5.3 Identification of 50-DOF lumped mass system with unknown mass 165

6.1 Accelerometer specification 193

6.2 GA parameters for baseline identification 193

6.3 GA parameters for identifying stiffness change due to cut and welding . . 194

6.4 Basic damage scenarios 195

6.5 Additional damage scenarios 195

6.6 Basic strengthening scenarios with stiffness increase 195

6.7 Additional strengthening scenarios 195

6.8 Identification of damage due to cut 196

6.9 Identification of strengthening due to welding 197

6.10 Effect of substructure size 198

7.1 Main findings from the thesis 205

A.1 Sampling method comparison via 10-DOF known mass system 222

A.2 Sampling method comparison via 20-DOF known mass system 223

A.3 Known mass system - Test on iSSRM method: 5-DOF 224

A.4 Known mass system - Test on iSSRM method: 10-DOF 225

A.5 Known mass system - Test on iSSRM method: 20-DOF 226

A.6 Known mass system - Test on iSSRM method: 50-DOF 227

A.7 Unknown mass system - Test on iSSRM method: 5-DOF 228

A.8 Unknown mass system - Test on iSSRM method: 10-DOF 229

A.9 Unknown mass system - Test on iSSRM method: 20-DOF 230

B.1 D2-Global identification: 17% damage at level 4 via complete measurement 233

B.2 D3-Global identification: 17% damage at level 4 and 4% damage at level 6 via complete measurement 233

B.3 D4-Global identification: 17% damage at level 4 and 4% damage at levels 3 and 6 via complete measurement 234

B.4 D6-Global identification: 17% damage at levels 3, 4 and 6 via complete measurement 235

B.5 S1-Global identification: moderate strengthening at level 4 via complete measurement 236

B.6 S4-Global identification: large strengthening at levels 4 and 6 via complete measurement 236

B.7 S5-Global identification: small strengthening at level 4 and moderate strengthening at level 6 via complete measurement 237

B.8 S7-Global identification: small strengthening at level 6 via complete measurement 237

B.9 D2-Global identification: 17% damage at level 4 via incomplete measurement 238

B.10 D3-Global identification: 17% damage at level 4 and 4% damage at level 6 via incomplete measurement 238

B.11 D4-Global identification: 17% damage at level 4 and 4% damage at levels 3 and 6 via incomplete measurement 239

B.12 D6-Global identification: 17% damage at levels 3, 4 and 6 via incomplete measurement 240

B.13 S1-Global identification: moderate strengthening at level 4 via incomplete measurement 241

B.14 S4-Global identification: large strengthening at levels 4 and 6 via incomplete measurement 241

B.15 S5-Global identification: small strengthening at level 4 and moderate strengthening at level 6 via incomplete measurement 242

B.16 S7-Global identification: small strengthening at level 6 via incomplete measurement 242

B.17 D2-“F-Sub” identification: 17% damage at level 4 via complete measurement and 2 substructures 243

B.18 D3-“F-Sub” identification: 17% damage at level 4 and 4% damage at level 6 via complete measurement and 2 substructures 243

B.19 D4-“F-Sub” identification: 17% damage at level 4 and 4% damage at levels 3 and 6 via complete measurement and 2 substructures 244

B.20 D6-"F-Sub" identification: 17% damage at levels 3, 4 and 6 via complete measurement and 2 substructures 245

B.21 S1-"F-Sub" identification: moderate strengthening at level 4 via complete measurement and 2 substructures 246

B.22 S4-"F-Sub" identification: large strengthening at levels 4 and 6 via complete measurement and 2 substructures 246

B.23 S5-"F-Sub" identification: small strengthening at level 4 and moderate strengthening at level 6 via complete measurement and 2 substructures . 247

B.24 S7-"F-Sub" identification: small strengthening at level 6 via complete measurement and 2 substructures 247

B.25 D2-"F-Sub" identification: 17% damage at level 4 via incomplete measurement and 2 substructures 248

B.26 D3-"F-Sub" identification: 17% damage at level 4 and 4% damage at level 6 via incomplete measurement and 2 substructures 248

B.27 D4-"F-Sub" identification: 17% damage at level 4 and 4% damage at levels 3 and 6 via incomplete measurement and 2 substructures 249

B.28 D6-"F-Sub" identification: 17% damage at levels 3, 4 and 6 via incomplete measurement and 2 substructures 250

B.29 S1-"F-Sub" identification: moderate strengthening at level 4 via incomplete measurement and 2 substructures 251

B.30 S4-"F-Sub" identification: large strengthening at levels 4 and 6 via incomplete measurement and 2 substructures 251

B.31 S5-"F-Sub" identification: small strengthening at level 4 and moderate strengthening at level 6 via incomplete measurement and 2 substructures 252

B.32 S7-"F-Sub" identification: small strengthening at level 6 via incomplete measurement and 2 substructures 252

B.33 D2-"F-Sub" identification: 17% damage at level 4 via complete measurement and 4 substructures 253

B.34 D3-"F-Sub" identification: 17% damage at level 4 and 4% damage at level 6 via complete measurement and 4 substructures 253

B.35 D4-"F-Sub" identification: 17% damage at level 4 and 4% damage at levels 3 and 6 via complete measurement and 4 substructures 254

B.36 D6-"F-Sub" identification: 17% damage at levels 3, 4 and 6 via complete measurement and 4 substructures 255

B.37 S1-"F-Sub" identification: moderate strengthening at level 4 via complete measurement and 4 substructures 256

B.38 S4-"F-Sub" identification: large strengthening at levels 4 and 6 via complete measurement and 4 substructures 256

B.39 S5-"F-Sub" identification: small strengthening at level 4 and moderate strengthening at level 6 via complete measurement and 4 substructures . 257

B.40 S7-"F-Sub" identification: small strengthening at level 6 via complete measurement and 4 substructures 257

B.41 D2-"T-Sub" identification: 17% damage at level 4 via complete measurement and 2 substructures 258

B.42 D3-"T-Sub" identification: 17% damage at level 4 and 4% damage at level 6 via complete measurement and 2 substructures 258

B.43 D4-"T-Sub" identification: 17% damage at level 4 and 4% damage at levels 3 and 6 via complete measurement and 2 substructures 259

B.44 D6-"T-Sub" identification: 17% damage at levels 3, 4 and 6 via complete measurement and 2 substructures 260

B.45 S1-"T-Sub" identification: moderate strengthening at level 4 via complete measurement and 2 substructures 261

B.46 S4-"T-Sub" identification: large strengthening at levels 4 and 6 via complete measurement and 2 substructures 261

B.47 S5-"T-Sub" identification: small strengthening at level 4 and moderate strengthening at level 6 via complete measurement and 2 substructures . 262

B.48 S7-"T-Sub" identification: small strengthening at level 6 via complete measurement and 2 substructures 262

B.49 D2-"T-Sub" identification: 17% damage at level 4 via incomplete measurement and 2 substructures 263

B.50 D3-"T-Sub" identification: 17% damage at level 4 and 4% damage at level 6 via incomplete measurement and 2 substructures 263

B.51 D4-"T-Sub" identification: 17% damage at level 4 and 4% damage at levels 3 and 6 via incomplete measurement and 2 substructures 264

B.52 D6-"T-Sub" identification: 17% damage at levels 3, 4 and 6 via incomplete measurement and 2 substructures 265

B.53 S1-"T-Sub" identification: moderate strengthening at level 4 via incomplete measurement and 2 substructures 266

B.54 S4-"T-Sub" identification: large strengthening at levels 4 and 6 via incomplete measurement and 2 substructures 266

B.55 S5-"T-Sub" identification: small strengthening at level 4 and moderate strengthening at level 6 via incomplete measurement and 2 substructures 267

B.56 S7-"T-Sub" identification: small strengthening at level 6 via incomplete measurement and 2 substructures 267

B.57 D2-"T-Sub" identification: 17% damage at level 4 via complete measurement and 4 substructures 268

B.58 D3-"T-Sub" identification: 17% damage at level 4 and 4% damage at level 6 via complete measurement and 4 substructures 268

B.59 D4-"T-Sub" identification: 17% damage at level 4 and 4% damage at levels 3 and 6 via complete measurement and 4 substructures 269

B.60 D6-"T-Sub" identification: 17% damage at levels 3, 4 and 6 via complete measurement and 4 substructures 270

B.61 S1-"T-Sub" identification: moderate strengthening at level 4 via complete measurement and 4 substructures 271

B.62 S4-"T-Sub" identification: large strengthening at levels 4 and 6 via complete measurement and 4 substructures 271

B.63 S5-"T-Sub" identification: small strengthening at level 4 and moderate strengthening at level 6 via complete measurement and 4 substructures . 272

B.64 S7-"T-Sub" identification: small strengthening at level 6 via complete measurement and 4 substructures 272

List of Figures

2.1 System identification using GA 54

2.2 Concept of simple genetic algorithm (SGA) 54

2.3 Modified GA based on migration and artificial selection (MGAMAS) . . . 55

2.4 Search space reduction method (SSRM) 56

2.5 Comparison of sampling method: 289 samples 57

2.6 SSRM with sampling test: an improved SSRM 58

2.7 Stiffness identification convergence histories of a 10-DOF lumped mass system under 0% noise 59

2.8 Stiffness identification convergence histories of a 20-DOF lumped mass system under 0% noise 59

2.9 Identification of a 10-DOF known mass system under noise 60

2.10 Typical identification of a 20-DOF known mass system under 10% noise . 60

2.11 Typical convergence history of a 20-DOF known mass system under 10% noise 61

3.1 Typical peak shifting of 1-DOF known mass system 96

3.2 Typical peak shifting of 2-DOF known mass system under 0% noise: 3D view 97

3.3 Typical peak shifting of 2-DOF known mass system under 0% noise: contour 97

3.4 Typical peak shifting of 2-DOF known mass system under 5% noise: 3D view 98

3.5 Typical peak shifting of 2-DOF known mass system under 5% noise: contour 98

3.6 Typical peak shifting of 2-DOF known mass system under 10% noise: 3D view 99

3.7 Typical peak shifting of 2-DOF system under 10% noise: contour 99

3.8 Peak shifting of 2-DOF known mass system under 10,000 cases: 0% noise 100

3.9 Peak shifting of 2-DOF known mass system under 10,000 cases: 5% noise 100

3.10 Peak shifting of 2-DOF known mass system under 10,000 cases: 10% noise 101

3.11 Typical peak shifting of 1-DOF unknown mass system under 0% noise: 3D view 101

3.12 Typical peak shifting of 1-DOF unknown mass system under 0% noise: contour 1 102

3.13 Typical peak shifting of 1-DOF unknown mass system under 5% noise: 3D view 102

3.14 Typical peak shifting of 1-DOF unknown mass system under 5% noise: contour 1 103

3.15 Typical peak shifting of 1-DOF unknown mass system under 10% noise: 3D view 103

3.16 Typical peak shifting of 1-DOF unknown mass system under 10% noise: contour 1 104

3.17 Typical peak shifting of 1-DOF unknown mass system under 0% noise: contour 2 104

3.18 Typical peak shifting of 1-DOF unknown mass system under 5% noise: contour 2 105

3.19 Typical peak shifting of 1-DOF unknown mass system under 10% noise: contour 2 105

3.20 Effect of data length on fitness function: noise free 106

3.21 Effect of multiple load cases on fitness function: noise free 106

3.22 Typical peak shifting of 2-element plate under 0% noise: contour 107

3.23 Typical peak shifting of 2-element plate under 5% noise: contour 107

3.24 Typical peak shifting of 2-element plate under 10% noise: contour 108

3.25 Enhanced optimization strategy: improved SSRM with local search 109

3.26 Convergence history of known mass systems using merely iSSRM method 110

3.27 Convergence history of unknown mass systems using merely iSSRM method 110

3.28 Typical iSSRM convergence of 20-DOF known mass system under 0% noise: 40,000 total evaluations 111

3.29 Typical iSSRM convergence of 20-DOF unknown mass system under 0% noise: 40,000 total evaluations 111

3.30 Allocation of total evaluations to iSSRM search and local search: based on a 20-DOF known mass system (Refer to Table 3.1 for the definition of Cases I to V) 112

3.31 Numerical example 1: 10-DOF lumped mass system 112

3.32 Numerical example 2: 16-element plate 112

3.33 Numerical example 3: 29-element truss 113

4.1 Illustration of substructural philosophy in frequency domain 138

4.2 Frequency domain substructural identification under random excitation . 139

4.3 Substructures of 12-DOF lumped mass system 140

4.4 Stiffness identification of 12-DOF system under 5% noise: complete measurement 141

4.5 Stiffness identification of 12-DOF system under 10% noise: complete measurement 141

4.6 Stiffness identification of 12-DOF system based on incomplete measurement 142

4.7 Identified stiffness integrity indices for damage scenario 1: 10% noise . . . 143

4.8 Identified stiffness integrity indices for damage scenario 2: 10% noise . . . 143

4.9 Substructures of 50-DOF lumped mass system 144

4.10 Stiffness identification of 50-DOF system under 5% noise: complete measurement 144

4.11 Stiffness identification of 50-DOF system under 10% noise: complete measurement vs incomplete measurement 145

4.12 Identified stiffness integrity indices for damage scenario 1: 5% noise 146

4.13 Identified stiffness integrity indices for damage scenario 2: 5% noise 146

4.14 Identified stiffness integrity indices for damage scenario 1: 10% noise . . . 147

4.15 Identified stiffness integrity indices for damage scenario 2: 10% noise . . . 147

5.1 Two-span truss structure and substructure 161

5.2 Ratio of identified stiffness to exact value for 50-DOF known-mass system under 5% noise 162

5.3 Ratio of identified stiffness to exact value for 50-DOF unknown-mass system under 5% noise 162

5.4 Ratio of identified mass to exact value for 50-DOF unknown-mass system under 5% noise 163

5.5 Comparison of divide-and-conquer methods in system identification based on the 50-DOF system (Sub-SOMI-RR taken from Tee *et al.* (2005)) . . . 163

6.1 Experimental model of frame building . . . 180

6.2 Static test set up . . . 180

6.3 Dynamic test set up . . . 181

6.4 Shaker used to excite the frame model . . . 181

6.5 Mounting of accelerometer and force sensor . . . 182

6.6 Welding at level 4, 6, and cut remained at level 3 . . . 182

6.7 Progressive strengthening at one level by welding: strengthening baseline (left), moderate strengthening (middle), large strengthening (right) . . . 182

6.8 Damage induced by cutting . . . 183

6.9 Strengthening by welding . . . 184

6.10 Damage case D2 (4L) with complete measurement: large damage (16.7%) at level 4 . . . 185

6.11 Damage case D3 (4L6S) with complete measurement: large damage (16.7%) at level 4 and small damage (4.1%) damage at level 6 . . . 186

6.12 Damage case D4 (4L3S6S) with complete measurement: large damage (16.7%) at level 4 and small damage (4.1%) at levels 3 and 6 . . . 187

6.13 Damage case D6 (3L4L6L) with complete measurement: large damage (16.7%) at levels 3, 4 and 6 . . . 188

6.14 Strengthening case S1 (4M) with complete measurement: moderate strengthening at level 4 . . . 189

6.15 Strengthening case S4 (4L6L) with complete measurement: large strengthening at levels 4 and 6 . . . 190

6.16 Strengthening case S5 (4S6M) with complete measurement: small strengthening at level 4 and moderate strengthening at level 6 . . . 191

6.17 Strengthening case S7 (6S) with complete measurement: small strengthening at level 6 . . . 192

List of Symbols

a	Lower bound of an unknown	28
b	Upper bound of an unknown	28
c	Constant in the fitness function	29
$\mathbf{C}$	Damping matrix of multiple degree-of-freedom systems	3
F_{sum}	Total fitness of a population in simple genetic algorithm	32
$\mathbf{g}$	Change in gradients	83
H	Transfer function	122
$\mathbf{K}$	Stiffness matrix of multiple degree-of-freedom systems	3
$\mathbf{M}$	Mass matrix of multiple degree-of-freedom systems	3
N_E	Total number of fitness evaluations	51
N_U	Total number of unknowns to be identified	51
$\mathbf{p}$	Search direction in gradient search methods	80
p_c	Crossover rate	33
p_m	Mutation rate	34
$\mathbf{r}$	Influence matrix in time domain substructural method	154
$\mathbf{S}$	Search space of unknowns to be identified	28
T	Temperature in simulated annealing algorithm	77
$\mathbf{u}$	Vector of displacements	3
$\dot{\mathbf{u}}$	Vector of velocities	3

$\ddot{\mathbf{u}}$	Vector of accelerations	3
$U(0,1)$	Uniform distribution	39
v	Chromosome in genetic algorithm	32
$\mathbf{x}$	Unknowns to be identified	28
α	Step size in gradient local searcher	80
γ	Substructural efficiency	131
ϵ_x	Convergence tolerance for variables	87
ϵ_g	Convergence tolerance for gradients	87
η	Exponential window size	129
ϑ	Objective function for local searchers	86
ξ	Damping ratio	153
ϕ	Fitness function for genetic algorithm	28
ω	Angular frequency	121
$\mathbf{\Lambda}$	Matrix of eigenvalues	5
$\mathbf{\Phi}$	Vector of eigenvectors	5

CHAPTER 1

Introduction

Health monitoring and safety evaluation of large structures have always been an important topic that draws significant governmental concerns and engineering interests. Early detection of damage will help to avoid catastrophic loss in properties and lives. Technically, structural health monitoring (SHM) is understood as an inverse problem in structural dynamics. The purpose is to determine the residual strength of structural resistance to known/unknown disturbance. Recognitions of SHM emerged in the early 1970s when a large number of observations of the 1971 San Fernando earthquake in California were recorded (Beck and Jennings, 1980). These observations provided knowledge of global stiffness by fitting the recorded response of a building to the response of a synthesized linear model subjected to the recorded base acceleration.

The developments in SHM are characterized by representative technical transitions from visual inspection to local non-destructive techniques, and then to structural identification methods. While visual inspection is widely used, especially in early days, it is often incomplete as it cannot investigate damage of inaccessible structural members. Local non-destructive techniques (NDT) such as ultrasound detection and acoustic emission method are suitable for individual structural components. But they are not suitable for large and complex structures, e.g. buildings, bridges and dams. Nevertheless, the rapid development of sensing systems and computer technology makes it possible to acquire

and analyze vibration signals in a more robust way than ever. Therefore, structural health monitoring of large systems is possible by measuring and analyzing the input and output signals, i.e., strain, displacement, or acceleration. To monitor structural health, system identification methods are the most extensively explored nowadays.

As an important branch of structural health monitoring, structural identification is the process of determining unknown parameters of a structural system based on observed input and output (I/O) of the system. Through the identified parameters, the structural state is to be monitored as well as non-destructively assessed. A common assumption made in structural system identification is that a mathematical model is available to accurately represent the physical system. Furthermore, good correlation is also assumed to be possible between the mathematical model and real observations such that damage will not introduce any violations to the baseline model. The subsequent section will elaborate typical mathematical models for structural response to external loadings. As models for response representation closely relate to the method used for structural identification, the immediately followed section will cover the classification of structural identification methods.

1.1 Mathematical Models on Structural Dynamics

The first important step in structural identification lies in the selection of a mathematical model for the structural system considered. Then the parameters of the chosen model will be estimated from the observed measurement. The models are usually expressed as second-order equations of motion or first-order state space equations.

1.1.1 Second-Order Model

For equilibrium of a dynamic system, three resisting forces resulting from the motion, i.e., the inertial force, the damping force and the spring force, counteract the external

force. The equilibrium can be formulated from the finite element perspective to achieve the ease of numerical implementation. If the corresponding mass, damping and stiffness distribution of an n degree-of-freedom (DOF) system are represented by $\mathbf{M}$, $\mathbf{C}$, and $\mathbf{K}$ matrices separately, the equations of motion are usually written as second-order differential equations.

$$\mathbf{M}\ddot{\mathbf{u}} + \mathbf{C}\dot{\mathbf{u}} + \mathbf{K}\mathbf{u} = \mathbf{B}\mathbf{f} \tag{1.1}$$

where $\mathbf{u}$, $\dot{\mathbf{u}}$ and $\ddot{\mathbf{u}}$ represent $n \times 1$ vectors of nodal displacements, velocities, and accelerations, respectively. The $n \times m$ matrix $\mathbf{B}$ defines the force locations. The vector $\mathbf{f}$ of dimension $m \times 1$ is the input vector acting on the system. In Eq. (1.1), the representation of damping is crucial. If classical normal modes, referred otherwise to undamped modes, are assumed in damped linear dynamic system, the damping force could be described analytically (Caughey, 1960). As a particular form of Caughey damping, Rayleigh damping proves to be useful to describe the dynamic response in a light damped system (Bathe, 1996). The system response can be computed to acceptable accuracy by the step-by-step integration method in time domain. Alternatively, this dynamic response can also be obtained by frequency domain method for linear systems, i.e., via mode displacement superstition or discrete Fourier Transform (DFT).

The second-order model is a good representation of a vibrating structure and able to account for linear as well as nonlinear behaviors of structures. However, this physical model is not established from the perspective of system identification, as it needs assumptions of damping and misses the modeling of noise in the I/O signals. The advantage of this second-order formulation lies in the ease of extracting the physical parameters directly relating to the structural stiffness.

1.1.2 First-Order Model

Different from the second-order model, the first-order state space model is originated from the classical control theory and extended to system identification. Within the framework

of control theory, state-space representation of system is widely used in electrical, mechanical and aerospace engineering. The representation is formulated by the following equations for a linear time invariant system.

$$\dot{\mathbf{x}}(t) = \mathbf{A}\mathbf{x}(t) + \mathbf{B}\mathbf{f}(t) \tag{1.2a}$$

$$\mathbf{y}(t) = \mathbf{D}\mathbf{x}(t) \tag{1.2b}$$

where $\mathbf{x}$ is an n-dimensional vector of state variables, $\mathbf{f}$ an m-dimensional vector of inputs to the system, and $\mathbf{y}$ a p-dimensional vector of outputs or measurements. Matrices $\mathbf{A}$, $\mathbf{B}$ and $\mathbf{D}$ describes the behavior of the system and are named, respectively, transition matrix, input matrix, and output matrix. The transition matrix $\mathbf{A}$ characterizes the dynamics of the system, i.e., a representation of mass, stiffness, and damping properties. The problem of system identification can be then stated as follows. Given the measurements $\mathbf{y}(t)$, construct constant matrices [**A, B, D**] such that the functions $\mathbf{y}$ are reproduced by the state space equations.

The second order differential equations can be converted to the state space equations by defining a state vector $\mathbf{x}_1$

$$\mathbf{x}_1 = \begin{bmatrix} \mathbf{u} & \dot{\mathbf{u}} \end{bmatrix}^T \tag{1.3}$$

Then Eq. (1.1) can be transformed to a state space representation as

$$\dot{\mathbf{x}}_1(t) = \mathbf{A}_1\mathbf{x}_1(t) + \mathbf{B}_1\mathbf{f}(t) \tag{1.4a}$$

$$\mathbf{y}(t) = \mathbf{C}_1\mathbf{x}_1(t) \tag{1.4b}$$

where

$$\mathbf{A}_1 = \begin{bmatrix} \mathbf{0} & \mathbf{I} \\ -\mathbf{M^{-1}K} & -\mathbf{M^{-1}C} \end{bmatrix}; \mathbf{B}_1 = \begin{bmatrix} 0 \\ \mathbf{M^{-1}B} \end{bmatrix}; \mathbf{C}_1 = \begin{bmatrix} \mathbf{C}_p & \mathbf{0} \end{bmatrix}$$

The modal parameters of the state space equations can be obtained by defining a measurement vector $\mathbf{y}$

$$\mathbf{y} = \begin{bmatrix} \mathbf{C}_p\mathbf{u} & \mathbf{C}_v\dot{\mathbf{u}} & \mathbf{C}_a\ddot{\mathbf{u}} \end{bmatrix}^T \tag{1.5}$$

Eq. (1.4a) can be alternatively written as follows

$$\begin{bmatrix} \mathbf{C} & \mathbf{M} \\ \mathbf{M} & \mathbf{0} \end{bmatrix} \dot{\mathbf{x}}_1 + \begin{bmatrix} \mathbf{K} & \mathbf{0} \\ \mathbf{0} & -\mathbf{M} \end{bmatrix} \mathbf{x}_1 = \begin{bmatrix} \mathbf{B} \\ \mathbf{0} \end{bmatrix} \mathbf{f} \tag{1.6}$$

with the measurement vector as

$$\mathbf{y} = [\ \mathbf{C}_p \quad \mathbf{0}\ ]\mathbf{x}_1 \tag{1.7}$$

where $\mathbf{y}$ includes any combination of nodal displacements, velocities, and/or accelerations. The matrix $[\ \mathbf{C}_p^T \quad \mathbf{C}_v^T \quad \mathbf{C}_a^T\ ]^T$ is of dimension $p \times n$, representing the output matrix that may incorporate position, velocity, and acceleration measurements, with p denoting the total number of outputs.

The advantage of rewriting Eq. (1.4a) into (1.6) is that the associated eigenvalue problems is kept symmetric and can be written in a matrix form as

$$\begin{bmatrix} \mathbf{C} & \mathbf{M} \\ \mathbf{M} & \mathbf{0} \end{bmatrix} \begin{bmatrix} \mathbf{\Phi} \\ \mathbf{\Phi\Lambda} \end{bmatrix} \mathbf{\Lambda} = \begin{bmatrix} -\mathbf{K} & \mathbf{0} \\ \mathbf{0} & \mathbf{M} \end{bmatrix} \begin{bmatrix} \mathbf{\Phi} \\ \mathbf{\Phi\Lambda} \end{bmatrix} \tag{1.8}$$

where $\mathbf{\Phi} = [\ \mathbf{\Phi}_1 \quad \mathbf{\Phi}_2 \quad \cdots \quad \mathbf{\Phi}_{2n}\ ]$ and the diagonal matrix $\mathbf{\Lambda}$ are of dimension $n \times 2n$ and $2n \times 2n$, respectively. The eigenvectors and eigenvalues are obtained by solving the following complex eigenvalue equation.

$$({\lambda_i}^2\mathbf{M} + \lambda_i\mathbf{C} + \mathbf{K})\mathbf{\Phi}_i = 0 \tag{1.9}$$

In this way, state-space representation provides a direct mapping between coordinates associated with measured inputs and outputs. More importantly, the representation is relevant to modal testing because the first-order form encompasses all linear system behavior, including damped structural system. The dynamic characteristics of a damped structure can be obtained by evaluating the complex roots, the intrinsic eigen pairs to the damped system, of a first-order system of equations.

The first-order representation provides a way to describe a dynamic system without assumptions on damping and allows more general mass, damping and stiffness properties

than normally applied. Therefore the identified complex mode shapes are directly employed in the system response predictions, especially if the damping matrix couples the modal equations. Furthermore, identification methods based on control algorithms such as observer/kalman filter identification (OKID) can be used to evaluate the response, since those methods will directly relate an input to an output. However, the physical parameters cannot be directly determined from the first-order representation. To relate the measurement to physical properties, the state space based system models has to be transformed to an equivalent second-order realizations (Bernal, 2000; De Angelis *et al.*, 2002; Lus *et al.*, 2003a,b).

1.2 Overview of Structural Identification Methods

Structural identification methods can be categorized in several different ways, e.g., frequency domain and time domain methods, parametric and nonparametric models, and deterministic and stochastic methods. Comprehensive literature reviews on system identification methods have also been given in Juang (1993), Ghanem and Shinozuka (1995), Ljung (1999), Ewins (2000), and Maia and Silva (2001). In this study, the identification methods will be classified into classical and non-classical methods.

1.2.1 Classical Methods

Classical methods often have sound mathematical basis. They are used to extract modal characteristics or physical properties through system identification. Based on the identified system, structural health can be monitored via detecting the potential damages by comparing a state of concern and the baseline/reference state.

1.2.1.1 Eigensystem Realization Algorithm (ERA)

Based on minimum realization and singular value decomposition (SVD), the ERA method constructs a discrete state-space model of minimal order that fits measured impulse re-

sponse functions (Juang and Pappa, 1985, 1986). The method reduces significantly the number of estimated modes that have to be considered. At the same time the method maintains the smallest state space dimension among the realized systems that has the same input-output relations. More importantly, the ERA method is an output-only time-domain modal identification technique using free vibration response signals. Closely spaced eigenvalues can be efficiently identified using data from more than one test (Juang and Pappa, 1985). Since its first appearance in 1985, ERA has been recognized as a successful modal identification method, and has achieved extensive engineering applications (Juang and Suzuki, 1988; Lus *et al.*, 1999; Qin *et al.*, 2001; Lus *et al.*, 2004; Siringoringo and Fujino, 2006; Nayeri *et al.*, 2007; De Callafon *et al.*, 2008; Majji and Junkins, 2008). However, one disadvantage is that this approach requires time-consuming computation in full singular value decomposition of the full rank Hankel matrix. In addition, the noise level of response data has significant effects on the identification accuracy.

1.2.1.2 Natural Excitation Technique (NExT)

Under the assumption that the system is excited by stationary white noise, the correlation functions between the response signals could be expressed as a sum of decaying sinusoids. Each decaying sinusoid has a damped natural frequency and damping ratio that are identical to those of a structural mode. Hence, the output correlation functions can be processed as the impulse response function of the system in order to extract modal parameters. This technique is generally referred to as NExT (James *et al.*, 1993, 1995), standing for Natural Excitation Technique. The method is basically a four-step process: acquisition of response data, calculation of auto- and cross-correlation functions from the measured time histories, time domain modal identification, i.e., using ERA to identify modal frequencies and damping ratios, and finally, extraction of the mode shape information. This approach does not require knowledge of the excitation. Thus it is applicable to the identifications subjected to ambient excitation. Extended to the harmonic excita-

tion, the NExT method has been used with least squares complex exponential method to extract modal parameters (Mohanty and Rixen, 2003). The NExT method has also been used in combination with ERA method for modal identification (Caicedo *et al.*, 2004; Yang *et al.*, 2006; Nayeri *et al.*, 2007; Qian *et al.*, 2007; Siringoringo and Fujino, 2008; Yun *et al.*, 2008). However, NExT fails to extract the modal parameters when closely spaced modes are present in the system (James *et al.*, 1993).

1.2.1.3 Random Decrement Technique (RDT)

Inspired by physical intuition instead of any mathematical development, Cole (1973) originally introduced the random decrement technique to detect damage in aerospace structures using single measurement. Based on the assumption of zero-mean, stationary random excitations, a random response of a structure is hypothesized to be composed of deterministic and random part. The idea is to obtain the deterministic response through sufficient samples of pre-selected segments of random response signals to average out the random part. A rigorous mathematical proof was given by Vandiver *et al.* (1982) on the equivalence between the random signals of a system through the RDT and the free decayed responses of the system. Nevertheless, it has been pointed out that the RD signature cannot be equal to the system free vibration curve if the random excitation is not white (Spanos and Zeldin, 1998). The RDT method is very attractive for system identification and damage detection when only the response data under random excitations is available. It was used to estimate modal parameters under ambient vibration in order to get the stiffness matrix (Feng *et al.*, 1998) and also adopted to extract modal parameters for damage detection using a neural network (Lee *et al.*, 2002). Owing to its efficiency, simplicity in processing vibration measurements and the lack of requirement for input excitation measurements, this method has been used extensively for damping estimation in offshore platform (Yang *et al.*, 1983), to study the effectiveness of tuned liquid dampers. It has been used for assessment of ship transverse stability, as RDT requires

no measurement of wave height (Haddara *et al.*, 1994). RDT was a versatile technique for characterization of random signal in the time domain, but it was not recommended for estimating cross-correlateion function for stochastic processes with low natural correlation (Brincker *et al.*, 1991). The method also produced biased modal estimates when subjected to forced excitation (Ku *et al.*, 2007).

1.2.1.4 Ibrahim Time Domain (ITD) Method

The Ibrahim Time Domain (ITD) method (Ibrahim and Mikulcik, 1977) used a set of free decay vibration measurements in a single analysis to simultaneously identify all parameters of the excited modes, i.e., the natural frequencies, modal damping ratios, and mode shapes. It was studied extensively in identifying dynamic characteristics of engineering structures. Using the data from a free vibration test, the ITD method was studied to identify the modal parameters of a highway bridge (Huang *et al.*, 1999) and a steel truss bridge (Rodrigues, 2002). Due to the effectiveness of identifying the closely spaced modes, the ITD method was also adopted to study the non-stationary ambient vibration data (Chiang and Lin, 2008). However, ITD technique is only applicable when free response data is presented, and also it favors the identification of modal frequencies and damping ratios. To obtain the complete mode shapes using ITD, a mode shape interpolation method was needed (Ueng *et al.*, 2000; Lin *et al.*, 2001). As the ITD method can only cope with free vibration data, it is usually used in combination with RDT method (Fujino *et al.*, 2000; Garibaldi *et al.*, 2003; Lin *et al.*, 2005; Siringoringo and Fujino, 2008).

1.2.1.5 Stochastic Subspace Identification

The methods of stochastic subspace identification have been comprehensively introduced in Van Overschee and De Moor (1996). The bulk of subspace methods have been matched by least squares method with applications in state space model (Ljung and McKelvey,

1996). They are established in the stochastic state space, the dynamic characteristics as natural frequencies, modal damping ratios and modal shapes of a structure can be extracted from the coefficient matrices of a state-space model. The SSI method does not require any preprocessing of the data to calculate auto/crosscorrelation functions or auto/cross-spectra of output data. Therefore, SSI method has been applied extensively in modal identification. By setting the reference sensors, the SSI method was validated with real ambient vibration data from a steel mast excited by wind load (Peeters and De Roeck, 1999). A subspace approach with an instrumental variable concept (Huang and Lin, 2001) was validated on a five-storey steel frame via ambient vibration, free vibration, and earthquake response data. The subspace identification method was also studied on a 15-story steel moment-resisting frame (Skolnik *et al.*, 2006). In the study, modal parameters were identified for the first nine modes using low-amplitude earthquake and ambient vibration data. The frequencies and mode shapes identified were then used to update a three-dimensional model to improve correlation between analytical and identified model for damage assessment. The SSI method was also applied to modal identification of steel arch bridge (Ren *et al.*, 2004), damage detection of a base-isolated building (Yoshimoto *et al.*, 2005), and health assessment of a 50-year old concrete bridge (Reynders *et al.*, 2007). However, the modal damping ratios were reported to be not identified reliably in the laboratory (Ndambi *et al.*, 2000) and field testing (He *et al.*, 2009). Another drawback was the stochastic subspace identification usually required large computational effort, although the good accuracy was achieved (Yi and Yun, 2004).

1.2.1.6 Time-Frequency Methods

The time-frequency methods are originally mathematical and signal processing tools. Compared to the traditional waveform or spectrum analysis by Fourier Transform, these methods have the advantage of revealing the event-related time and frequency domain information simultaneously. They are thus especially applicable for non-stationary signals

for which traditional Fourier analysis is limited. Typical time-frequency representation includes wavelet analysis (Mallat, 1999) and Hilbert-Huang Transform (HHT) (Huang *et al.*, 1998; Huang and Shen, 2005). Comparison of these two methods was studied by Kijewski-Correa and Kareem (2006) . Although they are essentially indirect structural identification methods, successful identification can be achieved by means of their fruitful resolution of the observations.

As a representative time-frequency method, wavelet has received increasing attention in the field of structural identification. To avoid ill-conditioning due to experimentally measured acceleration, Doyle (1997) applied wavelet deconvolution method for impact force identification. Wavelet transform was also used to extract impulse response function in linear systems, and the impulse response function was then utilized to identify the linear system via the realized state space models (Robertson *et al.*, 1998). By wavelet transformation, the equation of motion was translated into an algebraic equation of acceleration. The stiffness and damping matrices then can be identified by directly measuring acceleration (Sone *et al.*, 2004). By virtue of the time-invariance and filtering ability of the transform, wavelet transform was also used in modal identification (Huang *et al.*, 2005; Chakraborty *et al.*, 2006; Yang *et al.*, 2007a). Without modal identification, damage can be quantified directly as well by detecting the irregularity of wavelet coefficients observed near the location of the crack (Sun and Chang, 2004). Practical aspects of wavelet transform in damage detection such as sampling rate, filter frequency and length of signal were discussed by Quek *et al.* (2001). A good survey of wavelet based methods in the field of damage detection was given by Kim and Melhem (2004). However, wavelet analysis is an adaptive window Fourier analysis, and thus can deal with non-stationary but not nonlinear data. Thus its use makes sense only for linear systems (Huang and Shen, 2005).

Another commonly used time-frequency method, HHT, has been covered extensively in modal identification and damage detection. The feasibility of HHT was illustrated by

Quek *et al.* (2003) for locating an anomaly based on physically acquired propagating wave signals. Damage time instants, locations and natural frequencies as well as damping ratios were identified via HHT method (Yang *et al.*, 2004). The natural frequency and damping ratio of linear systems were identified by Yang *et al.* (2003a,b) via a single measurement of free response. Besides, mode shapes, physical mass, damping and stiffness matrices can also be identified if complete measurements were available. The advantage of the method has been illustrated by identifying closely spaced modes where the wavelet method is limited (Yang *et al.*, 2003a). By incorporating the RDT method, the identification is extended to identify in situ tall buildings using ambient wind vibration data from the only acceleration sensor (Yang *et al.*, 2004).

To sum up, modal identification methods have been considerably developed over the past decades. Through the measurements of response time history, modal parameters can be extracted with confidence (Juang, 1993; Ewins, 2000; Maia and Silva, 2001). These classical methods, including ERA, NExT, RDT, ITD, and SSI, are typically capable of extracting the modal parameters under operational conditions. They are attractive when only response data are measurable and the actual loading conditions are unknown. The time-frequency methods are fundamentally efficient signal processing tools and applicable for modal identification. However, modal parameters are extracted generally the first several modes, but the results are usually not reliable in higher modes due to the low signal to noise ratio. With only lower modes identified, however, the detectable damage by means of identified modal parameters usually has to be very large. In the field of structural health monitoring, it is important to detect the damage event in the early stage to provide warning and take remedial action. On the other hand, physical parameters such as stiffness have much more direct interpretation of structural health than modal parameters. Attempts have been made to extract physical properties from modal identification or state-space formulations, but they generally involve complicated mathematical operations (Alvin *et al.*, 1995; Chen *et al.*, 1996; De Angelis *et al.*, 2002; Ko and Hung, 2002;

Lus *et al.*, 2003a; Shi *et al.*, 2007). Determining physical parameter directly by using the measured acceleration time history has better potential of application. Recently, it is shown experimentally that very small damage, i.e., 4% can be detected using incomplete measurement, via physical domain system identification (Koh and Perry, 2007). Among all the 45 tested combinations, 89% of them successfully identified very small damage of 4% over the maximum false damage.

While modal identification aims to extract modal parameters from the observations, typical identification in the physical domain is posed as an optimization problem. The objective function is usually defined using the output signals from a mathematical model and real measurement. The mathematical model can be represented by a first-order state-space model or a second-order dynamic model. Physical parameters to be estimated can be stiffness, mass or damping coefficient. Because the relationship between model response and parameters is nonlinear generally, even if the model itself is linear in the state and linear in the parameters (Eykhoff, 1974), the unknown physical parameters cannot be explicitly expressed in terms of the objective function. Therefore the unknown parameters cannot be obtained directly by solving algebra equations. Through the optimization procedure, the parameters are deemed to be identified when the model estimated responses are in good agreement with the observations. Classical methods to solve this optimization problem in physical domain can be classified into four major groups: filtering methods, least squares method, the Bayesian method, and gradient search methods.

1.2.1.7 Filtering Methods

These methods are based on state estimation theory, and minimization is achieved by implicitly solving an initial value problem (Beck, 1979). A common feature of these methods is that they process the data sequentially and produce sequential estimates of both the parameters and the state. A typical drawback is that they give only an

approximation to the optimal estimates. The most popular filtering method used in system identification is Extended Kalman Filter (EKF), a general method applied in the field of modern control engineering. In the mathematical model, system dynamic motion is expressed as the first-order state space equation. State and observation equations are formulated and solved by the method of Extended Kalman Filter (EKF), and it is applicable in system identification by incorporating the system parameters to be identified as part of an augmented state vector. If the measured data at a number of locations are given and used in the observation vector, the EKF method can be applied to estimate the physical parameters of real systems as well as provide for uncertainty in the system model. Two main steps in EKF method are the update of state variables in time on basis of the system equations and the update of state variables based on measurements.

Application of EKF method for structural identification has attracted considerable interest in the civil engineering community. Yun and Shinozuka (1980) employed two filtering algorithms, namely the Extended Kalman Filter (EKF) and the iterated linear filter-smoother, to identify the hydrodynamic coefficient matrices of an offshore structure subjected to wave forces. To obtain stable and convergent solutions, Hoshiya and Saito (1984) incorporated a weighted global iteration (WGI) procedure to EKF for identifying dynamic systems. By means of the EKF-WGI method, Loh and Tsaur (1988) identified an equivalent linear system, a bilinear hysteretic restoring system and a system with stiffness degradation effect. Koh *et al.* (1991) formulated state and observation equations in a substructural approach, and solved them by EKF-WGI method. Nevertheless, the initial guess has to be within the vicinity of actual solution in order to get fast and stable convergence. The EKF method was also found to produce inaccurate estimations when nonlinear events dealt with, such as degrading strength or softening in materials (Corigliano and Mariani, 2004).

To deal with the non-stationary and nonlinear process, the filtering methods developed in system identification also include Monte Carlo Filter (MCF), H-infinity filter,

and particle filter. The MCF method was first proposed by Kitagawa (1996). It was to recursively identify the conditional distribution function of the state variable when observations up to the present time step are given. Several applications of the method have been reported. Sato *et al.* (2000) adopted MCF method to identify dynamic characteristics of structure systems. Yoshida and Sato (2002) applied MCF to identify the stiffness and damping ratio of a 5-DOF system. However, as the number of DOFs increases, the computer time increases drastically. Tanaka and Sato (2004) improved the classical MCF by developing a relaxation procedure in the filtering process to reduce the computational effort. Besides the Monte Carlo filter, an adaptive H-infinite filter was proposed to identify structural system with non-stationary dynamic characteristics (Sato and Qi, 1998). In addition, a particle filter was developed as well to estimate the parameters and Bayesian state via highly nonlinear models with non-Gaussian uncertainties (Ching *et al.*, 2006).

1.2.1.8 Least Squares Method

Least squares method is a classical strategy to find solutions for over-determined systems, usually interpreted as a method of fitting data. Evaluating the residual difference between the observed measurement and the value given by the model, the best candidate is estimated as the sum of squared residuals reaches the least value. In the application in structural identification, as long as enough measurement is available, the equation of motion can be transformed into an algebraic equation. The unknown damping and stiffness coefficients are identified by solving the algebraic equation. Due to the conciseness and ease of formulation, it has been applied often to identify physical structural systems. Caravani *et al.* (1977) developed a recursive least squares method in time domain identification, with an assumption that the number of acceleration measurements is equal to the number of DOFs. Agbabian *et al.* (1991) developed a least squares formulation to detect structural change by the identified stiffness and damping coefficient. Wang

and Haldar (1997) adopted the least squares and EKF method to identify structural parameters with unknown excitations. Loh *et al.* (2000) used a recursive least squares formulation to identify time-variant structures. Yang and Huang (2007) developed a sequential nonlinear least squares method to detect structure damage with unknown input and unknown output. However, the least squares method usually demands good initial guess and large computational burden in matrix inversion.

1.2.1.9 Bayesian Method

A general Bayesian statistical framework for system identification was presented by Beck and Katafygiotis (1998). Within the framework, probability models were established accounting for the parameter uncertainty and prediction uncertainty. Formulating the weighted probability models in the form of the initial predictive probability density function (PDF), Bayes' theorem was then applied to update the predictive PDF. However, the initial predictive PDF for the system output was usually a multidimensional integral which cannot be evaluated analytically or numerically. This difficulty was overcome by an asymptotic approximation. Globally maximizing the asymptotic approximation of the probability integral, the optimal structural parameter was then determined if the system was globally identifiable.

A significant characteristic of system identification using Bayesian statistical framework is that it can handle uncertainties such as modeling errors and non-uniqueness. Owing to these advantages, it has been implemented extensively in structural damage detection as well as structural health monitoring. Sohn and Law (2000) applied Bayesian approach to predict the location of plastic hinge deformation on a bridge column via dynamic experimental data. Vanik *et al.* (2000) simulated an on-line monitoring by a sequence of identified modal parameter to compute the updated probability of damage of structures. Yuen and Katafygiotis (2001) estimated the modal parameters and their uncertainties using only one set of ambient data. Yuen *et al.* (2004) combined the modal

identification and Bayesian system identification in a two-stage approach in damage detection of benchmark problem. It enabled the estimation of stiffness parameters as well as the probability that damage in any structural members that exceeded some specified threshold expressed in terms of a fractional stiffness loss. However, the application of Bayesian philosophy is confined to small scale identification problems. There were attempts by substructure concept to carry out on large scale identification, and the results were encouraging in terms of 5% measurement noise (Yuen and Katafygiotis, 2006).

1.2.1.10 Gradient Search Method

Some researchers have tried to tackle structural identification problems by gradient search methods, i.e., Gauss-Newton least squares (Bicanic and Chen, 1997; Chen and Bicanic, 2000) and Newton's method (Liu and Chen, 2002; Lee, 2009). However, they were often proved to be unsuccessful in the presence of noise (Liu and Chen, 2002), and also have other drawbacks such as requiring good initial guess and additional gradient information. More importantly, these classical methods commonly lack global search capability and tend to converge prematurely to local optima.

1.2.2 Non-classical Methods

Non-classical methods do not have rigorous mathematical formulations and are usually optimization methods established on heuristic rules such as natural evolution and self-organization. Typical strength of non-classical methods in structural identification is that they are more robust in achieving global optimum than classical methods. Furthermore they do not require good initial guess unlike many classical methods. The application of non-classical methods in structural identification is increasingly favored due to the rapid advancement in computer power. Owing to extensive applications in the inverse problems, two most commonly used non-classical methods are covered here, namely artificial neural network (ANN) and genetic algorithm (GA). Recently, other non-classical

methods have also been studied but marginal progresses have also been reported. For example, evolutionary strategy was studied to identify 3-DOF and 10-DOF lumped systems (Franco *et al.*, 2004). Simulated annealing was combined with genetic algorithm to detect damage of beam structures via static displacement and natural frequencies (He and Hwang, 2006). Particle swarm optimization (PSO) was used for structural identification due to its simple concept and quick convergence (Tang *et al.*, 2007). PSO coupled with simplex algorithm was found to perform better than simulated annealing and basic PSO in damage identification using frequency domain data (Begambre and Laier, 2009). The differential evolution strategy was investigated for identifying physical parameters in time domain (Tang *et al.*, 2008).

1.2.2.1 Artificial Neural Network

The working principle of neural network applied to computational structure is derived from the study of biological neurons (Haykin, 1994; Bishop, 1995). Fundamental elements in neural network are the linear/nonlinear neurons. They have multiple inputs and a single output. Neurons in different layers are connected through weighted links. A key characteristics of neural networks is the capability of self-organization or knowledge "learning". The capability allows automatic determination of the weights from the data containing the knowledge to be extracted. The process is often called training and implemented by adjusting the network neuron weights until output of network matches the target output within a provided tolerance. In the context of structural identification, the "learning" property of neural network makes it possible by avoiding comprehensive inverse analysis, where unknown parameters or damaged region can be recognized from given measurements by self-organization. Several properties of neural networks make them attractive to practical application. The algorithm can remain robust in the presence of noise and even complex nonlinearity. More importantly, no specific mathematical models are involved to define the relationship of input and output. This marvelous

capacity can even produce a sensible response from previously unseen data.

In the light of the above-mentioned advantages, many researches have applied artificial neural networks in civil engineering. Good review can be found in Flood and Kartam (1994a,b) and Adeli (2001). In structural identification, neural network was applied to process the non-parametric identification so that the responses are predicted by this unique mapping capacity instead of the physical model of the system (Chassiakos and Masri, 1996). Static load identification was carried out on aircraft wings using 11 inputs of strain responses and 11 outputs of concentrated load in each pattern and a total of 13 patterns were included (Cao *et al.*, 1998). Damage was identified by an iterative neural network with the introduction of orthogonal arrays (OA) to reduce the training data (Chang *et al.*, 2000). By initially establishing an emulator neural network to forecast the dynamic response in the forward analysis, a parametric evaluation neural network was used to identify a 5-degree of freedom lumped mass system. The 288 training patterns were chosen selectively from 0.6 to 1.0 times of the parameter to be identified (Xu *et al.*, 2004). In fact, artificial neural networks were anticipated to be more powerful to emulate higher level cognitive process rather than present simple I/O vector mapping problems in engineering (Flood, 2006). However, the sophisticated mapping capacity would be degenerated drastically as the number of unknowns increases in system identification. Much improvement is needed to handle the problems such as network size, network topology, selection of representative training patterns, as well as tedious training computation.

1.2.2.2 Genetic Algorithm

Genetic algorithm is known as an efficient global optimization method (Holland, 1975; Goldberg, 1989; Michalewicz, 1992). Based on the principle of "survival of the fittest", it imitates biological evolution by natural selection/reproduction, random crossover and mutation. The algorithm starts with an initial set of solutions, i.e., randomly generated population. In the population, each individual is termed as chromosome, representing a

set of trial parameters that define a possible solution to the problem. The priority of the chromosomes to breed is determined by their fitness from the objective function. Those with better fitness among the population are favored in the selection process. Employing specific selection criteria, such as roulette wheel, tournament, or rank selection, better chromosomes are given higher probabilities to be selected than worse chromosomes to reproduce new offspring through mutation and crossover.

Given its relative insensitivity to noise and initial guess, GA has good potential for solving inverse problems as structural identification. The procedure typically incorporates a forward analysis to evaluate fitness function and a backward analysis to search new possibilities. Generally, the mean-square error between the measured data and estimated response based on the mathematical model is used to define a fitness function. The best estimate for parameters is obtained when the error is minimized. Significant effort has been invested in the field of structural identification. The impact location of single load was identified using GA and the correlation of force reconstructions from the responses was defined as the fitness function (Doyle, 1994). The location and quantification of the extent of damage was performed by GA with the fitness function established in the forms of residual force vector (Mares and Surace, 1996). A GA-based structural damage detection strategy was proposed to identify the changes of characteristic properties in the structural member (Chou and Ghaboussi, 2001). GA was also used in the identification of moving masses on a multi-span beam by minimizing the errors between the measured and reconstructed accelerations (Jiang *et al.*, 2003).

However, most of the abovementioned references are concerned with simple structures with few degrees of freedom or few unknowns. Although using GA in structural identification is computationally intensive, particularly in the case of structures involving large numbers of DOFs or unknowns, it is still attractive as compared to many other methods because it allows the involvement of additional information or constraints as well as the use of parallel processing due to its high concurrency.

With the use of finite element methods in the forward analysis, increasing attention has been placed on identifying more complex and practical structures. To solve large scale problems, an efficient way is to use a divide-and-conquer method in the forward analysis. The computer time could be reduced in the forward analysis by conducting GA search in a much smaller modal domain instead of the usual physical domain (Koh *et al.*, 2000). Alternatively, by dividing the whole structure into smaller substructures, a novel concept of substructural identification was devised in the time domain (Koh *et al.*, 2003b). Subsequently a frequency domain substructure method was also developed under harmonic excitation (Koh and Shankar, 2003a,b).

Besides trying to reduce the computation cost in the forward analysis, it is imperative to improve the search capability of GA in the backward analysis. Recently considerable effort has been spent on the enhancement of identification strategies. It was proved that large time saving was possible by using distributed computing (Koh *et al.*, 2002). In a sequential programming, a search space reduction method (SSRM) was developed to accurately and reliably identify the structural systems (Perry *et al.*, 2006). The strategy adaptively adjusts the search space to expedite the search and incorporates a modified GA based on migration and artificial selection (MGAMAS). The SSRM method was applied successfully into the identification of the system as well as the input force using only limited output observations (Perry and Koh, 2008).

In addition to the modification of original GA architecture, research works in local searches also provide a promising way. The accuracy and robustness were greatly improved by embedding GA-compatible local searchers (Koh *et al.*, 2003a). However, they are in the inner loop of a general GA. The accuracy was achieved at the cost of computational time. Recently a Levenberg-Marquardt (LM) method local searcher was reported (Kishore Kumar *et al.*, 2007) to have good performance in identifying a 3-DOF nonlinear spring-damper system. It was shown that good accuracy was achieved by providing the initial guess using simple GA (SGA) runs. However, it might not be suitable for large

system identification because LM has to store the approximate Hessian matrix with $n \times n$ dimension and its expensive inversion has to be repeated. Besides, considerable preliminary SGA runs are needed to provide sufficiently good initial guess, especially for system with a large number of unknowns.

1.3 Objective and Scope

Substantial efforts have recently been devoted to the subject of structural health monitoring among researchers and practising engineers. The development of structural identification and damage detection gives birth to numerous classical and non-classical methods on this subject. Modal domain identification methods under the classical category have achieved significant advancement in the past decades. However, they do not work well in identifying small damages in local components of a complex system where robust identification of higher modes is required. while many time-domain classical methods, e.g. EKF, least squares method and gradient search methods, are sensitive to subtle changes in structures and used in identifying physical parameters via optimization, they unfortunately often suffer from the requirement of good initial guess and tend to have premature convergence due to the lack of global optimization capability.

In this study, to identify structural system physically, a non-classical method based on genetic algorithm is selected. The reasons are that GA inherently possesses global optimization capability and fairly loose requirement on initial guess, and is thus suitable for problems involving a large number of unknowns. More importantly, besides the potential in distributed computing, GA accommodates flexible modifications to achieve remarkable improvements in sequential programming. These strengths are unparalleled in many other methods.

Based on the literature review, key challenges in physical domain structural identification include: (1) better understanding of structural identification as an optimization

problem; (2) improvement on optimization method for identifying complex structures with large number of unknowns; (3) improvement on forward analysis for frequency domain substrucutral identification; and (4) experimental verification to verify the proposed identification strategy in presence of small damage and multiple damage with different magnitudes.

In view of the above key challenges, the main objective of this study is to develop a robust and efficient identification strategy for large-scale structural systems. To achieve this, research endeavor is taken in improving the convergence capability and reducing computer cost in both the backward analysis and forward analysis of the identification procedure. More specifically, the study covers the following scope:

(1) research on the characteristics of system identification when it is treated as an optimization problem;

(2) develop more efficient numerical optimization methods than recent published representative strategies in the backward analysis, based on the findings obtained in (1);

(3) investigate the performance of the proposed methods of (2) in substructural identification in both frequency domain and time domain; and

(4) validate the proposed methods of (2) and (3) in structural damage detection using experimental data.

It is hoped that the findings of this study will provide better understanding of structural identification as an optimization process. By virtue of these understanding, improvements on identification strategy will be intensively concentrated on sequential computing philosophy, allowing further extension to parallel computing for potential improvement. In this way, structural health monitoring can be carried out by structural identifications on practical engineering structures.

1.4 Organization of Thesis

The chapters of this study are arranged according to the development and application of the identification strategies.

In the first chapter, the mathematical models for dynamic system are summarized. After these representations for mathematical models, methods on structural identification are extensively presented in the literature review. They include classical and non-classical methods as well as their applications in modal domain and physical domain.

In Chapter 2, an improved search space reduction method (iSSRM) via sampling test is proposed. The method comprises an outer layer of sampling test and an inner layer of MGAMAS search. The sampling test is to determine a rough search space based on the first several samples. The MGAMAS search then finds the best candidate in the defined search space within limited evaluations. The search space is progressively scaled in the sampling test and a relaxation procedure. In addition, perturbation and jump-back procedures are developed to restore the search space from any possible deviation out of the real solution domain. Parametric study is carried out to propose suitable GA parameter for practical application.

Chapter 3 discovers the characteristics of structural identification as an optimization problem, leading to an efficient optimization strategy as uniformly sampled GA (namely, iSSRM) with gradient search. This chapter is motivated by the findings in Chapter 2 that an increasing fitness over generation does not necessarily indicate an improved identification. Therefore a fitness surface study is carried out on lower-order dynamic systems with concerns on the effect of measurement noise, data length and number of load cases. A noise induced "peak-shifting" is typically observed. That is, there is only one global peak which is surrounded by several local optima. The increase in noise level will introduce shifting and decrease of the global peak while local optima will seldom be produced. The observation results in the development of a uniformly sampled GA

with gradient search. Through the studies on the numerical examples, the Broyden-Fletcher-Goldfarb-Shanno (BFGS) method is recommended over the conjugate gradient (CG) method and simulated annealing (SA) method. The switch point between the global search and local search is given based on the studies on Chapter 2. The proposed identification strategy is then tested in the subsequent chapters.

In Chapter 4, the frequency domain substructural method (F-Sub) is extended to accommodate random excitation. Through introducing the exponential window method, the effect of initial condition is damped out within arbitrary data length. Therefore despite of the periodic assumption of discrete Fourier transform, the steady state formulation can be applied to non-periodic loading. An obvious advantage of using the exponential window is that it results in great reductions in computer time especially for lightly damped system, over the traditional strategy of zero padding.

In Chapter 5, the proposed hybrid identification strategy is studied at a substructural level in time domain, i.e., T-Sub method. The purpose is to verify the proposed strategy on the known mass identification as well as the unknown mass identification, which is rarely studied by other researchers.

Chapter 6 presents the performance of the proposed identification strategy using experimental data. The laboratory experiment is carried out statically and dynamically on a 7-level steel frame. Baseline identification is implemented using the iSSRM method, iSSRM with BFGS method in global identification, and T-Sub with iSSRM plus BFGS in substructural identification. The subsequent investigation embraces the damage from cut as well as stiffness increase due to welding. In the detection phrase, the T-Sub, F-Sub and global identification will be studied. Results will be compared to the recent studies.

The study is concluded in Chapter 7 with highlight of main findings and recommendations. The detailed results for Chapter 2 and 6 are provided in Appendices A and B, respectively.

CHAPTER 2

Uniformly Sampled Genetic Algorithms: An Improved SSRM

The identification strategy proposed in this chapter is a search space reduction method via Hammersley sequence sampling (Hammersley, 1960). It is a two-layer system identification strategy based on genetic algorithm. At the inner layer, candidates are explored within a search limit using MGAMAS, a modified GA based on migration and artificial selection (Perry *et al.*, 2006). At the outer layer, the search limit is defined by a set of Hammerley sequence samples. A relaxation procedure is incorporated to make the sampling driven search space reasonable. In addition, perturbation and jump-back procedures are also invoked when necessary to restore possible deviation from the real search limit.

To formulate the proposed identification strategy, the essential ideas of simple GA (SGA) and search space reduction method (SSRM) (Perry *et al.*, 2006) will be introduced. An improved SSRM (iSSRM) based on sampling test is then proposed. The purpose of sampling test is to obtain a rough contour of the fitness surface before GA search so as to define an appropriate search limit. Usually a uniform sampling is desired to have unbiased samples in the multi-dimensional solution space. Thus four possible sampling methods will be investigated, incorporating random uniform distribution, Latin hypercube, orthogonal array (OA), and Hammersley sequence. To compare these sampling

methods in conjunction with the iSSRM tests, stiffness identification is implemented numerically on 10-DOF and 20-DOF lumped mass systems. Based on this comparison, the sampling test that performs best in terms of robustness and accuracy of identification will be recommended. Finally, a comprehensive parametric study is carried out to study the trade off between exploration and exploitation, e.g. to determine the sizes of samples for sampling test, and generations, populations, as well as total runs for MGAMAS search.

2.1 System Identification Using Genetic Algorithms

Treating the identification of physical parameters as an optimization problem, traditionally referred as output-error issue (Bekey, 1970; Bowles and Straeter, 1972), the statement of problem can be written typically in terms of maximization as

$$\begin{aligned} &\max \phi(\mathbf{x}) \quad \text{subject to} \quad \mathbf{x} \in \mathbf{S}, \\ &\text{where} \quad \mathbf{S} = \left\{ \mathbf{x} \in \Re^k | a_i \leq x_i \leq b_i, \forall i = 1, 2, \cdots k \right\} \end{aligned} \tag{2.1}$$

Here ϕ is scalar-valued functions of the variables $\mathbf{x}$ to be identified, and $\mathbf{S}$ is the search space. The value of a_i and b_i are the lower bound and upper bound of the individual parameters set from an engineering viewpoint. In terms of global optimization, GA is a good candidate owing to its strengths in robustness with respect to measurement noise and initial guess, ease of adding constraints of optimization, and high concurrency for distributed computing. Using GA in structural identification, the idea can be illustrated in a block diagram in Fig. 2.1.

To control the computational cost, the convergence criterion is typically set as the achievement of maximum number of fitness evaluations. The fitness function is defined by the errors between the measured acceleration $\ddot{u}^m$ and estimated response $\ddot{u}^e$ from the mathematical model. They are responses collected from p measurements with q data length. In the literature, there are different definitions of fitness function on the basis of response errors. Nevertheless, the present study follows the simplest formulation as in

Eq. (2.2).

$$\phi = \frac{1}{c + \sum_{i=1}^{p} \sum_{j=1}^{q} (\ddot{u}_{ij}^{m} - \ddot{u}_{ij}^{e})^2} \tag{2.2}$$

In Eq. (2.2), c is a constant that plays an important role in measuring fitness. It helps to set clear upper boundary in the best fitness on one hand and avoids a potential zero denominator on the other hand. The value of c is better chosen to have the similar magnitude as the error term. As the constant c will take 0.001 in this study, the best fitness is then 1,000 within the limit of computer tolerance. The system is deemed as identified when the estimated output $\ddot{u}^e$ agrees with the measured response $\ddot{u}^m$, resulting in the best estimate of parameters that maximizes the fitness function within the total evaluations.

The identifiability of the system is implicitly based on the assumption that unique mapping is available between the measurement and the unknown parameters. Although few researchers provide rigorous proof on the identification uniqueness, it is reasonable to avoid non-uniqueness by putting the measurement location as sufficient and distributed as possible, based on the available results of limited research works (Udwadia and Sharma, 1978; Udwadia, 1985; Franco *et al.*, 2006). In the present study, the second assumption is that the mathematical model used in the forward analysis can capture the physical behavior of the structures. Thus the modeling error is neglected. This means that good understanding and modeling of the structural behavior is important.

In the following sections, the original idea of GA will be introduced. Focusing on the GA application in structural identification, a recent research on the improvement of GA, i.e., the SSRM method will be reviewed. Then a more advanced version of SSRM, iSSRM, will be presented on the basis of uniform sampling tests.

2.2 Simple GA

The beginning of genetic algorithms can be traced back to the early 1950s when several biologists and computer scientists used computers for simulations of biological systems. Nevertheless, the work of developing evolution-inspired algorithms in 1950s drew limited attentions that evolutionary computation, i.e., evolution strategies, evolutionary programming, and genetic algorithms, has ever seen (Box, 1957; Friedman, 1959). In the 1960s, the field of evolutionary computation remained an active area of research. Rechenberg (1965) introduced "evolution strategies" to optimize real-valued parameters for devices such as airfoils. The program structure was fixed and primarily search operator such as mutation and selection allowed the solution to evolve. Fogel *et al.* (1966) developed "evolutionary programming", where the evolutionary computing was implemented with no fixed structure. Candidate solutions to given tasks were represented as finite-state machines and the evolutionary operators are selection and mutation. Furthermore, the work done in late 1960s and early 1970s at the University of Michigan under the direction of John Holland led to GAs as they are known today. A genetic algorithm is an adaptation procedure based on the mechanics of natural genetics and natural selection, including two fundamental components as survival-of-the-fittest and variation (Holland, 1975; Goldberg, 1989). However, Holland was the first to attempt to put computational evolution on a firm theoretical basis (Mitchell, 1996). More importantly, Holland's introduction of a population-based algorithm with crossover, inversion, and mutation provided better variation than Rechenberg's evolutionary strategies (Rechenberg, 1965) and Fogel, Owens, and Walsh's evolutionary programming (Fogel *et al.*, 1966) .

The classical concept of GA is well established in a simple genetic algorithm (SGA). In SGA, the initial population is randomly generated, with each chromosome representing a possible solution to the target optimization problem. Based on a user-defined fitness function, the performance of each chromosome is evaluated in the population.

Subsequently, a set of simple operations inspired by biological evolution are repetitively implemented to generate a new population for the next generation. The main operations of SGA include reproduction, crossover and mutation. In the evolution of a generation level, user-defined criterion of reproduction allows the fitter chromosomes in the population higher chance to produce new offspring. Crossover by recombination makes it possible for the heuristically offspring to inherit the strengths of "fitter" chromosomes in the past generations. Furthermore, mutation facilitates the achievement of population diversity through generating offspring with distinct characteristics. The probability of crossover and mutation operations in a population depends on the crossover and mutation rates, which are defined as the ratios of the chosen chromosomes out of the population size. These three SGA operations are repeated in the old population until a new population of the same size of n_p is formulated. By this generic way, the solution space is explored generation after generation. After some sufficient number of generations or when no significant improvement is observed, the best chromosome is deemed to represent the optimal solution.

Without any loss of generality, the heuristic procedure of SGA can be explained by a maximization problem. Suppose we wish to maximize a function of k variables, $\phi(x_1, \cdots x_k) : \Re^k \rightarrow \Re$. Suppose further that each variable x_i can take values from a domain $\mathbf{S}_i = [a_i, b_i] \subseteq \Re$, and $\phi(x_1, \cdots x_k) > 0$ for all $x_i \in \mathbf{S}_i$. Now, one element in each chromosome is represented by a real number, for example, $x_i \in [a_i, b_i]$. To initialize a population, a total number of n_p chromosomes are randomly set before standard GA operations. The critical stages of the algorithm are reproduction, crossover and mutation.

2.2.1 Reproduction

Reproduction, also referred to as selection, is an operator to simulate the natural selection. Through this process, individual strings are copied according to their fitness. The chromosomes with higher fitness have a higher probability of contributing one or more

offspring in the next generation. Once selected, the chromosome is then entered into a "breeding" pool which is a tentative new population for further genetic operator action. The reproduction can be carried out in a number of ways. A simple way for SGA is to carry out reproduction by a roulette wheel method. The selection process is explained in the following steps.

- Calculate the fitness value for each chromosome $v_i(x_1, x_2, \cdots x_k)$ where $i = 1, \cdots, n_p$ assuming the fitness values are positive. The value n_p determines the population size. The fitness for a chromosome is $\phi(v_i)$.

- Find the total fitness of the population F_{sum}

$$F_{sum} = \sum_{i=1}^{n_p} \phi(v_i) \tag{2.3}$$

- Calculate the probability of a selection p_i for each chromosome $v_i(i = 1, \cdots, n_p)$

$$p_i = \phi(v_i)/F_{sum} \tag{2.4}$$

- Calculate a cumulative probability q_i for each chromosome $v_i(i = 1, \cdots, n_p)$

$$q_i = \sum_{j=1}^{i} p_j \tag{2.5}$$

- Generate a random (float) number r from the range [0,1]

- If $r < q_1$, then select the first chromosome v_1; otherwise select the i-th chromosome $v_i(2 \leq i \leq n_p)$ such that $q_{i-1} < r \leq q_i$

The procedure of roulette wheel selection shows that each individual is assigned a selection probability proportional to its fitness. The selection is made with replacement until the new population is full. Through this procedure, multiple selections of fitter individuals are encouraged while the weakest individuals are filtered out.

2.2.2 Crossover

Crossover is to exchange information or to cause the juxtaposition of different chromosomes that have good performance in the past generations. In the operation, new offspring are produced by recombination of the selected parents from the tentatively formed new population by reproduction. Strengths of the past are thus transferred through this heuristic swapping. Therefore crossover is a one of the most critical GA operations to exploit the solution space.

A simple crossover is used in SGA to facilitate the recombination operation. By the principle of simple crossover, the information before and after a randomly selected breakpoint of a parent pair are swapped. To carry out crossover operation in SGA, one of the critical parameters in a genetic system needed is probability of crossover p_c. This probability gives the expected number $p_c \times n_p$ of chromosomes which undergo the crossover operation in the new population. The procedure can be demonstrated as below.

- Generate a random (float) number r from the range [0,1]
- If $r < p_c$, select the given chromosome for crossover, an integer position j along the string is then selected uniformly at random between 1 and the string length minus one, i.e., $[1, l-1]$. Two new chromosomes are created by swapping all elements before and after the split point j . For example, consider chromosomes v_1 and v_2, the new resulting offspring after simple crossover are $v_1{}'$, and $v_2{}'$

$$\begin{array}{l} v_1 = (x_1, x_2, \cdots x_{j-1}, x_j, x_{j+1}, \cdots x_k) \\ v_2 = (y_1, y_2, \cdots y_{j-1}, y_j, y_{j+1}, \cdots y_k) \end{array} \rightarrow \begin{array}{l} v_1{}' = (x_1, x_2, \cdots x_{j-1}, x_j, y_{j+1}, \cdots y_k) \\ v_2{}' = (y_1, y_2, \cdots y_{j-1}, y_j, x_{j+1}, \cdots x_k) \end{array} \tag{2.6}$$

2.2.3 Mutation

Although crossover effectively searches via exploiting the extant best strings, they may lose some potentially useful genetic material in exploring the solution space. The reason is

that crossover operator simply recombines information which already exists, while cannot explore the solution space that are not covered by the current population. To introduce diversity and avoid a prematurely homogeneous population, mutation is necessary in the artificial genetics to protect against such an irrecoverable loss. This operator, in fact, plays a secondary role in the operation of genetic algorithms. Once a chromosome is chosen to mutate, the mutation operator in SGA is simply implemented by random alteration of the value in a string position.

In order to mutate in the mating pool, another parameter of the genetic system, probability of mutation p_m, gives the expected number $p_m \times n_p$ of chromosomes which undergo the mutation operation in the new population. The mutation in SGA is given as follows.

- Generate a random (float) number r from the range $[0, 1]$
- If $r < p_m$, mutate the chromosomes: In SGA, mutation works to change a specific variable by random walking throughout the whole string. If the original string is marked as v, the mutated one will be processed to be $v^{'}$ as below.

$$v = (x_1, x_2, \cdots x_{j-1}, x_j, x_{j+1}, \cdots x_k) \rightarrow v^{'} = (x_1, x_2, \cdots x_{j-1}, x_j^{'}, x_{j+1}, \cdots x_k) \quad (2.7)$$

Each element within the chromosome has the same chance of undergoing the mutative process. The mutated element $x_j^{'}$ is actually a random value from the domain of the corresponding parameter domain $[a_j, b_j]$. After selection, crossover, and mutation, a new population is ready for the next evaluation. This evaluation is used to build the probability distribution for the next selection process. The rest of the evaluation is cyclic repetition of the above steps. To sum up the philosophy of SGA, a flowchart is shown in Fig. 2.2.

It is obvious that the occurrence of crossover and mutation is dependent on the ratios as p_c and p_m. They determine the so-called "EE" tradeoff between exploitation

and exploration in GAs. For example, small values of these breeding ratios lead to small scale exploration around the current solution and tend to protect the heuristics from being destroyed. Large values of these ratios produce larger scatter of new solutions and explore more new areas are searched but at the expense of possibly losing the good strength from the past generations. Nevertheless, a good performance in SGA is attainable by adopting a high crossover probability prevailing in the space search, an occasionally active mutation with small probability. At the same time, the population size should be kept in a moderate scale. By this guideline of choosing GA parameters (Goldberg, 1989), the diversity and convergence in the evolution can be reasonably optimized in the "EE" tradeoff.

Besides the crucial operators demonstrated above, representation of the chromosomes is another key issue in genetic algorithm. The representation scheme can severely limit the window by which the system observes its world. There are many ways of encoding in GAs such as binary encoding, tree encoding, including the real representations adopted in this study (Mitchell, 1996). The success of some coding is largely problem dependent. For example, a problem involving simple on/off control is ideally suited to binary coding. When applying to real world, the binary string may have inherent problems as "hamming cliffs" that will have difficulties in continuously representing the real numbers. For example, the value of 15 is represented as 01111 in binary encoding, but for GA operation to have a value of 16 requires change of all the bits to achieve the string as 10000. For this reason, real representation is preferred in this study as it can represent the parameters itself directly and is applicable to meet general purposes.

Many variants of GA can be formulated for a given problem. Such variants may differ in many ways, i.e., methods for creating an initial population, genetic operators for transforming individuals, and parameters such as population size, breeding ratios (possibilities of applying different operators). However, they share a common principle: a population of individuals undergoes some transformations, and during this evolution

process the individuals strive for survival. Good review of the transformation mechanisms as mutation and crossover, the balance of exploration and exploitation, as well as application can be found in Goldberg (1989) and Michalewicz (1992).

2.3 Search Space Reduction for Genetic Algorithm

The application of GA in structural identification began in early 1990s for relatively simple problems (Yao *et al.*, 1993; Doyle, 1994). It was introduced in identifying physical parameters, i.e., stiffness, damping, and mass of larger structural systems, in 2000s (Koh *et al.*, 2000, 2002, 2003a; Perry *et al.*, 2006; Koh and Htun, 2004). In these research works, GA has been investigated in direct application, distributed computing, GA-compatible local searcher, architectural modification, and GA-associated identification uncertainty. To tap the full potential and versatility of GAs in large-scale structural health monitoring, the major task is to improve the search capability. The most recent improvement of sequential GA in physical domain identification is the SSRM method, with versatile applications in structural identification, damage detection, and offshore applications (Perry, 2006). The success of SSRM motivates its concept demonstration in this section and further advancement in the following section.

Treating the physical domain identification as optimization problems, the solution space is substantially huge and incorporates local optima and global optima. For stochastic optimization methods like GA, there is no specifically defined search direction unlike in gradient-based methods. The operation mechanisms have to be specially devised for exploiting good solutions available and exploring in the search space for new solutions. In SGA, this tradeoff is expected to reach a balance within each generation by selecting suitable crossover rate and mutation rate. However, the solution space explored in one run is limited since there is only one set of such probability based ratios in SGA. To explore as much as possible in the solution domain, the evolution via single population in SGA is improved by using MGAMAS algorithm (Perry *et al.*, 2006). The basic concept is

to use multiple species instead of only a single of them. One of the species is used mainly to keep the best solutions while the others are used to search for new solutions. Different mutation and crossover strategies are used in the breeding species in order to enhance the search diversity. Furthermore, it is desirable that the computational effort could be adaptively focused on more new dimensions in the exploration process when some of the parameters have converged. This is achieved by an outer SSRM loop. Through several preliminary MGAMAS runs, the mean μ_i^h and standard deviation σ_i^h of the identified parameters were computed. Therefore the new search space is defined, i.e., Eq. (2.8)

$$\begin{cases} \widehat{a}_i^h = \mu_i^h - w \times \sigma_i^h \\ \widehat{b}_i^h = \mu_i^h + w \times \sigma_i^h \end{cases} \qquad (i = 1, 2 \cdots k) \tag{2.8}$$

where $\widehat{a}_i^h$ and $\widehat{b}_i^h$ are the lower and upper boundaries of the current SSRM search limit. The value w defines the window size, k is the number of variables and h represents the present run. The ideas of MGAMAS and SSRM are illustrated as Fig. 2.3 and Fig. 2.4, respectively. Convergence history is traced by the mean μ_i^h and standard deviation σ_i^h of the parameters. At the later runs of SSRM, the standard deviation tends to decrease as the corresponding parameter is in convergence. Then the search limit of the parameter reduces accordingly. The scale of search limit reduction is governed by the window size w (Perry *et al.*, 2006). To sum up, SSRM works by reducing the search space for those parameters that converge quickly. Computer time will not then be spent on exploring the area far away from the optimal solution. Instead, the computational effort is expected to be saved by attempting to focus on the more promising solution space.

2.4 Improved SSRM by Sampling Test

A drawback of SSRM is that the search space reduction is not activated right from the beginning. Several initial MGAMAS runs are necessary to make the means and standard deviation statistically meaningful. Hence, using SSRM too early may result in "jump out", i.e., the scaled search space is out of the real solution domain. Nevertheless, these

initial MGAMAS runs cost up to 30% to 40% of total fitness evaluations (Perry *et al.*, 2006). Furthermore, the initial population may not cover the search space as uniform as it could, for example, by some sampling method. In this section, an enhanced way is proposed to sample in the search space and the search limits are then defined according to the fitness of the samples. At the same time, the original way of defining search space by SSRM is retained as a fall back, in case that sampling method provides an inappropriate search limit. The following sections present a rational way to take samples in the search space.

2.4.1 Sampling Methods

As a multi-dimensional optimization problem, the identification of multi-DOF (MDOF) system involves a huge solution space. Sampling in a grid manner is impractical as computational effort will increase exponentially with the identification dimensions. For example, with k parameters and s points per parameter, a total of s^k fitness evaluations are required. An increase in grid density will of course provide more information of fitness surface. However, it will also pose an expensive demand on computer time. Therefore, an economical way to take samples is desired, as it is better to conduct small scale logical sampling experiments for hyper plane search. These samples could be much more sparse than the s^k sampling manner, but remains as uniform as well in the solution space. In the present study, four sampling methods will be investigated, incorporating orthogonal arrays (OA) (Hedayat *et al.*, 1999), randomly uniform distribution, Latin hypercube (McKay *et al.*, 1979), and Hammersley sequence (Hammersley, 1960). Typical distributions of these four sampling methods are given in Fig. 2.5 for comparison, and 289 samples are considered herein.

2.4.1.1 Random Uniform Distribution

Within the search limit, it is possible to make trials in the solution space by uniform samples. If originally sampled between 0 and 1, an element of the j-th trial sample $(x_1, \cdots, x_i, \cdots, x_k)_j$, $(j = 1, 2, \cdots n)$ in the new search space is

$$x_i = \widehat{a}_i^h + U(0,1) \times (\widehat{b}_i^h - \widehat{a}_i^h) \tag{2.9}$$

where $U(0,1)$ stands for uniform probability distribution. The samples are randomly generated using pseudo random numbers. They can be shown to pass standard statistical tests for randomness like a Kolmogorov-Smirnov test.

2.4.1.2 Latin Hypercube

Latin hypercube was introduced by McKay *et al.* (1979) to study the output distribution of computer program by selecting random input variables. This technique is often applied in uncertainty analysis. Through Latin hypercube sampling, one will find that there is only one sample in each row and each column of a square grid. The idea is that Latin hypercube sampling subdivides the unit cube into N intervals along each dimension. Then the samples are chosen randomly such that each interval contains exactly one point. Latin hypercube sampling is generally not quasi-random in the sense of minimizing discrepancy as the Hammersley sequence later. This could be attributed to the restrictions to the placement of Latin hypercube samples. However, the stratified random sampling procedure by Latin Hypercube can also reproduce the uniformity via sparse samples, instead of in an s^k sampling manner. Thus it is a cost-effective way to exploring the solution space by Latin Hypercube sampling based on Eq. (2.9).

2.4.1.3 Orthogonal Array (OA)

Orthogonal arrays were originally proposed in statistics (Rao, 1947). They are now often referred to as Taguchi method (Taguchi *et al.*, 2004), widely applied in medicine,

manufacturing and quality engineering in the planning of experiments. The purpose is to examine that how changes in the levels of various factors affect a response variable of interest. This is a typical issue of k factor with s levels, conventionally solved through a full factorial experimental design. OA samples are essentially selected out of these full factorial combinations, but OA reduces the experimental trials drastically. For an experiment with k variables at s different settings, a full factorial experiment would require s^k experiments. By OA, this number reduces to $k(s-1)+r(s-1)(s-1)+1$ and r is the number of potential interaction among the variables (Besterfield *et al.*, 1995). Actually orthogonal array is a type of experiment, by which the independent variables are statistically "orthogonal". The samples generated by OAs will be uncorrelated to one another in a statistical manner.

Typically OA is represented as $OA(n, k, s, t)$. The number of rows n is the array size and measures the number of samples. The value of k defines the number of factors or variables. The value of s actually represents the number of levels that has been evenly divided along one variable dimension of a solution. The value t is the strength of OAs, which is the number of columns that all the paired possibilities can be seen an equal number of times. When OAs are applied to sample in the search space for system identification, n represents the total number of samples and k is the number of unknown parameters to be identified. Thus, a typical variable x_i in the sample $(x_1, \cdots, x_i, \cdots, x_k)_j,\ \ j = 1, 2, \cdots n$ in terms of OA is expressed in Eq. (2.10), where m_{OA} is one of the items in a row of OAs.

$$x_i = \widehat{a}_i^h + \frac{m_{OA}-1}{s-1} \times (\widehat{b}_i^h - \widehat{a}_i^h) \qquad i = 1, 2, \cdots k;\ \ m_{OA} \in [1, s] \tag{2.10}$$

Specific values of n, k, s, and t are not continuously varied by themselves as they depend on the way to construct OAs. There are a number of techniques for constructing OAs (Hedayat *et al.*, 1999). Generally, the larger the desired strength, the harder it is to construct the array. It may not be easy to find exact OAs suitable for a particular identification. However, the following property of OAs (Hedayat *et al.*, 1999) makes the application more flexible: any $n \times k'$ subarray of an $OA(n, k, s, t)$ is an $OA(n, k', s, t')$,

where $t' = \min(k', t)$. The significance of OAs is to have as much as information of fitness surface but uses the smallest number of samples. Therefore, the computational cost of sampling is reduced.

2.4.1.4 Hammerley Sequence

Hammersley sequence sampling can also provide uniform samples of search space. It is part of the quasi-Monte Carlo methods or low-discrepancy sampling family, which are originally used to calculate multi-dimensional integrals without a closed-form solution. "Quasi" here means a sampling approach that employs a strictly deterministic algorithm to generate samples in an n-dimensional space. "Discrepancy" refers to a quantitative measure of how much the distribution of samples deviates from an ideal uniform distribution. Unlike the pseudo random sequences, quasi-random sequences fail many statistical tests for randomness. However, these random number generators seek to produce highly uniform samples of the unit hypercube. With new interpretation of $U(0, 1)$ in a Hammersley manner, Eq. (2.9) is applicable for sampling test via Hammersley sequence samples. The definition of Hammersley sequence, together with the way to establish the uniformity of points, is shown as follows. An arbitrary integer n can be written in radix-R notation

$$n \equiv n_m n_{m-1} \cdots n_2 n_1 n_0.0 = n_0 + n_1 R + n_2 R^2 + \cdots n_m R^m \tag{2.11}$$

where $m = [\log_R(n)] = [\ln(n)/\ln(R)]$, the square brakets [ ] extracts the integer part of the numbers inside. Then an inverse radix number, a unique fraction between 0 and 1, can be constructed by reversing the order of the digits of n. It is

$$\psi_R(n) = 0.n_0 n_1 n_2 \cdots n_m = n_0 R^{-1} + n_1 R^{-2} + n_2 R^{-3} + \cdots + n_m R^{-m-1} \tag{2.12}$$

The Hammersley points on a k-dimensional cube are

$$x_k(n) = [\ n/N, \quad \psi_{R_1}(n), \quad \psi_{R_2}(n), \quad \cdots \quad \psi_{R_{k-1}}(n)\ ] \tag{2.13}$$

where $n = 0,1, 2, \cdots, N-1$ and the values for $R_1, R_2, \cdots, R_{k-1}$ are the first $k-1$ prime numbers. For quasi-randomness, the integers R_i must be mutually prime. Because of

the way in which quasi-random sequences are generated, they may contain undesirable correlation for the higher coordinates of the sequence. This is significant in their initial segments and in the case of higher dimensions. In that case, the uniformity is strongly affected as the samples cannot uniformly cover the hyper plane any more. To alleviate this problem, leaping is adopted in this study (Kocis and Whiten, 1997). Setting a leap value to the next prime number larger than the largest prime base can help maintain uniformity when generating sample sets for high dimensions (Robinson and Atcitty, 1999).

The significance of these four sampling methods lies in that they can generate highly uniform samples in exploring the multi-dimensional solution space. This uniformity of samples, however, is achieved at a drastically reduced cost of fitness evaluations from the exponential manner of s^k to only a productive manner of sk. In summary, uniform samples can be randomly generated by random uniform distribution and Latin hypercube, while these samples can be produced as well in determinate ways by OA and Hammersley sequence. Furthermore, the number of variables via OA in Eq. (2.10) is limited, i.e., only 33 by $OA(512, 33, 16, 2)$ with level s above 3 (Hedayat *et al.*, 1999). The limitation, however, is not applicable for the other three sampling methods, as which have no construction difficulty like OA.

2.4.2 Relaxation, Perturbation and Jump-back: Treatment after Sampling

The philosophy of using sampling test to reduce search space is shown in Fig. 2.6. Sampling in the new search range, each variable limit is resized by the minimums and maximums of the first n_b best samples. However, convergence will be compromised if too large a value is selected for n_b. In this study, a rather small value, i.e., 5, is found to work well for the present investigation. To make the search limit defined by samples more efficient, relaxation, perturbation and jump-back procedures are necessarily constructed.

The purpose of relaxation is to revise the sampling-defined search space, and ensure

that the next exploration will start from the neighborhood of the present best solution. As sampling test will work before each MGAMAS run, the search space may be over reduced such that the rescaled space does not contain the real solution space. In order to alleviate this problem, the relaxation procedure is necessary to adjust the search space defined by the n_b samples. It requires that the newly found best solutions via MGAMAS should be covered by the larger radius of the present search range $[a_i^h, b_i^h]$, but should not exceed the most originally defined search range $[a_i^0, b_i^0]$. This is expressed as

$$\begin{cases} a_i^{h+1} = \max[x_i^h - |x_i^h - b_i^h|, a_i^0], & if \quad |x_i^h - a_i^h| < |x_i^h - b_i^h| \\ b_i^{h+1} = \min[x_i^h + |x_i^h - a_i^h|, b_i^0], & if \quad |x_i^h - a_i^h| > |x_i^h - b_i^h| \end{cases} \quad (i = 1, 2 \cdots k) \tag{2.14}$$

where h represents the current number of runs, x_i^h is one of the variables in the current best solution $(x_1^h, \cdots, x_i^h, \cdots, x_k^h)$. $[a_i^{h+1}, b_i^{h+1}]$ is the search space for the next sampling. Using this relaxation procedure, the balance is considerably improved between reducing the search space and ensuring the solution is within the new space.

On the other hand, if the mean fitness of n_b best samples is not improved, the search space defined by samples may risk overshooting and missing the proper search space. Therefore a restoring mechanism is expected to recover the search limit, which leads to the proposed perturbation procedure and jump-back procedure.

The purpose of perturbation is to discover the best candidate by a decoupled SSRM search. This automatic correction of search limits is essential in exploring the parameter space. The perturbation procedure requires running the current MGAMAS loop in an independent search limit defined by SSRM rather than those defined by samples. The search space is described in Eq. (2.8). The mean and variance are based on all the best chromosomes up to the present run. In fact, the SSRM is able to restore the search range to a reasonable limit, even if misled by the search limit defined by sampling test. The reason is that SSRM-defined search space provides a robust alternative by tracing the mean and standard deviation of the best parameter in each run. The standard deviation

provides an indication of the convergence uncertainty of the identified parameter and the search space can be adjusted accordingly. If sufficient runs are carried out, the statistically defined search limit will become significant as it can always suggest a promising area containing optimal solution. More importantly, this SSRM-defined search space requires no additional evaluation of fitness function.

If perturbation is activated, a jump-back procedure is then followed to make the next run start from one of the previous search ranges. The historical search range of each run has been recorded as the program goes. This is shown in Fig. 2.6. Because the best candidate explored by SSRM in the perturbation procedure suppose to be inside the search limit, the current range will keep jumping back until it covers the newly found best solution. Finally, the jump back procedure will keep the search range as $[a_i^{h-l}, b_i^{h-l}]$, which satisfies

$$x_i^h \in [a_i^{h-l}, b_i^{h-l}] \qquad (i = 1, 2 \cdots k) \tag{2.15}$$

where $l \in [1, h]$, denotes the number of runs that has jumped back to satisfy Eq. (2.15). When the jump-back is finished, it will step into the usual relaxation procedure. Then a new search space is modified by Eq. (2.14) on basis of the jumped search range $[a_i^{h-l}, b_i^{h-l}]$. That is

$$\begin{cases} a_i^{h+1} = \max[x_i^h - |x_i^h - b_i^{h-l}|, a_i^0], & if \quad |x_i^h - a_i^{h-l}| < |x_i^h - b_i^{h-l}| \\ b_i^{h+1} = \min[x_i^h + |x_i^h - a_i^{h-l}|, b_i^0], & if \quad |x_i^h - a_i^{h-l}| > |x_i^h - b_i^{h-l}| \end{cases} \quad (i = 1, 2 \cdots k) \tag{2.16}$$

It is noted that the search space will be reset in three cases including sampling test, relaxation and jump-back procedures. The relaxation will be active regardless of the activation of perturbation procedure, and helps much if over-reduction is discovered by the samples. However, jump-back will not work if there is no perturbation, as the search space defined by the samples proves to be capable of producing progressive improvement with better solutions. Using these search space resizing processes, the balance could be considerably improved between the reduction of search space and ensuring a new search

space that incorporates the optima.

In summary, the proposed iSSRM method with sampling test carries out an inner MGAMAS loop and an outer sampling exploration. The inner MGAMAS is to find the best solution in each run, which is set as the center of new search limit. The outer sampling test is to define a radius of the search limit for the next run. Whether a new search limit defined in this way contains the real solution is judged by the improvement of the measure of mean fitness value of the first n_b samples. If the measure is not improved compared to the previous sampling run, a wrong search limit is implied. In order to restore the search limit, changes are proposed to conduct in redefining the center and radius of search in this study. The center, i.e., the best solution, is to be determined by a perturbation procedure via SSRM search. The radius is, however, enlarged by the jump-back and relaxation procedures.

2.5 Numerical Examples

To test the four sampling methods for the proposed sampling based SSRM, two examples are investigated including lumped mass systems (Perry *et al.*, 2006) of 10 degree-of-freedom (DOF) and 20-DOF. As a result of random excitations, accelerations are generated by constant-average-acceleration Newmark method. Rayleigh damping of 2% is set equally for the first two modes. The search space is typically set as from 0.5 to 2.0. That is, the lower and upper bounds are set to be half and twice of the actual values. In the identification, the mass distribution of the structures is assumed as known while the stiffness distribution and two Rayleigh damping coefficient are to be identified. Both the input and output are assumed to be contaminated by Gaussian white noise with zero mean and variance of one. The noise levels considered are 0%, 5%, and 10%. GA parameters recommended by Perry (2006) will be used both for SSRM and iSSRM methods herein, which are given in Tables 2.1 and 2.2. These parameters will be studied for iSSRM until the best sampling method is suggested from this investigation. The sample size adopted

in this study differs with examples. To comply with the ease of constructing, especially OAs, we use 289 samples for 10-DOF system and 512 samples for 20-DOF system. Especially, orthogonal arrays used in this study are $OA(289, 12, 17, 2)$ and $OA(512, 22, 16, 2)$, respectively. They are extracted from $OA(289, 18, 17, 2)$ and $OA(512, 33, 16, 2)$. To avoid possible bias reporting, the input forces and noise pattern are freshly generated for each run. The results reported in the following sections are the average from 25 runs, except for Fig. 2.10 which is a typical result from one run. Total fitness evaluations are 5,000 for 10-DOF system with 12 unknowns and 10,000 for 20-DOF with 22 unknowns.

As shown in Fig. 2.7 and 2.8 which are free of noise, convergence histories of fitness and mean error consistently prove that the iSSRM via sampling test is much better that original SSRM and SGA. For a given 5,000 fitness evaluations, the identified results by iSSRM via sampling provides the highest fitness. It identifies almost exact values, corresponding to fitness equals to 1,000 in the 10-DOF system. In the mean error plot, the sudden drop around 0.4 normalized evaluation of SSRM is reasonable, as 4 out of total 10 runs are used for calculating mean and standard deviation in Eq. (2.8). The mean error plot also shows that SGA converges rather slowly in almost 80% evaluations. The reason is that GA has to search new possibilities in the same $[0.5, 2.0]$ range in each generation. However, both SSRM and iSSRM reduce the search space in each run. The fitness evaluations are then strategically allocated for the most worthy solution space. Typically, the mean errors of identified stiffness by iSSRM via sampling test are less than 1% at the end of 5,000 fitness evaluations.

Fig. 2.9 illustrates that consistent improvements are achieved by the iSSRM methods in the presence of 0%, 5%, and 10% noise. It is noted that the present comparison is based on the recommended parameters for SSRM. As the sampling test is introduced in iSSRM, balanced exploration and exploitation in original SSRM are necessary to be re-examined for iSSRM via a parametric study. Before an extensive parametric study for GA parameters, however, a scalable sampling method has to be suggested for iSSRM.

This is different from a previous study (Zhang *et al.*, 2009), where parametric study is restricted due to the limit of OA construction. For example, the maximum number of unknowns with more than 3 levels allowed by OA is 33 presently via $OA(512, 33, 16, 2)$ (Hedayat *et al.*, 1999).

To recommend a better sampling method for iSSRM, a comparison study is performed. Without loss of generality, a simple statistical study is carried on those 25 runs for the noise free case. The CPU time reported is based on a workstation with two 3.0GHz-CPUs. The results are summarized in Table 2.3 and 2.4 for 10-DOF and 20-DOF lumped mass systems. A further study on 20-DOF system is included, as it allows more extensive investigation of the consistency of the proposed methods on a more unknowns involved case. Compared to OA and Hammersley sequence, random uniform distribution and Latin hypercube provide a less robust identification, since the corresponding standard deviations in the identification error, i.e., in Table 2.3 and 2.4, are consistently greater than OAs and Hammersley sequence. However, Hammersley sequence is recommended not only because it can provide equally good results with OA, but it is much more flexible to construct than OA.

There is no perturbation found in the study of this section, although its performance has been reported (Zhang *et al.*, 2009). This indicates the sampling defined search limit for the current problem happens to be successful in balanced exploration and exploitation such that the optima are accurately bracketed for each run. More importantly, an iSSRM run without activating the perturbation and jump-back procedures implies that additional computer time in the fitness evaluation is avoided for restoring the search limit.

2.6 Parametric Study

The comparison study of four sampling methods suggests that Hammersley sequence is the best candidate for iSSRM based on consideration of sampling uniformity, accuracy and scalability. It shows that the quasi-random sequence provides uniform samples in the solution space. The Hammersley sequence is much more flexible to construct than OA, as well as gives much more robust and accurate results than random uniform distribution and Latin hypercube. Compared to a recent work on improving GA, the proposed sampling based GA achieves significantly better accuracy based on the same number of fitness evaluations. In the comparison of sampling methods, however, GA parameters adopted are based on the best performance of SSRM, which may not be equally suitable for iSSRM. Due to the involvement of sampling test, trade off of exploitation-and-exploration has to be re-examined. The reason is that the original balanced exploration and exploitation pattern will be affected with additional allocation of total evaluations on the sampling tests. This trade off investigation is readily carried out by virtue of the scalability in quasi-random sequences construction, i.e. Hammersley sequence in this study.

To achieve better performance of iSSRM, parametric study is conducted in this section. Without loss of generality, this study is investigated based on noise-free measurements. The purpose is to find suitable GA parameters for the best iSSRM performance. The criterion used herein is to compare the accuracy that can be achieved in a given number of fitness evaluations. Total fitness evaluations are determined by the size of population, generation, sampling, and runs. It can be expressed as

$$TotalEval = (PopSize \times GenSize \times 3 + SampleSize) \times Runs \tag{2.17}$$

The present parametric study considers only typical combinations, and thus the parameters of interest will vary while other parameters will be fixed. It is an efficient way to study the effect of different parameters. In this way, huge computer time is avoided by

only considering typical parameter combinations. For example, if 3 different values are considered for each of 10 parameters of concerns, there will be 59,049 combinations in total.

The current parametric study is focused on the allocations of total evaluations into outer sampling test and inner MGAMAS search, with special considerations in the size of samples as well as populations, generations, and the number of MGAMAS runs. The test on parameters will comprise two sections. First, the main test will be carried out for the evaluation allocation into sampling and MGAMAS exploring. The GA parameters such as crossover ratio, mutation ratio, migration ratio, etc, will be fixed, using the recommended values (Perry *et al.*, 2006). The size effect of MGAMAS exploration will be studied by three typical values for samples, population, and runs. The number of generations will be given via Eq. (2.17). This will introduce totally 27 cases for each investigation. Second, additional test will further tune the sampling size and also determine the n_b value, which governs the convergence performance. The value of n_b is investigated with two other possibilities, i.e., 4 and 7. Sample size is further tuned by reducing or increasing 2 times the number of unknowns N_u. When the main test is finished, additional test will continue by fixing the other parameters and only vary n_b and sample size. Both identifications on known mass systems and unknown mass are conducted in the parametric study.

2.6.1 Known Mass System

In the first part, known mass case is considered for 5-DOF, 10-DOF, 20-DOF, and 50-DOF lumped mass system. The "total evaluations" refers to the number of times to evaluate the fitness function, as defined in Eq. (2.2). It is set to be 5,000, 10,000, 40,000, and 250,000 for the four different systems, respectively. On a two-CPU 3.0-GHz workstation, the computational time is approximately 0.8s, 3s, 26s, and 419s for 5, 10, 20 and 50-DOF systems, respectively. The total evaluations are chosen such that the mean error for iSSRM by Hammersley sequence, using some basic GA parameters, is about 2% al-

lowing for further fine tuning of GA parameters. The 50-DOF system will be investigated after the 10-DOF and 20-DOF systems, as the 50-DOF system involves more unknowns and thus will be time-consuming in parametric studies. Better understanding of 10-DOF and 20-DOF system from the parametric study will be helpful to choose more suitable parameter for examining the 50-DOF system. The fixed parameters for iSSRM are in Table 2.5. The parameters to be varied and their trial values are listed in Table 2.6.

2.6.2 Unknown Mass System

In the second part of parametric study, unknown mass is considered for 5-DOF, 10-DOF and 20-DOF systems. This is a more challenging problem which might introduce more local optima. The reason is that different combinations of mass and stiffness can possibly produce the same eigenpairs, thus resulting in ridges in the fitness contour. Using the formulation Eq. (2.2), there will be regions producing the same fitness. On the other hand, the 50-DOF system is not involved in this part of the study, since huge computer time will be incurred for a total of 27 cases in 50-DOF system. While the identification is more difficult for unknown mass problem, the total evaluations are increased to 40,000, 80,000 and 600,000 for the 5-DOF, 10-DOF and 20-DOF systems, respectively. The computer times are approximately 15s, 65s and 1,029s. The various values for three parameters, i.e., the size of population, samples, and total number of MGAMAS runs, are chosen based on the results of known mass cases. Similar to the previous known mass problem, a total of 27 cases are carried out in this part of the parametric study. The fixed parameters are listed in Table 2.7 and the investigated GA parameters in Table 2.8.

2.6.3 Recommended GA Parameters

After an elaborate study, the best parameters are summarized in Table 2.9 with some brief comparison. In the case of known-mass identification, iSSRM yields much better accuracy than SSRM and this is achieved at half of the total evaluations of SSRM. The

relative computational effort is presented as the evaluation ratio equal to the total evaluations by iSSRM over that by SSRM (Perry *et al.*, 2006). Typically, only 0.07% and 0.15% mean error lies in identified stiffness for 10-DOF and 20-DOF system, whereas the corresponding errors are 0.43% and 0.52% reported by Perry *et al.* (2006). In the unknown mass case, the results listed in Table 2.9 are based on 10% noise in the measurements. The mean errors of identified stiffness and mass are consistently better than those reported by Perry *et al.* (2006). The global performance of the iSSRM method can be observed from Table 2.10, where identifications are reported in presence of different levels of noise. Typical identification of 20-DOF lumped mass system under 10% noise is shown in Fig. 2.10.

Full results of parametric tests conducted on the known-mass and unknown-mass cases are presented in Appendix A. From the main test on the size effect of population, samples, and runs, the following sets of parameters performs best out of 27 cases. In the known-mass case, $0.3\sqrt{N_E}/30N_U/15$, i.e., "BCB" in Table A.3 of Appendix A, are suggested for 5-DOF system where N_E is the total number of fitness evaluations and N_U is the total number of unkowns to be identified. $0.15\sqrt{N_E}/30N_U/15$, i.e., "ACB" in Table A.4 and Table A.5 of Appendix A, are recommended for 10-DOF and 20-DOF lumped mass system. $0.15\sqrt{N_E}/45N_U/20$, i.e., "ACB" in Table A.6, are better for 50-DOF system. In unknown-mass case, $0.15\sqrt{N_E}/18N_U/25$, i.e., "AAC" in Table A.8 and A.9 of Appendix A, are recommended for 10-DOF and 20-DOF lumped mass system. The additional test on n_b value and sample size gives marginal benefits. Typically, $0.15\sqrt{N_E}/32N_U/15$, i.e., in additional test of Table A.8 and A.9, may be better for 10-DOF and 20-DOF system. However, the parameters recommended in the main tests are remained as "ABB" for consistency consideration. The value of n_b is recommended to be 5 throughout this study, as it performs better than 4 or 7 in the present parametric study of all the cases.

To apply iSSRM method in different number of unknowns, GA parameters can be

interpolated based on the current study. For even larger systems, several recommendations would be beneficial for good identification. Small population, i.e., $0.15\sqrt{N_E}$ is favored regardless of whether mass is known or not. For stiffness identification, more computational effort should put in sampling test than in MGAMAS. In simultaneously identifying mass and stiffness parameters, however, more intensive effort should be put on MGAMAS rather than the outer sampling test. As it will be implied in the next chapter that the unknown mass case often introduce more local optima and ridges than the known mass case, finer sampling meshes in the solution space tend to define a smaller search limit and thus risk more in overshooting the global optima.

When studying the iSSRM method, two interesting phenomena are observed as shown in Fig. 2.11. First, convergence of fitness value is progressively improved, especially in the first half of total evaluations. The corresponding convergence of mean error is, however, not as smooth as that of fitness. This indicates the existence of local optima in the first half the history as greater fitness does not necessarily mean better candidate. Besides, the uneven curves lie typically more in the earlier part than the later part. Second, the convergence rate by the earlier 50% evaluations achieves better performance than the subsequent 50% evaluations, in terms of mean error in identified parameters. It implies that the later 50% evaluations might be spent in fine tuning for the global peak, since marginal improvement is found on the identification errors, and the errors are as small as only 5% in the presence of 10% noise.

2.7 Conclusions

In this study, an iSSRM method is presented for system identification. By taking samples in the search space, it allows the inner MGAMAS search intensively with focus on the most promising solution possibilities. The Hammersley sequence out of the four sampling methods considered is recommended. Numerical investigation gives consistent identification on the stiffness values of 10-DOF and 20-DOF lumped mass systems. It shows

that quasi-random sequence is able to provide acceptably uniform samples in the solution space. They are much easier to construct than OA, and gives much more robust and accurate results than random uniform distribution and Latin hypercube. In comparison to the recent similar work on improving GA, the iSSRM method could achieve remarkably better accuracy using slightly more than half of evaluations of SSRM (Perry *et al.*, 2006). Besides, the present study can be readily extended to other quasi-random sequences if necessary, e.g. Holton and Sobol sequences, which is not covered in this study. For more general applications in structural identification, the GA parameters can be interpolated through the values listed in Table 2.11.

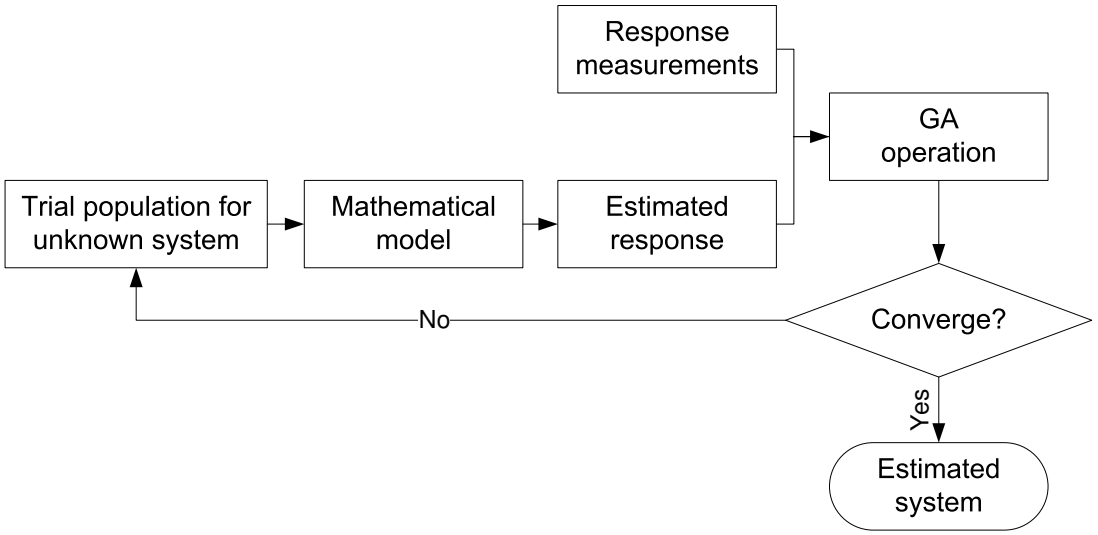

Figure 2.1: System identification using GA

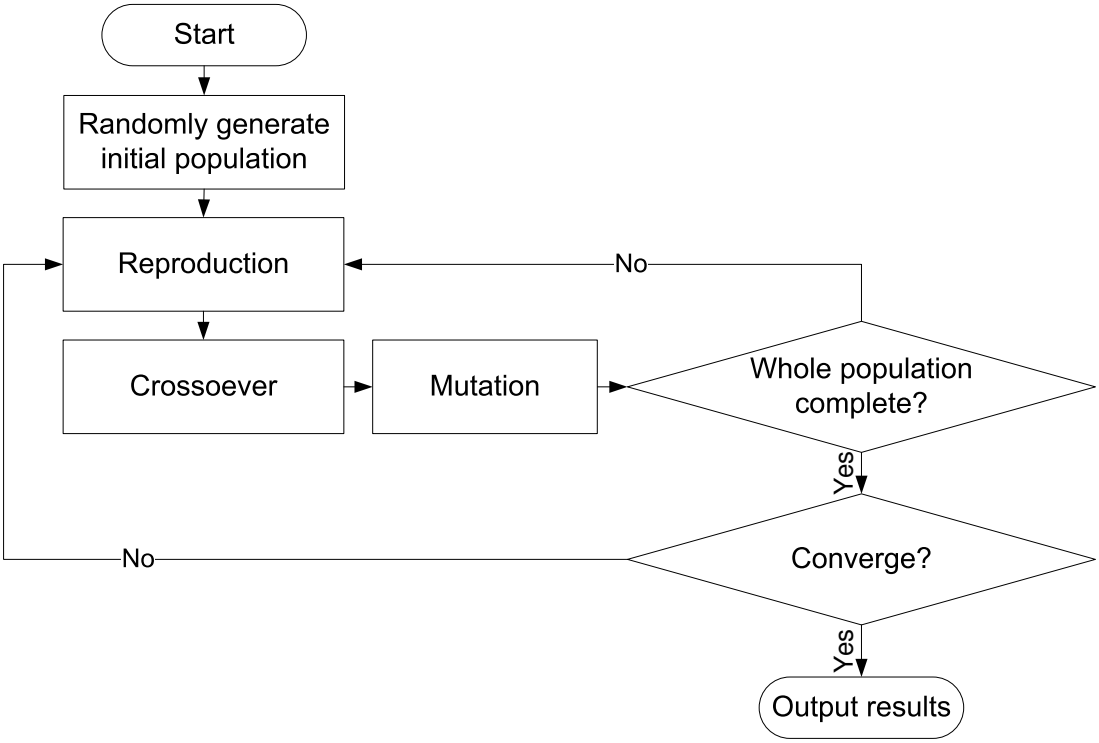

Figure 2.2: Concept of simple genetic algorithm (SGA)

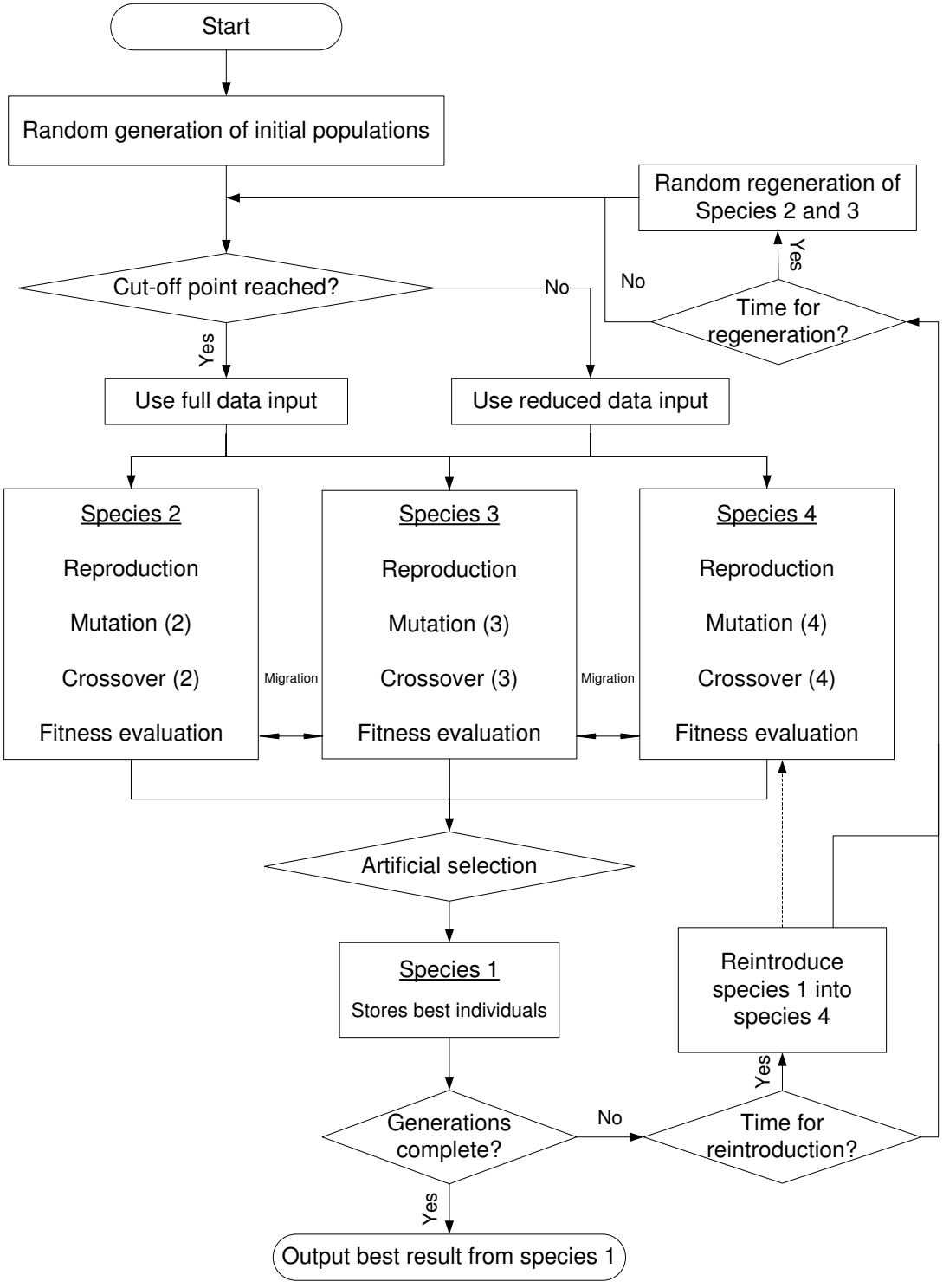

Figure 2.3: Modified GA based on migration and artificial selection (MGAMAS)

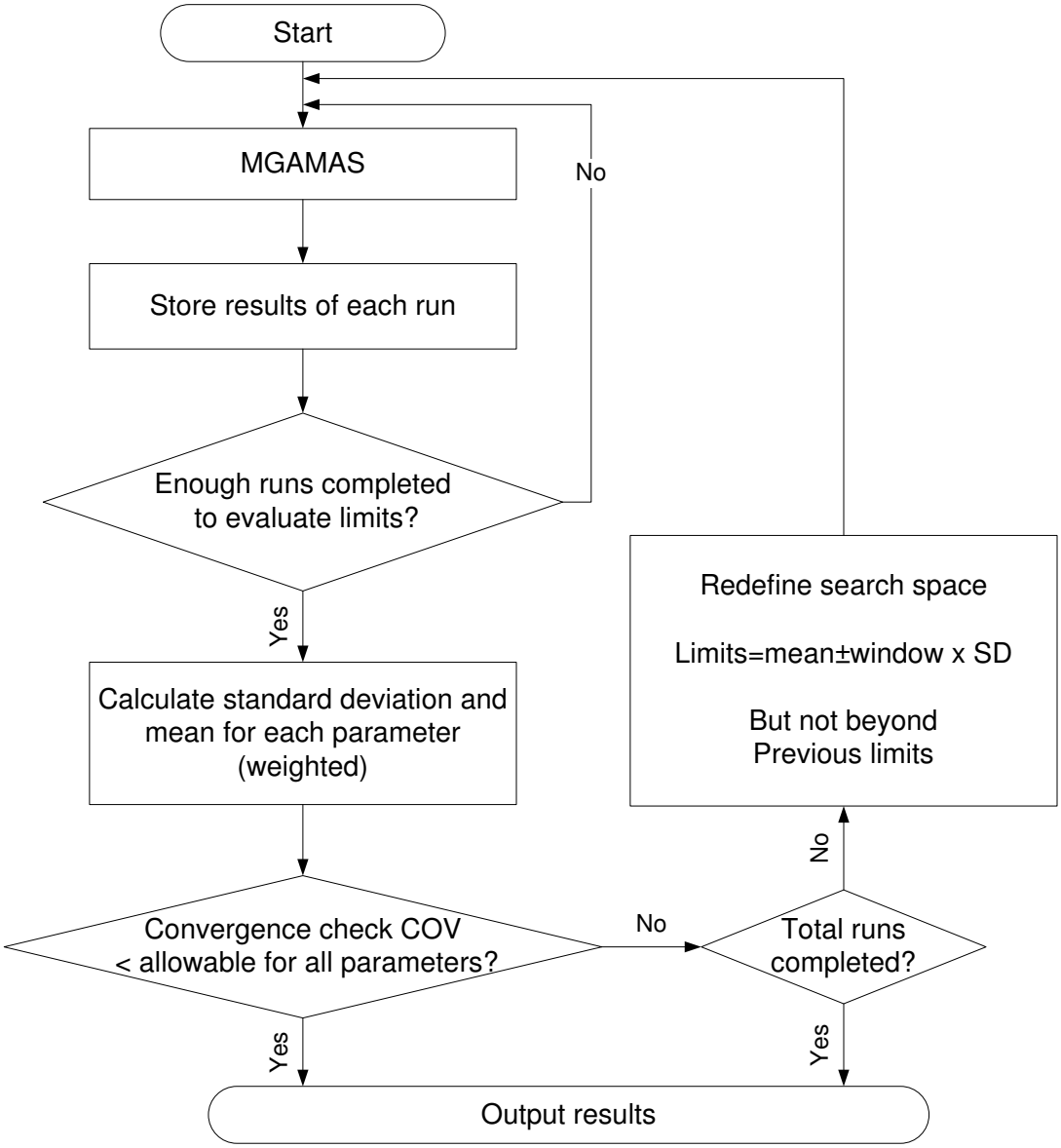

Figure 2.4: Search space reduction method (SSRM)

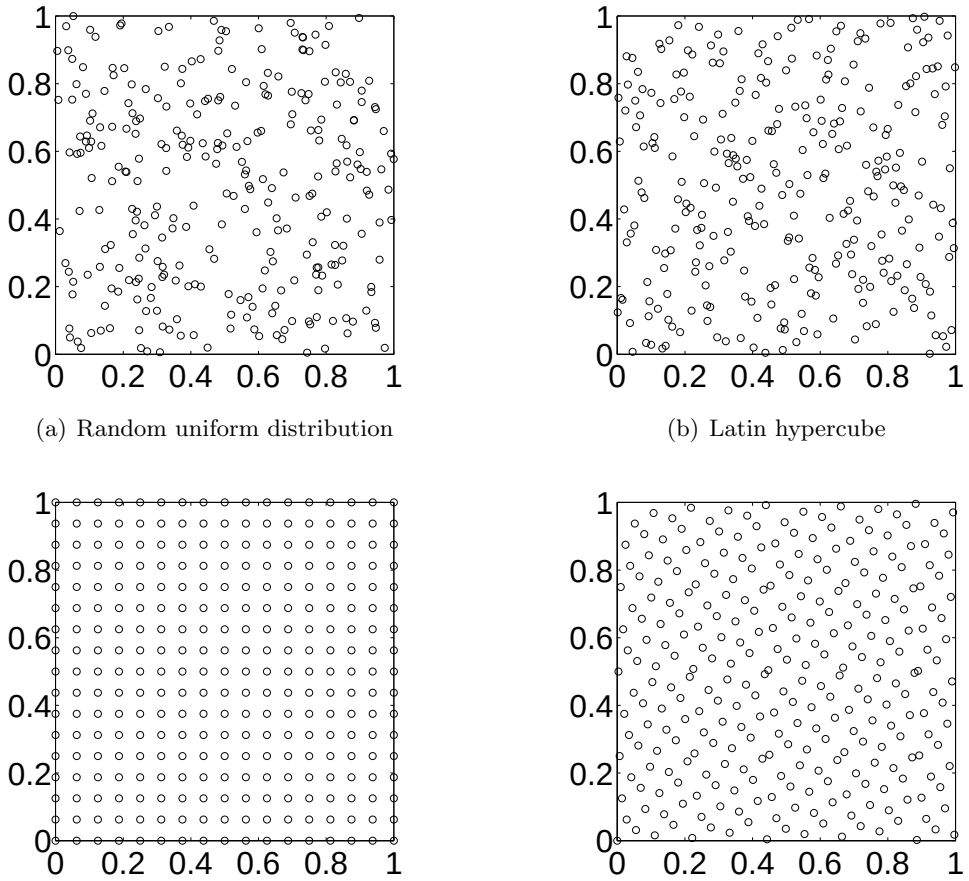

(a) Random uniform distribution

(b) Latin hypercube

(c) Orthogonal arrays

(d) Hammersley sequence

Figure 2.5: Comparison of sampling method: 289 samples

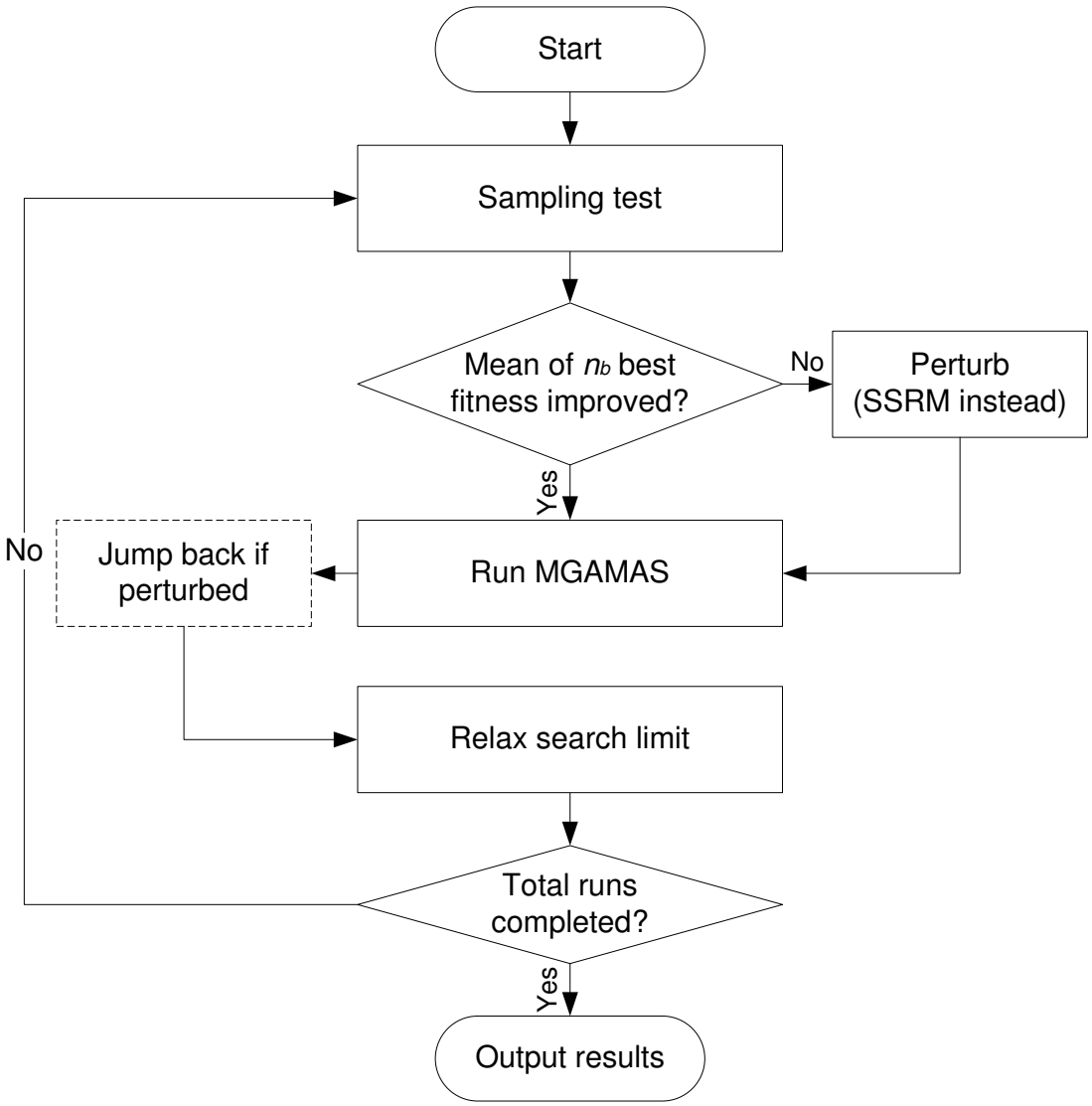

Figure 2.6: SSRM with sampling test: an improved SSRM

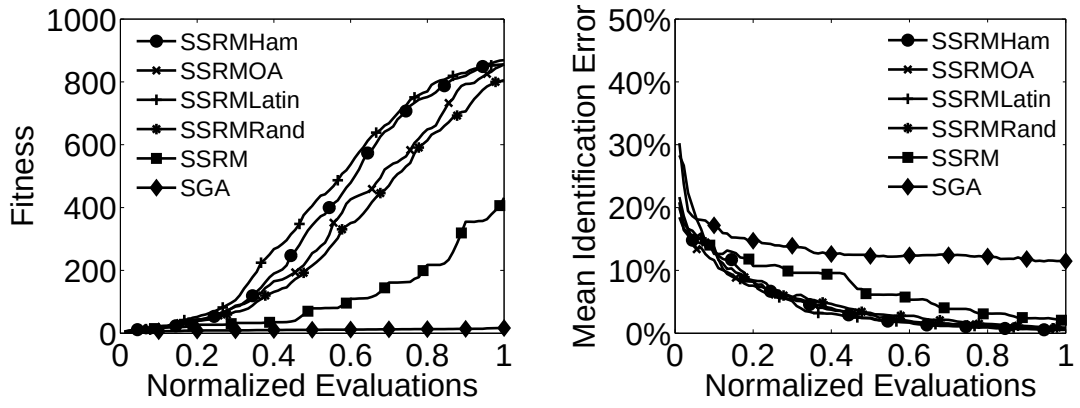

Figure 2.7: Stiffness identification convergence histories of a 10-DOF lumped mass system under 0% noise

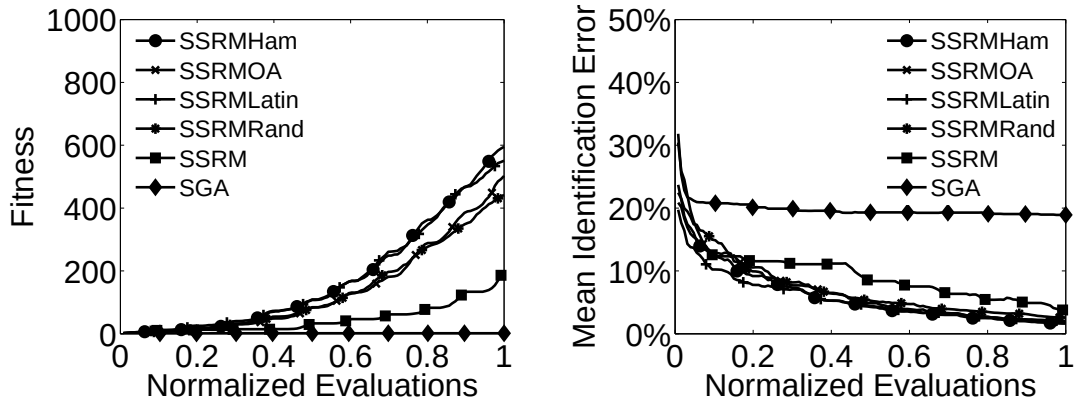

Figure 2.8: Stiffness identification convergence histories of a 20-DOF lumped mass system under 0% noise

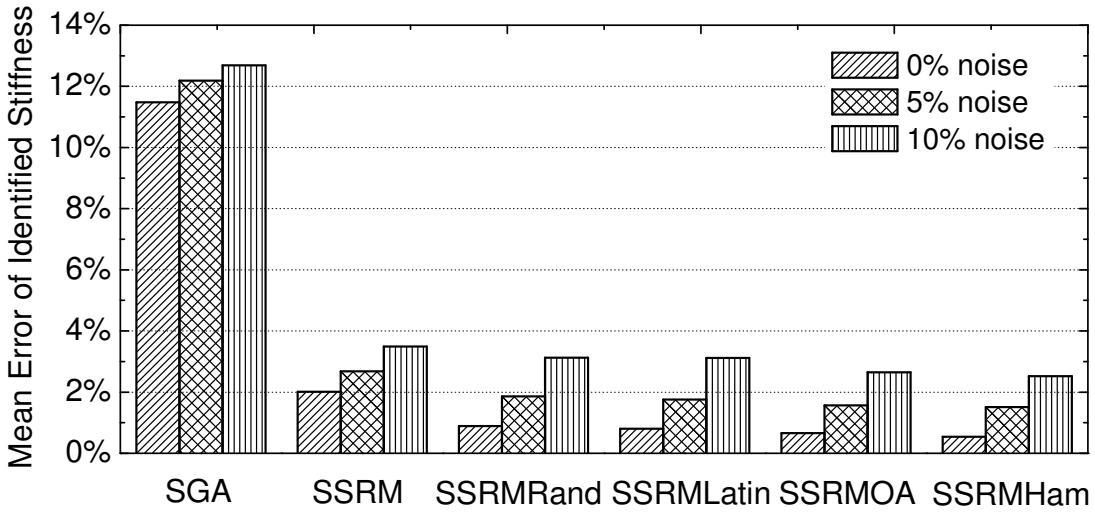

Figure 2.9: Identification of a 10-DOF known mass system under noise

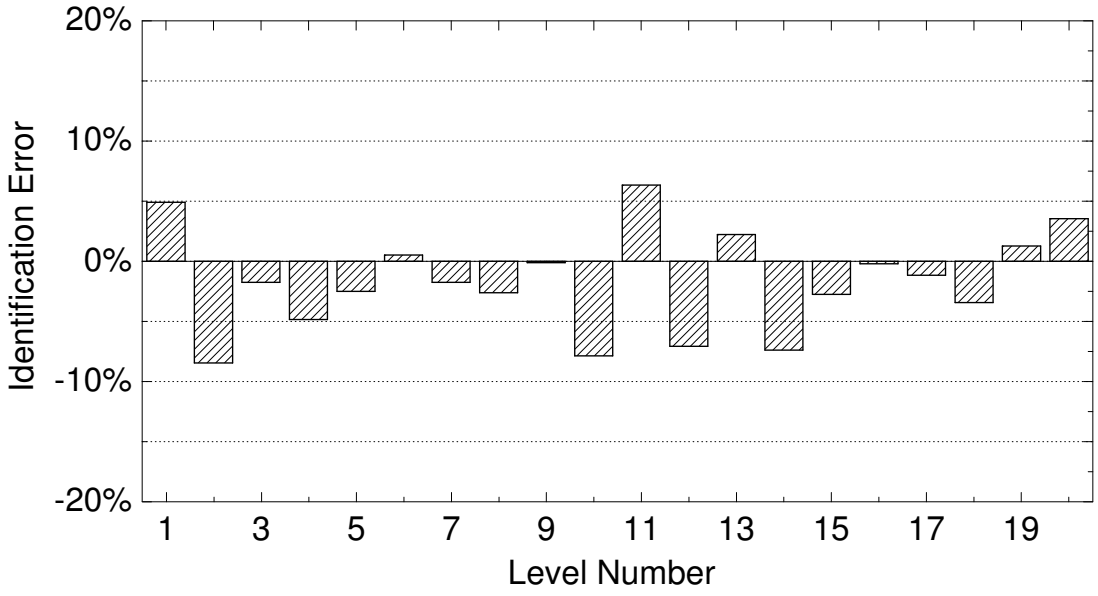

Figure 2.10: Typical identification of a 20-DOF known mass system under 10% noise

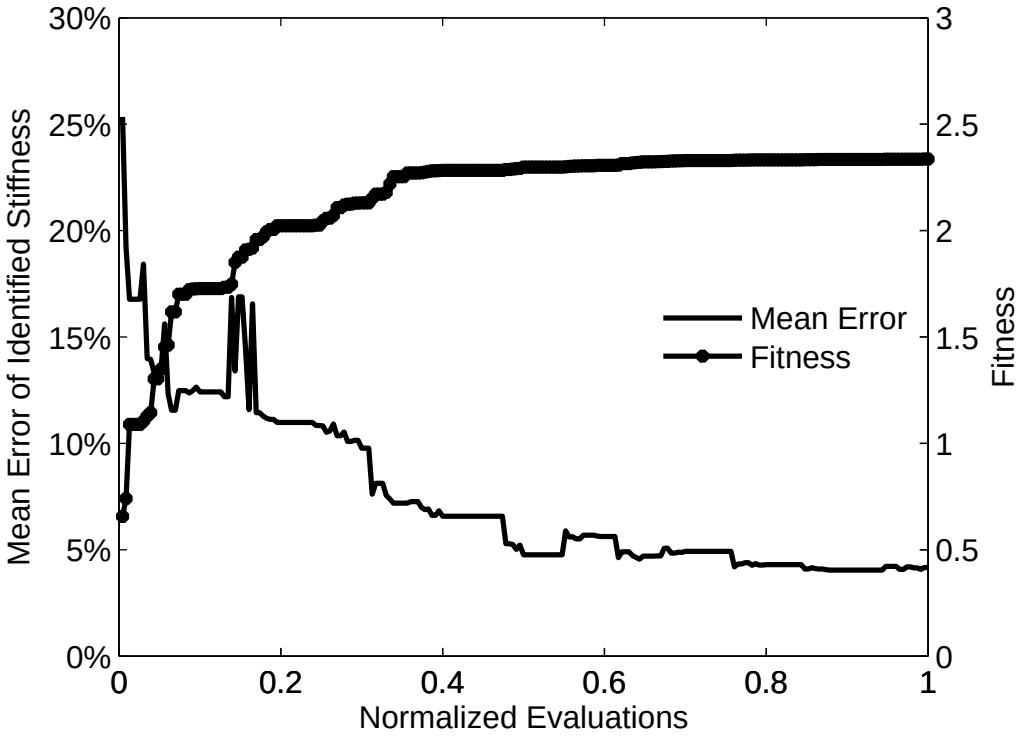

Figure 2.11: Typical convergence history of a 20-DOF known mass system under 10% noise

Table 2.1: GA parameters for iSSRM with sampling test: 10-DOF system

GA parameters	10-DOF lumped mass system					
	SGA	SSRM	SSRMRand	SSRMLatin	SSRMOA	SSRMHam
Population size	57	5×3	5×3	5×3	5×3	5×3
Generations	90	34	14	14	14	14
Sample size	-	-	289	289	289	289
Total runs	-	10	10	10	10	10
Crossover rate	0.95	0.8	0.8	0.8	0.8	0.8
Mutation rate	0.05	0.2	0.2	0.2	0.2	0.2
Migration rate	-	0.05	0.05	0.05	0.05	0.05
Regenerations	-	2	2	2	2	2
Reintroductions	-	30	10	10	10	10
Window width	-	4	4	4	4	4
Total evaluations	5,130	5,100	4,990	4,990	4,990	4,990

Table 2.2: GA parameters for iSSRM with sampling test: 20-DOF system

GA parameters	20-DOF lumped mass system					
	SGA	SSRM	SSRMRand	SSRMLatin	SSRMOA	SSRMHam
Population size	80	7×3	7×3	7×3	7×3	7×3
Generations	126	48	23	23	23	23
Sample size	-	-	512	512	512	512
Total runs	-	10	10	10	10	10
Crossover rate	0.95	0.8	0.8	0.8	0.8	0.8
Mutation rate	0.05	0.1	0.1	0.1	0.1	0.1
Migration rate	-	0.05	0.05	0.05	0.05	0.05
Regenerations	-	3	3	3	3	3
Reintroductions	-	40	20	20	20	20
Window width	-	4	4	4	4	4
Total evaluations	10,080	10,080	9,950	9,950	9,950	9,950

Table 2.3: Comparison of sampling methods: 10-DOF lumped mass system with 0% noise

Test	Fitness			Stiffness Error (%)		CPU Time	Evaluations	Perturb-
	Mean	SD[a]	Median	Mean	SD[a]	(sec)		ation
SGA	17	(2)	12	11.48	(0.68)	1	5,130	-
SSRM	431	(33)	412	2.01	(0.22)	1	5,100	-
SSRMRand[b]	806	(43)	890	0.89	(0.20)	1	4,990	0
SSRMLatin[b]	856	(41)	953	0.80	(0.19)	1	4,990	0
SSRMOA[b]	856	(21)	887	0.66	(0.09)	1	4,990	0
SSRMHam[b]	869	(33)	947	0.54	(0.10)	1	4,990	0

[a] SD=standard deviation

[b] SSRMRand, SSRMLatin, SSRMOA, and SSRMHam are the iSSRM method sampled by random uniformly, Latin hypercube, orthogonal arrays, and Hammersley sequence, respectively.

Table 2.4: Comparison of sampling methods: 20-DOF lumped mass system with 0% noise

Test	Fitness			Stiffness Error (%)		CPU Time	Evaluations	Perturb-
	Mean	SD[a]	Median	Mean	SD[a]	(sec)		ation
SGA	2	(0)	1	18.91	(0.93)	6	10,080	-
SSRM	199	(18)	191	3.70	(0.34)	6	10,080	-
SSRMRand[b]	441	(34)	456	2.56	(0.36)	6	9,950	0
SSRMLatin[b]	551	(48)	556	2.06	(0.36)	6	9,950	0
SSRMOA[b]	502	(29)	502	1.79	(0.19)	6	9,950	0
SSRMHam[b]	595	(30)	580	1.61	(0.15)	6	9,950	0

[a] SD=standard deviation

[b] SSRMRand, SSRMLatin, SSRMOA, and SSRMHam are the iSSRM method sampled by random uniformly, Latin hypercube, orthogonal arrays, and Hammersley sequence, respectively.

Table 2.5: GA parameter test values for known mass system: fixed parameters

Fixed parameters	Lumped mass systems			
	5-DOF	10-DOF	20-DOF	50-DOF
Total evaluations	5,000	10,000	40,000	250,000
Crossover rate	0.8	0.8	0.8	0.8
Mutation rate	0.2	0.2	0.2	0.2
Migration rate	0.05	0.05	0.05	0.05
Regeneration	2	2	3	3
Reintroduction	5	20	50	100
Window width	4	4	4	4

Table 2.6: GA parameter test values for known mass system: investigated parameters

Parameters	Cases		
	A	B	C
Main test			
Population size	$0.15\sqrt{N_E}$	$0.3\sqrt{N_E}$	$0.5\sqrt{N_E}$
Sample size	$10{N_U}^a/18{N_U}^b$	$18{N_U}^a/30{N_U}^b$	$30{N_U}^a/45{N_U}^b$
Number of runs	$9^a/15^b$	$15^a/20^b$	$20^a/25^b$
Additional test			
n_b trails	4	5^c	7
Sample size	-$2N_U$	+$2N_U$	

[a] Parameters are considered in 10- and 20-DOF cases.

[b] Parameters are used in 50-DOF case.

[c] Default value in main test

Table 2.7: GA parameter test values for unknown mass system: fixed parameter

Fixed parameters	Lumped mass systems		
	5-DOF	10-DOF	20-DOF
Total evaluations	40,000	80,000	600,000
Crossover rate	0.4	0.4	0.4
Mutation rate	0.2	0.2	0.1
Migration rate	0.05	0.05	0.05
Regeneration	3	3	3
Reintroduction	50	50	100
Window width	4	4	4

Table 2.8: GA parameter test values for unknown mass system: investigated parameters

Parameters	Cases		
	A	B	C
Main test			
Population size	$0.15\sqrt{N_E}$	$0.3\sqrt{N_E}$	$0.5\sqrt{N_E}$
Sample size	$18N_U$	$30N_U$	$45N_U$
Number of runs	15	20	25
Additional test			
n_b trails	4	5[a]	7
Sample size	$-2N_U$	$+2N_U$	

[a] default value in main test

Table 2.9: Performance comparison for SSRM and iSSRM methods

Results	Known mass systems			Unknown mass systems	
	10-DOF	20-DOF	50-DOF	10-DOF	20-DOF
Time (h:m:s)	00:00:03	00:00:26	00:06:59	00:01:05	00:17:18
Evaluation ratio[a]	0.5	0.5	-	0.08	0.3
Mean error - k (%)	0.07(0.43)[b]	0.15(0.52)	0.87	2.05(2.98)	2.43(2.78)
Max error - k (%)	0.19(1.21)	0.38(1.60)	3.12	5.08(6.62)	6.78(8.64)
Mean error - m (%)	-	-	-	1.98(3.00)	2.60(3.00)
Max error - m (%)	-	-	-	4.69(6.81)	7.54(10.40)

[a] Evaluation ratio is obtained by current total evaluations divided by total evaluations by Perry *et al.* (2006).

[b] Data in the brackets are by Perry *et al.* (2006): 0% noise for known mass system and 10% noise for unknown mass case.

Table 2.10: Identification of lumped mass systems via iSSRM method

Results	Known mass systems			Unknown mass systems	
	10-DOF	20-DOF	50-DOF	10-DOF	20-DOF
			0% Noise		
CPU time (h:m:s)	00:00:03	00:00:26	00:06:59	00:01:05	00:17:18
Mean error - k (%)	0.07	0.15	0.87	0.11	0.07
Max error - k (%)	0.19	0.38	3.12	0.26	0.28
Mean error - m (%)	-	-	-	0.11	0.08
Max error - m (%)	-	-	-	0.30	0.26
			5% Noise		
CPU time (h:m:s)	00:00:03	00:00:26	00:06:59	00:01:05	00:17:18
Mean error - k (%)	1.65	1.97	4.28	1.11	1.17
Max error - k (%)	4.16	4.91	18.76	2.63	3.19
Mean error - m (%)	-	-	-	1.04	1.31
Max error - m (%)	-	-	-	2.04	3.77
			10% Noise		
CPU time (h:m:s)	00:00:03	00:00:26	00:06:59	00:01:05	00:17:18
Mean error - k (%)	2.78	4.17	7.85	2.05	2.43
Max error - k (%)	7.0	10.84	34.38	5.08	6.78
Mean error - m (%)	-	-	-	1.98	2.60
Max error - m (%)	-	-	-	4.69	7.54

Table 2.11: Recommended GA parameters for iSSRM method

Parameters	Known mass systems				Unknown mass systems		
	5-DOF	10-DOF	20-DOF	50-DOF	5-DOF	10-DOF	20-DOF
Total Evaluations	5,000	10,000	40,000	250,000	40,000	80,000	600,000
Population size	7	5	10	25	10	14	39
Generations	6	20	67	135	55	80	246
Sample size	$7^a/210^b$	$12^a/360^b$	$22^a/660^b$	$52^a/2340^b$	$12^a/360^b$	$22^a/660^b$	$42^a/1260^b$
Number of runs	15	15	15	20	20	20	20
n_b value	5	5	5	5	5	5	5
Crossover rate	0.8	0.8	0.8	0.8	0.4	0.4	0.4
Mutation rate	0.2	0.2	0.1	0.1	0.2	0.2	0.2
Migration rate	0.05	0.05	0.05	0.05	0.05	0.05	0.05
Regeneration	2	2	3	3	3	3	3
Reintroduction	5	10	30	50	20	40	100
Window width	4.0	4.0	4.0	4.0	4.0	4.0	4.0
Time (m:s)	00:0.78	00:03	00:26	06:59	00:15	01:05	17:18

[a] the number of unknowns

[b] the number of samples

CHAPTER 3

Improved SSRM with Gradient Search

Structural identification in physical domain is usually posed as an optimization problem. By adopting some heuristic rules to maximize a prescribed fitness function, genetic algorithms (GA) have proved to be a relatively robust method in identifying the unknown system. In Chapter 2, improved search space reduction method (iSSRM) via uniform samples makes it possible to achieve more accurate results with about half of computer time by Perry *et al.* (2006). However, the reasons on why GA with reduced search space can work are not well established. An interesting finding on the convergence history of 20-DOF system in Chapter 2 indicates the significance of having knowledge on the contour of fitness surface. Although traditionally treated as an optimization process, the information on the fitness surface of structural identification has not been investigated in the past literatures. With better understanding of the fitness surface, the computational efficiency is expected to improve further with more advanced optimization strategies.

In this chapter a "peak shifting" observation is reported on the fitness surface. It implies that there is only one global peak surrounded by various local optima in the fitness contour. In the presence of measurement noise, the global peak will shift and its

magnitude decreases. At the same time, new local optima are seldom produced even as the noise level increases. The observation of peak shifting strongly suggests the use of hybrid optimization for system identification. Within a reasonable search range, iSSRM is presented to overcome the local optima away from the global peak. As the solution gets sufficiently close to the vicinity of the global peak, peak finding is then investigated by local search. The local search is investigated using gradient based and non-gradient based methods, including conjugate gradient (CG) method, Broyden-Fletcher-Goldfarb-Shanno (BFGS) method, as well as simulated annealing (SA) method. Based on the knowledge of parametric study in Chapter 2, reasonable switch point for iSSRM search and local search is recommended in this chapter. The efficiency of the proposed hybrid optimization strategy is demonstrated by three numerical examples, i.e., a lumped mass system, a plate structure, and a truss model. Supported by "peak shifting", even better results are obtained with further reduction of computational effort.

3.1 Characteristics of Structural Identification as an Optimization Problem

In the field of numerical optimization, it is well recognized that there is no single best algorithm for general application. However, good knowledge on the shape of fitness surface will help to choose a problem-suitable strategy. Practical identification of structural system is usually associated with a large number of variables. This poses considerable difficulties to make the fitness surface visible though two- or three-dimensional plots. However, through small scale testing, i.e., variables equal to or less than 2, the nature of structural identification can be discovered in an optimization perspective. To gain some insight, the investigation of fitness surface will be conducted for single DOF and 2-DOF lumped mass system. In this study, fitness function is evaluated on basis of Eq. (2.2),

which is recalled here as

$$\phi = \frac{1}{0.001 + \sum_{i=1}^{p}\sum_{j=1}^{q}(\ddot{u}_{ij}^{m} - \ddot{u}_{ij}^{e})^2} \tag{3.1}$$

To investigate the fitness surface, each unknown parameter will result in an independent solution dimension. As the contour of fitness surface is unknown in advance, the search domain will be meshed evenly in a grid manner. The method is to evaluate the fitness function at each point on the regular grid of parameters. It is usually called an s-level problem if s possibilities of each variable are tried along its search space. Obviously the accuracy of resultant surface inevitably depends on the grid density. As more parameters are included in the model, the number of evaluations can be excessive. In the present investigation, examples of only one and two unknowns will be examined with sufficiently fine grid mesh. Nevertheless, this will provide good understanding to the optimization for structural identification, especially the effect due to measurement noise, recorded data length, and the use of multiple load cases. It should be noted that, based on the assumptions in Section 2.1, modeling error is negligible and thus is assumed to have no effect on the fitness surface.

The investigation will cover the known mass case and unknown mass case in the generally defined $[0.5 - 2.0]$ search space. The effect of measurement noise, data length, and number of load cases will be examined. In the known mass case, 1-DOF and 2-DOF system will be studied for checking the observation consistency. Sampling in a uniform grid, 10,000 points are evenly taken in the K_1 space for 1-DOF system and 100 points are taken along each parameter of K_1 and K_2 for 2-DOF system. In the unknown mass case, 1-DOF system will be considered with 100 points extracted evenly in the K_1 and M_1 dimension. The resolutions of sampling mesh are taken in the above way so that the fitness surface can be representatively described without unnecessarily additional fitness evaluations. In addition, a further 10 times finer meshes for these systems is found to make no difference in the shape of fitness function.

3.1.1 Effect of Measurement Noise

The 1-DOF known mass system is considered with 500 kg mass and a damping ratio of 1%. The system is excited by a random force at the top. The acceleration is measured at the only mass point. The stiffness K_1 of 600 kN/m, normalized as one in the figures, is to be identified. Fig. 3.1 gives the distribution of fitness under a 10,000 grid mesh. In the noise free case, there is one extremely high peak surrounded by several local optima within the search range of 0.5 to 2.0. It is found that, with the increase of noise level, the peak of fitness function decreases and shifts as well. However, noise in the measurements induces no additional local optima. In this study, this observation is referred to as "peak shifting". The observation of peak shifting in fact substantiates the idea of applying reduced search space strategy in optimizations. The reason is that SSRM cannot work efficiently in the case of more than one global peak or when there is no significant difference in fitness height between global peak and local optima.

To further investigate the problem, a 2-DOF system of known mass is analyzed in the same way. The stiffness and mass are 600 kN/m and 500 kg for the first level, and 350 kN/m and 300 kg for the second level. Rayleigh damping of 1% is considered in both modes. Similar observations are shown in Figs. 3.2 to 3.7 for noise levels of 0%, 5%, and 10%. The contour line of fitness peak supports the peak shifting hypothesis. Of great importance is that the extension (or flattening) of "peak ridge" indicates that noise in the measurement will have more influence to the lower-level stiffness K_1 than the upper-level stiffness K_2. This observation concurs with the previous finding (Koh *et al.*, 2003b). That is, it is usually more difficult to identify the stiffness at lower-level of a lumped mass system. The reason is that the response excited is usually smaller at the lower level than at the upper level. Statistical analysis of 10,000 cases of peak shifting under 0%, 5%, and 10% levels of noise, i.e., Figs. 3.8 to 3.10, reveals that the peak tends to move roughly in a -45° direction on the K_1-K_2 contour plot. This means that the identified values for K_1 and K_2 are equally affected by the increase of noise level.

The noise effect on the fitness surface is also of interest for unknown mass systems, because a model of unknown mass allows more flexibility in calibrating the physical parameters but the identification becomes more challenging. The reason lies not only in the increase in search dimensions due to doubling the number of unknowns, but also in the fact that the simultaneously changed stiffness and mass parameters are possible to produce the same eigenpairs. An insight to the lower-dimension fitness shape of unknown mass case will be constructive to understand the physical meaning of higher-dimension identification. To this end, the 1-DOF system is again investigated but assuming that both the stiffness and mass are unknown.

As observed from Figs. 3.11 to 3.19, the shape of fitness function is strongly affected by the additional involvement of the unknown mass to the unknown stiffness. Besides the noise-induced peak shifting, a rather long ridge is discovered along the direction of 45° in the K_1-M_1 domain while the slope in the perpendicular direction is rather steep. This is because eigen values and eigen modes will not be affected by simultaneously scaling the stiffness and mass by the same factor. The fitness surface analysis shows that more local optima and ridges are in the fitness surface than the known mass case.

Of great importance is that peak shifting is a significant optimization characteristic of the global peak. The observation of peak shifting has nothing to do with specific formulation of the fitness function. The essential use of fitness function is to evaluate the performance of individual solution candidate. Therefore, using different fitness functions might change the relative magnitude between the global peak and local optima, the distribution of local optima away from the global peak, and the sensitivity of individual variables to be identified. The sensitivity can be expressed as first-order fitness derivatives, i.e., gradients, or second-order fitness derivatives, i.e., Hessian matrix. Nevertheless, these three affected items will not have influence on the location and magnitude of global peak. Under the practical measurement noise, the observation will be valid as long as the mathematical model can capture the physical behavior of the structures.

In fact, this assumption on modeling error has been made in Section 2.1 and can be reasonably satisfied in reality.

3.1.2 Effect of Data Length and Number of Load Cases

The effects of measured data length and the number of load cases are studied herein in the absence of measurement noise. Fig. 3.20 shows that in the noise free case, the shorter the data length, the fewer the local optima. From the frequency domain viewpoint, a longer time history provides finer frequency resolution. Thus it is easier to capture the resonance between the system and external forces than using a shorter time history. Hence, by using longer data length in the measurement, more local optimum due to the resonance will be found within the search limit. Nevertheless, the shorter the data length, the more negative influence due to noise will be present in the identification. The signal will be adversely affected as the relative peak height decreases with shorter data length. Besides, it should be noted that the peaks of all the three data-length cases are coincident at the global peak, i.e., the point with fitness value 1,000. The coincident peaks indicate that the unknown 1-D system will be unique in the noise free case, regardless of the length of measurement.

Fig. 3.21 illustrates that there will be fewer local optima if data are collected from more load cases. This is reasonable because the length of response data is the same for multiple load cases so that the contribution on the dominant frequencies tends to be superimposed but canceled out at other frequencies. Because the number of local optima tends to be smoothed out when combining the measurements from the white noise excited system. However, if multiple load cases will be used in structural identification, the recommended number of load cases is between 5 and 10, as more load cases make the global peak sharper and taller but this actually makes the identification tougher through optimization.

The fitness surface is also investigated for one-element and two-element plates. As the one-element plate plots show not much difference compared to SDOF lumped mass system, only the two-element plate results are shown from Figs. 3.22 to 3.24. Consistent "peak shifting" is observed again. It should be noted that the shape of fitness surface and the magnitude of peak shifting depend on the formulation of fitness function, i.e., Eq. (3.1), and thus on the location of measurements as well as data length. This is because the layout of sensor network will determine the richness of modal information contained in the measurements. Since modal participation will reflect the stiffness and mass distribution, identification of structures will be accordingly affected by measuring the accelerations from different parts of the structures. Nevertheless, of great importance is that peak shifting observed in lower dimension makes it possible to devise a novel and efficient hybrid optimization strategy as explained below.

3.2 Gradient and Non-Gradient Local Search

The fitness surface analysis indicates that local search methods will be beneficial for fine tuning near the peak. In this region, the gradient-based methods usually have better performance than GA. This is because new candidates in GA are estimated by random variation, i.e., mutation and crossover, in the breeding process. It is easy for GA to overcome local optima and reach the vicinity of the global optimal peak, but it is rather inefficient to find the exact peak through trying randomly varied candidates. The computation will be intensive for species evolution to cover the solution neighborhood and converge to the peak.

In this connection, a hybrid optimization strategy is proposed to improve the convergence of identification as well as to verify the "peak shifting" observation. The essential concept is shown in Fig. 3.25. This algorithm embraces a preliminary iSSRM search and a local search for fine tuning. The local searchers considered herein include gradi-

ent based conjugate gradient method, Broyden-Fletcher-Goldfarb-Shannon method, and non-gradient based simulated annealing method. As a result, the identification by non-gradient local searcher will serve as a reference to check whether the peak found by gradient based methods is the global peak, by judging the achievement of the same identification accuracy. This is because simulated annealing starts a random search from the neighborhood of best estimates, and thus has better chance for locating the global peak than GA, which carry out species evolution within the whole search range. More importantly, simulated annealing is much better in capturing the global peak than the other two local searchers, i.e., CG and BFGS, as they are based on the gradients and easily converge to local optima. For the purpose of discussion and ease of reference, the fundamental concepts of these algorithms are briefly outlined in the subsequent sections.

3.2.1 Simulated Annealing

The idea of simulated annealing (SA) is inspired from annealing in metallurgy, especially in the way that liquids freeze and crystallize, or metals cool and anneal. At high temperatures, heat causes atoms to become active from their initial positions and move freely and randomly through states of higher energy. If it cools slowly, the atoms will have more chances of finding configurations with lower energy than the initial state. Analogizing with this physical process, simulated annealing was firstly presented as an optimization algorithm to locate a good approximation of the global optima (Kirkpatrick *et al.*, 1983). Starting from an initial configuration, SA identifies the initial value of fitness function as a local optima. The initial configuration is then perturbed in the neighbourhood by taking a finite step away from it. The local optima will be updated if a better candidate is found within this neighbourhood. When an optimization problem is treated as a minimization problem, any downhill step is accepted and the process repeats from this new point. By allowing an uphill step selectively, it helps to escape from getting trapped in local optima. Therefore, the uphill or downhill decision and annealing scheme play

important roles in SA.

The uphill implementation is based on the "Metropolis algorithm" (Nicholas *et al.*, 1953). It accepts the uphill possibilities on a statistical basis. The algorithm is as follows.

Algorithm 1 Metropolis algorithm

If $\Delta f = f(\mathbf{x}) - f(\mathbf{x}_0) \leq 0$ **Then**

accept the good new point: $\mathbf{x} = \mathbf{x_{new}}$

Else

accept the bad new point with probability:

$$\mathrm{P}(\Delta f) = \exp\left(-\frac{\Delta f}{T_h}\right) > \textit{ a random number between } (0,1)$$

End if

The probability depends on a global temperature and differences between the energies, e.g. Δf. The global temperature T_h is gradually decreased during the process. In fact the system sometimes goes uphill as well as downhill. But the lower the temperature, the less likely the uphill movement is activated. These uphill and downhill movements allow the solver to escape from local optima and then explore more possible solution space.

Each of uphill and downhill processes at a certain temperature is called a "sweep". The system will be in equilibrium at a low temperature and frozen into a global energy minimum after prescribed sweeps or another convergence criterion is satisfied. In each sweep, there will be N_t times of adjusting the search neighborhood. At one neighborhood, N_s cycles are used to accept enough uphill and downhill candidates through perturbing each unknown parameter in turn. Therefore, if n is the number of unknown variables, a total of $n \times N_s$ evaluations of objective function are incorporated before the next neighborhood is explored. After N_t times of such iterations, namely $n \times N_s \times N_t$ evaluations, are accomplished in a complete sweep at one temperature, the temperature will be low-

ered by a ratio. Then the annealing will continue including such an iterative sweeping and temperature reduction process. In this study, if the tolerance of four successive temperatures is satisfied by a convergence criterion or a fixed number of evaluations are met, the system is considered frozen and hence annealing stops.

Besides making uphill or downhill decision by Metropolis algorithm, it is important to select an efficient annealing or cooling schedule, which is to lower the temperature T over time. An annealing schedule includes the starting temperature T_0, the rate of cooling, and the amount of time to spend at each temperature. Considering the trade off between efficiency and ease of implementation, the annealing schedule chosen herein is the exponential cooling strategy. The system is to start at a high temperature and then cool exponentially

$$T_{h+1} = r_T T_h \tag{3.2}$$

The ratio r_T is typically chosen from 0.7 to 0.9, because rapid cooling will result in a system frozen into a meta-stable state far from the optimal configuration.

In addition to uphill decision and annealing schedule, it is necessary to search in the neighborhood that only valid configurations are generated without spending more computer time than necessary in attempting the unknown solution space. To fulfill this purpose, Corana's method is adopted to define the neighborhood for simulated annealing algorithm (Corana *et al.*, 1987). In this regard, the neighborhood range is adjusted to keep the acceptance rate of 0.5 for Metropolis criteria. The generation of a new solution is in principle random, but in the following way as

$$\mathbf{x}_{new} = \mathbf{x}_{old} + r\mathbf{m} \tag{3.3}$$

where $\mathbf{x}_{old}$ is the current solution vector, and r is a uniform random scalar within the interval $[-1, 1]$. The neighborhood range is governed by the step length $\mathbf{m}$ (Corana *et al.*, 1987). The step length $\mathbf{m}$ is varied according to the acceptance rate p, e.g. 0.5. The acceptance ratio can be calculated from the number of acceptance n within the period

N_s, as n/N_s.

Algorithm 2 Simulated annealing

Select an initial temperature

Start from an initial configuration $\mathbf{x_0}$, and set it as current optimum, i.e., $\mathbf{x_{opt}} = \mathbf{x_0}$

Sweeps: **While** not converge

Do N_t times

Cycles: **Do** N_s times

Do n times

Perturb the current configuration via Corana's method to get the possibilities

Besides those downhill points, accept uphill points based on the Metropolis criteria (Algorithm 1)

End Do

End Do: Cycles

Adjust the search length $\mathbf{m}$ by Corana's method

End Do

If convergence criteria are met**, then**

Stop

Else

Restart from the current best optimum $\mathbf{x} = \mathbf{x_{opt}}$

Adjust temperature by cooling rule $T = r_T \times T$

End If

End While: Sweeps

Thus as the temperature declines, downhill movements are less likely to be accepted and the percentage of rejections rise. Given the scheme for the selection for the step length vector $\mathbf{m}$, it will fall also. Finally the reduction of temperature will make $\mathbf{m}$ smaller, and then SA focuses on the most promising area for optimization. The initial value of $\mathbf{m}$ is not very important as it will be reset quickly from the initials by Corana's method. Nevertheless, the initial system temperature T_0 is crucial for the success of SA

method. For a small T_0, the step length $\mathbf{m}$ may be too small and leads to insufficient evaluations of objective function to find the global optima. However, the relationship between the initial temperature and the step length $\mathbf{m}$ is problem dependent. In summary, the complete process of simulated annealing is given by the Algorithm 2 which is used in this study. As a result of Corana's method, new candidates are generally explored in its local neighborhood. However, a global optimum is guaranteed by virtue of Metropolis algorithm, as both uphill and downhill choices are considered whereas uphill movements, i.e., worse solution, are rejected in most optimization algorithms.

3.2.2 Conjugate Gradient Method

Generally gradient search methods begin from some initial guess $\mathbf{x}_0$, and then the initial guess is updated in stages with predefined search direction and step length. The process is often expressed in this formulation.

$$\mathbf{x}_{h+1} = \mathbf{x}_h + \alpha_h \mathbf{p}_h \tag{3.4}$$

where vector $\mathbf{p}_h$ represents a search direction, and scalar α_h determines the length of the step. The search direction could be selected to minimize the objective function with respect to α_h at each run.

Unlike the traditional steepest descent method, the search direction defined in CG methods is a conjugate direction instead. The conjugate property is defined in the manner that if a set of nonzero vectors $\{p_0, p_1, \cdots p_n\}$ is conjugate, it suffices the following relationship with respect to the symmetric positive definite matrix $\mathbf{H}$.

$$p_i^T \mathbf{H} p_j = 0 \ , \quad \text{for all } i \neq j \tag{3.5}$$

For a function approximated as a quadratic form, $\mathbf{H}$ is the Hessian matrix. In this regards, the search direction will be conjugate to the previous directions. The conjugate property is maintained from $\mathbf{p}_{h-1}$ to $\mathbf{p}_h$ by choosing each $\mathbf{p}_h$ to be a linear combination

of the steepest descent direction $-\nabla \mathbf{f}_h$ and the previous direction $\mathbf{p}_{h-1}$ (Nocedal and Wright, 1999). It can be simplified to iterations of the form

$$\mathbf{p}_h = -\nabla \mathbf{f}_h + \beta_h \mathbf{p}_{h-1} \tag{3.6}$$

where β_h is a scalar to be defined by requiring that $\mathbf{p}_{h-1}$ and $\mathbf{p}_h$ must be conjugate with respect to $\mathbf{H}$. In generating a set of conjugate vectors, the new vector $\mathbf{p}_h$ is computed using only the previous vector $\mathbf{p}_{h-1}$. This remarkable property implies that the method requires little storage and computation.

After determining the search direction $\mathbf{p}_h$, the following section is to evaluate the step length of searching as α_h. In computing the step length α_h, a trade-off is needed. The selection of α_h will give a substantial reduction of the objective function, but with a rather economical computational effort. The generally recognized belief is that α_h should be chosen to solve the one-dimensional minimization problem accurately, which is normally referred to as a line search or line minimization algorithm (Dennis and Schnabel, 1996). The line search is to determine the step length in one direction by minimizing a function of one variable without calculation of the derivative. In conjugate gradient method, a standard subroutine of Brent's method (Press *et al.*, 1992) is adopted herein to conduct line minimization.

Considering the nonlinear relations between stiffness, damping parameters and the objective function, only nonlinear variants of conjugate gradient method are covered here. Nonlinear CG methods differ from each other mainly in the choice of the parameter β_h. However, equivalent results will be produced for quadratic functions whichever β_h is chosen. Among these variants, the most commonly used one is proposed by Polak and Ribire (1969); Nocedal and Wright (1999). In their formulation, this parameter is defined as

$$\beta_{h+1} = \frac{\nabla \mathbf{f}_{h+1}^T (\nabla \mathbf{f}_{h+1} - \nabla \mathbf{f}_h)}{\nabla \mathbf{f}_h \cdot \nabla \mathbf{f}_h} \tag{3.7}$$

Normally, the first search direction $\mathbf{p}_0$ is chosen as the steepest descent direction at the

initial point $\mathbf{x}_0$. As in the general CG methods, we perform successive one-dimensional minimizations to determine a suitable step length along the conjugate search directions. Therefore a complete CG algorithm of Polak-Ribire version adopted in this study is formally as in Algorithm 3.

Algorithm 3 Conjugate gradient method

Given $\mathbf{x_0}$, convergence tolerance ϵ

Evaluate $f_0 = f(\mathbf{x_0})$, $\nabla \mathbf{f}_0 = \nabla \mathbf{f}(\mathbf{x}_0)$

Set initial search direction $\mathbf{p_0} = -\nabla \mathbf{f_0}$

$k \leftarrow 0$

While $\|\nabla \mathbf{f}_h\| > \epsilon$

Compute the step length α_h through 1D line minimization

Set $\mathbf{x}_{h+1} = \mathbf{x}_h + \alpha_h \mathbf{p}_h$

Evaluate $\nabla \mathbf{f}_{h+1}$

$$\beta_{h+1} \leftarrow \frac{\nabla \mathbf{f}_{h+1}^T (\nabla \mathbf{f}_{h+1} - \nabla \mathbf{f}_h)}{\nabla \mathbf{f}_h \cdot \nabla \mathbf{f}_h}$$

$\mathbf{p}_{h+1} \leftarrow -\nabla \mathbf{f}_{h+1} + \beta_{h+1} \mathbf{p}_h$

$h \leftarrow h + 1$

End While

Obviously in each run of the local search in system identification, the above CG method requires the evaluation of the objective function and its gradient. However, no matrix operations are performed unlike in classical Newton's method. It is observed that only a few vectors of storage are required in the CG method.

3.2.3 BFGS Method

The Broyden-Fletcher-Goldfarb-Shanno method is one of the most popular Quasi-Newton algorithms (Broyden, 1970; Fletcher, 1970; Goldfarb, 1970; Shanno, 1970; Nocedal and Wright, 1999). Before introducing the method, we consider finding a minimum through

Newton's method. It is based on the second-order Taylor series:

$$f(\mathbf{x}_{h+1}) = f(\mathbf{x}_h + \Delta\mathbf{x}_h) \approx f(\mathbf{x}_h) + \nabla\mathbf{f}^T(\mathbf{x}_h)\Delta\mathbf{x}_h + \frac{1}{2}\Delta\mathbf{x}_h{}^T\mathbf{H}_h\Delta\mathbf{x}_h \tag{3.8}$$

In this quadratic model, $\mathbf{H}_h$ is an $n \times n$ symmetric positive definite Hessian matrix. It will be revised or updated at every iteration. The underlying principle of Newton's method is to determine the stationary point of this quadratic approximation. Therefore it satisfies

$$\nabla\mathbf{f}(\mathbf{x}_h) + \mathbf{H}_h\Delta\mathbf{x}_h = 0 \tag{3.9}$$

where $\Delta\mathbf{x}_h = \mathbf{x}_{h+1} - \mathbf{x}_h = \alpha_h\mathbf{p}_h$, it is defined by the product of the step size and the vector of search direction. Hence Newton's method leads to

$$\mathbf{x}_{h+1} = \mathbf{x}_h - \alpha_h\mathbf{H}_h^{-1}\nabla\mathbf{f}(\mathbf{x}_h) \tag{3.10}$$

Normally Newton's method only converges if the initial point is sufficiently close to the solution. In each loop the inverse of Hessian matrix $\mathbf{H}_h^{-1}$ has to be computed and stored, and this is prohibitively expensive in storage even for moderate systems. By introducing the idea of Quasi-Newton, however, the inverse Hessian matrix is iteratively approximated instead. That is

$$\lim_{i\to\infty}\mathbf{A}_i = \mathbf{H}^{-1} = (\nabla^2\mathbf{f})^{-1} \tag{3.11}$$

Without computing the Hessian matrix at every iteration, this inverse Hessian approximation $\mathbf{A}$ is used instead to achieve a more economical computational effort. Hence Eq. (3.10) is rewritten as

$$\mathbf{x}_{h+1} = \mathbf{x}_h - \alpha_h\mathbf{A}_{h+1}\nabla\mathbf{f}(\mathbf{x}_h) \tag{3.12}$$

The difference of various Quasi-Newton methods lies in the Hessian approximation matrix $\mathbf{H}$. If the change in gradients $\mathbf{g}$ is

$$\mathbf{g}_h = \nabla\mathbf{f}_{h+1} - \nabla\mathbf{f}_h \tag{3.13}$$

then in the most popular Quasi-Newton method, i.e., BFGS, this Hessian approximation is defined as

$$\mathbf{A}_{h+1} = \left(I - \frac{\Delta \mathbf{x}_h \mathbf{g}_h{}^T}{\mathbf{g}_h{}^T \Delta \mathbf{x}_h} \right) \mathbf{A}_h \left(I - \frac{\mathbf{g}_h \Delta \mathbf{x}_h{}^T}{\mathbf{g}_h{}^T \Delta \mathbf{x}_h} \right) + \frac{\Delta \mathbf{x}_h \Delta \mathbf{x}_h{}^T}{\mathbf{g}_h{}^T \Delta \mathbf{x}_h} \tag{3.14}$$

The Hessian approximation matrix $\mathbf{A}$ updates through combining the most recently observed information about the objective function with the existing knowledge within the current Hessian approximation. It is observed that Quasi-Newton methods require only the gradient of the objective function to be supplied at each iteration. By measuring the changes in gradients, a model of the objective function can be constructed that is good enough to produce super linear convergence (Nocedal and Wright, 1999). For practical implementation the complete loop of BFGS is shown in Algorithm 4.

Algorithm 4 BFGS method

Given $\mathbf{x}_0$, convergence tolerance ϵ

Set inverse Hessian approximation $\mathbf{A_0}$

$k \leftarrow 0$

While $\|\nabla \mathbf{f}_h\| > \epsilon$

Compute search direction $\mathbf{p}_h = -\mathbf{A}_h \nabla \mathbf{f}_h$

Compute the step length α_h through 1D line minimization

Set $\mathbf{x}_{h+1} = \mathbf{x}_h + \alpha_h \mathbf{p}_h$

Compute $\mathbf{A}_{h+1}$

$h \leftarrow h + 1$

End While

In the above procedure, the initial approximation $\mathbf{A}_0$ is generally set to be the identity matrix. One dimensional minimization for choosing α_h is implemented by standard backtracking line search subroutine (Press *et al.*, 1992). Quasi-Newton methods are often more efficient than Newton's method as the second derivatives are not required. Compared to BFGS method, Newton's method converges quadratically and more rapidly than the super linear convergence of BFGS, but the cost per iteration is much higher. As for

quasi-Newton methods and CG, the former is usually efficient in small problems than the latter. But for large problems the CG is believed to be more powerful in efficiency, since CG uses only function and gradient information in minimizing a function. A superior strength is that CG does not store any approximation to the second-derivative matrix.

3.3 Formulation of Objective Function, Gradient, and Convergence Criteria

To implement the hybrid optimization strategy, namely iSSRM with local search, the formulation of fitness function, the gradient and convergence criteria are derived in this section. The objective function and its derivatives will have significant influence on the numerical convergence, and they have to be defined specifically for the two parts of search. In this study, the formulation by Koh *et al.* (2003a) is used for the preliminary iSSRM search. The strength lies in the incorporation of an equivalent influence factor for all measurements. By construction, measurement locations that have smaller response magnitude can contribute equally to the fitness function. The formulation is given as

$$\phi = \frac{1}{0.001 + \varepsilon} \tag{3.15}$$

where $\varepsilon = \frac{1}{p}\sum_{i=1}^{p} w_i \varepsilon_i$; $\varepsilon_i = \frac{1}{q}\sum_{j=1}^{q} (\ddot{u}_{ij}^m - \ddot{u}_{ij}^e)^2$; $\mu = \sqrt{\frac{1}{q}\left(\sum_{j=1}^{q} (\ddot{u}_{ij}^m)^2\right)}$; $\bar{\mu} = \sum_{i=1}^{p} \frac{\mu_i}{p}$; $w_i = \frac{\bar{\mu}_i}{\mu_i}$

These data are collected from p measurements with the data length of q. Error ε_i is weighted based on the root mean square of each measurement. On the other hand, among the three proposed local searchers, two of them, i.e., BFGS and CG are gradient based search relying heavily on the derivatives of objective function. These two methods will be inefficient if the objective function produces a considerably sharp peak in fitness surface, as the step length has to be adjusted frequently to approach the peak. Therefore in the second part of the hybrid strategy, the fitness function is modified to conduct

minimization via objective function ϑ defined in

$$\vartheta = -\ln(\phi) \tag{3.16}$$

Based on the idea of peak shifting, a "ln" function will beneficial to reduce the relative magnitudes of fitness peaks. The CG and BFGS local searchers will then be easier to locate the global peak. The reason is that, for the gradient based search methods, too sharp a global peak will induce expensive iterations to progressively adjust the search direction and step length.

In the local search, both BFGS and CG methods require that the gradient or the first partial derivatives of fitness function can be computed at arbitrary points. Rigorously speaking, these methods require analytical expression of the derivatives. They are therefore applicable only to differentiable functions. In the present problem, however, the objective function cannot be explicitly expressed as a function of unknowns. The gradient at the trial point would not be evaluated exactly. Therefore if a set of solution $\mathbf{x}$ is expressed as $\mathbf{x} = \{x_1, x_2 \cdots x_k\}$, representing stiffness, damping and/or mass, the gradient of fitness function has to take the form as numerical approximation, for example, in a forward-difference expression as

$$\nabla\vartheta(x) = \left[\begin{array}{cccc} \dfrac{\partial\vartheta_h}{\partial x_1} & \dfrac{\partial\vartheta_h}{\partial x_2} & \cdots & \dfrac{\partial\vartheta_h}{\partial x_k} \end{array} \right]^T \tag{3.17}$$

where $\dfrac{\partial\vartheta_h}{\partial x_i} \approx \dfrac{1}{\delta}\left[\vartheta(x_1^h, x_2^h \cdots x_i^h + \delta \cdots x_k^h) - \vartheta(x_1^h, x_2^h \cdots x_i^h \cdots x_k^h)\right]$, δ is the step length.

In the present study, damping ratios are treated as unknown together with the stiffness parameters. However, the damping parameters are of drastically different orders in magnitudes from the stiffness parameters. It will pose significant numerical difficulty for gradient based local searchers as CG and BFGS. Consider the gradient approximation defined in Eq. (3.17), change in one direction can induce much larger variations in the fitness function than that in another direction. The gradient will therefore differ substantially from one to another, as the sensitivity of parameters varies considerably.

Consequently the algorithms will end up with a set of exaggerated derivatives such that the parameters with relatively smaller magnitudes will not be sensitive at all to reflect the rational evolution. A diagonal scaling procedure (Dennis and Schnabel, 1996) is adopted to transform all the unknowns into a new set of variables, which will be within an order of magnitude of one. Therefore the variance in the gradient will be more balanced.

The convergence of the proposed hybrid optimization strategy is determined in two steps. For the global search by iSSRM, the convergence is set as a fixed number of fitness evaluations. Because the iSSRM method is used for preliminary search and it is not required to ensure convergence. For local search, two convergence criteria are established. One is based on the relative changes in successive values of $\mathbf{x}$

$$\frac{|\mathbf{x}_{h+1}^i - \mathbf{x}_h^i|}{\max\{|\mathbf{x}_{h+1}^i|, \text{typ}(\mathbf{x})\}} \leq \epsilon_x \ , \quad (1 \leq i \leq n) \tag{3.18}$$

and the other is to use the relative gradients

$$\max_{1 \leq i \leq n} \frac{\nabla\vartheta(\mathbf{x}_h^i)\max\{|\mathbf{x}_{h+1}^i|, \text{typ}(\mathbf{x})\}}{\max\{|\vartheta(\mathbf{x}_{h+1}^i)|, \text{typ}(\vartheta)\}} \leq \epsilon_g \tag{3.19}$$

where $\text{typ}(\mathbf{x})$ and $\text{typ}(\vartheta)$ are the user-defined typical magnitudes of the variables $\mathbf{x}$ and the value of ϑ, respectively. Setting typical magnitudes of variables and objective function values here is to avoid numerical difficulties of measuring relative change when the argument is near zero (Dennis and Schnabel, 1996). For example, a good trial start for these two values could be 1.0 which would only be unsatisfactory when the magnitudes of the variable and objective function are always much smaller than 1.0. ϵ_x and ϵ_g are the predefined tolerances for the variables and gradients. The local search is considered to have converged when any one of the convergence criteria is satisfied.

3.4 Parametric Study for Balanced Global and Local Search

Parametric study on the hybrid strategy is necessary in order to have an allocation of total evaluation effort in a balanced iSSRM search and local search. The investigation

here includes the determination of the "switch point" between the global iSSRM search and the local search. As for the GA parameters in iSSRM method, the parameters recommended in Chapter 2 cannot be used directly herein since they are obtained by testing iSSRM itself under fixed evaluations for certain problems. If the number of evaluations changes, the trade-off by the recommended set of exact iSSRM parameter will be changed accordingly. Nevertheless, it is reasonable to assume that the allocation of total evaluations into different iSSRM component search is scalable to the number of total evaluations. To be specific, the ratios of evaluations used for outer sampling test and inner MGAMAS of iSSRM are constant regardless of the total evaluations for different problems.

To avoid tedious computations herein, the investigation in this section will take advantage of the available experience based on the previous chapter. First, the total evaluations follow those used in Chapter 2, i.e., Table 2.11. Second, the effort in sampling test will be simplified by using the same sampling ratio for the corresponding system. The sampling ratio is defined by the evaluations in sampling test divided by total iSSRM evaluations, which can be derived from Table 2.11 of Chapter 2. For example, the ratio is taken as 0.63, 0.54 and 0.248, for 5-DOF, 10-DOF, and 20-DOF systems, respectively, in the known mass case. The ratio is taken 0.18, 0.165, and 0.042 for these systems in the unknown mass case. With known total evaluation and sampling ratio, the evaluations used for sampling test and MGAMAS are then fixed.

The allocation of total evaluations to MGAMAS search will not be repeated with further considerations in the sampling size, population size, generation size, and total number of runs. They are considered in a much simplified way herein. Following the recommendations in Chapter 2 to keep population size small , the population size is taken as $0.15\sqrt{N_E}$, where N_E is the number of total evaluations. Furthermore, the number of total runs will follow those obtained in Chapter 2. Therefore, if the evaluations used for iSSRM is determined, the size of generation can be established, i.e., by Eq. (2.17), with

given sample size, population size, and number of total runs.

The final task is to select the switch point for iSSRM search and local search in the enhanced strategy. Instead of concluding a switch point from time consuming parametric studies, a reasonable switch point will be determined from the convergence history by using merely iSSRM method. It should be noted that the identification reported herein is performed in the absence of noise, since measurement noise will not introduce local optima and thus makes not much difference for the convergence behavior to be investigated. From the identification of different systems, Figs. 3.26 and 3.27 show a consistent performance of iSSRM method based on average over 25 runs. Using merely iSSRM method, the convergence speed is much faster in the first half than the rest of the whole history. This indicates that the switch point could be in the first half of the whole history.

Therefore the switch from iSSRM to local search will be determined by comparing the following five cases, i.e., 10%, 20%, 30%, 40%, and 50% of total evaluations based on using merely iSSRM search. The present investigation is implemented on a 20-DOF system with noise-free measurement and known mass. The BFGS method is considered as local searcher. According to the results presented in Table 2.11, the total evaluations are 40,000 for 20-DOF known mass system. Therefore the evaluations used for “10%”, “20%”, “30%”, “40%”, and “50%” initial iSSRM search of the enhanced strategy are 4,000, 8,000, 12,000, 16,000, and 20,000, respectively. The results are given in details in Table 3.1. The corresponding performance of iSSRM and gradient search are shown in Fig. 3.30. The results conservatively suggest 20% of total evaluations should be recommended for the switch point for the enhanced identification strategy. The reason is that 10% of total evaluations, i.e., 4,000 for ”Case I”, will give identification error of 5.79% and 20% of total evaluations will significantly reduce the identification error to 2.77%. Further more evaluations out of the total evaluations allocated for iSSRM will only make marginal reduction of the identification error.

Besides the considerations in convergence speed, it has to be ensured as well that there will be no more local optima after switching to local search, especially gradient search. The mean identification errors in Figs. 3.26 and 3.27 show fairly uneven curves in convergence in the first 20% of the whole history, particularly for the unknown mass systems. These results suggest that a closer investigation is necessary for representative convergence histories. Therefore typical convergence histories of 20-DOF system are presented in known and unknown cases, i.e., Figs. 3.28 and 3.29. The stepped jump in the fitness history with uneven improvement in the identification error history indicates that at least the first 20% of the whole history should focus on iSSRM search to overcome local optima far away from the global peak. Furthermore, similar conclusions can be drawn from identifying the 20-DOF system under 10% noise, i.e., Fig. 2.11. In addition, if there is a tight requirement on limiting the number of total evaluations, the 10% case is also possible for known mass identification as it reduces identification error with an acceptable computational cost.

3.5 Numerical Examples

To verify the "peak shifting" hypothesis and the proposed hybrid optimization strategy, three examples are investigated. They are a 10-DOF lumped mass system, a plate structure and a truss model, shown in Figs. 3.31, 3.32, and 3.33. The search space is typically set from 0.5 to 2.0. That is, the lower and upper bounds are half and twice of the actual values. In the identification, mass distribution of the structures is assumed as known while the stiffness and two damping coefficient are to be identified. Due to random excitations, accelerations are generated by constant-average-acceleration Newmark method. Both the input and output are assumed to be contaminated by Gaussian white noise with zero mean and variance of one. The noise level is considered at 0%, 5%, and 10%. The parametric study has been carried out for the proposed iSSRM and the local search methods, leading to the values used in this study. Considering the random nature

of iSSRM, the results reported in the following are the average from 25 runs. Computer time is reported on basis of a two-processor workstation with 3.0-GHz CPU.

3.5.1 Lumped Mass System of 10 DOFs

In order to compare the performance of proposed identification strategy, a 10-DOF lumped mass system is used Koh *et al.* (2003a). The structure is a plane shear building modelled as a 10-DOF lumped mass system. As shown in Fig. 3.31, the input random forces are applied at the 10^{th} level, and accelerations are instrumented at levels 2, 4, 6, 8, and 10. The actual damping is set to be 5% to the first two modes.

In the hybrid optimization strategy, i.e., iSSRM method with local search, the convergence tolerance is set to be 10^{-6} and the step length δ in Eq. (3.17) is taken as 10^{-6} for numerical evaluation of the gradients. For SA method, the ratio of annealing is set to be 0.9, the starting temperature is 3.0. The iteration will exit when the convergence limit of 10^{-6} or the maximum evaluations of 20,000 is reached. By adopting Corana's method (Corana *et al.*, 1987) to define the neighbourhood, the initial step length vector is 1.0 and the adjustment vector of step length is 2.0. A comprehensive comparison with published methods (Perry *et al.*, 2006) and results (Koh *et al.*, 2003a) is presented in Table 3.4 with the parameter setting in Table 3.3. As shown, improvements by the local searchers are so significant that almost the exact value can be identified in the absence of noise. The maximum errors in these cases are found to be practically zero for gradient based CG and BFGS, which are better than non-gradient based SA. The result implies that the global peak is captured by three local searchers in all runs.

In the presence of 10% noise, the accuracy of the results is similar to that reported in Koh *et al.* (2003a). Nevertheless, the total evaluations by iSSRM with BFGS are 2,590 evaluations which are much faster than the reported result of 30,000 evaluations used in Koh *et al.* (2003a). The global peak is believed to be identified since the result by BFGS

and CG local search can reach the same accuracy as that by the non-gradient based SA. Furthermore, the gradient based local searchers CG and BFGS are rational to be more efficient than non-gradient based SA in locating the sharp peak. As shown in Table 3.4, the total evaluations are 2,590 for BFGS, 2,766 for CG, and 21,980 for SA in the case of 10% noise. Besides, it is also observed in Table 3.4 that the number of evaluations required by CG is larger than that of BFGS. The reason is that the line minimization adopted by BFGS is more efficient than CG.

3.5.2 Cantilever Plate of 16 Elements and 168 DOFs

To investigate the proposed method in a different structure, a 1-cm thick aluminum plate with a dimension 0.8 m long and 0.6 m wide is considered, i.e., Fig. 3.32. The plate is supported rigidly along a single edge. At one of free corners of the plate, a random force with white noise distribution is applied as external excitation. The plate is modeled as a 4×4 mesh via 8-node Mindlin plate element, with selective integration to avoid spurious modes (Hinton and Owen, 1984). Therefore a total number of 168 DOFs are involved. Out of them only 6 translational accelerations are measured for identifying the whole plate. The accelerations are measured within 500 time steps of a sampling rate of 40 kHz. The very high sampling rate is to ensure that the higher frequencies of the structure can be accurately captured. Damping ratio of 1% is equally set for the 1^{st} and 2^{nd} modes of the whole plate.

Compared to the previous example, the following modifications are found to be constructive to carry out the hybrid optimization strategy. For SA local search, the ratio of annealing is set to be 0.85, the initial temperature is 5.0 and the maximum evaluations are 20,000. All the other settings remain the same as the previous example of lumped mass system. Results in Table 3.6 show that the global peak is accurately identified by the local searchers in noise free case. The mean and maximum errors are found to be zero for all three local searchers. This indicates that there is only one global fitness peak

for present identification in the noise free case. An interesting phenomenon in Table 3.6 is that total number of evaluations and computer time decrease significantly for CG in 10% noise case. The identification accuracy reached is still of the same magnitude as SA. This tendency in the results reasonably reflects the effect of "peak-shifting". As noise level increases, the global extreme of fitness function will reduce and shift simultaneously. Brent's method of line minimization is used in CG, where a parabolic interpolation is used to determine the step length without information of gradients. When the shape of objective function is as smooth as a parabola, this algorithm will be efficient to determine the step length by using the approximated minimum of the fitted parabolic function. Therefore it will be easier for CG local searcher to locate the global peak in the noise case than the noise free case. Nevertheless, the superiority of BFGS local search is found to outperform over CG and SA. It can accomplish the identification with good accuracy as well as reduce the computational time significantly.

3.5.3 Truss of 29 Elements and 28 DOFs

The proposed method is now tested for in a more challenging structure. Measurements available in this truss example are much less than the previous two examples in relation to the number of unknown stiffness parameters, i.e., higher ratio of unknown parameters to measurements available. The present structure is a model of steel truss bridge. Young's modulus of the material is 200 GPa, and density is 7800 kg/m^3. The outer diameter of the steel tube is 1.55 cm and the inner diameter is 1.09 cm, resulting in a sectional area of 0.9538×10^{-4} m^2. The structure is excited by two random forces and accelerations are measured at 5 locations, as illustrated in Fig. 3.33. Proportional damping ratio of 2% is assumed for the first two modes. To identify this structure, parameters of the proposed algorithm are listed in Table 3.7.

The results in Table 3.8 show that the performance for the proposed hybrid optimization strategy is consistently excellent in the noise free case. The global peak is

believed to be found by CG and BFGS with and without noise, because their accuracy of the identification results are similar to those by SA. It is also noted that the mean identification error by iSSRM with BFGS is as small as 3.23% under 10% noise. At the same time, the computer time is only around 3 minutes and almost a quarter of that is used by SSRM. Local search by CG will generally use more fitness evaluations, and accordingly cost more time than BFGS. Most of the computer time is found to be used in line search procedure. Most of the computer time is found to be used in line search procedure. As mentioned before, the line minimization implemented in CG is of less efficiency than in BFGS, because much less function evaluations are carried out to find an acceptable step length.

3.6 Conclusions

In this study, noise induced peak shifting is observed for optimization oriented structural identification. This observation leads to a more efficient hybrid solver for system identification. The hybrid identification strategy involves an improved SSRM via sampling and local search. The method of iSSRM facilitates adaptively rescaling of search limit by an initial sampling test. It is used to deal with local optima and provides a starting point for local search. As an efficient local searcher, BFGS is recommended over CG and SA methods in this study. Numerical investigation includes a 10-DOF lumped mass system, a 168-DOF plate structure and a 28-DOF steel truss model. The proposed hybrid optimization strategy has been successfully applied in the identification of the structural stiffness distribution. The conclusions and recommendations could be drawn as follows.

(1) Treated as an optimization problem, measurement noise makes the peak of fitness function shift and decrease. An increase in the noise level seldom produces new local optima in the vicinity of the original extreme peak.

(2) Among the three local searchers, the BFGS method is more efficient than the CG

and SA methods in achieving good accuracy. In fact, this method can be readily extended to larger system identification problems by using limited-memory BFGS (L-BFGS) method (Liu and Nocedal, 1989). However, it may be impractical to use other methods including Gauss-Newton or Levenberg-Marquardt algorithms, which require evaluating and storing a modified Jacobian matrix in every step.

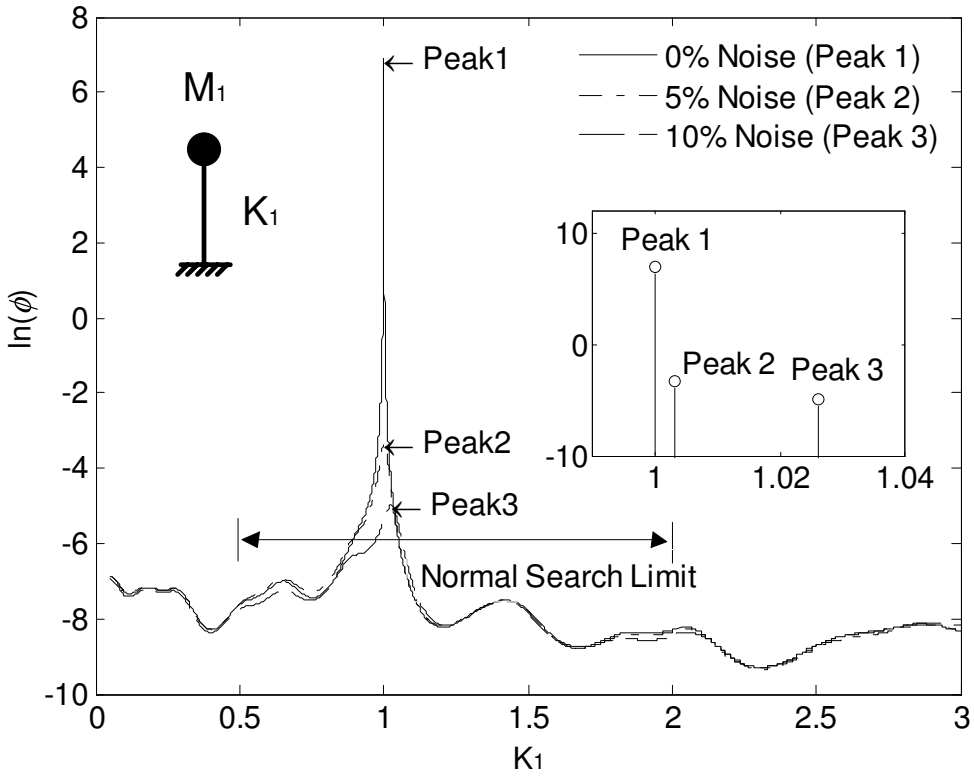

Figure 3.1: Typical peak shifting of 1-DOF known mass system

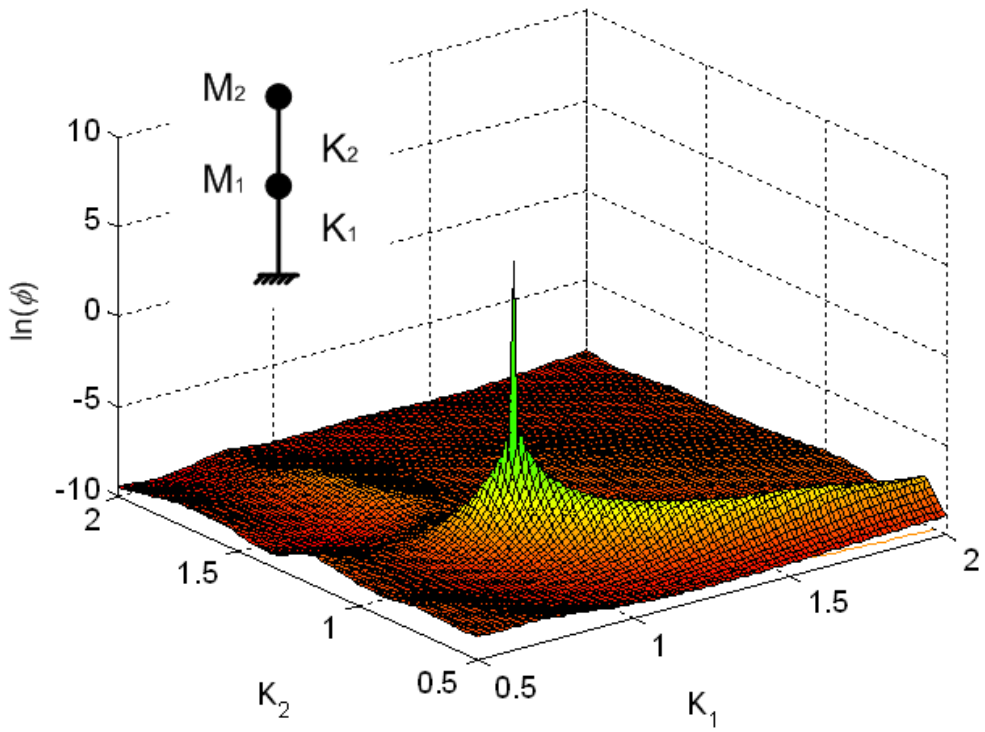

Figure 3.2: Typical peak shifting of 2-DOF known mass system under 0% noise: 3D view

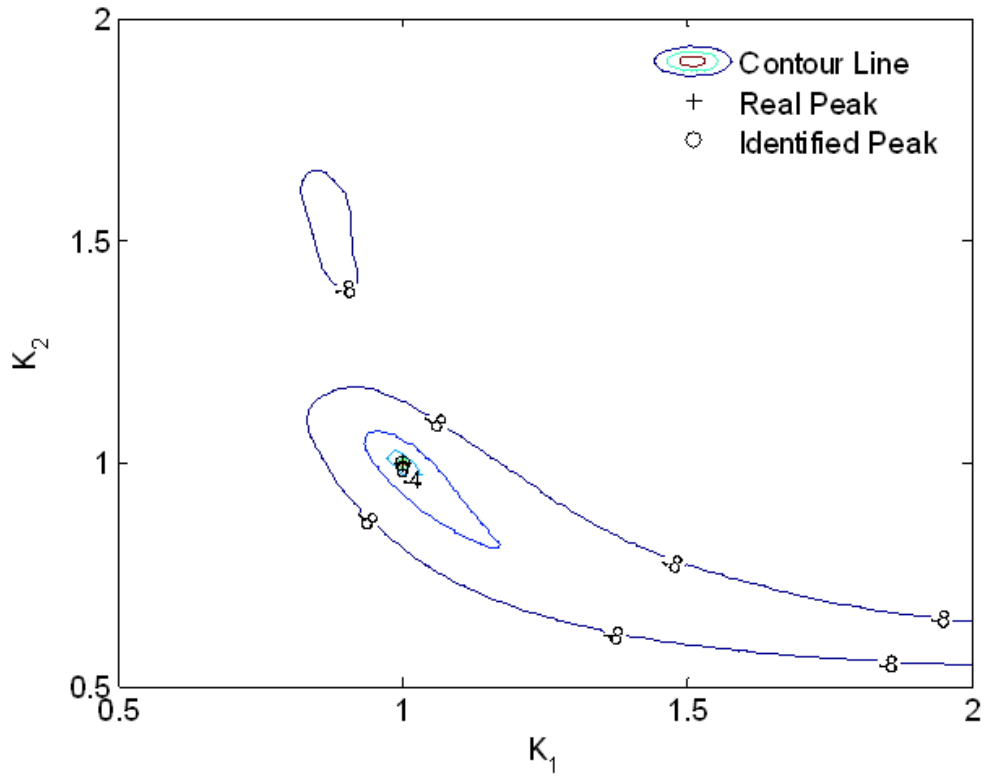

Figure 3.3: Typical peak shifting of 2-DOF known mass system under 0% noise: contour

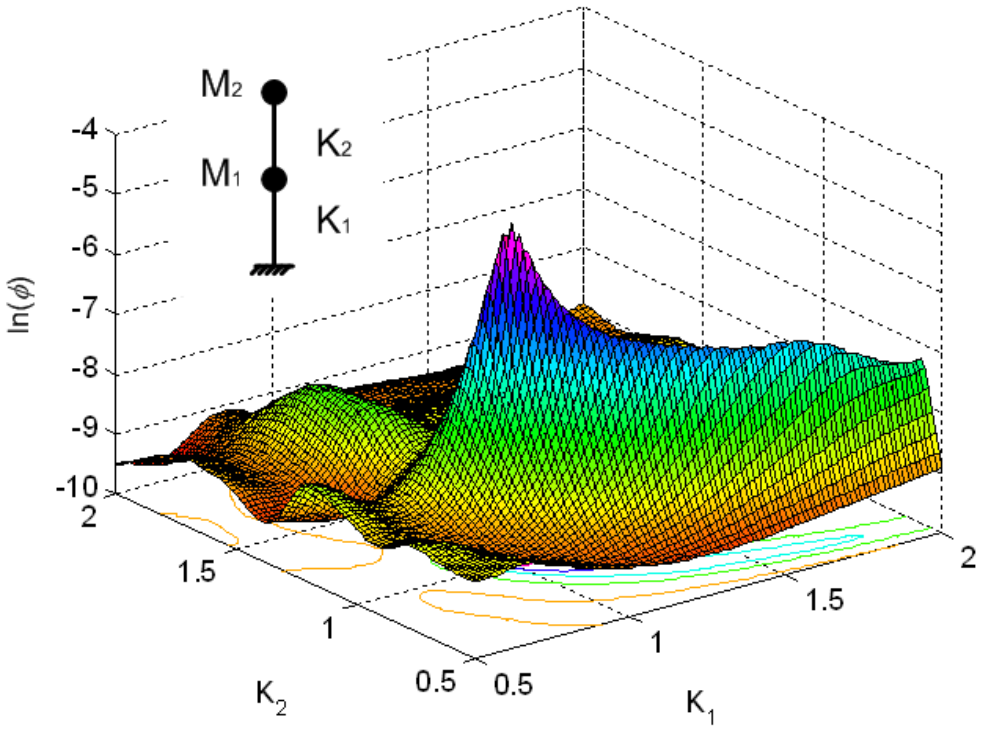

Figure 3.4: Typical peak shifting of 2-DOF known mass system under 5% noise: 3D view

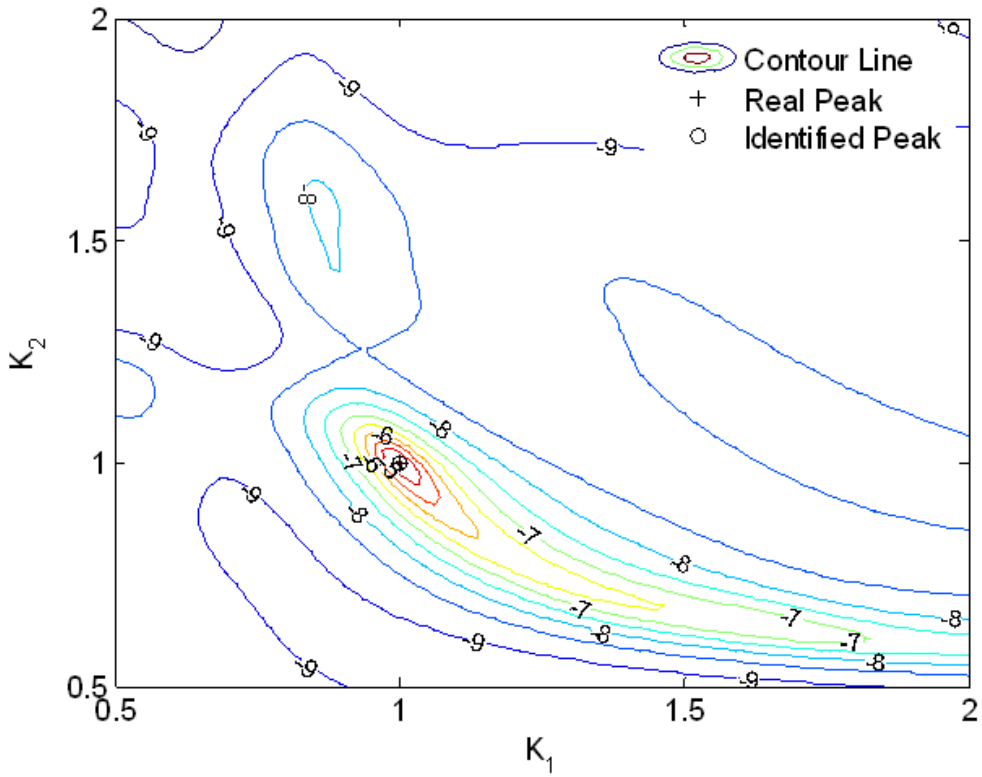

Figure 3.5: Typical peak shifting of 2-DOF known mass system under 5% noise: contour

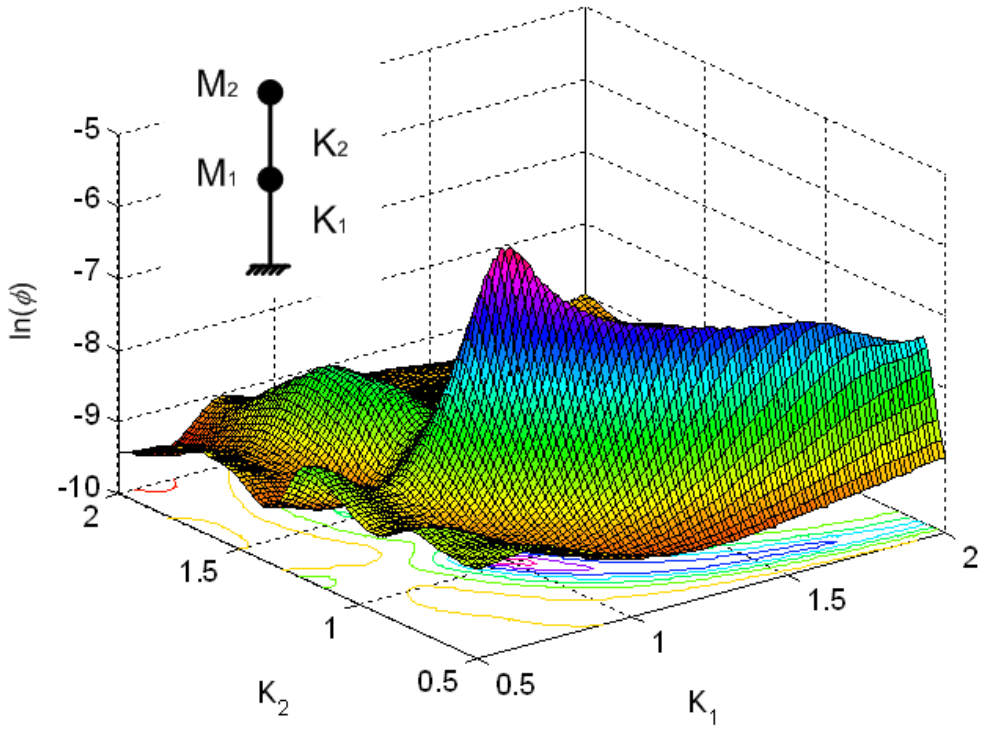

Figure 3.6: Typical peak shifting of 2-DOF known mass system under 10% noise: 3D view

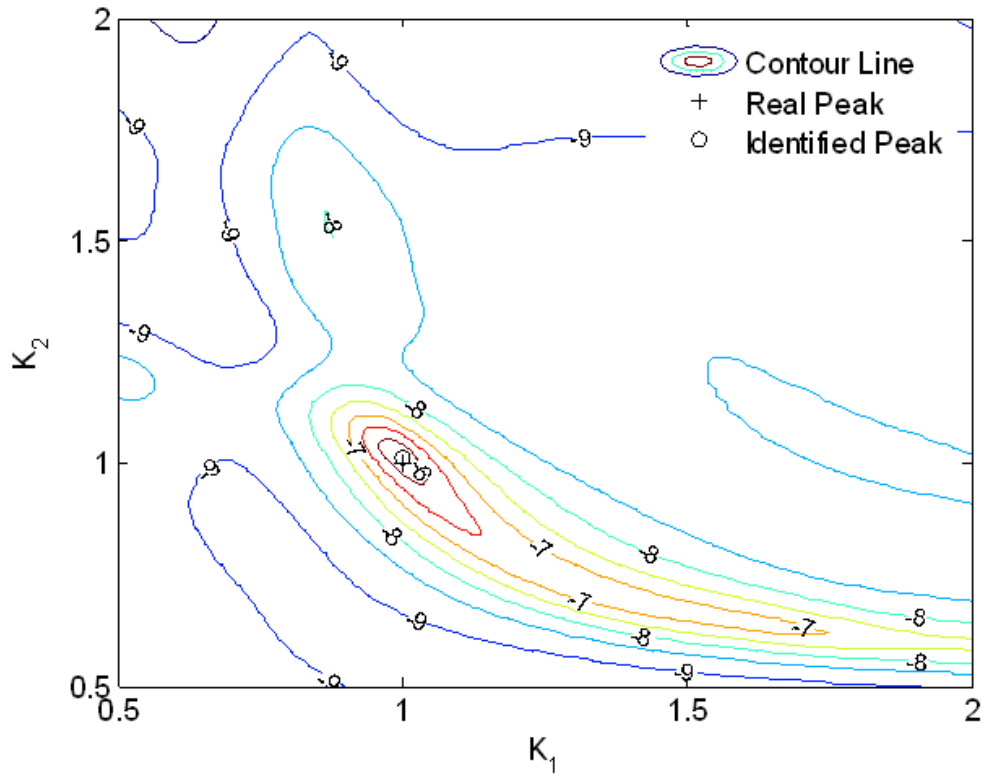

Figure 3.7: Typical peak shifting of 2-DOF system under 10% noise: contour

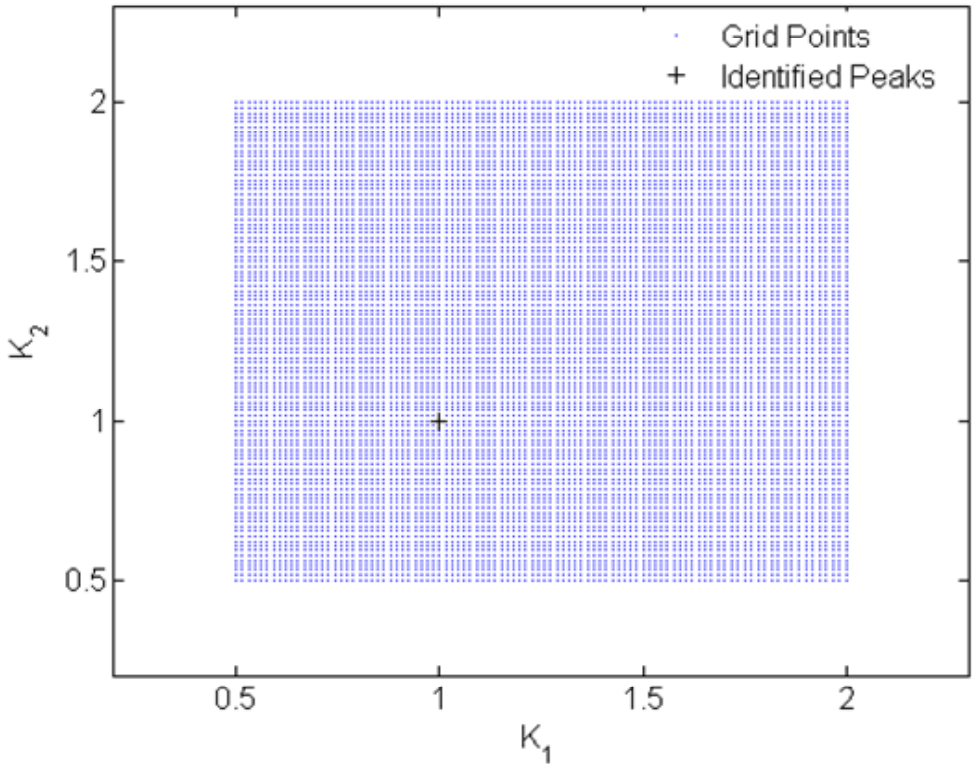

Figure 3.8: Peak shifting of 2-DOF known mass system under 10,000 cases: 0% noise

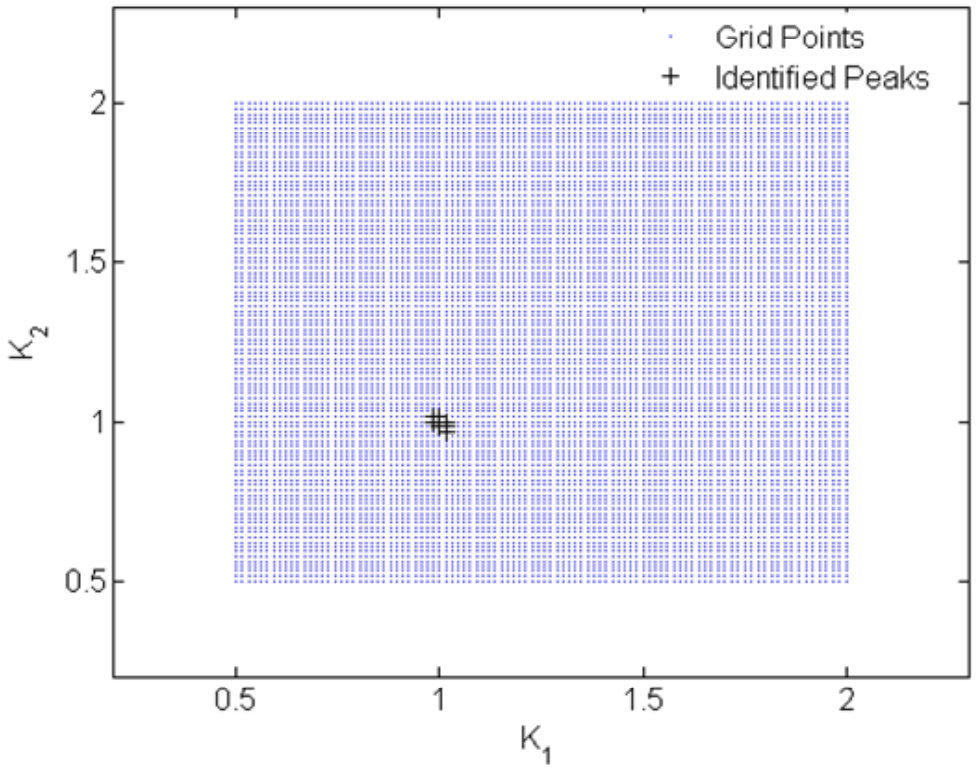

Figure 3.9: Peak shifting of 2-DOF known mass system under 10,000 cases: 5% noise

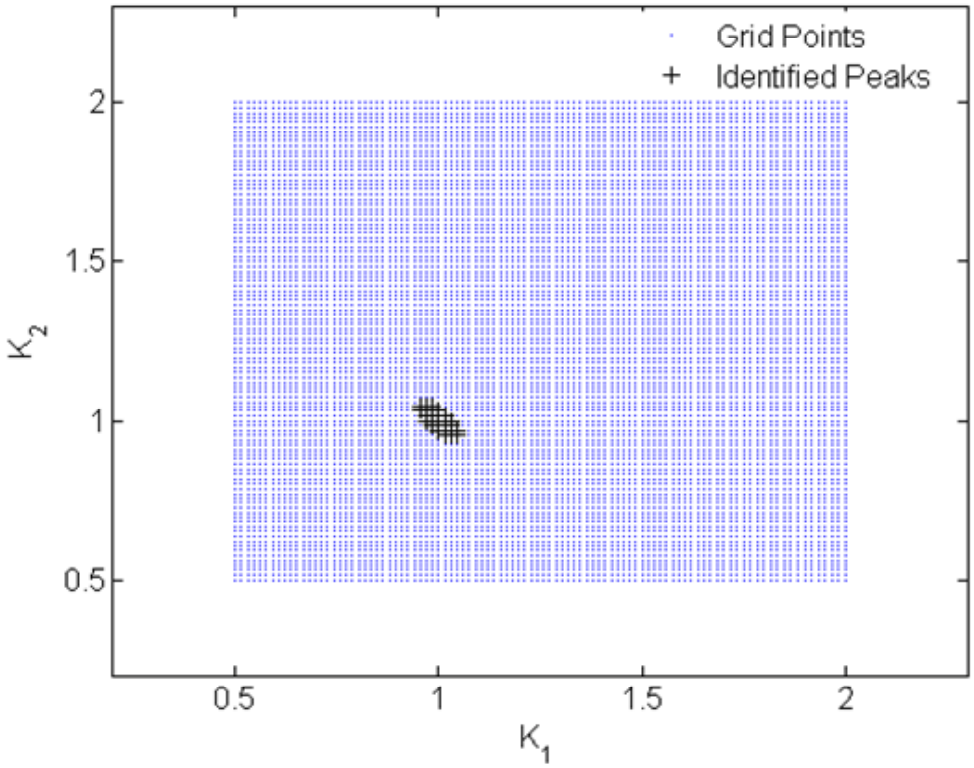

Figure 3.10: Peak shifting of 2-DOF known mass system under 10,000 cases: 10% noise

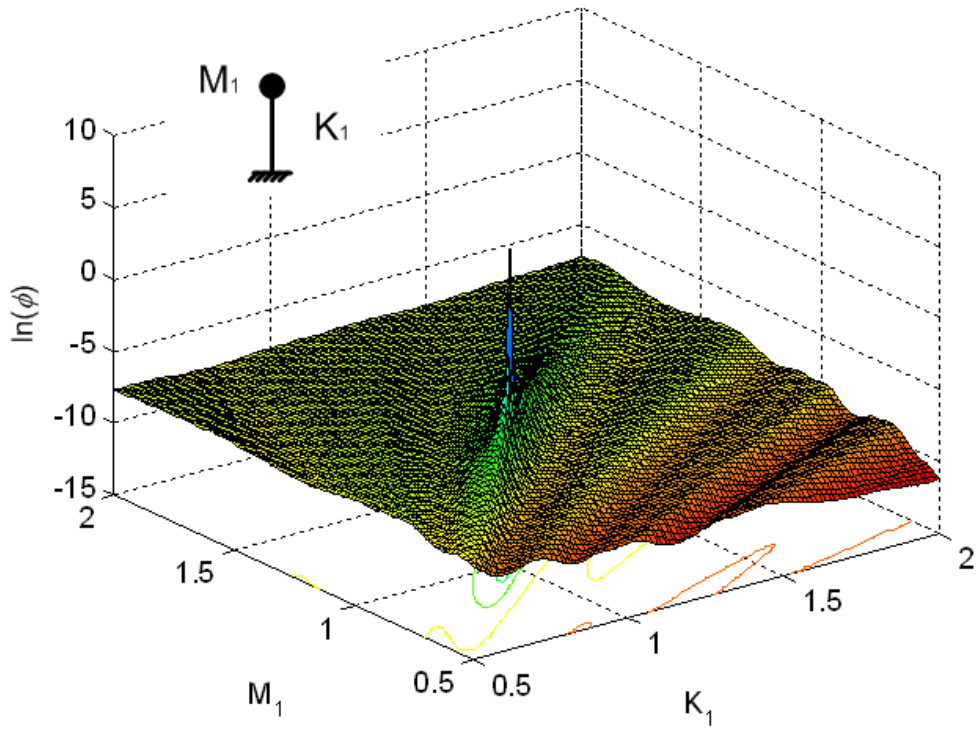

Figure 3.11: Typical peak shifting of 1-DOF unknown mass system under 0% noise: 3D view

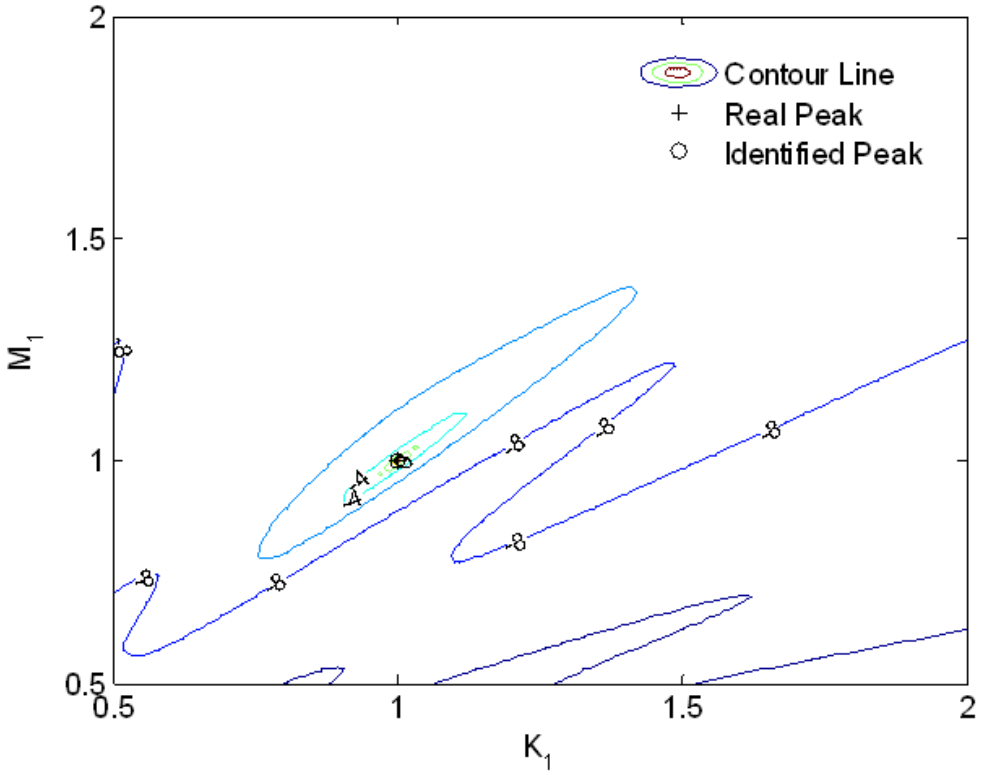

Figure 3.12: Typical peak shifting of 1-DOF unknown mass system under 0% noise: contour 1

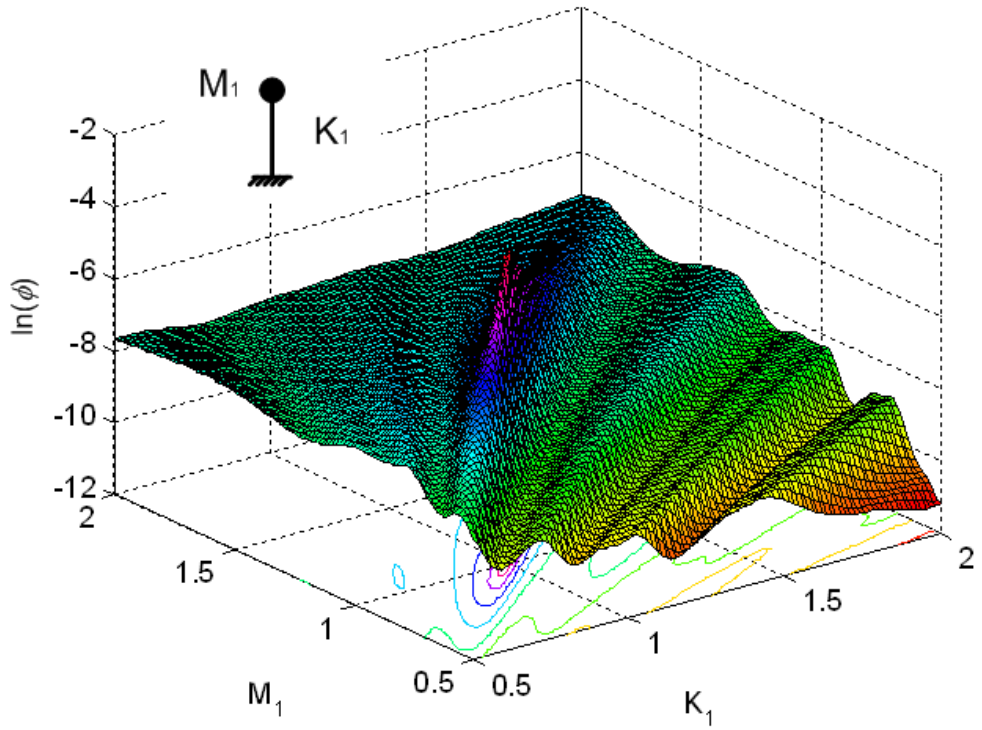

Figure 3.13: Typical peak shifting of 1-DOF unknown mass system under 5% noise: 3D view

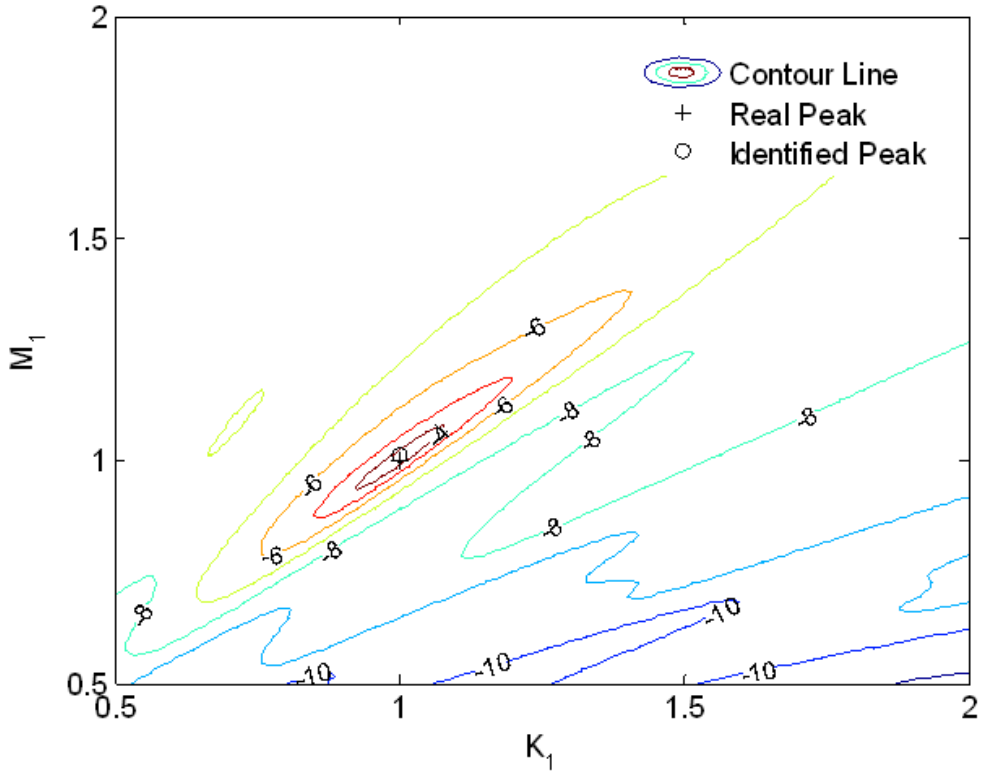

Figure 3.14: Typical peak shifting of 1-DOF unknown mass system under 5% noise: contour 1

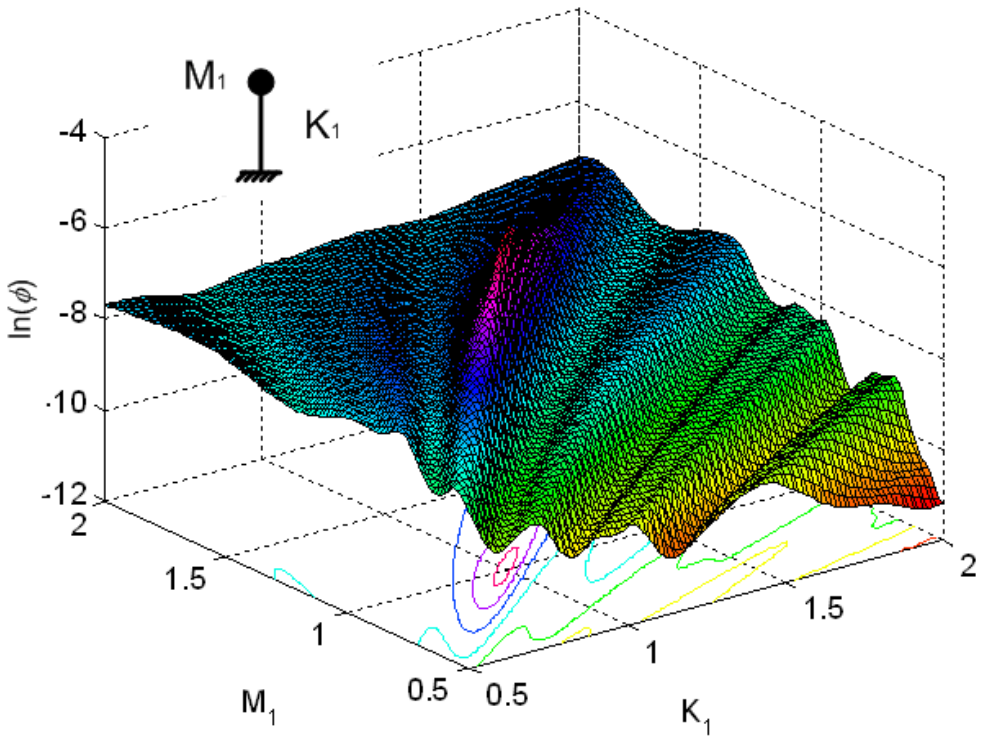

Figure 3.15: Typical peak shifting of 1-DOF unknown mass system under 10% noise: 3D view

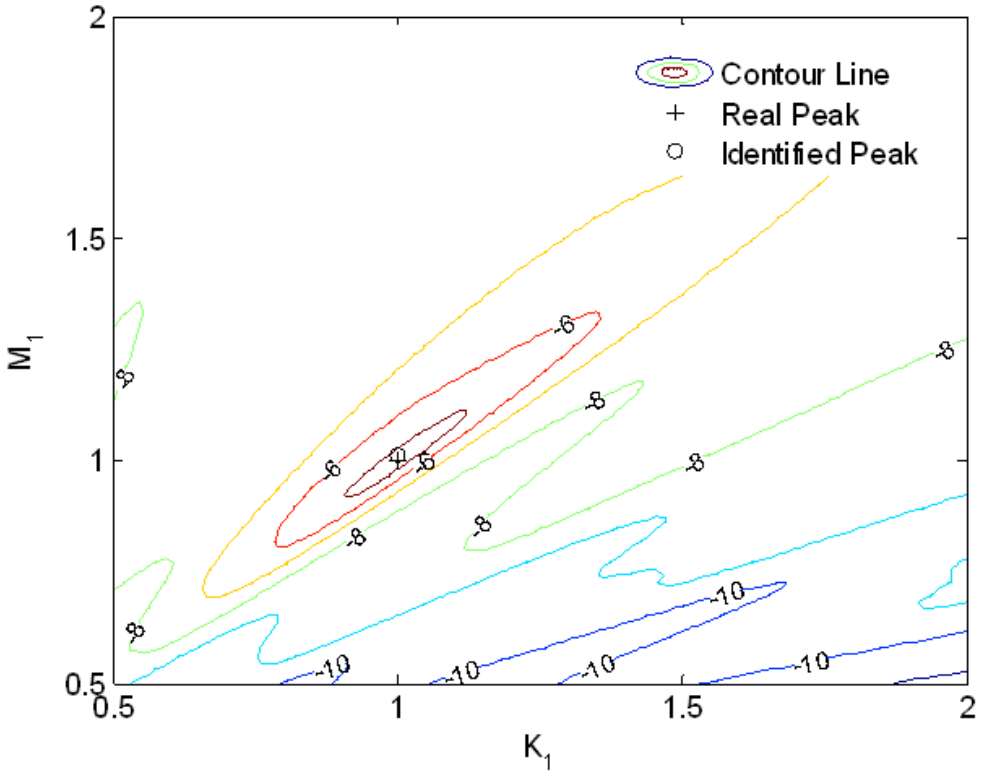

Figure 3.16: Typical peak shifting of 1-DOF unknown mass system under 10% noise: contour 1

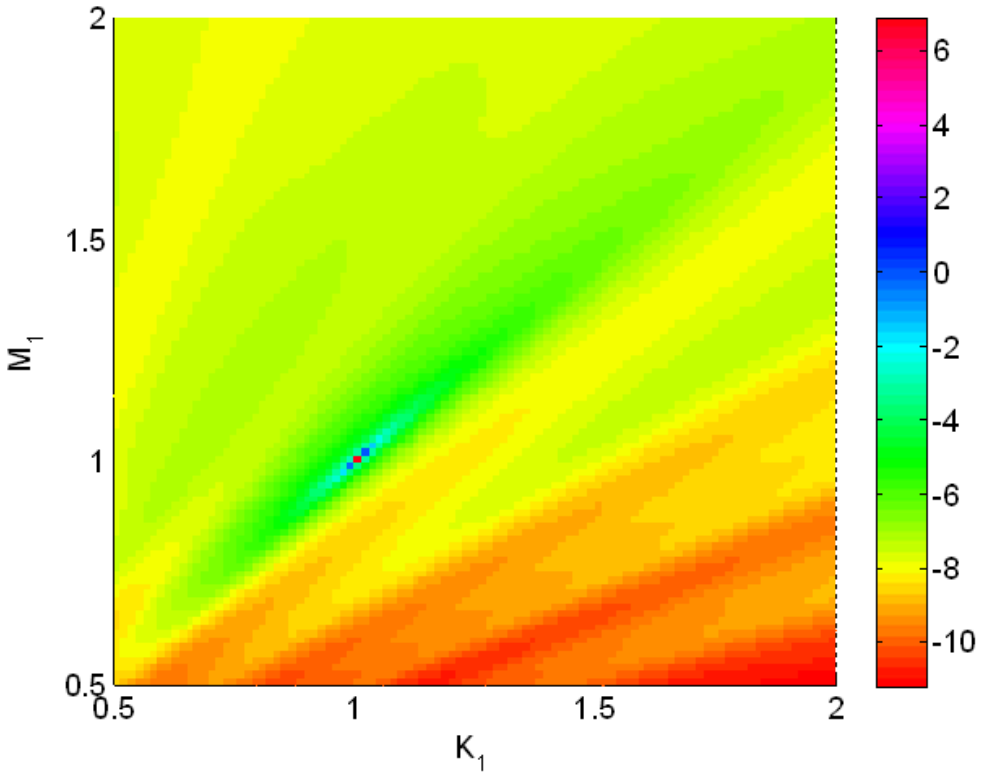

Figure 3.17: Typical peak shifting of 1-DOF unknown mass system under 0% noise: contour 2

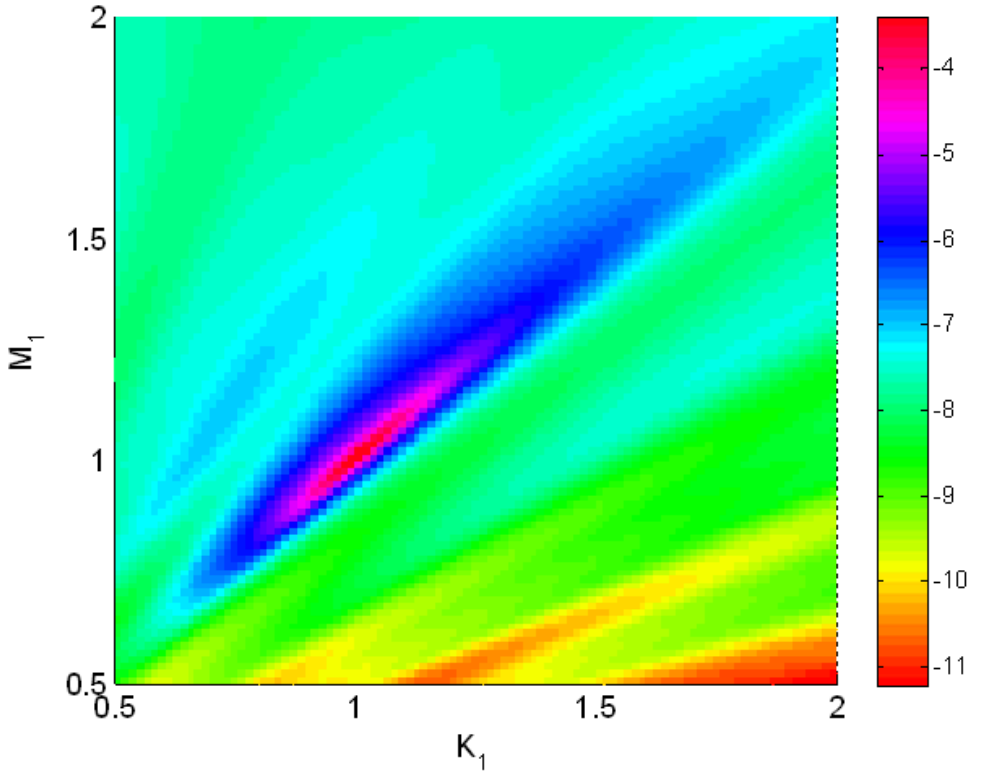

Figure 3.18: Typical peak shifting of 1-DOF unknown mass system under 5% noise: contour 2

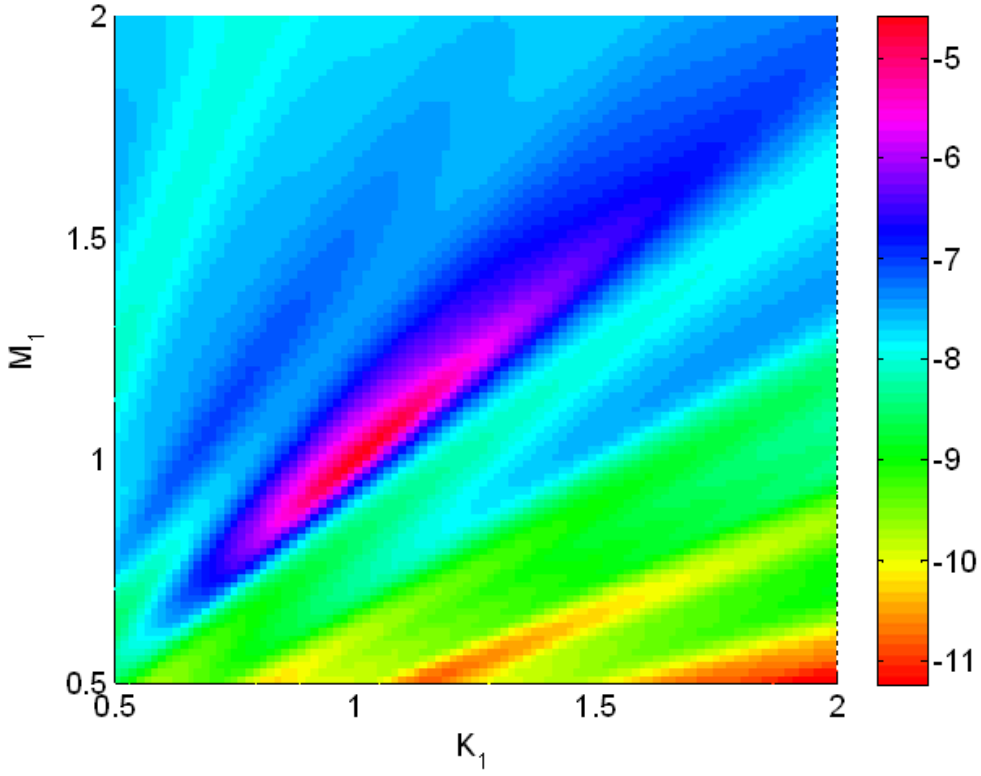

Figure 3.19: Typical peak shifting of 1-DOF unknown mass system under 10% noise: contour 2

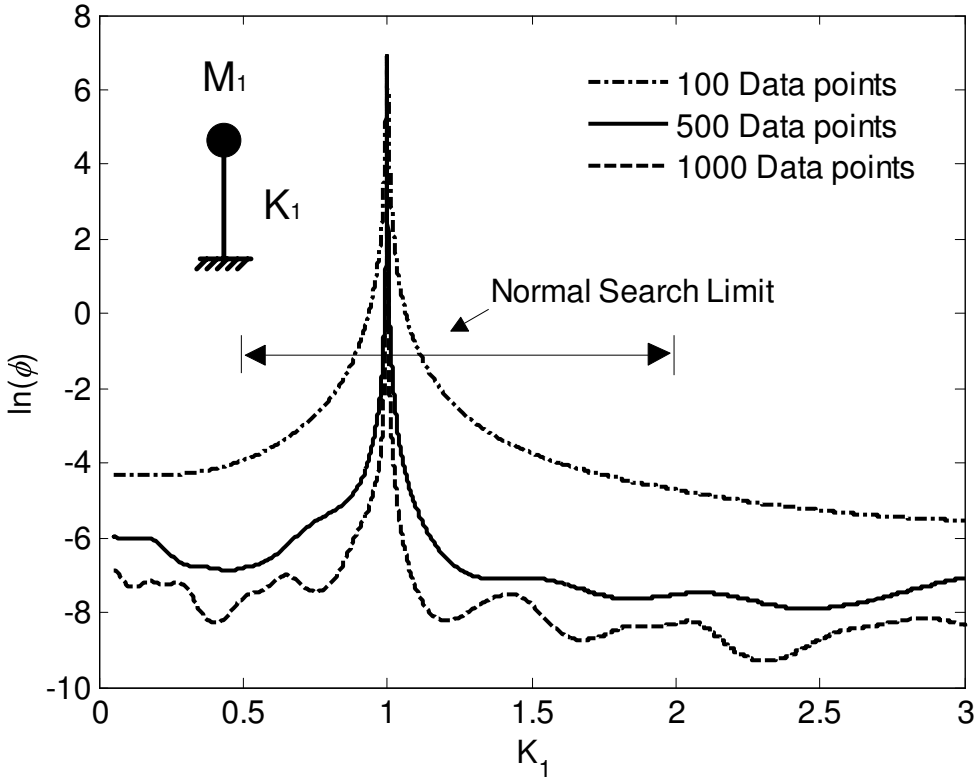

Figure 3.20: Effect of data length on fitness function: noise free

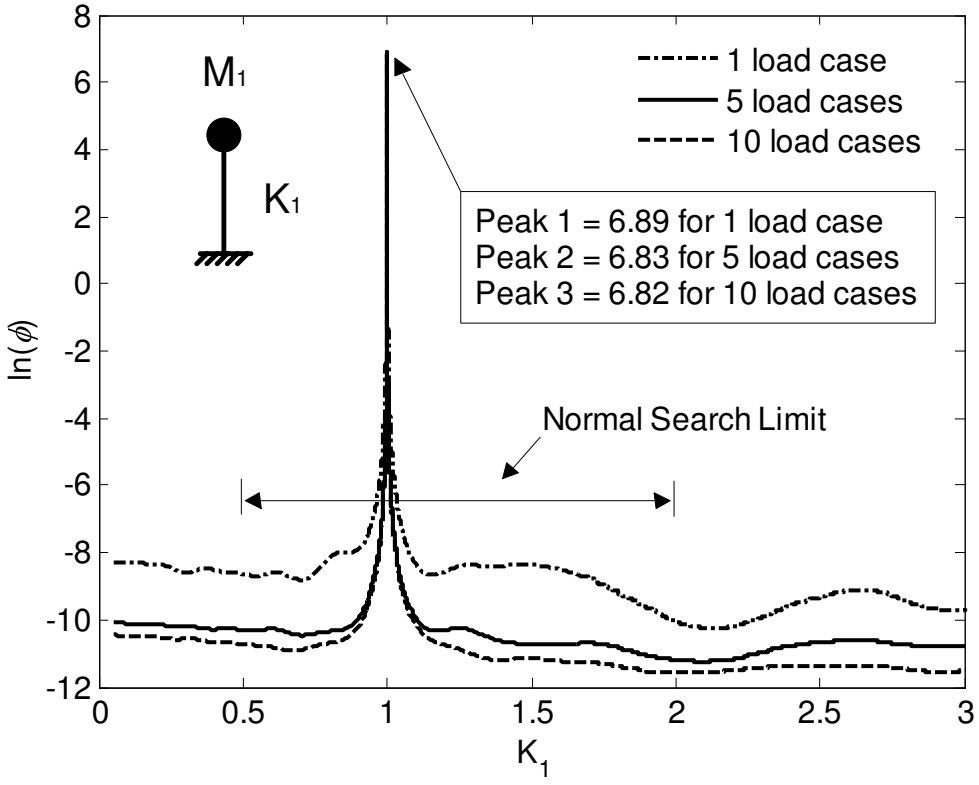

Figure 3.21: Effect of multiple load cases on fitness function: noise free

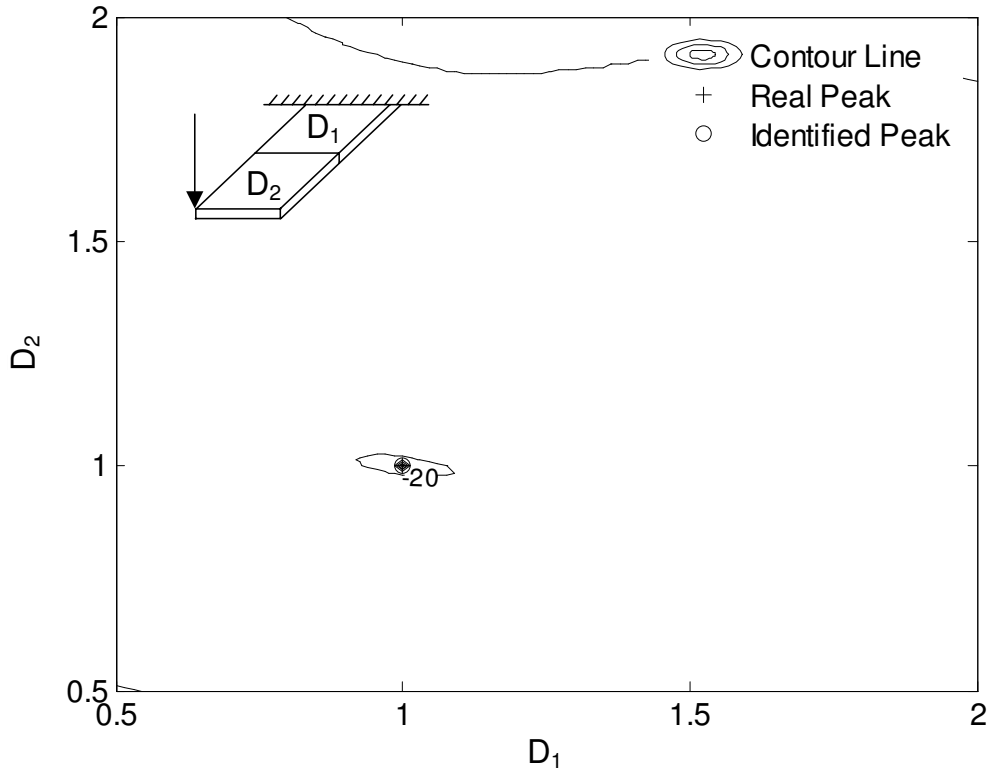

Figure 3.22: Typical peak shifting of 2-element plate under 0% noise: contour

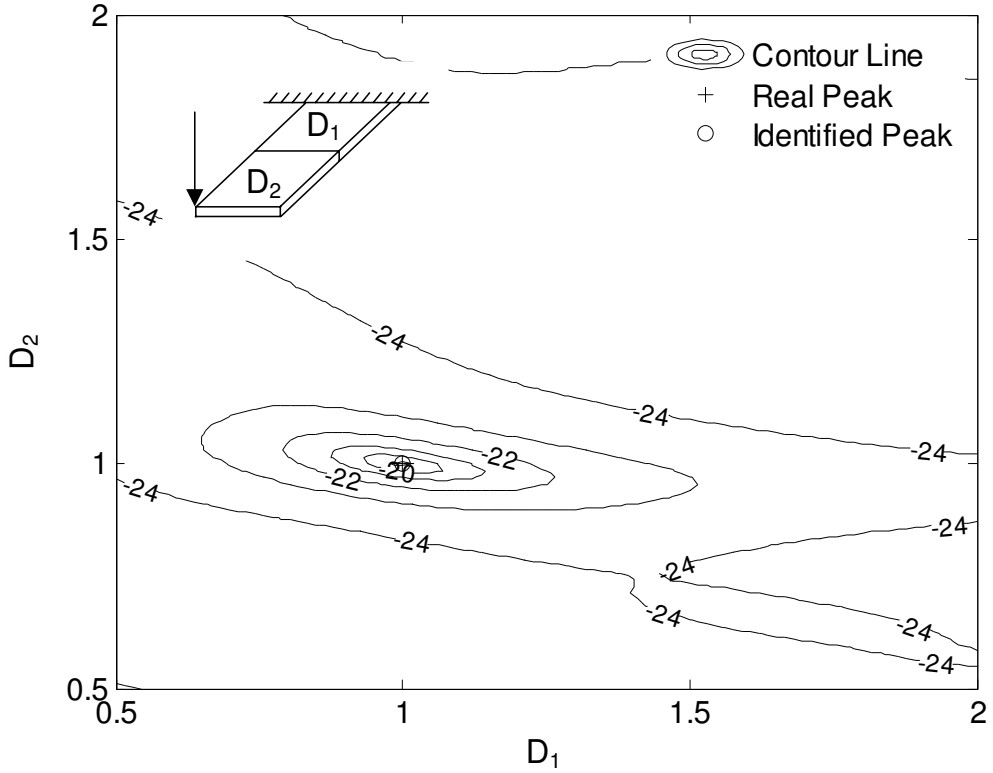

Figure 3.23: Typical peak shifting of 2-element plate under 5% noise: contour

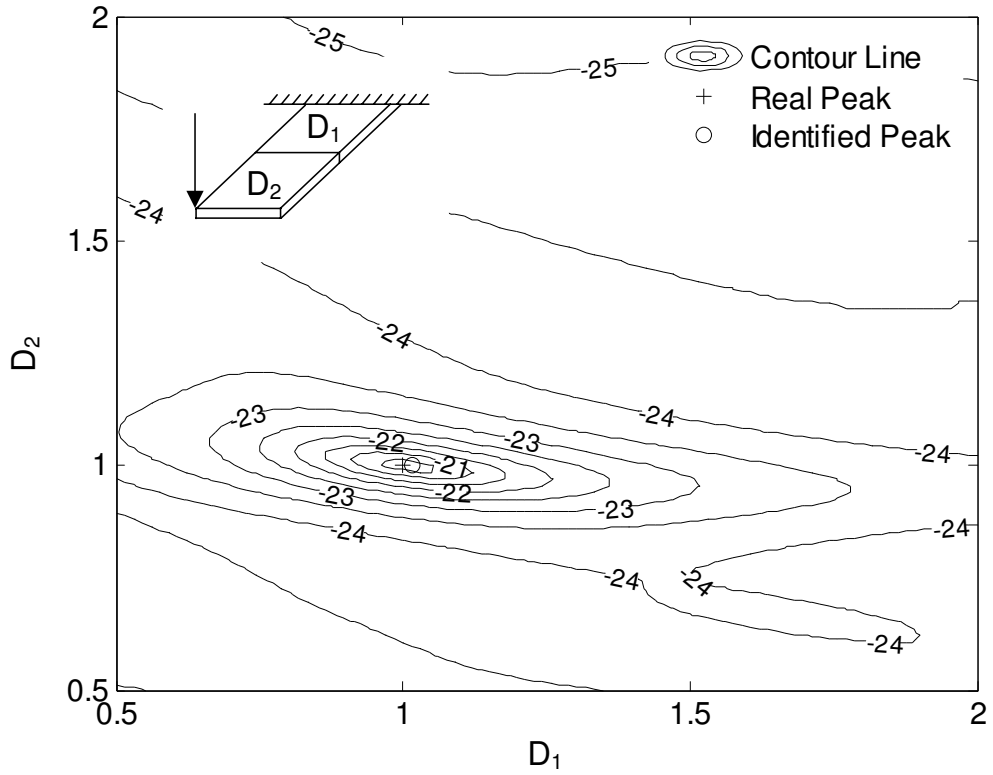

Figure 3.24: Typical peak shifting of 2-element plate under 10% noise: contour

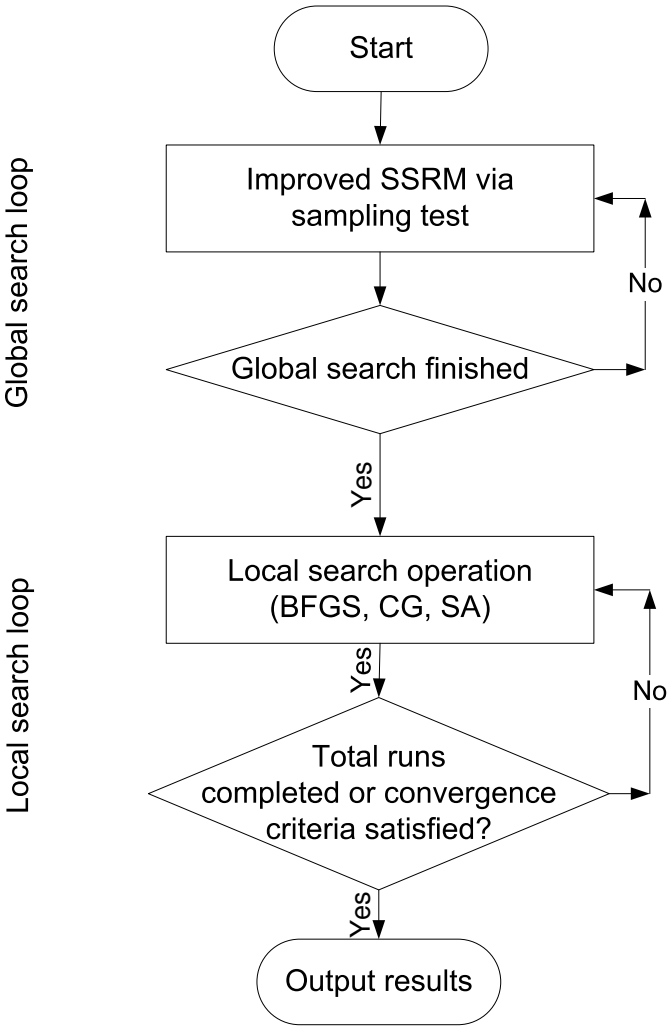

Figure 3.25: Enhanced optimization strategy: improved SSRM with local search

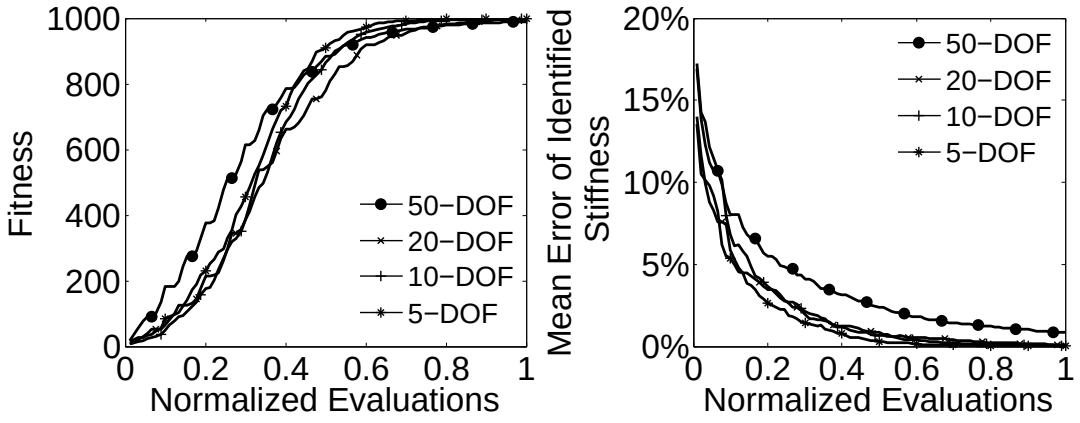

Figure 3.26: Convergence history of known mass systems using merely iSSRM method

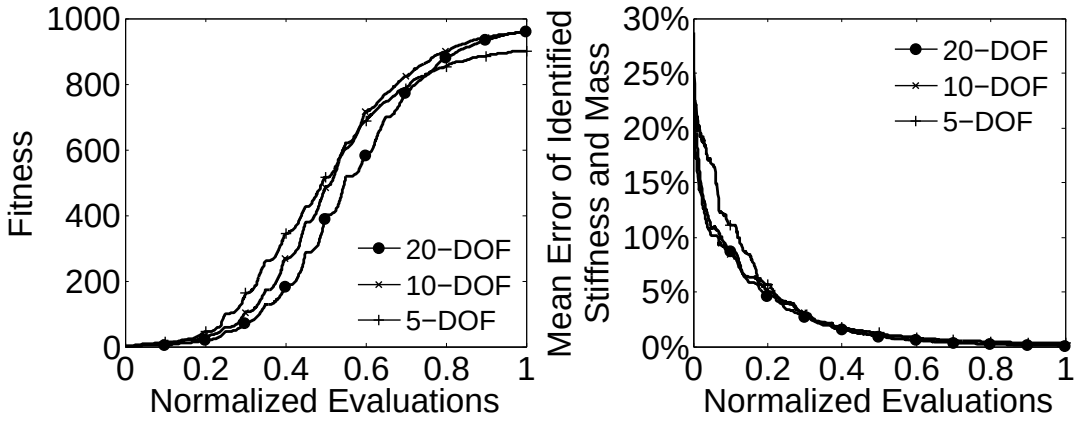

Figure 3.27: Convergence history of unknown mass systems using merely iSSRM method

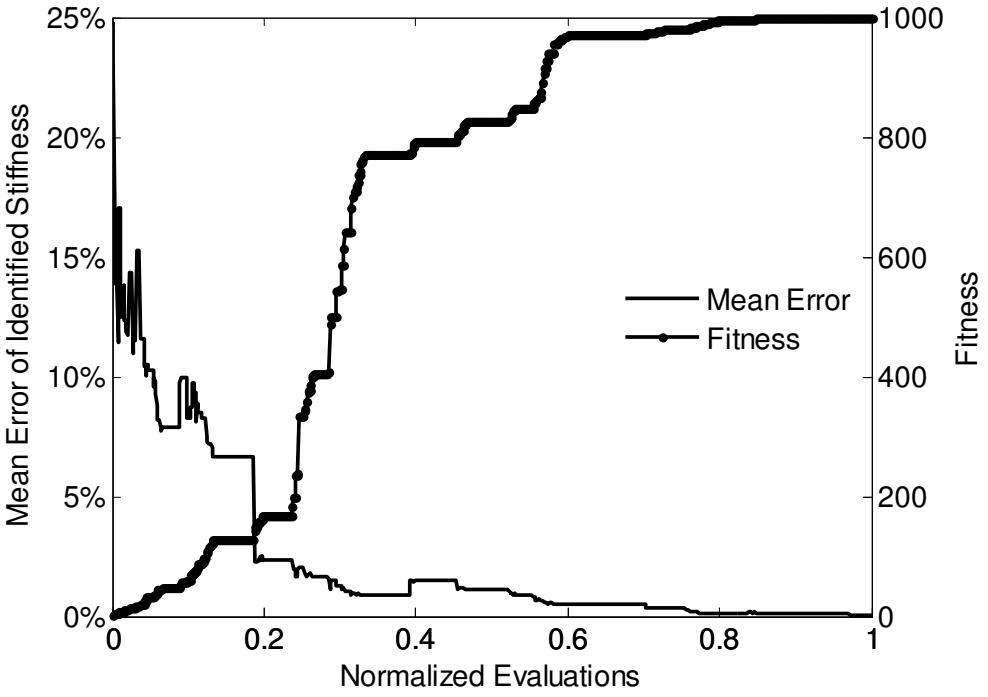

Figure 3.28: Typical iSSRM convergence of 20-DOF known mass system under 0% noise: 40,000 total evaluations

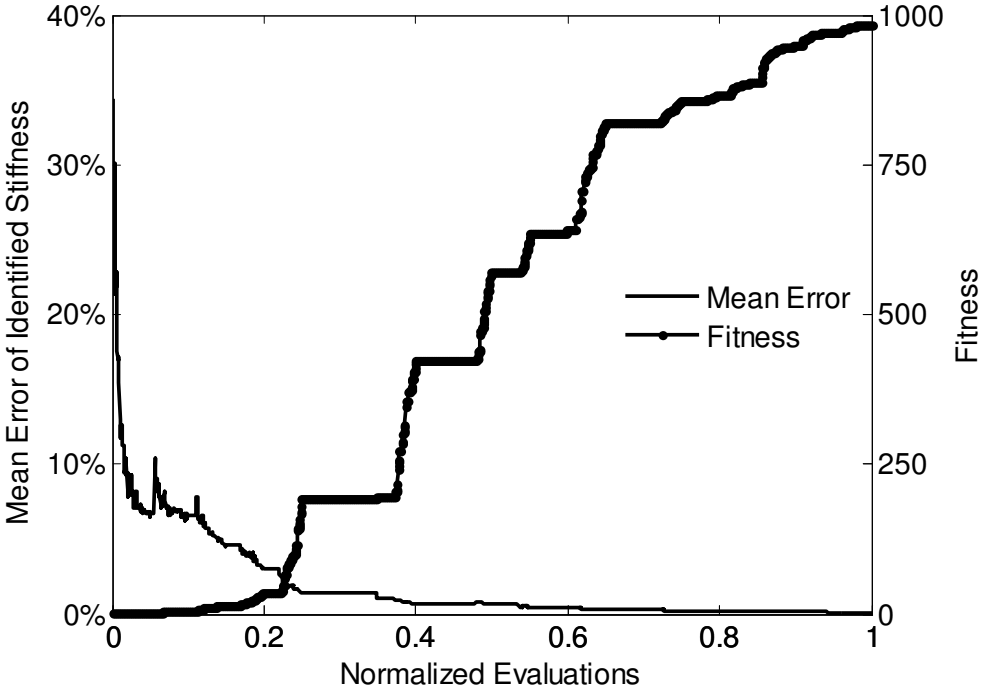

Figure 3.29: Typical iSSRM convergence of 20-DOF unknown mass system under 0% noise: 40,000 total evaluations

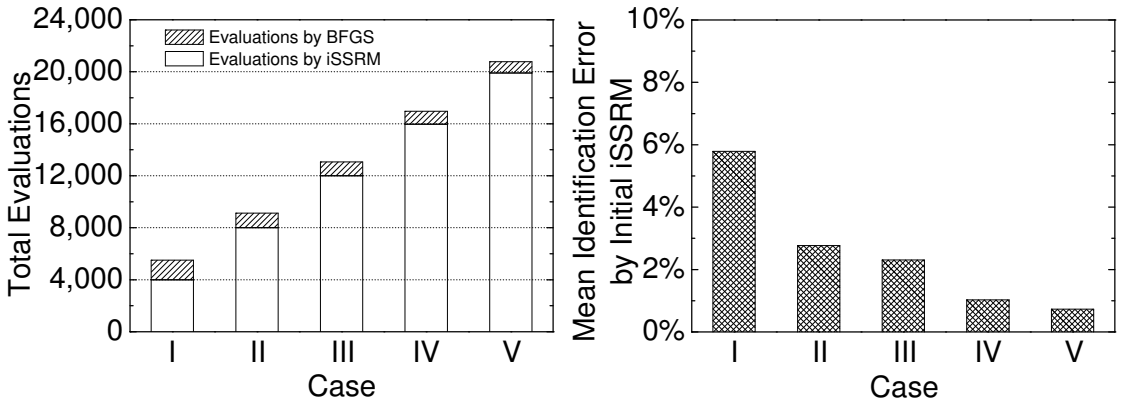

Figure 3.30: Allocation of total evaluations to iSSRM search and local search: based on a 20-DOF known mass system (Refer to Table 3.1 for the definition of Cases I to V)

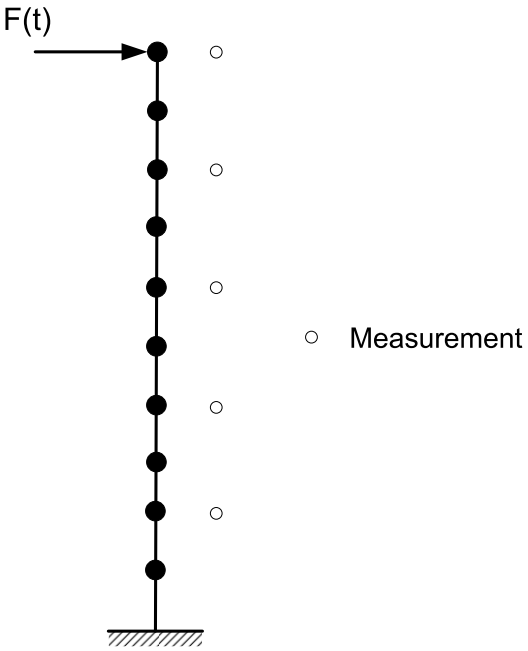

Figure 3.31: Numerical example 1: 10-DOF lumped mass system

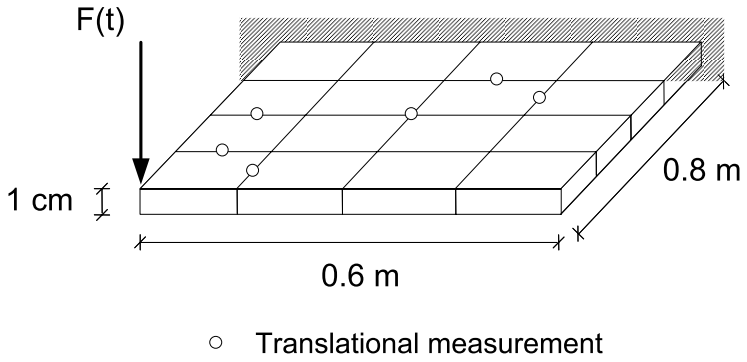

Figure 3.32: Numerical example 2: 16-element plate

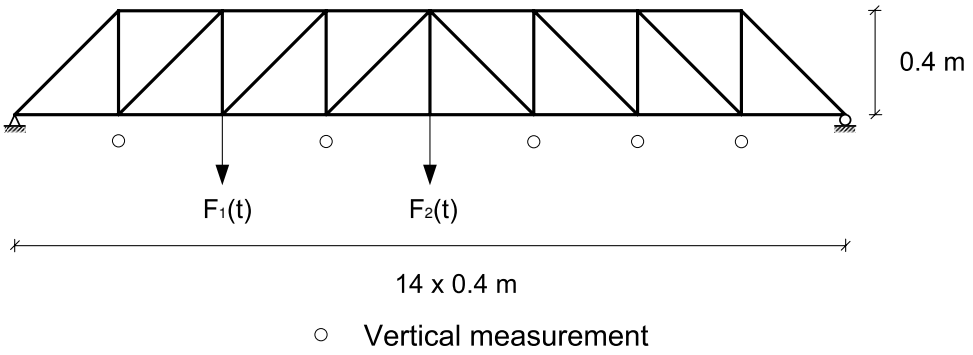

Figure 3.33: Numerical example 3: 29-element truss

Table 3.1: Allocations of total evaluation to iSSRM and local search in the enhanced optimization strategy: based on a 20-DOF known mass system

Switch point[a]	Case I: 10%	Case II: 20%	Case III: 30%	Case IV: 40%	Case V: 50%
Allocation by global/local search	4,000/1,505	8,000/1,133	12,000/1,067	15,970/987	19,910/861
Mean error - k (%)	5.79/0.00	2.77/0.00	2.31/0.00	1.03/0.00	0.73/0.00
Fitness value[b]	117/1,000	377/1,000	504/1,000	773/1,000	861/1,000
Time (s:ms)	02:844/01:226	05:417/00:815	08:217/00:793	10:937/00:727	13:552/00:709

[a] Based on the total evaluations concluded in Table 2.11, the percentage means the effort used for iSSRM as a initial global search in the enhanced optimization strategy over the effort by merely iSSRM method. For example, "10%" means 4,000/40,000 for 20-DOF known mass system.

[b] Fitness is measured by Eq. (3.1).

Table 3.2: Recommended parameters for iSSRM in the enhanced optimization strategy

GA parameters	Known mass systems			Unknown mass systems		
	5-DOF	10-DOF	20-DOF	5-DOF	10-DOF	20-DOF
Total evaluations	1,000	2,000	8,000	8,000	16,000	120,000
Population size	3×3	3×3	5×3	5×3	7×3	17×3
Generations	4	10	40	29	42	150
Sample size	63	108	200	96	176	336
Sampling ratio[a]	0.630	0.540	0.248	0.180	0.165	0.042
Number of runs	10	10	10	15	15	15
n_b value	5	5	5	5	5	5
Crossover rate	0.8	0.8	0.8	0.4	0.4	0.4
Mutation rate	0.2	0.2	0.1	0.2	0.2	0.1
Migration rate	0.05	0.05	0.05	0.05	0.05	0.05
Regeneration	2	2	3	3	3	3
Reintroduction	3	10	20	20	30	100
Window width	4.0	4.0	4.0	4.0	4.0	4.0
Data length	200	200	200	500	500	500

[a] Sampling ratio is defined as the evaluations used for sampling test divided by the total evaluations.

Table 3.3: GA parameters for numerical example 1: 10-DOF lumped mass system

GA parameters	10-DOF lumped mass system						
	SGA[a]	SSRM	Hybrid[a] GA-SW	Hybrid[a] GA-MV	iSSRM -BFGS	iSSRM -CG	iSSRM -SA
Initial evaluations	-	-	-	-	1,980	1,980	1,980
Population size	50	12×3	50	50	3×3	3×3	3×3
Generations	600	83	100	100	10	10	10
Sample size	-	-	-	-	108	108	108
Number of runs	-	10	-	-	10	10	10
Crossover rate	0.6	0.8	0.6	0.6	0.8	0.8	0.8
Mutation rate	0.001	0.2	0.001	0.001	0.2	0.2	0.2
Migration rate	-	0.05	-	-	0.05	0.05	0.05
Regeneration	-	3	-	-	2	2	2
Reintroduction	-	40	-	-	5	5	5
Window width	-	4.0	-	-	4.0	4.0	4.0
Data length	1,000	1,000	1,000	1,000	1,000	1,000	1,000
Time step (sec)	0.002	0.002	0.002	0.002	0.002	0.002	0.002

[a] Results by Koh *et al.* (2003a)

Table 3.4: Results for numerical example 1: 10-DOF lumped mass system

Results	10-DOF lumped mass system						
	SGA[a]	SSRM	Hybrid[a] GA-SW	Hybrid[a] GA-MV	iSSRM -BFGS	iSSRM -CG	iSSRM -SA
			0% Noise				
Total evaluations	30,000	30,000	30,000	30,000	2,295	2,951	21,980
CPU time (h:m:s)	-	00:00:52	-	-	00:00:04	00:00:05	00:00:34
Mean error - k (%)	2.90	0.58	0.40	0.20	0.00	0.00	0.06
Max error - k (%)	7.80	2.13	1.20	1.00	0.00	0.00	0.17
			10% Noise				
Total evaluations	30,000	30,000	30,000	30,000	2,590	2,766	21,980
CPU time (h:m:s)	-	00:00:52	-	-	00:00:04	00:00:05	00:00:34
Mean error - k (%)	5.10	5.37	2.70	3.00	2.90	2.79	3.40
Max error - k (%)	15.00	14.26	12.20	7.60	7.63	7.03	9.20

[a] Results by Koh *et al.* (2003a)

Table 3.5: GA parameters for numerical example 2: 16-element plate

GA parameters	16-element plate				
	SGA	SSRM	iSSRM-BFGS	iSSRM-CG	iSSRM-SA
Initial evaluations	-	-	3,020	3,020	3,020
Population size	140	12×3	4×3	4×3	4×3
Generations	214	83	16	16	16
Sample size	-	-	110	110	110
Number of runs	-	10	10	10	10
Crossover rate	0.8	0.8	0.8	0.8	0.8
Mutation rate	0.05	0.1	0.1	0.1	0.1
Migration rate	-	0.05	0.05	0.05	0.05
Regeneration	-	3	3	3	3
Reintroduction	-	40	10	10	10
Window width	-	4.0	4.0	4.0	4.0
Data length	500	500	500	500	500
Time step (sec)	2.5×10^{-5}	2.5×10^{-5}	2.5×10^{-5}	2.5×10^{-5}	2.5×10^{-5}

Table 3.6: Results for numerical example 2: 16-element plate

GA parameters	16-element plate				
	SGA	SSRM	iSSRM-BFGS	iSSRM-CG	iSSRM-SA
			0% Noise		
Total evaluations	30,000	30,000	4,548	18,565	23,020
CPU time (h:m:s)	04:04:52	04:13:13	00:39:12	02:29:29	02:57:43
Mean error - D^a (%)	11.94	3.02	0.00	0.00	0.00
Max error - D^a (%)	35.86	9.71	0.00	0.00	0.02
			10% Noise		
Total evaluations	30,000	30,000	4,972	6,373	23,020
CPU time (h:m:s)	04:05:19	04:14:18	00:41:41	00:55:58	02:55:44
Mean error - D^a (%)	15.84	5.81	4.72	4.77	5.73
Max error - D^a (%)	42.87	16.68	13.17	13.03	15.67

[a] D=flexural rigidity

Table 3.7: GA parameters for numerical example 3: 29-element truss

GA parameters	29-element truss				
	SGA	SSRM	iSSRM-BFGS	iSSRM-CG	iSSRM-SA
Initial evaluations	-	-	5,960	5,960	5,960
Population size	196	16×3	4×3	4×3	4×3
Generations	306	125	38	38	38
Sample size	-	280	140	140	140
Number of runs	-	10	10	10	10
Crossover rate	0.9	0.8	0.8	0.8	0.8
Mutation rate	0.05	0.1	0.1	0.1	0.1
Migration rate	-	0.05	0.05	0.05	0.05
Regeneration	-	3	3	3	3
Reintroduction	-	50	10	10	10
Window width	-	4.0	4.0	4.0	4.0
Data length	500	500	500	500	500
Time step (sec)	1.0×10^{-2}	1.0×10^{-2}	1.0×10^{-2}	1.0×10^{-2}	1.0×10^{-2}

Table 3.8: Results for numerical example 3: 29-element truss

GA parameters	29-element truss				
	SGA	SSRM	iSSRM-BFGS	iSSRM-CG	iSSRM-SA
			0% Noise		
Total evaluations	60,000	60,000	10,780	110,169	25,960
CPU time (h:m:s)	00:14:07	00:13:25	00:02:42	00:24:19	00:05:55
Mean error - EA (%)	18.84	2.91	0.00	0.00	0.76
Max error - EA (%)	49.96	11.32	0.00	0.02	5.08
			10% Noise		
Total evaluations	60,000	60,000	12,619	54,324	25,960
CPU time (h:m:s)	00:14:21	00:14:01	00:02:55	00:11:54	00:06:00
Mean error - EA (%)	20.87	3.63	3.23	3.22	4.15
Max error - EA (%)	54.81	14.60	15.69	16.13	20.93

CHAPTER 4

Frequency Domain Substructural Identification under Random Excitation

In Chapter 3 we examine the nature of structural identification as an optimization problem, leading to a uniformly sampled genetic algorithm and gradient search method. Compared to similar research efforts recently (Koh *et al.*, 2003a; Perry *et al.*, 2006), equally good accuracy is achieved with around only one-tenth of computer time. This result is definitely very encouraging, making it possible to identify even larger systems on today's personal computer platform.

For better numerical performance, it is not a good idea to identify the target structures as a whole using the enhanced optimization strategy, or, for that matter, any other strategy. The reason is two-fold: the identification of a whole structural system usually comes with a large number of unknowns and also a large number of DOFs in the finite element model. The large number of unknowns will result in a huge search space for identification using the optimization strategy, posing a formidable challenge for convergence. The large number of DOFs will require extensive computer time for evaluating the objective function in the forward analysis. These two problems can be addressed

by reducing the size of the structural system to be identified, for example, by means of substructuring. To this end, a frequency domain substructural method is investigated in this chapter. The original idea of substructuring is that the measured responses are divided into base points and check points (Koh and Shankar, 2003a,b). The base points are used to calculate the unknown force of interfaces and the check points are then used to compare with the estimated response and formulate the objective function. However, this idea was presented on the basis of steady-state dynamics in the forward analysis, confining to sinusoidal excitations. This is not applicable to more general random excitations.

To extend the current sine wave excitation to random forced vibration, the merely use of Discrete Fourier transform (DFT) is insufficient. As the assumption of DFT is that the basic function has to be periodic in the integral domain. This is, however, usually not achievable in reality. A traditional way is to assume the whole data length as one period, and zero padding is needed to ensure that the response dies out at the end of the period, meeting the necessary causality condition. Zero padding guarantees the periodic requirement for Fourier transform on one hand but results in a long time history on the other hand. This is particularly so for lightly damped dynamic systems. Therefore, zero padding is obviously a disadvantage for structural identification using optimization strategies, as the long time history will substantially increase the computer time. The need for arbitrary data length in the measurements is expected.

To overcome the above-mentioned problem, the substructural method is extended in this chapter to random excitations, by introducing the exponential window method. With the exponential window, the response can be guaranteed to disappear within one period even for lightly damped dynamic systems. The measured data length can be arbitrary as no zero padding is involved. The steady state formulation is then applicable to non-periodic loading. For comparison purpose, two numerical examples (Tee *et al.*, 2005) will be presented on the extended substrucural method in the forward analysis. The

proposed optimization strategy of Chapter 3 will be considered in the inverse analysis. The first example is a 12-DOF lumped mass system to test the performance of the proposed method in structural identification and damage detection. The second 50-DOF system is investigated to verify the consistency of the method in a much larger system.

4.1 Frequency Response Function

In the forward analysis, the steady state response is obtained by transfer function, which is usually referred to as frequency response function (FRF). The formulation is readily derived based on the harmonic excitation. For a multi-DOF dynamic system, the motion is characterized by the following second order differential equation.

$$\mathbf{M}\ddot{\mathbf{u}} + \mathbf{C}\dot{\mathbf{u}} + \mathbf{K}\mathbf{u} = \mathbf{f} \tag{4.1}$$

where $\mathbf{M}$, $\mathbf{C}$ and $\mathbf{K}$ are the mass, damping and stiffness matrix of the system. $\mathbf{f}$ is the external excitation. $\ddot{\mathbf{u}}$, $\dot{\mathbf{u}}$ and $\mathbf{u}$ represent the acceleration, velocity, displacement, respectively. If the structure is excited harmonically by a set of forces all at the same frequency ω, but with their respective amplitudes and phases. Then

$$\mathbf{f} = \mathbf{F}(\omega)e^{i\omega t} \tag{4.2}$$

and at the same time, the response exists in the form of

$$\mathbf{u} = \mathbf{U}(\omega)e^{i\omega t} \tag{4.3}$$

where $\mathbf{F}(\omega)$ and $\mathbf{U}(\omega)$ are $n \times 1$ vectors of time-independent complex amplitudes.

The equation of motion then becomes

$$(\mathbf{K} - \omega^2\mathbf{M} + i\omega\mathbf{C})\mathbf{U}(\omega)e^{i\omega t} = \mathbf{F}(\omega)e^{i\omega t} \tag{4.4}$$

Rearranging for the response

$$\mathbf{U}(\omega) = \mathbf{H}(\omega)\mathbf{F}(\omega) \tag{4.5}$$

where $\mathbf{H}(\omega)$ is the $n \times n$ receptance Frequency Response Function (FRF) matrix for the system and is given by

$$\mathbf{H}(\omega) = (\mathbf{K} - \omega^2\mathbf{M} + i\omega\mathbf{C})^{-1} \tag{4.6}$$

In fact, this is a common analysis method in the frequency domain, especially when using a transfer function approach. As shown in Eq. (4.5), it is based on the simple relationship, that exists for linear, time-invariant systems between the Fourier transform of the input, $\mathbf{F}(\omega)$ and $\mathbf{U}(\omega)$. These transforms are related through the complex-valued transfer function, $\mathbf{H}(\omega)$. This relationship assumes zero initial conditions for the input and output and implies that their full time histories are used in calculating $\mathbf{F}(\omega)$ and $\mathbf{U}(\omega)$. In practice, they are calculated at discrete frequencies from finite records, using a fast Fourier transform (FFT) algorithm. The formulation of Eq. (4.5) represents the steady-state response to a periodic extension of the excitation.

The general element in the receptance FRF matrix is defined as follows:

$$H_{pq}(\omega) = \frac{U_p}{F_q} \tag{4.7}$$

It is clearly possible to determine values for the elements of $\mathbf{H}(\omega)$ at any frequency of interest simply by substituting the appropriate values into Eq. (4.6). However, this involves the inversion of a system matrix at each frequency and this has several disadvantages. First, it becomes costly for large order systems where n is fairly large. Second, it is inefficient if only a few of the individual FRF expressions are required. Third, it provides no insight into the form of the various FRF properties.

For these reasons, an alternative means of deriving the various FRF parameters is to make use of the modal properties for the system in lieu of the spatial properties. Returning to Eqs. (4.5) and (4.6), we can write

$$(\mathbf{K} - \omega^2\mathbf{M} + i\omega\mathbf{C}) = \mathbf{H}(\omega)^{-1} \tag{4.8}$$

Premultiply both sides by φ^T and postmultiply both sides by φ to obtain

$$\varphi^T(\mathbf{K} - \omega^2\mathbf{M} + i\omega\mathbf{C})\varphi = \varphi^T\mathbf{H}(\omega)^{-1}\varphi \tag{4.9}$$

If

$$\mathbf{K}_n = \varphi^T \mathbf{K} \varphi; \mathbf{M}_n = \varphi^T \mathbf{M} \varphi; \mathbf{C}_n = \varphi^T \mathbf{C} \varphi \tag{4.10}$$

Then

$$(\mathbf{K}_n - \omega^2 \mathbf{M}_n + i\omega \mathbf{C}_n) = \varphi^T \mathbf{H}(\omega)^{-1} \varphi \tag{4.11}$$

we have

$$\mathbf{M}_n(\omega_r^2 - \omega^2 + i\omega {\mathbf{M}_n}^{-1} \mathbf{C}_n) = \varphi^T \mathbf{H}(\omega)^{-1} \varphi \tag{4.12}$$

where ω_r is angular frequency associated with the r-th mode. Eq. (4.12) leads to

$$\mathbf{H}(\omega) = \varphi \mathbf{M}_n(\omega_r^2 - \omega^2 + i\omega \cdot 2\omega_r \xi_r)^{-1} \varphi^T \tag{4.13}$$

where ξ_r is the damping ratio associated with the r-th mode. It is clear from this equation that the recepetance matrix $\mathbf{H}(\omega)$ is symmetric, and this is recognized as the principle of reciprocity which applies to many structural characteristics. Its implication in this situation is that:

$$H_{pq}(\omega) = \frac{U_p}{F_q} = H_{qp}(\omega) = \frac{U_q}{F_p} \tag{4.14}$$

Eqs. (4.13) and (4.14) permit us to compute any individual FRF parameter $H_{pq}(\omega)$ using the following formula

$$H_{pq}(\omega) = \sum_{r=1}^{n} \frac{\varphi_{pr} \varphi_{qr}}{\omega_r^2 - \omega^2 + i \cdot 2\omega\omega_r \xi_r} \tag{4.15}$$

Note that the resulting expression is delivered by multiplying the p-th row of φ by the diagonal frequency matrix by the q-th column of φ^T. In fact, this is very much simpler and more informative than the use of direct inverse as given in Eq. (4.6).

If the response is acceleration instead of displacement, the corresponding frequency domain FRF functions are called accelerance $A_{pq}(\omega)$ relating the output acceleration spectrum $a_p(\omega)$ at location p to input excitation frequency spectrum $F_q(\omega)$ at location q. Therefore, the accelerance is given as follows.

$$A_{pq}(\omega) = -\omega^2 H_{pq}(\omega) = \sum_{r=1}^{n} \frac{-\omega^2 \varphi_{pr} \varphi_{qr}}{\omega_r^2 - \omega^2 + i \cdot 2\omega\omega_r \xi_r} \tag{4.16}$$

4.2 Frequency Domain Substructural Method under Harmonic Excitation

Based on the concept of divide-and-conquer, the response of part or whole structure can be obtained individually from each substructure. As established in the original formulation (Koh and Shankar, 2003a), the response of the substructure is given by

$$\mathbf{U} = \mathbf{H}_{\mathbf{E}}^{*}\mathbf{F}_{\mathbf{E}} + \mathbf{H}_{\mathbf{I}}^{*}\mathbf{F}_{\mathbf{I}} \tag{4.17}$$

where $\mathbf{F_E}$ is the excitation force applied inside the substructures. $\mathbf{F_I}$ is the unknown interface force vector, and $\mathbf{H}^*$, including $\mathbf{F_E}$ and $\mathbf{F_I}$, represents the receptance of a "free-free" substructure. The receptance can be directly measured using Eq. (4.14) or evaluated by Eq. (4.6) or Eq. (4.15) within a substructure. It should be noted that, substructures are "free-free" components that are unconstrained at the interface except those supported at physical boundaries. Thus rigid body modes, if any, of the substructures with zero natural frequency should be counted in when Eq. (4.15) is used to calculate the receptance. If the excitation force is applied outside of the substructure, the $\mathbf{F_E}$ terms vanish, leading to output-only identification.

In the present substructure method, the response measurements embrace "base points" and "check points". "Base points" represent the substructurally selected points that used to calculate the unknown interface force. If the "free-free" substructure has s interface forces, the number of "base points" has to be s, and the unknown interface can be obtained by solving the following equation.

$$\mathbf{F_I} = \mathbf{H}_{\mathbf{I}}^{*-1}(\mathbf{U}_b - \mathbf{H}_{\mathbf{E}}^{*}\mathbf{F_E}) \tag{4.18}$$

where $\mathbf{H}_{\mathbf{I}}^{*}$ is a matrix with a dimension of $n_i \times n_{DOF}$. The number n_i represents the total number of nodes at the interface, and n_{DOF} is the total number of DOFs per node. Obviously, s is at least the product of n_i and n_{DOF} so that the number of equations will be sufficient to solve for the unknowns in Eq. (4.18). Therefore the substructure of

interest has to be large enough to contain sufficient number of available measurements for the sum of "base points" and the subsequent "check points".

"Check points" are to provide additional measurements used to check whether the candidate system can generate the same output as the measured responses. In this way, the objective function formulated by the estimated and measured "check point" response, i.e., Eq. (4.17), is able to identify the system. Theoretically, only one check point is required to identify the unknown system, but more check points can reduce the sensitivity of identification result to the chosen check point and thus improve the numerical accuracy.

To illustrate the philosophy of substructuring, a lumped mass system shown in Fig. 4.1 is studied for example. Typically, a and b represent two interfaces, p and q are two base points, c is the check point and e is the location of internal force (if any). The interface forces are represented by F_a and F_b. The two unknown interface forces can be solved from two measurements within the substructure.

$$\mathbf{F_I} = \left\{ \begin{array}{c} F_a \\ F_b \end{array} \right\} = \left[\begin{array}{cc} H^*(p,a) & H^*(p,b) \\ H^*(q,a) & H^*(q,b) \end{array} \right]^{-1} \left[\left\{ \begin{array}{c} u_p \\ u_q \end{array} \right\} - \left\{ \begin{array}{c} H^*(p,e) \\ H^*(q,e) \end{array} \right\} \mathbf{F_E} \right] \tag{4.19}$$

Once the interface force $\mathbf{F_I}$ is solved, it is substituted back into Eq. (4.17) to compute the response at the check point

$$u_c = H^*(c,e)\mathbf{F_E} + H^*(c,a)F_a + H^*(c,b)F_b \tag{4.20}$$

The above example of one dimensional structure implies that the size of the $\mathbf{H_I^*}$ matrix is determined by the number of the interface unknowns, i.e., 4 by 4 for the Euler beam case and even larger for plates and shells. Furthermore, the size of this matrix is also determined by the number and type element used and the connectivity mechanism from the substructure to the whole structure.

4.3 Frequency Domain Substructural Method under Random Excitation

The previous section presents the frequency domain substructure concept for periodic excitation. Under a harmonic force, the response is readily evaluated by applying Eq. (4.5) to a specific excitation frequency ω. This formulation gives the response under the assumption that the system is initially at rest and the forcing function is periodic. Using Fourier transform, a periodic forcing function is thus expressed as a linear combination of harmonics of different frequencies, amplitudes and phase angles, and the total response is the superposition of component frequency response.

To extend the substructure method from harmonic loading to random excitations, the key issue is to make Eq. (4.5) applicable for non-periodic forcing functions. It is then necessary to recall the continuous representation of Eq. (4.5), which is essentially applicable for arbitrary excitations. The response is estimated by the convolution of the forcing function and the unit impulse response function. The formulation is summarized in the following expressions.

$$\mathbf{u}(t) = \frac{1}{2\pi}\int_{-\infty}^{\infty} \mathbf{H}(\omega)\mathbf{F}(\omega)e^{i\omega t}d\omega \tag{4.21}$$

where

$$\mathbf{H}(\omega) = \int_{-\infty}^{\infty} \mathbf{h}(t)e^{-i\omega t}dt$$

$$\mathbf{F}(\omega) = \int_{-\infty}^{\infty} \mathbf{f}(t)e^{-i\omega t}dt$$

Basically, $\mathbf{H}(\omega)$ and $\mathbf{F}(\omega)$ are the Fourier transforms of $\mathbf{h}(\mathbf{t})$ and $\mathbf{f}(\mathbf{t})$. In the continuous formulation, i.e., Eq. (4.21), the response due to a non-periodic loading can be theoretically integrated in time from $-\infty$ to $+\infty$ in the Fourier transform integral. In numerical implementation, the use of discrete Fourier transform (DFT) prevails instead. Sampled at regular intervals, the infinite integration domain is decretized and the continuous Fourier integral is then replaced by summation over one period. An important

difference between the continuous and discrete Fourier transforms is that, the continuous FT provides a true representation of the given function while the discrete FT represents only a periodic version of the function. These two versions of Fourier transform will not become similar unless the original function happens to be periodic with the whole data length. The problem now is to convert the non-periodic forcing function $\mathbf{f}(\mathbf{t})$ and the unit impulse response function $\mathbf{h}(\mathbf{t})$ into periodic forms.

As a result of the periodic assumption for DFT, the causality is required in the signals such that the initial condition achieved at the start of the next cycle will be the same as the initial condition attained at the beginning of the present cycle. With the assumption of zero initial condition, the resulting response has to be "quiet" at the end of the period. Otherwise, it cannot ensure the zero initial condition for the next cycle. Traditionally, a quiet ending in the response of a damped system is achieved by adding sufficient length of zeros to the original forcing function. The length of trailing zeros is dependent on fundamental period of the system and the damping of the system. The damping, however, plays an important role in the free vibration section where zeros has been padded additionally to the original time history. Through sufficiently long period and large enough damping, the impulse response $\mathbf{h}(\mathbf{t})$, corresponding to the digitally sampled complex response function $\mathbf{H}(\omega)$, can then practically be silent towards the end of the period (Humar, 1990). Otherwise the initial conditions in the periodic response by DFT are not identical to the true initial condition.

However, zero padding incurs extensive computer time particularly for lightly damped and undamped systems. First, increasing the length of zero-padding augments the number of data points in the time history, decreases the step length of frequency increment, and increases the frequency resolutions in DFT. These changes will eventually increase the computational effort in calculating the associated $\mathbf{F}(\omega)$ and $\mathbf{H}(\omega)$, which will be considerably significant for multi-DOF systems. Second, the response will be incorrectly estimated if damping is not large enough in the system. Typically, for a lightly damped

system, i.e., 5% damping ratio, the errors in responses are substantial even when the data length of padded zeros is increased to be 10 times of the original length of excitations (Veletsos and Ventura, 1985). If not resolved, these problems tend to compromise the advantages of the proposed strategy than other substructuring ideas in the identification.

4.3.1 Exponential Window Method

As explained in the previous section, the use of DFT may introduce spurious initial conditions in the response due to the preceding periods of the exciting force. The calculated response by the steady state formulation may be in significant error unless enough damping and sufficient long time history of padded zeros are ensured. Instead of adding long zeros to maintain the causality, a more promising way is to adopt an Exponential Window (EW) method (Kausel and Roesset, 1992) to introduce an artificial damping to damp out this spurious initial condition. To compensate the error caused by the spurious initial conditions, the EW method is superior to supposition of corrective force impulse (Veletsos and Ventura, 1984) and fast convolution method (Humar, 1990), which are not readily extended to general multi-DOF systems or continuous systems.

Sound mathematical derivation can be found from Kausel and Roesset (1992). The use of exponential window herein, rather than other window methods like cosine bell window in signal processing, gives a clear physical interpretation as well as a concise numerical implementation. The problem here is to deal with transient signals and thus emphasis is placed on the effect of initial conditions. Therefore the capacity on minimizing "leakage" dominates the selection of windows. A properly applied exponential window will cause the impulse response to be completely contained within the sampling window; thus leakage will be reduced to a minimum in its spectrum. More importantly, the exponential window is one of the few windows whose effects can be removed by post-processing. While processing the transient signals, the exponential window adds artificial damping to all of the modes of the structure in a known manner. As this artificial

damping is known, it is very easy to restore the original signals by compensating an inverse exponential window.

Using the EW method, both the forcing function and the unit impulse response function will be scaled such that the functions die rapidly toward the end of a selected period, so that the causality is maintained in their convolution. Let the forcing function be $\mathbf{f(t)}$ and impulse function be $\mathbf{h(t)}$. Through the EW, the histories of $\mathbf{f(t)}$ and $\mathbf{h(t)}$ are scaled by an EW function as $\bar{\mathbf{f}}(t)$ and $\bar{\mathbf{h}}(t)$ as follows

$$\bar{\mathbf{f}}(t) = e^{-\eta t}\mathbf{f}(t) \text{ and } \bar{\mathbf{h}}(t) = e^{-\eta t}\mathbf{h}(t) \text{ where } \eta > 0 \tag{4.22}$$

The Fourier transform then gives

$$\bar{\mathbf{F}}(\omega) = \mathbf{F}(\omega - i\eta) = \int_{-\infty}^{\infty} [e^{-\eta t}\mathbf{f}(t)]e^{-i\omega t}dt \tag{4.23}$$

and

$$\bar{\mathbf{H}}(\omega) = \mathbf{H}(\omega - i\eta) = \int_{-\infty}^{\infty} [e^{-\eta t}\mathbf{h}(t)]e^{-i\omega t}dt \tag{4.24}$$

Scaled with EW, the total response is given by inverse Fourier transform as

$$\bar{\mathbf{u}}(t) = \frac{1}{2\pi}\int_{-\infty}^{\infty} \mathbf{U}(\omega - i\eta)e^{i\omega t}d\omega = \frac{1}{2\pi}\int_{-\infty}^{\infty} \mathbf{H}(\omega - i\eta)\mathbf{F}(\omega - i\eta)e^{i\omega t}d\omega \tag{4.25}$$

By taking the inverse EW, the expected response is given by

$$\mathbf{u}(t) = e^{\eta t}\bar{\mathbf{u}}(t) \tag{4.26}$$

To achieve sufficient attenuation of EW without loss of numerical precision, the window size factor η is given by

$$\eta = \frac{2\pi}{T} \tag{4.27}$$

which corresponds to a 54.6 dB attenuation of exponential window and produces good enough results (Kausel and Roesset, 1992).

To carry out the algorithm numerically, the corresponding discrete formulation is

$$\bar{\mathbf{u}}(t) = \frac{1}{2\pi}\sum_{n=0}^{N-1} \mathbf{H}(n\Delta\omega - i\eta)\mathbf{F}(n\Delta\omega - i\eta)e^{i(2\pi kn/N)}\Delta\omega,\ k = 0, 1, \cdots (N-1) \tag{4.28}$$

The folding frequency is $\pi/\Delta t$. $\mathbf{H}(\omega_j - i\eta)$ of $\pi/\Delta t$ to $2\pi/\Delta t$ is the complex conjugate of those located symmetrically between 0 and $\pi/\Delta t$. Only the first half before the folding frequency is physically meaningful. Then the time domain response is

$$\mathbf{u}(k\Delta t) = e^{\eta \cdot k\Delta t}\bar{\mathbf{u}}(k\Delta t) \tag{4.29}$$

4.3.2 Frequency Domain Substructural Identification Using Steady State Formulation

Using the EW method, Eq. (4.5) is now applicable for non-periodic loadings. For substructural analysis under random excitations, Eq. (4.18) is used to get the unknown interface force, and to calculate the check point response. In the case of random excitation $\mathbf{F_E}$, the response of an arbitrary point at each frequency component is evaluated through Eq. (4.17), i.e.

$$\mathbf{u}(\omega_k - i\eta) = \mathbf{H}^*_{\mathbf{E}}(\omega_k - i\eta)\mathbf{F_E}(\omega_k - i\eta) + \mathbf{H}^*_{\mathbf{I}}(\omega_k - i\eta)\mathbf{F_I}(\omega_k - i\eta) \tag{4.30}$$

The total response in time domain is then the summation of all the contributions from individual harmonic components as

$$\mathbf{u}(t) = e^{\eta \cdot k\Delta t}\frac{1}{2\pi}\sum_{n=0}^{N-1}\mathbf{u}(\omega_k - i\eta)e^{i(2\pi kn/N)}\Delta\omega \tag{4.31}$$

where the frequency component $\omega_k = \dfrac{2\pi k}{N\Delta t}$, and $k = 0, 1, \cdots (N-1)$. It should be borne in mind that the resulting folding frequency has to be high enough to incorporate the highest modes of interest. The implementation of frequency domain substructural identification (F-Sub) is illustrated in Fig. 4.2.

In practice, acceleration is preferred in measurement to displacement. In that case, Eqs. (4.30) and (4.31) which correspond to displacement response can be reformulated for acceleration as follows.

$$\ddot{\mathbf{u}}(\omega_k - i\eta) = \mathbf{A}^*_{\mathbf{E}}(\omega_k - i\eta)\mathbf{F_E}(\omega_k - i\eta) + \mathbf{A}^*_{\mathbf{I}}(\omega_k - i\eta)\mathbf{F_I}(\omega_k - i\eta) \tag{4.32}$$

where the accelerance is given by Eq. (4.16), and

$$\ddot{\mathbf{u}}(t) = e^{\eta \cdot k\Delta t} \frac{1}{2\pi} \sum_{n=0}^{N-1} \ddot{\mathbf{u}}(\omega_k - i\eta) e^{i(2\pi kn/N)} \Delta\omega \tag{4.33}$$

4.4 Substructural Efficiency: A Measure of Divide-and-Conquer Methods

For the ease of quantifying and comparing the performance of different divide-and-conquer methods for system identification, a measure called "substructural efficiency" is proposed in this study to compare the computer times used by a substructural identification and by global identification. Suppose a whole structure is divided into n substructures of similar sizes for identification, and suppose further the computer times used for identifying the i-th substructure and the whole structure are t_i and t_g, respectively, then the substructrual efficiency γ is defined, based on the equal number of fitness evaluations used by n substructures and by global identification, as

$$\gamma = 1 - \frac{\sum_{i=1}^{n} t_i}{t_g} \tag{4.34}$$

The total evaluations for substructural and global identification are chosen in such a manner that both of the methods achieve the best of their performance and the final identification errors are at the same level, i.e., approaching zero in the noise free case. Obviously, this ratio should be within the range from 0 to 1. The closer the value of γ comes to 1, the better the efficiency of dividing-and-conquering. Of course, a negative γ is possible and indicates that the substructural method takes longer time than the global identification. In such a case, the substructural method may be suitable to identify part of a structure but cannot be efficiently applied to identify a whole structure by substructuring.

4.5 Numerical Examples

Two numerical examples are presented in the present section. The proposed frequency-domain substructural identification under random excitation, "F-Sub" in short from here onwards, is firstly tested on a 12-DOF system to check the applicability. Then the method will be investigated on a larger 50-DOF system to test the consistency. For these two systems, both system identification and damage detection will be carried out using the iSSRM with gradient search strategy in Chapter 3. The input excitation and the mass properties are assumed to be known. For both structures, the system identification is carried out using the whole structure and F-Sub method. The total fitness evaluation is expected to be 3,800 for 12-DOF system and 12,000 for 50-DOF system. The GA parameters to be used in the identification strategy are given in Table 4.1. The results of the present research will be compared with the previous study by Tee *et al.* (2005). Only the result by Sub-SOMI-RR method, i.e., substructural second-order model identification with relative response, of Tee *et al.* (2005) is covered, as it is the mostly recommended method in the paper. As concluded in the paper, the Sub-SOMI-RR method was more practical than the Sub-FOMI method, i.e., substructural first-order model identification, in requiring no collocated acuators and sensors at all the interface DOFs as well as avoiding numerical difficulties by converting the first-order model to the second-order model at the substructural level. Furthermore, the Sub-SOMI-RR method was better than the Sub-SOMI-AR method, i.e., with absolute response, in demanding less velocities and displacements at the interface DOFs. It should be noted that the computer time is measured by the same 450-MHz Pentium III CPU as used by Tee *et al.* (2005).

4.5.1 Stiffness Identification of A 12-DOF System

In the stiffness identification, the structure is divided into three substructures: $S_1 = [1-4]$, $S_2 = [3-8]$, and $S_3 = [7-12]$. Two random forces with white noise distribution

are imposed at level 3 and level 7. The structure to be identified is illustrated in Fig. 4.3. Based on substructural identification with overlap, the identified element in the common part will be reported by the averaged value. Full measurement of accelerations is assumed in the first stage to compare with the performance with the algorithm, Sub-SOMI-RR by Tee *et al.* (2005). For the dynamic system, Rayleigh damping is assumed to be 1.5% for the first two modes. In the second phase of identification, 50% measurement availability is investigated. The location of the incomplete measurement are at levels 1, 2, 4, 6, 8, and 10.

The result in the case of no noise is not presented as the exact values are achieved by both F-Sub and Sub-SOMI-RR methods. Results under measurement noise are presented in Table 4.2. Using complete measurement, the results are demonstrated in Figs. 4.4 and 4.5 under measurement noise of 5% and 10%, respectively. It is clear that the identification using the proposed optimization strategy are consistently better than those in the reference Tee *et al.* (2005). In the case of 10% measurement noise, identifying the 12-DOF system as a whole, the mean error/maximum error/computer time by Tee *et al.* (2005) are 8.8%/9.9%/50min while the corresponding values are 1.15%/2.73%/63min in the current research by F-Sub. The results in substructural level by Sub-SOMI-RR and F-Sub are fairly encouraging. The mean error/maximum error is 6.4%/9.1%/35min for Sub-SOMI-RR, and 1.37%/4.39%/7min for F-Sub. Besides great improvement in accuracy, the substructural efficiency by Eq. (4.34) is 0.9 for F-Sub while the efficiency is only 0.3 for Tee *et al.* (2005). In the presence of 5% measurement noise, the computer time is unaltered and the mean error/maximum error are 5.7%/9.0% for Sub-SOMI-RR (Tee *et al.*, 2005), and 0.66%/1.86% for F-Sub. The results show good performance of F-Sub over Sub-SOMI-RR by considerably improved accuracy and time reduction. In the case of incomplete measurement, the superior performance is still maintained as shown in Fig. 4.6. The mean error/maximum error are 0.92%/2.58% for 5% noise case and 2.50%/6.04% for 10% noise.

4.5.2 Damage Detection of A 12-DOF System

In the numerical simulation, damage is measured in terms of stiffness reduction and quantified by a scalar index called the stiffness integrity index. The stiffness integrity index is defined as the ratio of the stiffness identified in the damage state divided by that in the reference state. In this section the reference state is taken as the intact state. Two damage scenarios are studied. Damage scenario 1 involves single damage occurring in S_1 with 30% stiffness reduction in level 4. Damage scenario 2 embraces two damages in S_2: 20% stiffness reduction in level 2 and the other is 40% in level 5. The results listed in Fig. 4.7 and 4.8 are the two scenarios for the noise level of 10%. The identification of damage indices in the whole structure use F-Sub method yields mean/ maximum errors of 2.01%/5.47% for damage scenario 1 and 1.72%/4.12% for scenario 2. In the reference Tee *et al.* (2005) for comparison, the corresponding errors are 3.3%/5.1% and 3.7%/6.9% for Sub-SOMI-RR method. The identification result by F-Sub is very encouraging as the accuracy is achieved at the cost of only around 7 min compared to 35 min by Tee *et al.* (2005).

4.5.3 Stiffness Identification of A 50-DOF System

In the example of 12-DOF system, the proposed F-Sub method incorporating the use of improved identification strategy exhibit superior performance to the Sub-SOMI-RR recommended by Tee *et al.* (2005). A much larger 50-DOF system Tee *et al.* (2005) is studied here to check the robustness and consistency of the proposed method. The whole structure is divided into 5 substructures, within each of which there is a force applied at the corresponding top level, i.e., levels 10, 20, 30, 40, and 50 as illustrated in Fig. 4.9. The 5 substructures are defined as $S_1 = [1-10]$, $S_2 = [9-20]$, $S_3 = [19-30]$, $S_4 = [29-40]$, and $S_5 = [39-50]$. Rayleigh damping with ratio of 1.5% is set equally to the first two modes of the global structure. Full accelerations are assumed available in the first phase

of identification. In the second phase of identification, only 36% measurement availability is assumed. The locations of incomplete measurement are at levels 1, 2, 3, 5, 8, and 10 in each substructure.

The identification results are summarized in Table 4.3. Based on complete measurement, the identification results are given in Fig. 4.10. The accuracy is consistently better than that presented by Tee *et al.* (2005). When identifying the 50-DOF system as a whole in presence of 5% noise, the mean/maximum error/computer time are 23.5%/53.1%/190min was given by Tee *et al.* (2005), and 0.85%/4.16%/1,740min using the proposed iSSRM with gradient search. A point to note is that the CPU time is measured by a 450-MHz Pentium III CPU. It is clear that the improvement on efficiency is not as good as the improvement on accuracy. However, this disadvantage is overcome by a substructural identification. The use of F-Sub method gives mean/maximum error/time as 1.63%/6.88%/65min for 5 substructures combined. However, the corresponding values are worse, i.e., 11.0%/18.3%/210min, for Sub-SOMI-RR method. Based on the same number of fitness evaluations as in Table 4.1, the substructural efficiency by Eq. (4.34) is 0.963 for F-Sub method while that is -0.11 for Sub-SOMI-RR method. Obviously, F-Sub method shows an excellent efficiency over Sub-SOMI-RR method, as negative substructural efficiency implies that the method is inefficient for identifying a whole substructure by substructuring. In case of 10% measurement noise, the mean/maximum errors are 2.81%/9.90% for F-Sub method and 1.84%/7.44% for identification as a whole. Although the accuracy can be achieved in the same level, the computer time is reduced to around 4% only by using F-Sub method. Typically, it will cost 13 minutes to identify one of the 5 substructures of a 50-DOF system.

The comparison of complete measurement to incomplete measurement is presented in Fig. 4.11 and Table 4.3. With 36% measurement availability by F-Sub identification, the mean/maximum errors are 4.79%/20.94% for 5% noise and 9.63%/42.93% for 10% noise. Such an increase in identification error from complete measurement to incomplete

measurement is expected. The reason is the incomplete measurement will significantly affect the number of higher modes that can be captured in a substructure level. With less information on higher modes, it will be more difficult to identify local stiffness of the whole structure.

4.5.4 Damage Detection of A 50-DOF System

Two damage scenarios are investigated in this section. The damage is identified at substructure level. The first damage occurs in a substructure $S_{DS1} = [25 - 30]$ with 15% stiffness reduction in level 28 and 25% reduction in level 30. The second damage scenario is a multiple-damage case in substructure $S_{DS2} = [19 - 30]$, involving 20% stiffness reduction in level 21, 15% reduction in level 25 and 25% reduction in level 26. The incomplete measurements of damage scenario 1 are located at levels 24, 25, 28 and 30. For damage scenario 2, the measurements are available at levels 18, 20, 25, 28 and 30.

In the case of 5% noise with complete measurement, the results of two damage scenarios are shown in Fig. 4.12 and 4.13. The identification of stiffness integrity index achieves mean/maximum errors of 1.55%/2.81% for the first damage scenario with 5% noise, and 1.29%/3.41% for the second damage scenario. In the presence of 10% measurement noise (refer to Fig. 4.14 and 4.15), the errors increase to 4.11%/7.38% for damage scenario 1 and 3.24%/6.84% for damage scenario 2. With incomplete measurement, the mean/maximum errors are 6.05%/11.27% for damage scenario 1 in 10% noise, and 10.10%/30.39% for damage scenario 2 in 10% noise. It is observed that the influence of incomplete measurement is considerably large, even using the proposed identification strategy in the two damage scenarios. Therefore it is strongly recommended that sufficient measurement should be presented especially in the case of multiple-damage in a substructure.

4.6 Conclusions

A substructural identification method in frequency domain, i.e., F-Sub, has been presented in this chapter, which is applicable to random excitations. The extension of F-Sub method from harmonic loading to random excitation is achieved in preserving the periodic assumption of DFT, through the use of the exponential window method. Therefore the requirement of causality is maintained within arbitrarily chosen length of response time histories.

The proposed identification strategies consist of the proposed F-Sub method in the forward analysis and the optimization strategy of Chapter 3 in the backward analysis. The strategies are then tested on 12-DOF and 50-DOF lumped mass systems in system identification and damage detection. Results are definitely very encouraging compared to the recent research by Tee *et al.* (2005). Besides much better identification accuracy is achieved by the use of F-Sub method than the Sub-SOMI-RR method (Tee *et al.*, 2005), i.e., less than 2% versus 11% in mean identification error, impressive efficiency of F-Sub method in substructuring is reported by investigating a 50-DOF lumped mass system under 5% noise. Based on Eq. (4.34), a significant substructural efficiency is reached as 0.963 for the F-Sub method while that is of -0.110 by the Sub-SOMI-RR method (Tee *et al.*, 2005). This finding indicates as well that the merely use of F-Sub method in identification will reduce the computer time to around 4% over global identification, via adopting 5 substructures in a 50-DOF system.

With incomplete measurement, the identification error reasonably increases. Engineering implication arising from the results is that, sufficient measurements have to be available within the substructure of interest if a substructural method in identification. This is to capture as many higher modes as possible for better identification.

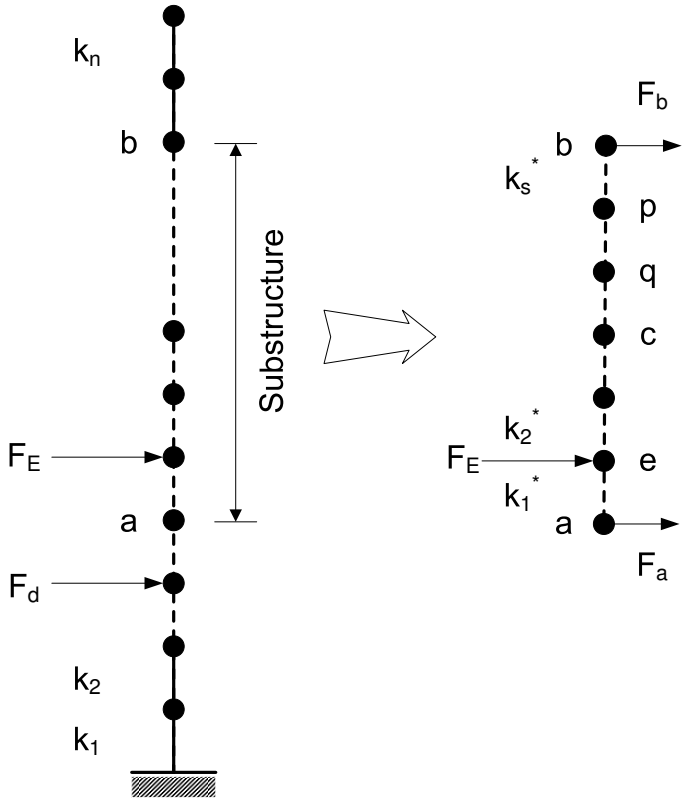

Figure 4.1: Illustration of substructural philosophy in frequency domain

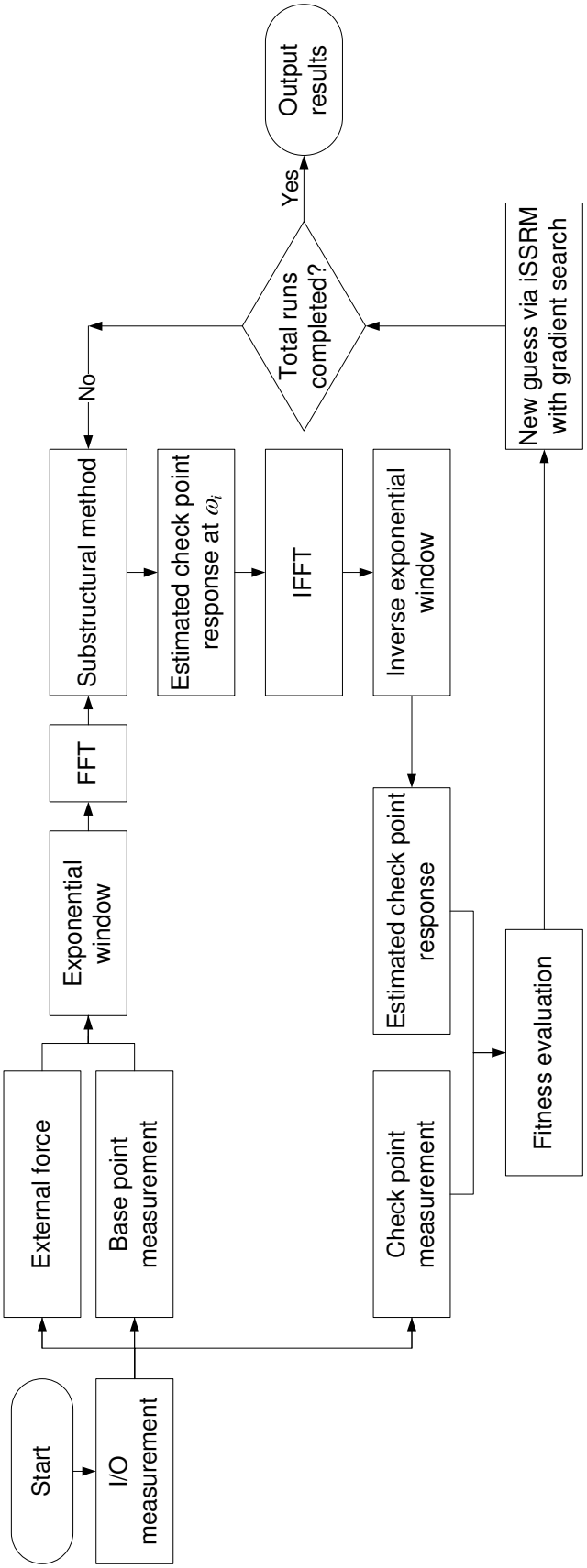

Figure 4.2: Frequency domain substructural identification under random excitation

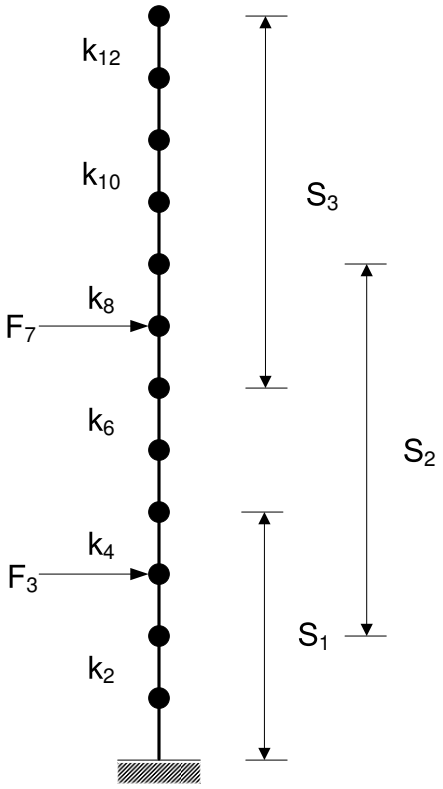

Figure 4.3: Substructures of 12-DOF lumped mass system

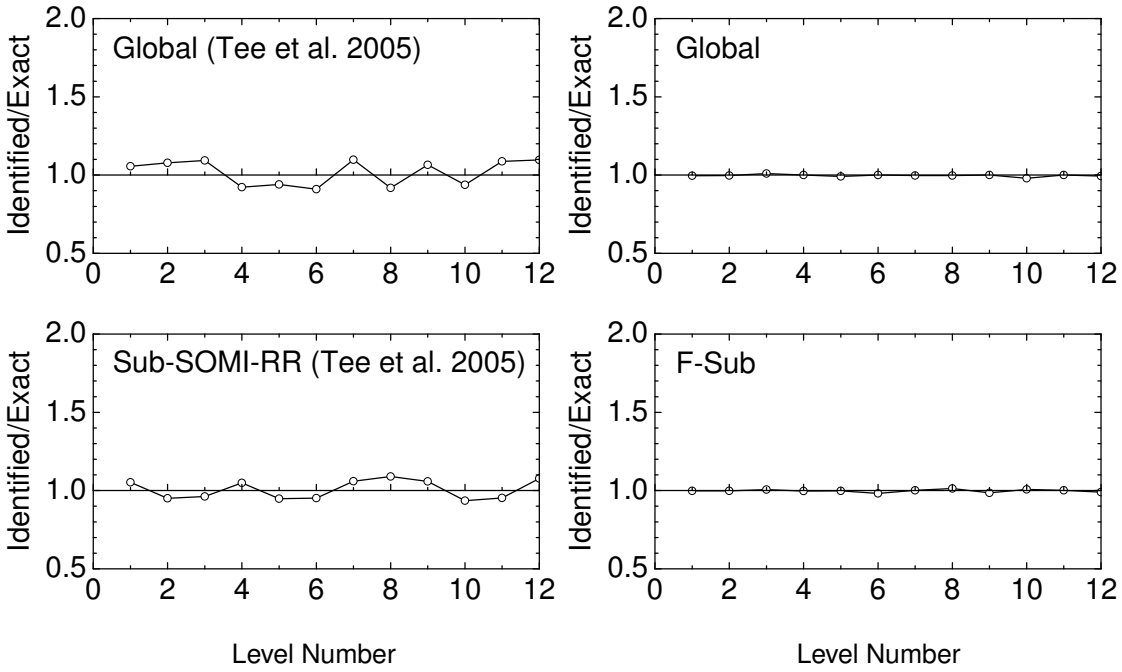

Figure 4.4: Stiffness identification of 12-DOF system under 5% noise: complete measurement

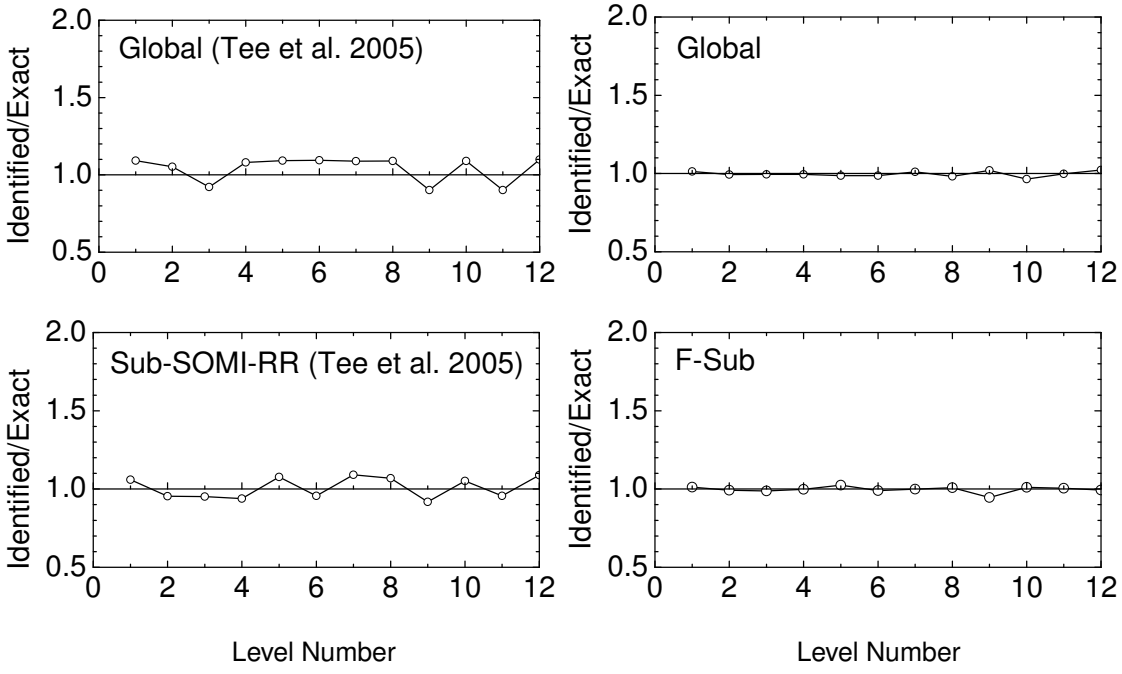

Figure 4.5: Stiffness identification of 12-DOF system under 10% noise: complete measurement

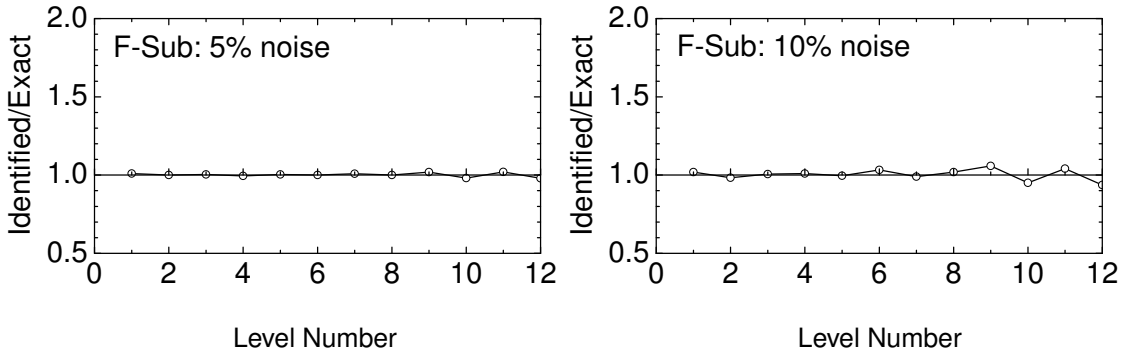

Figure 4.6: Stiffness identification of 12-DOF system based on incomplete measurement

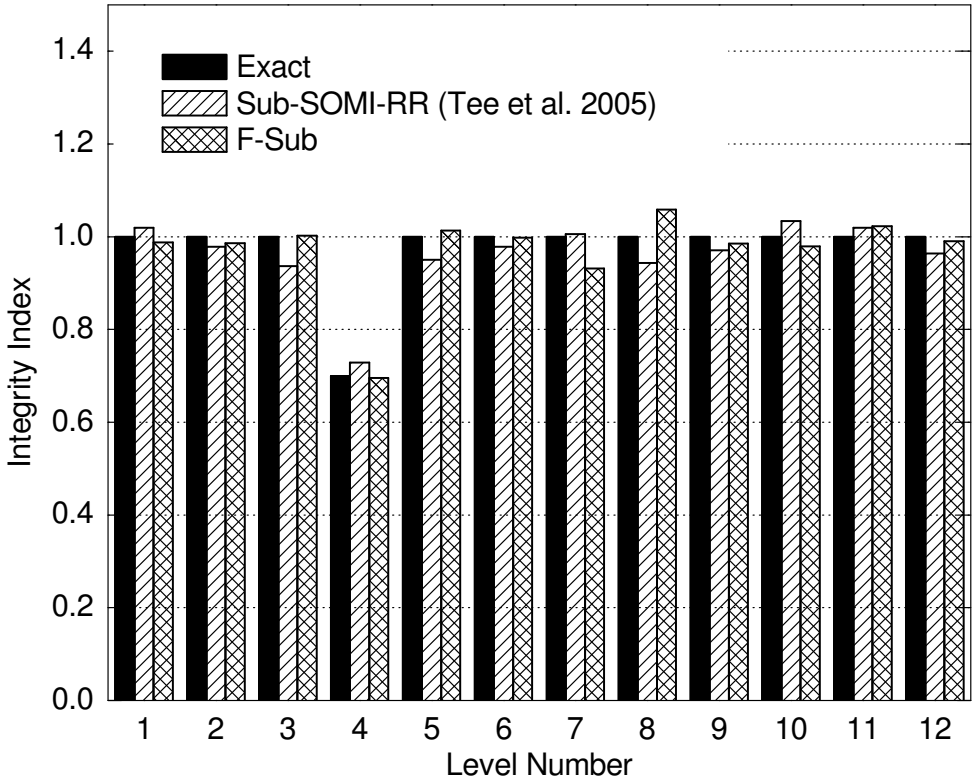

Figure 4.7: Identified stiffness integrity indices for damage scenario 1: 10% noise

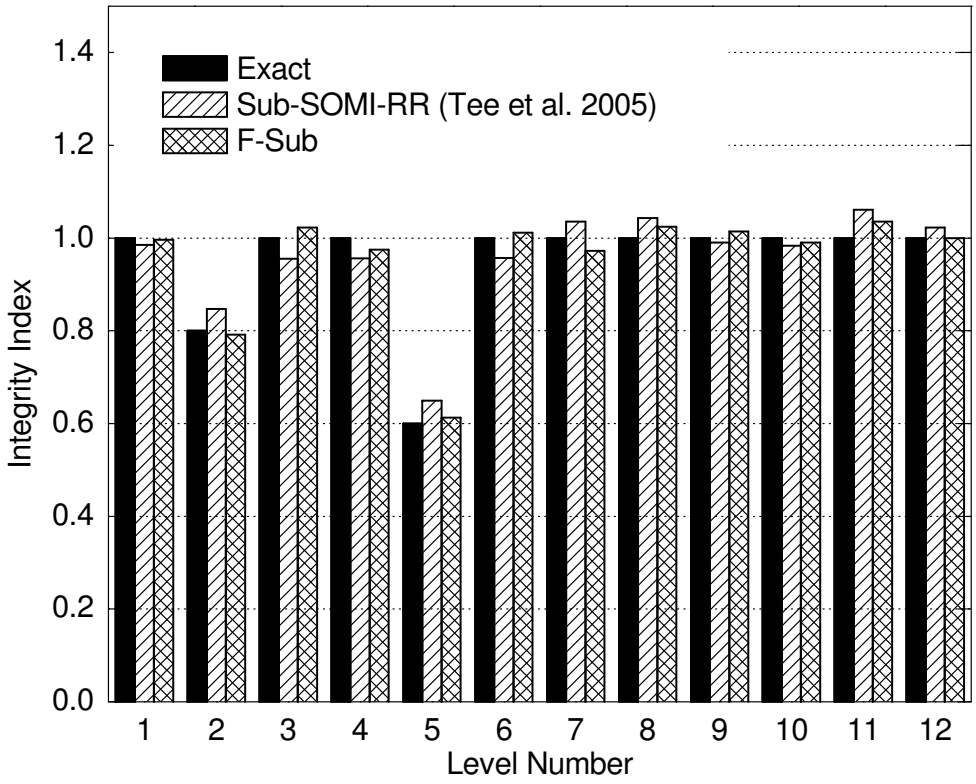

Figure 4.8: Identified stiffness integrity indices for damage scenario 2: 10% noise

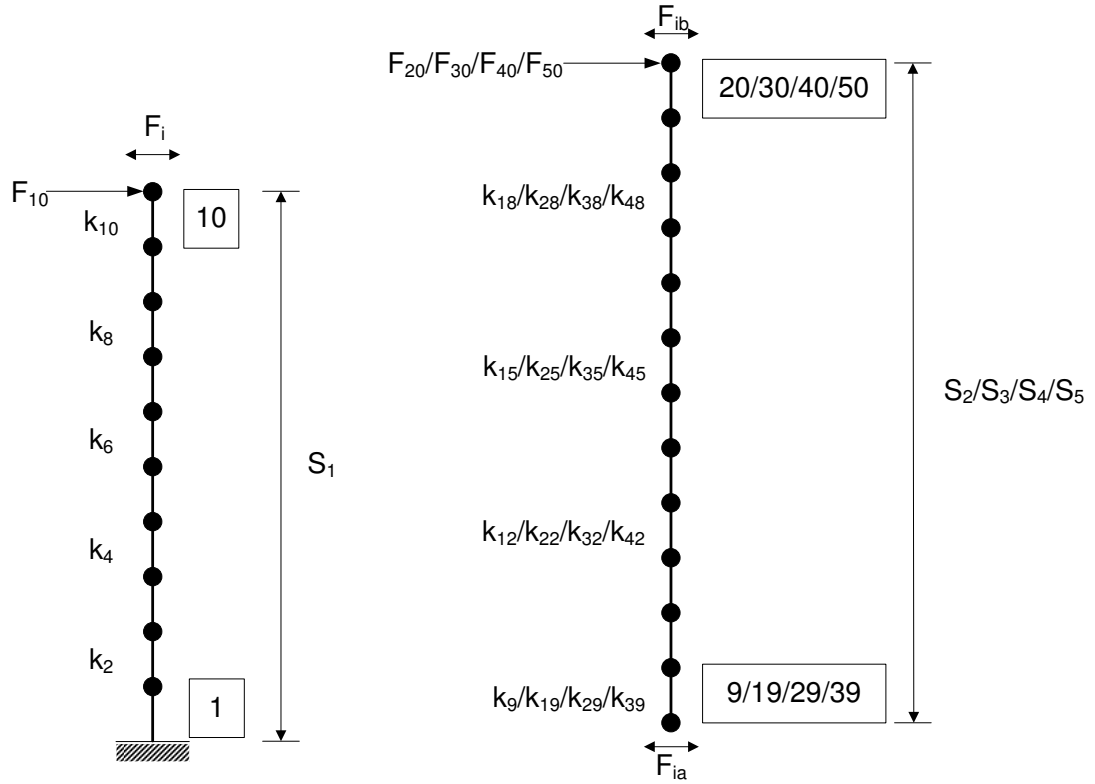

Figure 4.9: Substructures of 50-DOF lumped mass system

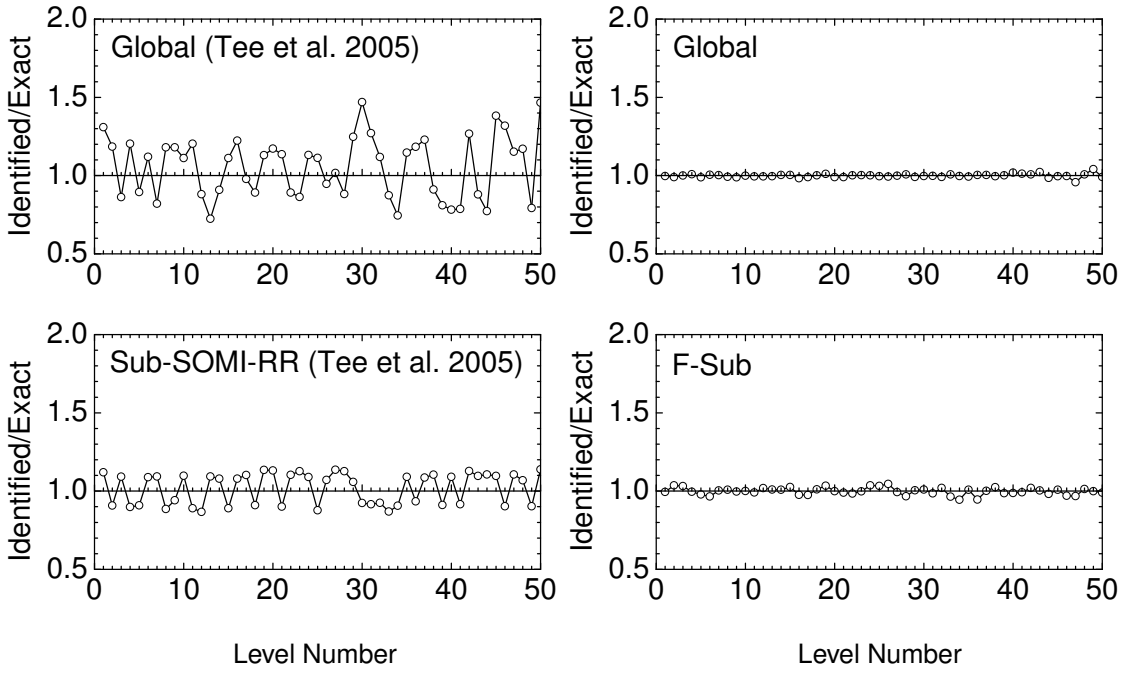

Figure 4.10: Stiffness identification of 50-DOF system under 5% noise: complete measurement

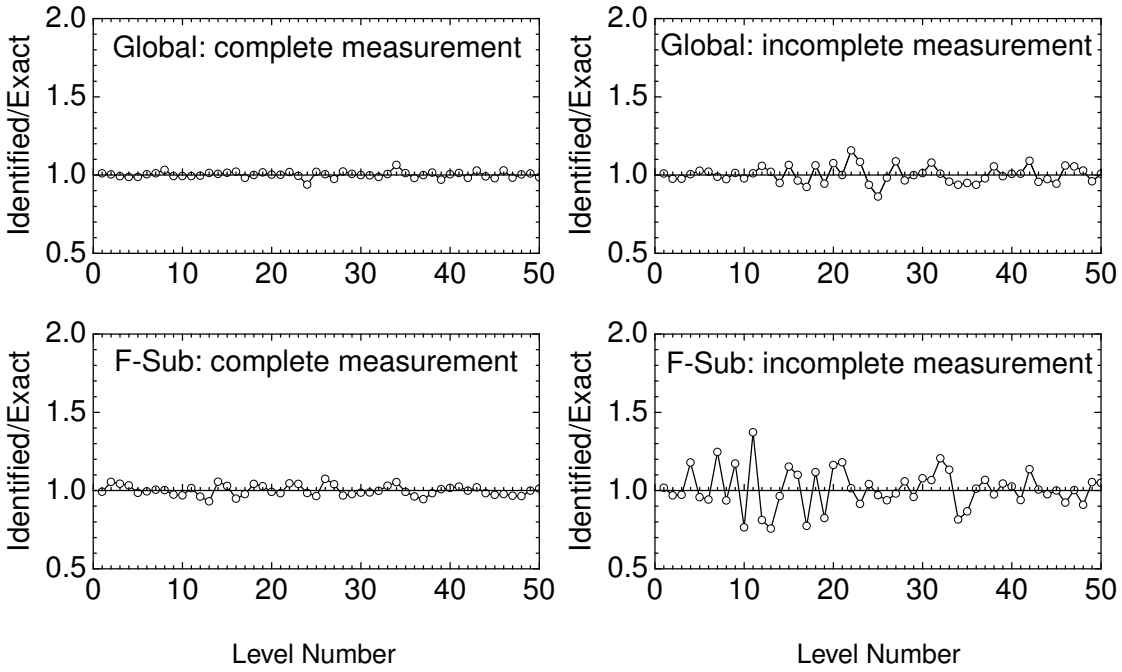

Figure 4.11: Stiffness identification of 50-DOF system under 10% noise: complete measurement vs incomplete measurement

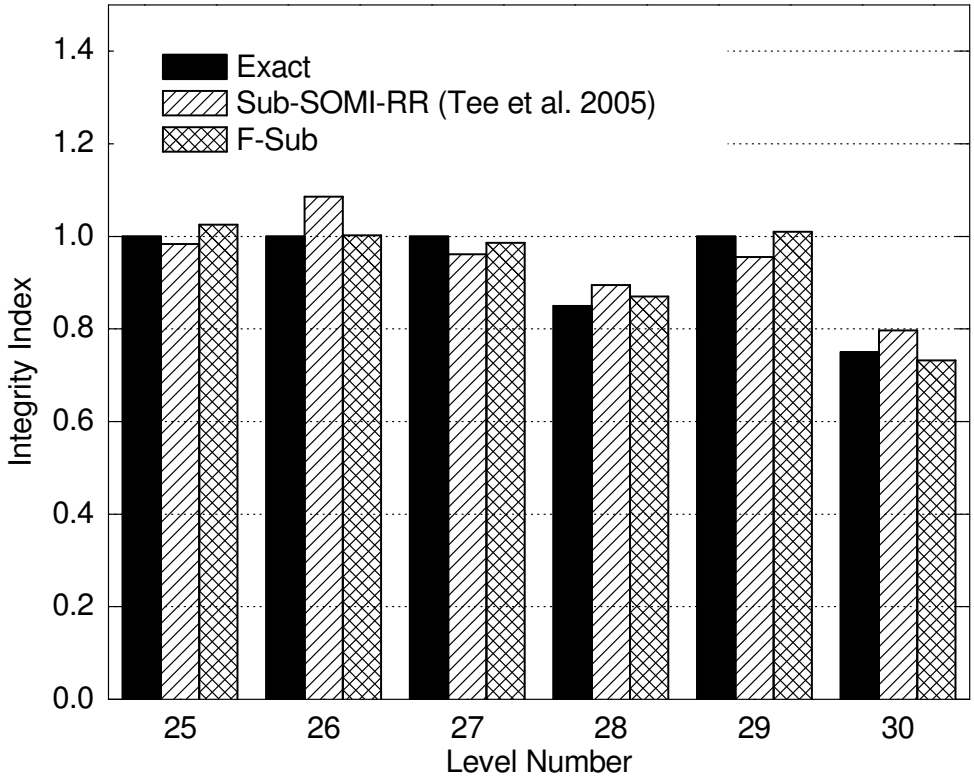

Figure 4.12: Identified stiffness integrity indices for damage scenario 1: 5% noise

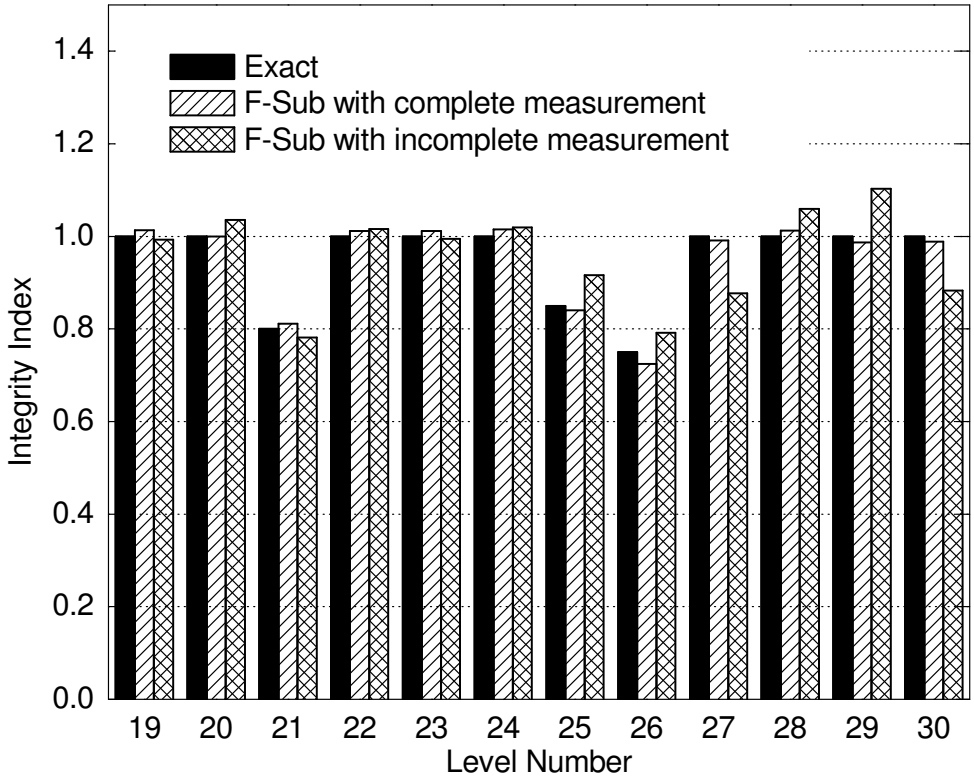

Figure 4.13: Identified stiffness integrity indices for damage scenario 2: 5% noise

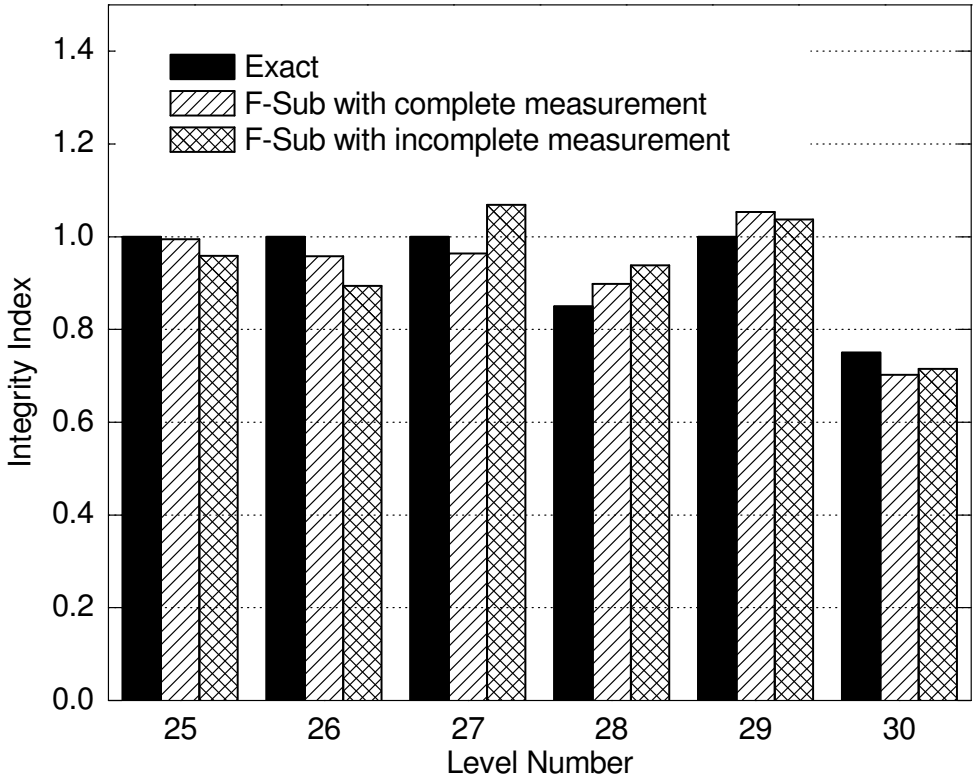

Figure 4.14: Identified stiffness integrity indices for damage scenario 1: 10% noise

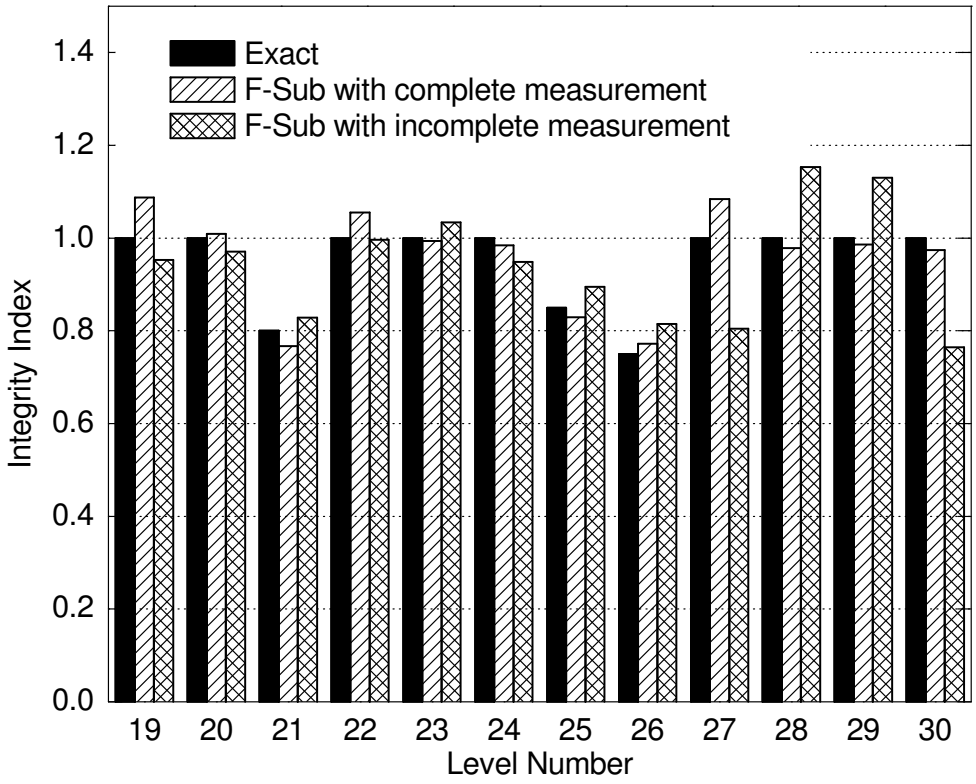

Figure 4.15: Identified stiffness integrity indices for damage scenario 2: 10% noise

Table 4.1: GA parameters for system identification and damage detection in numerical studies

GA parameters	12-DOF system		50-DOF system	
	F-Sub (3S[a])	Global structure	F-Sub (5S[a])	Global structure
Total Evaluations	1,250	3,800	2,400	12,000
Population size	3×3	3×3	3×3	5×3
Generations	4	15	10	50
Sample size	63	162	108	248
Number of runs	10	10	10	10
n_b value	5	5	5	5
Crossover rate	0.8	0.8	0.8	0.8
Mutation rate	0.2	0.2	0.2	0.2
Migration rate	0.05	0.05	0.05	0.05
Regeneration	2	2	2	2
Reintroduction	3	5	5	20
Window width	4.0	4.0	4.0	4.0

[a] S=substructure

Table 4.2: Structural identification of 12-DOF lumped mass system

Noise	Error	Global	Sub-SOMI-RR	Global		F-Sub	
		Complete[a]	(Tee *et al.*, 2005)	Complete	Incomplete	Complete	Incomplete[a]
5%	Mean error (%)	7.9	5.7	0.51	0.66	0.66	0.92
	Maximum error (%)	9.8	9.0	1.39	1.62	1.86	2.58
10%	Mean error (%)	8.8	6.4	1.15	1.47	1.37	2.5
	Maximum error (%)	9.9	9.1	2.73	3.19	4.39	6.04
CPU Time (min)		50	35	63	63	7	7

[a] Complete/Incomplete means the availability of measurement.

Table 4.3: Structural identification of 50-DOF lumped mass system

Noise	Error	Global	Sub-SOMI-RR	Global		F-Sub	
		Complete[a]	(Tee *et al.*, 2005)	Complete	Incomplete	Complete	Incomplete[a]
5%	Mean error (%)	23.5	11.0	0.85	1.99	1.63	4.79
	Maximum error (%)	53.1	18.3	4.16	8.38	6.88	20.94
10%	Mean error (%)	-[b]	-[b]	1.84	5.14	2.81	9.63
	Maximum error (%)	-[b]	-[b]	7.44	19.25	9.90	42.93
CPU Time (min)		190	210	1,740	1,740	65	65

[a] Complete/Incomplete means the availability of measurement.

[b] "-" indicates results are not presented.

CHAPTER 5

Time Domain Substructual Identification

As shown in the previous chapter, the proposed identification strategy, the iSSRM with gradient search and the F-Sub method, offers considerable ease in convergence and significant time cost reduction in computation. The success attributes not only to the conception of the enhanced optimization strategy, but also to the philosophy of substructuring in frequency domain. The use of efficient optimization with a robust divide-and-conquer method is very attractive and of great engineering significance for identifying large scale structures. It is found that, however, F-Sub method requires that the size of substructure has to be large enough to provide sufficient measurement for base points and check points. This requirement will compromise slightly the advantages as a divide-and-conquer strategy. Another disadvantage is that the F-Sub confronts non-uniqueness when identifying stiffness, mass, and damping with known input.

Divide-and-conquer strategies in structural identification have achieved good developments since 1990s. A substructural identification method in time domain were presented using extended Kalman filter to estimate the stiffness and damping coefficient (Koh *et al.*, 1991). The measurement of displacement, velocity and acceleration at the

interface were required. Later this time domain substructural method was improved, referred to as T-Sub method in this study, in identification using GA (Koh *et al.*, 2003b). The enhancement lies in that only the acceleration measurement is needed. A modal domain identification was conducted with GA (Koh *et al.*, 2000), allowing the identification to be carried out in a much smaller domain than physical domain. The component mode synthesis method (Craig and Bampton, 1968) was adopted in substructural damage quantification. The identification was carried out by neural networks with natural frequencies and mode shapes as input and damage cases as output (Yun and Bahng, 2000). Besides, a substructural identification framework is proposed to avoid directly measuring rotations via the strain and translational measurements (Reich and Park, 2001). Recently, a Bayesian based probabilistic approach was also proposed to identify the location and probable level damage in a substructure level (Yuen and Katafygiotis, 2006). Among these research works, the paper by Koh *et al.* (2003b) demonstrated the T-Sub method in maintaining two-fold benefits in convergence and computational efficiency as a general divide-and-conquer method, as well as simultaneously identifying stiffness, mass and damping.

The research in this chapter is to study the feasibility of the proposed iSSRM with gradient search method in identifying substructures in time domain. Specifically, the purpose is to explore an alternative divide-and-conquer identification strategy to F-Sub in the following cases: (1) to identify part of a whole structure and identify the whole structure by substructuring, and (2) to identify stiffness and damping when mass is unknown. Therefore, the first step of the study will investigate the applicability of the enhanced optimization strategy and the T-Sub method in known mass case, including local identification of part of a whole structure and identification of a full structure via progressive substructuring. The second step is then to examine the identification strategy with unknown mass.

5.1 Substructural Method in Time Domain

The motion equation of a multiple degree of freedom dynamic systems can be described as

$$\mathbf{M}\ddot{\mathbf{u}} + \mathbf{C}\dot{\mathbf{u}} + \mathbf{K}\mathbf{u} = \mathbf{f} \tag{5.1}$$

where $\mathbf{M}$, $\mathbf{C}$ and $\mathbf{K}$ are the mass, damping and stiffness matrix of the structural system, respectively. $\ddot{\mathbf{u}}$, $\dot{\mathbf{u}}$ and $\mathbf{u}$ represent the acceleration, velocity and displacement response when the structure is excited by input force $\mathbf{f}$.

In this study, Rayleigh damping is used. That is, the damping is assumed to be proportional to a combination of the mass and the stiffness matrices and given as

$$\mathbf{C} = a_0\mathbf{M} + a_1\mathbf{K} \tag{5.2}$$

It is evident that this proportional damping leads to the following relation between damping ratio ξ_n and frequency ω_n of the n-th mode. Through this relation, the associated coefficient a_0 and a_1 could be determined.

$$\xi_n = \frac{a_0}{2\omega_n} + \frac{a_1\omega_n}{2} \tag{5.3}$$

As the identification procedure involves computing the dynamic response repeatedly, identification of the whole structure would be inevitably time consuming. Instead of solving Eq. (5.1) as a whole, the measured response at the interface can be used to "zoom in" on a given part of the structure, thereby significantly reducing the computational effort and number of parameters leading to improved performance. The equation of motion for a substructure can be written as

$$\begin{bmatrix} \mathbf{M}_{rj} & \mathbf{M}_{rr} \end{bmatrix} \begin{Bmatrix} \ddot{\mathbf{u}}_j \\ \ddot{\mathbf{u}}_r \end{Bmatrix} + \begin{bmatrix} \mathbf{C}_{rj} & \mathbf{C}_{rr} \end{bmatrix} \begin{Bmatrix} \dot{\mathbf{u}}_j \\ \dot{\mathbf{u}}_r \end{Bmatrix} + \begin{bmatrix} \mathbf{K}_{rj} & \mathbf{K}_{rr} \end{bmatrix} \begin{Bmatrix} \mathbf{u}_j \\ \mathbf{u}_r \end{Bmatrix} = \mathbf{f}_r \tag{5.4}$$

where, subscript 'r' denotes internal DOFs of the substructure while subscript 'j' represents the interface DOFs. Treating interface responses as 'input' for the substructure concerned, the above Eq. (5.4) can be rearranged as,

$$\mathbf{M}_{rr}\ddot{\mathbf{u}}_r + \mathbf{C}_{rr}\dot{\mathbf{u}}_r + \mathbf{K}_{rr}\mathbf{u}_r = \mathbf{f}_r - \mathbf{M}_{rj}\ddot{\mathbf{u}}_j - \mathbf{C}_{rj}\dot{\mathbf{u}}_j - \mathbf{K}_{rj}\mathbf{u}_j \tag{5.5}$$

The kinematic responses in the substructural level, $\ddot{\mathbf{u}}_r$, $\dot{\mathbf{u}}_r$, and $\mathbf{u}_r$ are considered to be composed by a quasi-static component and a relative dynamic component. Taking the displacement for example, the internal displacement can be expressed as the sum of quasi-static displacement $\mathbf{u}_r^s$ and relative dynamic displacement $\mathbf{u}_r^*$. That is

$$\mathbf{u}_r = \mathbf{u}_r^s + \mathbf{u}_r^* \tag{5.6}$$

where quasi-static part is the response of structures ignoring all inertial effects and damping, the relative dynamic part is simply the difference between the total response and the quasi-static response. Neglecting the time-derivatives in Eq. (5.5), the quasi-static displacements can then be obtained as

$$\mathbf{K}_{rr}\mathbf{u}_r^s = -\mathbf{K}_{rj}\mathbf{u}_j \tag{5.7}$$

or alternatively,

$$\mathbf{u}_r^s = -{\mathbf{K}_{rr}}^{-1}\mathbf{K}_{rj}\mathbf{u}_j = \mathbf{r}\mathbf{u}_j \tag{5.8}$$

Based on the concept of "quasi-static displacement" vector (Koh *et al.*, 2003b), we have

$$\dot{\mathbf{u}}_r^s = -{\mathbf{K}_{rr}}^{-1}\mathbf{K}_{rj}\dot{\mathbf{u}}_j = \mathbf{r}\dot{\mathbf{u}}_j \tag{5.9}$$

and

$$\ddot{\mathbf{u}}_r^s = -{\mathbf{K}_{rr}}^{-1}\mathbf{K}_{rj}\ddot{\mathbf{u}}_j = \mathbf{r}\ddot{\mathbf{u}}_j \tag{5.10}$$

where $\mathbf{r} = -{\mathbf{K}_{rr}}^{-1}\mathbf{K}_{rj}$, referred to as the influence coefficient matrix and used to relate the internal DOFs to interface DOFs under the quasi-static condition.

Substituting Eq. (5.8), (5.9), and (5.10) into Eq. (5.6), and rearranging Eq. (5.5), we have

$$\mathbf{M}_{rr}\ddot{\mathbf{u}}_r^* + \mathbf{C}_{rr}\dot{\mathbf{u}}_r^* + \mathbf{K}_{rr}\mathbf{u}_r^* = \mathbf{f}_r - (\mathbf{M}_{rj} + \mathbf{M}_{rr}\mathbf{r})\ddot{\mathbf{u}}_j - (\mathbf{C}_{rj} + \mathbf{C}_{rr}\mathbf{r})\dot{\mathbf{u}}_j \tag{5.11}$$

Eq. (5.11) shows the relative motion, i.e., $\ddot{\mathbf{u}}_r^*$, $\dot{\mathbf{u}}_r^*$ and $\mathbf{u}_r^*$, actually defines the dynamic motion, i.e., it can take into consideration of inertial and damping effects. As the damping

term is usually small in comparison to the others, the above equation can be simplified as

$$\mathbf{M}_{rr}\ddot{\mathbf{u}}_r^* + \mathbf{C}_{rr}\dot{\mathbf{u}}_r^* + \mathbf{K}_{rr}\mathbf{u}_r^* = \mathbf{f}_r - (\mathbf{M}_{rj} + \mathbf{M}_{rr}\mathbf{r})\ddot{\mathbf{u}}_j \tag{5.12}$$

This actually means that the forces induced by the quasi-static damping are much smaller than the forces arising from the quasi-static inertia effects. Furthermore, if there is no force applied within the substructure, $\mathbf{f}_r$ vanishes and the response of internal DOFs are determined by the motion of interface nodes induced force. Therefore,

$$\mathbf{M}_{rr}\ddot{\mathbf{u}}_r^* + \mathbf{C}_{rr}\dot{\mathbf{u}}_r^* + \mathbf{K}_{rr}\mathbf{u}_r^* = -(\mathbf{M}_{rj} + \mathbf{M}_{rr}\mathbf{r})\ddot{\mathbf{u}}_j \tag{5.13}$$

Obviously, the T-Sub method needs to solve the internal response on the left hand side while treating the other on the right hand side of equation of motion as interfaces.

5.2 Numerical Examples

In order to verify the applicability of the proposed hybrid strategy in a time domain substructural identification, the same three numerical examples as used by Koh *et al.* (2003b) are studied: a two-span truss structure, a 50-DOF system with known mass distribution, and a 50-DOF system with unknown mass distribution. As concluded by Koh *et al.* (2003b), T-Sub without overlap is recommended for identifying only part of a structure while another version of T-Sub, known as the progressive substrucutral identification (PSI), is good for identification of the whole structure by adaptive substructuring. Therefore, the first two examples are to investigate feasibility of the hybrid optimization strategy in known-mass identification, including identifying a part of the structure by T-Sub without overlap and as a whole by PSI. The third example is to illustrate the PSI method in identifying large systems when the stiffness, mass, and damping are not known a priori.

For each of these three systems considered, Rayleigh damping is adopted with damping ratio of 5% for the first two modes. Treating the two damping coefficients as un-

knowns, the total numbers of parameters to be identified are thus 13, 52, and 102 for the three examples. The input forces are assumed to comply with Gaussian white noise distribution, and known for all the cases, except that they are outside the substructures of concern. In the identification, a data length of 2-second time histories is collected at a sampling rate of 500 Hz. The measurement noise is defined as the ratio of standard deviation of the zero-mean white Gaussian noise to the root-mean-square value of the unpolluted signals. The GA parameters of the identification strategy are given in Table 5.1.

5.2.1 A Two-Span Truss Structure

The two-span truss is composed of 57 elements, out of which, an 11-element substructure illustrated in Fig. 5.1 is to be identified. Typical length of the structural members is 4 m. For each member, Young's modulus and sectional area are 200 GPa and 0.0015 m^2, respectively. The axial rigidity EA is identified through T-Sub method without overlap. In the global structure, eight random forces in total are imposed while only four of them are within the substructure of interest. The accelerations are assumed to be available in 11 locations. As illustrated in Fig. 5.1, 3 of the measurements are inside the substructure and the rest of them are at the interfaces. The identification results are very good in the case of 5% and 10% noise levels are summarized in Table 5.2. In identifying the 11-element truss substructure, the mean/maximum errors are 0.85%/2.60% in the presence of 5% noise and 1.37%/4.07% for 10% noise. The results are significantly better than the earlier results by Koh *et al.* (2003b), which give errors 8.99%/18.90% for 10% noise.

5.2.2 A 50-DOF System with Known Mass

The purpose is to identify the stiffness distribution with assumed mass properties but unknown damping ratios. Exact parameters of the 50-DOF system are $K_1 = K_2 = \cdots = K_{50} = 700$ kN/m, and $M_1 = 600$ kg, $M_2 = M_3 = \cdots = M_{50} = 300$ kg. External

forces are applied at the respective 3^{rd}, 6^{th}, 9^{th} nodes of every 10 levels. Accelerations are measured at the 3^{rd}, 5^{th}, 8^{th}, and 10^{th} node of each 10 levels and the interested substructural interfaces. For the SSI method with overlap, the whole structure is divided into 10 substructures: $S_1 = [45-50)$, $S_2 = [40-50)$, $S_3 = [35-50)$, $\cdots$, $S_{10} = [0-50)$. A square bracket "[" means that the acceleration at the level indicated is required as interface and used as input whereas a parenthesis ")" indicates the measurement at that level is optional. The search limit is set from 0.5 to 2.0 times of real values. Using the proposed identification strategy, the total evaluations are 12,000 for both complete structural identification (CSI) and PSI so that a fair comparison of accuracy can be done.

Typical identification results of the present investigation at 5% noise are illustrated in Fig. 5.2. The results give a consistent picture that the proposed identification strategy is much better than the previous T-Sub method by Koh *et al.* (2003b) for both CSI and PSI. In terms of identified-to-exact ratios, the mean absolute error of 7.3% for CSI and 3.1% for PSI in the identified stiffness parameters were reported in Koh *et al.* (2003b). The saving in computational time was 37% for PSI compared to CSI. With the proposed identification strategy, the mean/maximum absolute error/time are reduced to 0.75%/2.48%/12min for CSI and 1.32%/4.73%/5min for PSI. The computer time achieves a 42% reduction for PSI as compared to CSI. When the noise level of measurement goes up to 10%, the mean/maximum absolute error are 1.36%/5.15% for CSI and 2.84%/11.04% for PSI. However, the results in the case of 10% noise were not reported in the reference Koh *et al.* (2003b), and thus comparison cannot be made.

5.2.3 A 50-DOF System with Unknown Mass

The third example will further illustrate the outstanding feature of T-Sub, that is identifying stiffness and damping without knowledge of mass distribution. It is obviously more challenging as the stiffness, mass and damping are to be identified simultaneously. To illustrate the point, the same 50-DOF system is investigated again with unknown mass.

The whole structure is to be identified via 25 substructures which are $S_1 = [48 - 50)$, $S_2 = [46 - 50)$, $S_3 = [44 - 50)$, $\cdots$ $S_{25} = [0 - 50)$. Considering the increased number of unknowns and thus a much bigger search space, 50,000 evaluations are adopted for fair comparison with the work by Koh *et al.* (2003b). For each substructure by PSI, 2,000 evaluations will be computed to find the candidate sub-system. The force locations are maintained the same as in Example 2. However, the accelerations taken herein are at the 2^{nd}, 4^{th}, 6^{th}, 8^{th}, and 10^{th} level of each substructure. For the first substructure $S_1 = [48 - 50)$, an additional measurement is taken at the 49^{th} level. The reason is that the size of the first substructure is too small to be identified through the lower modes contributions. If the first substructure is not accurately identified, the error will propagate to subsequent substructural identification as S_1 will be then treated as known but inaccurate.

The results are excellent in the sense that both stiffness and mass are fairly well identified, as summarized in Table 5.3. The T-Sub method is associated with negligible modeling error in the formulation. The error originates from ignoring the time-derivative forces in the interface. It is reflected in Table 5.3 in the identification of noise free case. By CSI method, both the mean and maximum absolute errors are found to be zero. However, the errors do not vanish but are small for PSI method.

The comparison of results with previous research (Koh *et al.*, 2003b) is presented in Fig. 5.3 and 5.4. In Koh *et al.* (2003b), the mean errors of identified stiffness are 5.1% and 21.0% for PSI and CSI, respectively, in the case of 5% noise, while the corresponding errors are 1.46% and 1.17% in the present study. Reduction in computer time for PSI compared to CSI is 37% in the present study, and this is quite close to the 40% reduction reported in Koh *et al.* (2003b). This finding actually highlights the success of substructuring in reducing the forward analysis time. As the total evaluations are fixed equally, the time spent on the iterations on a substructure is of course much less than using the whole structure. The identification of a 50-DOF system with unknown mass takes only

19 min by the PSI method, using a two-processor workstation with each processor having quad-core CPU at 3.00 GHz.

It is discovered in the two examples on 50-DOF system, however, that the CSI method yields slightly better identification accuracy than the PSI method. The observation is predominant especially in the case of incomplete measurement. This is reasonable in that, for the same type of sensor distribution, the modal information picked up in the global structure will always be richer than in a substructural level. The contribution from the lower modes is reflected as rigid body response in a substructural level. Only deformable modes will exhibit the participation from component stiffness.

5.3 Conclusions

It has been verified in this chapter that the proposed uniformly sampled genetic algorithm plus gradient search is applicable in time domain substructural identification (T-Sub). Through the numerical investigation of different type of structures, several remarks can be given as

(1) The PSI method was recommended (Koh *et al.*, 2003b) to be a successful variant of T-Sub method for identifying a whole structure by dividing and conquering. It is discovered in the two examples on 50-DOF system, however, the CSI method yields slightly better identification over that by PSI method. The reason is that, for the same layout of sensors, more modal information will be collected in a global level than a substructural level, although more unknowns are involved in a global identification. The engineering implication of this finding is that it is better to have more measurements in a substructure of interest, especially for the first several substructures for PSI identification.

(2) By completing the same number of total evaluations, it is discovered in this study that the substructural efficiency achieved by the PSI method over the CSI method

is not sensitive to the optimization method used in the backward analysis, although the enhanced optimization strategy can help to reduce computer time by either CSI or PSI method. However, the substructural efficiency will vary with the substructural size and the structural type that to be identified. It is of confidence to expect that the substructural ratio will reduce further when the number of DOFs increases.

(3) Based on the studies of the 50-DOF system (Tee *et al.*, 2005), F-Sub method is recommended over T-Sub and Sub-SOMI-RR (Tee *et al.*, 2005) for large structural identification in terms of accuracy and efficiency. The results are shown in Fig. 5.5.

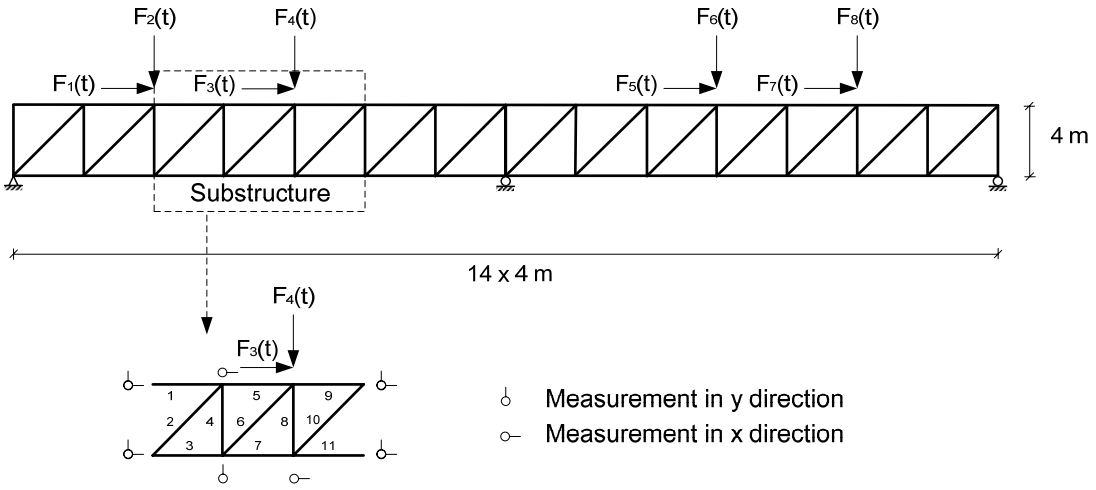

Figure 5.1: Two-span truss structure and substructure

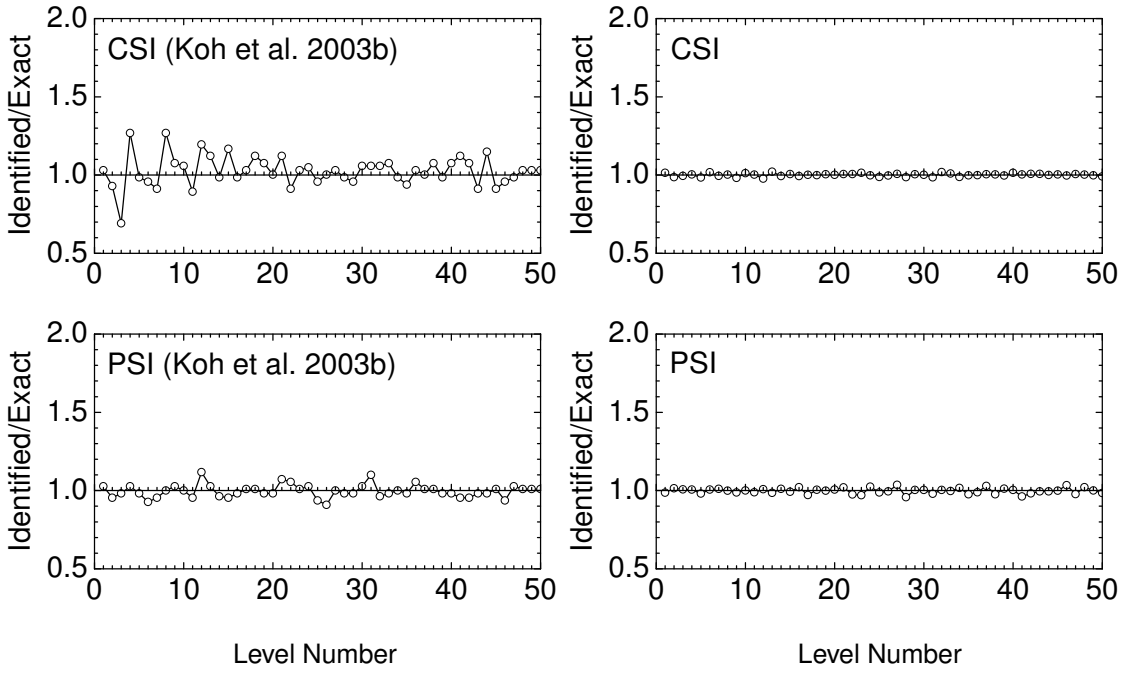

Figure 5.2: Ratio of identified stiffness to exact value for 50-DOF known-mass system under 5% noise

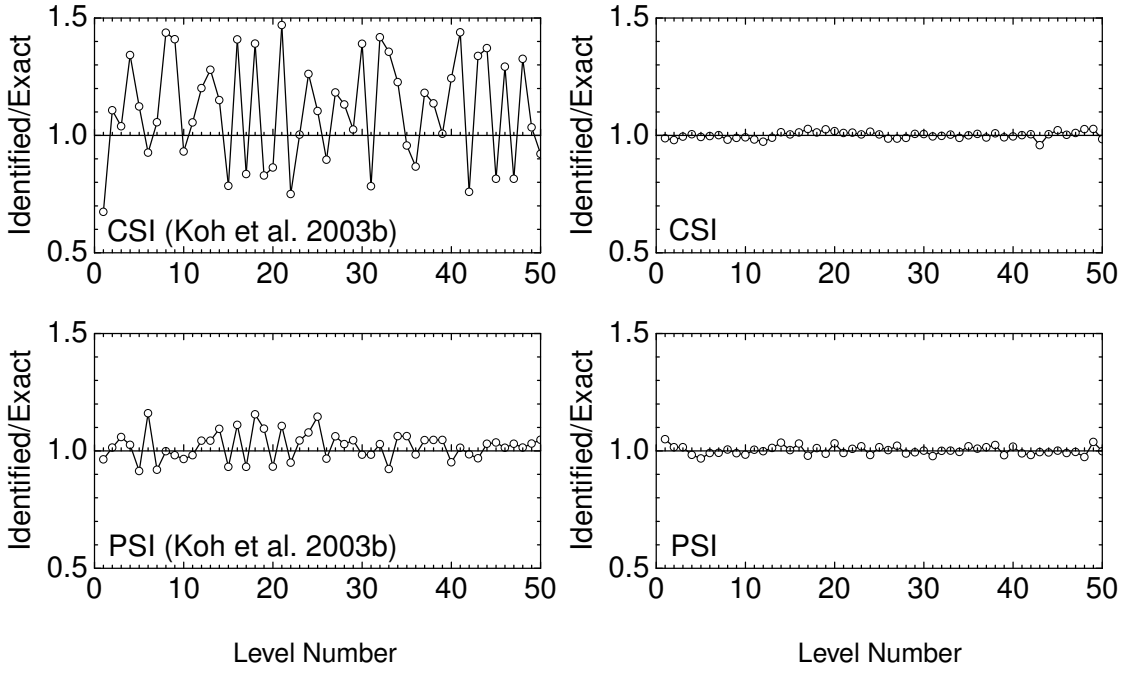

Figure 5.3: Ratio of identified stiffness to exact value for 50-DOF unknown-mass system under 5% noise

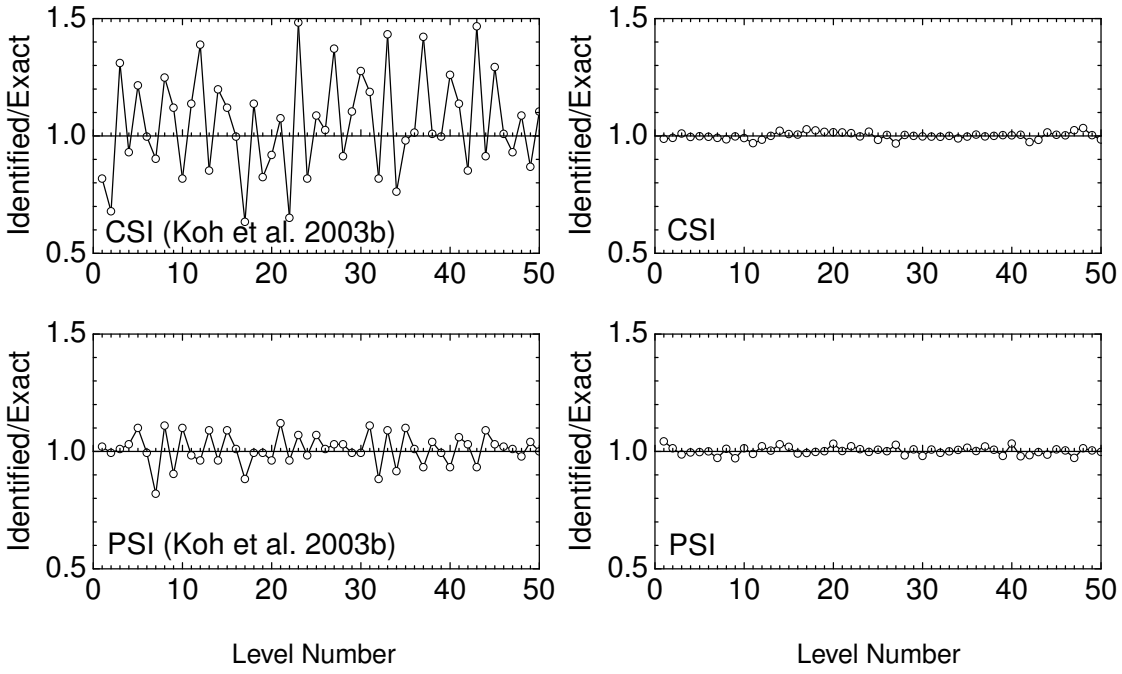

Figure 5.4: Ratio of identified mass to exact value for 50-DOF unknown-mass system under 5% noise

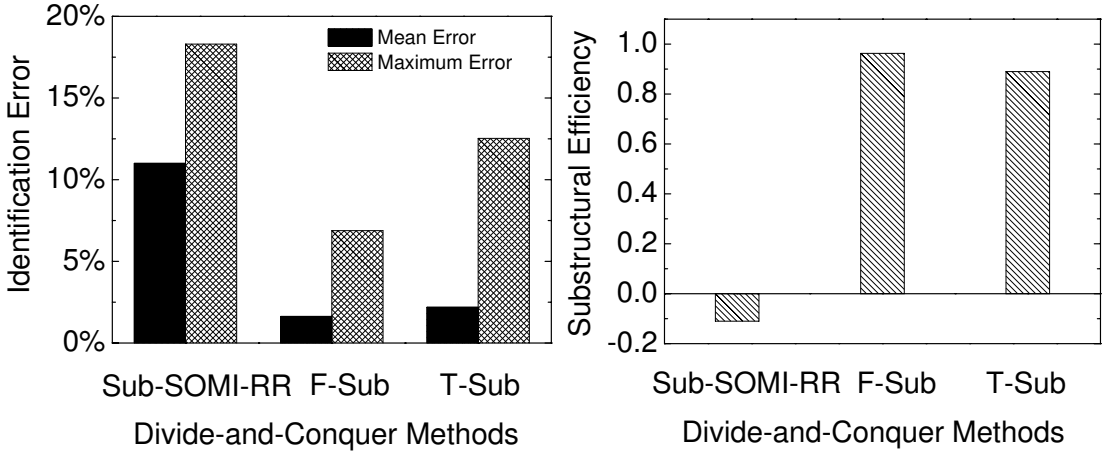

Figure 5.5: Comparison of divide-and-conquer methods in system identification based on the 50-DOF system (Sub-SOMI-RR taken from Tee *et al.* (2005))

Table 5.1: GA parameters for system identification in numerical examples

GA parameters	Truss	50-DOF system: known mass		50-DOF system: unknown mass	
		CSI	PSI (10S[a])	CSI	PSI (25S[a])
Total Evaluations	2,400	12,000	1,200	2,400	12,000
Population size	3×3	5×3	3×3	10×3	3×3
Generations	10	48	4	128	16
Sample size	108	238	63	168	34
Number of runs	10	10	10	10	10
n_b value	5	5	5	5	5
Crossover rate	0.8	0.8	0.8	0.4	0.4
Mutation rate	0.2	0.2	0.2	0.2	0.2
Migration rate	0.05	0.05	0.05	0.05	0.05
Regeneration	2	3	2	3	3
Reintroduction	5	20	3	50	5
Window width	4.0	4.0	4.0	4.0	4.0

[a] S=substructure

Table 5.2: Identification of truss substructure by SSI without overlap

Member number	Exact EA (MN)	Estimated EA		
		5% noise	10% noise	10% noise (Koh *et al.*, 2003b)
1	300	299.70	290.60	338.27
2	300	304.00	297.00	289.00
3	300	296.50	304.30	326.54
4	300	300.60	298.30	285.19
5	300	300.10	305.00	243.26
6	300	298.80	298.70	315.98
7	300	302.30	294.70	319.50
8	300	298.60	302.60	305.13
9	300	299.40	299.50	251.76
10	300	306.40	300.00	316.57
11	300	307.80	287.80	256.15
Mean absolute error (%)		0.85	1.37	8.99
Maximum absolute error (%)		2.60	4.07	18.90

Table 5.3: Identification of 50-DOF lumped mass system with unknown mass

Methods	Identification error	Noise level for stiffness			Noise level for mass		
		0%	5%	10%	0%	5%	10%
CSI	Mean error (%)	0.00	1.17	2.43	0.00	1.12	2.27
	Maximum error (%)	0.00	3.65	7.74	0.00	3.45	7.99
PSI	Mean error (%)	0.58	1.46	3.05	0.53	1.34	2.89
	Maximum error (%)	2.24	4.89	10.11	2.20	4.77	9.69

CHAPTER 6

Identification of Structural Changes: Experiment Study

In Chapters 2 and 3, a uniformly sampled genetic algorithm, i.e., iSSRM, with gradient search is proposed for identifying large structural systems. Extensive parametric studies have been carried out to reach a balanced optimization in the initial non-gradient search and the latter gradient search. In Chapter 4, the proposed identification strategy is investigated in an extended frequency domain substructural identification (F-Sub). The original substructural method under sinusoidal excitation is improved to accommodate random excitation (Koh and Shankar, 2003a). The identification strategy is also applied in Chapter 5 for time domain substructural identification (T-Sub). These two chapters have served to test the validity of "peak-shifting" in a substructural level, paving the way to identifying even larger systems with much less computer cost. It has been shown numerically in the global identification that the proposed strategy is able to achieve equally good result with an impressive 90% reduction in computer time, when compared to recent similar works (Koh *et al.*, 2003a; Perry *et al.*, 2006). With the aid of substructural method, the proposed identification strategy has the potential to identify a 50-DOF structure (Koh *et al.*, 2003b) with only 4% computer time. It should be noted that this is done without parallel computing, although the proposed identification strategy can

readily be parallelized due to its high concurrency.

Nevertheless, such good numerical results as demonstrated in the previous chapters should be supported by experimental evidence. To investigate the performance of the proposed strategies in global/substructural identification, the experiment conducted by Koh and Perry (2007) is considered. The experiment is also extended in order to identify the stiffness change associated with welding, which serves to model the effect of structural strengthening, for example, by means of retrofitting. Together with the cut-induced damage data, new data are used to test the proposed methods in a more challenging way, where the stiffness increased by welding is to be determined in the presence of initial damage.

In the first part of this chapter, static test will be implemented to serve as as-built for dynamic test by different methods. The second part will cover vibration testing setup, data processing, and dynamic baseline state identification. The third part will then be on the arrangement of damage and strengthening scenarios. The last part will present the damage identification results based on post analysis of the experimental data. To this end, it is important to bear in mind that subsequent identifications are carried out based on known mass properties, which are taken from the baseline identification using the dynamic test data.

6.1 Static Testing for Baseline Quantification

The original model used by Koh and Perry (2007) was a 7-storey steel frame. The six columns were made of steel plates with 25×4.6 mm rectangular cross section. At each level, a rigid frame of a width to length ratio 1:2 was fabricated by a $25 \times 25 \times 3.0$ mm square hollow section. With symmetrically distributed flexible columns around a rather rigid floor, the structure can be simplified as a shear building with a single translation at each level. For ease of load application, the model was erected horizontally to a rigid

vertical supporting frame, as shown in Fig. 6.1.

Static experiment was carried out as a supplement to dynamic testing. By hanging weights at each level, the static displacements were recorded from transducers. Two 10-mm displacement transducers (Tokyo Sokki Kenkyuio) were used to measure the left-hand side and right-hand side deflection at each loaded level. This was illustrated in Fig. 6.2. The average of two displacements was taken as the deflection d_i for each storey. The weight hanging test was conducted storey by storey, and every 5 kg is added until a maximum of 25 kg was reached. This procedure was repeated from the supporting end level 1 to the free end level 7. Therefore five data points were obtained for each level, from which a linear force-displacement line can be obtained by linear regression. The total stiffness from level 1 to an arbitrary level i can be expressed as

$$K_i = \ell\left(\frac{F_i}{d_i}\right) \qquad (i = 1, 2, \cdots 7) \tag{6.1}$$

where $\ell(\cdot)$ denotes the linear regression obtained from the load-displacement data points. Then the stiffness of each level k_i can be obtained accordingly by Eq. (6.2)

$$k_i = \begin{cases} K_1 \\ \\ (K_i^{-1} - K_{i-1}^{-1})^{-1} \quad (i = 2, 3, \ldots 7) \end{cases} \tag{6.2}$$

6.2 Dynamic Testing

Dynamic experiment is the main focus of the chapter, to identify stiffness change of the tested frame in each damage/strengenthening phase. Three methods, i.e., global identification, T-Sub method, and F-Sub method were used to carry out identification on the basis of dynamic testing data. Among these three methods, global identification and T-Sub method would be used to identify the baseline model of unknown mass. Then the baseline mass by different methods would be used to identify the stiffness change via the corresponding methods. As the F-Sub method cannot be used to identify the unknown mass case, the required baseline mass was obtained by T-Sub method.

6.2.1 Vibration Testing Setup

In vibration testing, dynamic force was applied through a function generator (Signametrics function generator, model SM-1020), where the force history was converted into voltage time signal. By a power amplifier, the signal was adjusted to the workable level and to produce sufficient movement for an electromagnetic shaker (model Labworks ET-126B). The shaker was clamped to a rigid base. As illustrated in Fig. 6.3, force generated by the shaker was transferred to the frame by a connecting rod and a bolted connection. The output force of shaker was captured by a force sensor, which was attached up to the connecting rod through an aluminum plate and fastened down to the shaker via a threaded stainless steel stringer. Detailed connection of shaker, force sensor and the tested frame was shown in Fig. 6.4 and 6.5.

The dynamic response was measured at each level of the frame using three types of accelerometers. Performance specifications of the seven accelerometers used are given in Table 6.1. These accelerometers were mounted at the center column of the upper side in each level. To avoid inducing external damping due to mounting, thin double sided tape and thin layer epoxy were adopted. The excitation was measured through a force sensor. The sensitivity, force range, and frequency range of the force sensor were 11.16 mV/N, 445 N, and 36 kHz.

With battery-powered signal conditioner, signals from the accelerometers and force sensor were transmitted to a 16-channel high-speed digital oscilloscope (Yokogawa model DL716E). In the experiment, eight channels were used for data acquisition. The data was recorded at a sampling rate of 5 kS/s. The record length was taken as 10k, i.e., 10,000 points were recorded for each signal during the vibration test.

6.2.2 Data Processing

Noise is inevitable in the measured response and excitation signals. There are two major sources of noise in vibration test: electrical noise of the measurement system and background noise. The electrical noise is undesired electromagnetic interference in a transmission cable or device. It comes from (1) a coupling between circuits in the measurement system with power circuits, (2) vibration-sensitive elements other than the sensor, e.g. cable, and (3) improper selection/setting of system components such that achievable signal-to-noise ratio is not attained (Harris and Piersol, 2001). Background or ambient noise, on the other hand, is mainly caused by the unknown background vibration sources, for instance, occasional heavy equipment operating in the laboratory.

Therefore data processing comprises two steps of noise filtering. The first step is to remove the non-zero mean offset caused by electrical noise. In the study, the mean of the first 500 points of the whole 10K-event is computed, accounting for the potential offset before the force application. Then the first step of de-noising is done by subtracting the computed mean value from the whole data record. The second step is to remove the response due to higher frequency inputs which exceeded the bandwidth of the tested structure. The measured 7th frequency of the intact seven level frame is 123 Hz (Perry, 2006). Hence, a low-pass filter is designed with a cut-off frequency of 256 Hz. The ripples at the pass band and stop band are set to be 3 dB and 60 dB.

6.3 Baseline Identification

The baseline of stiffness change would be established via vibration data in this section. As the stiffness changes would cover cut-induced damage and structural strengthening by welding, the baseline of these two cases had to be identified in advance. The intact state would be considered as baseline for cut-induced damage case whereas the final scenario of cut-induced damage would be used for baseline for strengthening case. Baseline

identification is to map the experimental model into the mathematical model used, i.e., a shear building which can have lateral motion in one direction at each level.

The following sections identify the baseline model using system identification methods that are applicable without the knowledge of mass, stiffness, and damping properties. For comparison, the proposed iSSRM with gradient search as well as the companion methods SSRM and iSSRM are used in the backward analysis. Both global identification and T-Sub method are considered in the forward analysis. Substructural identification is examined by PSI method recommended in the case of unknown mass (Koh *et al.*, 2003b). Two substructuring arrangements are adopted, while maintaining the same number of total evaluations. The first arrangement is to use 2 substructures, for instance, $S_1 = [4-7]$ and $S_2 = [1-7]$. The second is to use 4 substructures, i.e., $S_1 = [6-7]$; $S_2 = [4-7]$; $S_3 = [2-7]$; $S_4 = [1-7]$. For the 7-level model, the PSI is carried out step by step. For example, the outer substructures, away from the supporting end, are identified first and the identified stiffness values are treated as known in successive identifications. Experimental data from previous static testing would serve as a good reference for dynamic testing. Once the two baseline states of damage and strengthening are established using global/substructural identification, the identified mass properties are taken as known in the corresponding method for further damage/strengthening detection.

To carry out baseline identification and the subsequent detection of stiffness change, total evaluations have to be determined for the identification strategies. The numerical examples presented in Chapter 2 and 3 have demonstrated that using iSSRM method would reduce the fitness evaluations by half compared to the original SSRM method, and using iSSRM with BFGS will reduce the evaluations further to only 10% for global identification. In addition, the use of PSI substructuring typically achieves a further reduction of computer time to 40% compared to the same number of total evaluations with global identification. With this knowledge of reduction in total evaluations, typical GA parameters for baseline state identification as well as subsequent damage and strength-

ening detection are given in Table 6.2 and 6.3. In these tables, the total evaluations by T-Sub and F-Sub method are only 40% of the total evaluations by global identification. In Table 6.2, 80% of the total evaluations are expected to spend on iSSRM global search and 20% for gradient local search. For substructural identification, GA parameters used for each substructure are given in Table 6.2. This evaluation allocation is adopted throughout the present chapter.

6.4 Scenarios of Structural Change Identification

This section describes various scenarios of structural changes, including damage induced by physical cut and strengthening by welding. In the cut-induced damage detection, the original experimental data of 6 basic damage cases and 3 additional damage cases by Perry (2006), as shown in Tables 6.4 and 6.5, are used. The intact state before any cut of frame is taken as the baseline for cut-induced damage detection. As an extension of the experiment, strengthening by welding is considered in 5 basic scenarios and 3 additional scenarios, i.e., Tables 6.6 and 6.7. The 6^{th} damage scenario D6, involving large damage in levels 3, 4 and 6, will be considered as the baseline for quantifying the strengthening effect due to welding.

These tests are all conducted using specified input of random forces A, B, C, D and E. For each input, three tests are carried out at a sampling rate of 5 kS/s. Note that the large damage in level 3 remained unaltered in all the strengthening case, i.e., Fig. 6.6. Cut-induced damages in levels 4 and 6 were repaired by welding progressively from level 4 to level 6, as illustrated in Fig. 6.7. This led to increase in stiffness which is to be identified. It should be noted that small, moderate and large damage or strengthening are short for “S”, “M”, and “L”, respectively, in the tables and figures of this chapter. Illustrations of the magnitudes in cut-induced damage and strengthening are given in Figs. 6.8 and 6.9, respectively.

6.5 Analysis of Experimental Data

The main purpose of this section is to investigate the stiffness change using the proposed identification strategies. Based on the parameter setting in baseline identification, i.e., Table 6.2, the GA parameters used for identifying cut-induced damage and structural strengthening are given in Table 6.3. Damping parameters are treated as unknown and mass is assumed to be known and remain unaltered as the reference state. For consistency and better identification, the same method will be used for stiffness change detection if it is used in the reference state identification. An exceptional case is the F-Sub method, which is not applicable in the unknown mass case. Thus the T-Sub method will be adopted instead in the reference state identification for the F-Sub method.

To have a comprehensive investigation on the proposed strategies, the success of identification should account for potential uncertainties in the identified stiffness change. The uncertainties may arise from modeling error, measurement noise, incompleteness in the forward analysis, as well as the identification strategy in the backward analysis.

First, modeling error is unavoidable in structural identification (Koh and See, 1994; Beck and Katafygiotis, 1998). In the forward analysis, an adequate mathematical model is needed to represent the physical system. The mathematical model should be as general as possible, and be capable of capturing the main physical behavior of the structure. However, differences exist between a mathematical model and real physics, due to variations of material properties inexact modeling of constitutive behavior and boundary conditions, and insufficient spatial discretization of the distributed structural system. As a result, there will be uncertainty in accuracy in the predicted response.

Second, measurement noise would introduce uncertainties for identification (Koh and See, 1994; Beck and Katafygiotis, 1998; Xia *et al.*, 2002). Using classical identification methods, input/output noise would pose great challenge for numerical convergence of identified parameters. From an optimization angle, measurement noise of input and

output will induce peak shifting and decreasing as reported in Chapter 3. Therefore, the final identification will be accordingly affected. Another source of uncertainty is due to measurement incompleteness. In practice, the set of observed DOFs is usually a smaller subset of the whole model DOFs. Because of incomplete measurement, the richness of collected modal information is limited and thus the sensitivities of unknown parameters in optimization are affected accordingly.

Third, identification uncertainty may originate from the stochastic characteristics of the optimization method (Htun, 2004; Koh and Htun, 2004). Due to the random choices or probabilistic operations incorporated, these methods produce different best estimates in different runs.

Existence of these uncertainties may cause difficulty in identifying less pronounced damage, while reporting false damage on intact structural elements. To access the effect of these uncertainties, final identification would be reported on a statistical basis in this study. The database of statistics is established on a combination of load cases. For instance, each damage/strengthening scenarios was tested using five different forces A, B, C, D, and E. For each force, three tests were carried out. In total there were fifteen sets of data for each scenario. In the identification, force is assumed to be the same in the reference state identification and damage/strengthening detection. For example, if force A is used in the three tests of undamaged case D0, the same force A will be used in damaged case D1 for the other three tests. Thus in the identification by force A, nine combinations are studied. Eventually, for each damage/strengthening scenario, 45 combinations are studied as 5 different forces are used. Final identification of each damage/strengthening scenario is presented in terms of success rate, in Tables 6.8 to 6.10. Representative stiffness change scenarios would be reported by the average of total 45 combinations, i.e., from Fig. 6.10 to Fig. 6.17.

The success of identification is reported as “1x”, if the smallest real change (dam-

age/strengthening) in the investigated scenarios is greater than maximum false change. In particular, if there are two or more small changes in the scenario, the one close to the supporting end would be taken as the success reference, because it is often difficult to identify small change near the fixed end. For example, in the basic damage case D4 (Table 6.4), 4.1% small damage occurs in both level 3 and 6 with 16.7% large damage in level 4, the "1x" success would be reported when the maximum false damage is less than 4.1%. In order to provide as much damage information as possible, success rate is reported up to "4x" in the Appendix B, indicating that the identified change is 4 times as large as the maximum false change. Collecting all the success cases in each investigated scenario, the final success is recorded as a percentage over a total of 45 cases. The maximum false change is reported not only in magnitude but also its location. The details are presented in Appendix B. For concise reporting in this chapter, the results on the effect of incomplete measurement and the effect of substructural size are summarized in Tables 6.8, 6.9, and 6.10, and are discussed below.

6.5.1 Effect of Incomplete Measurement

The fitness evaluations required for global and substructural identification using the proposed strategy reduced to only 10% and 4% of the evaluations, respectively, by Koh and Perry (2007). With the knowledge of time reduction in computational effort, the results presented in Table 6.8, and 6.9 are excellent for complete measurement. For global structural identification, the "1x" success rates obtained by Koh and Perry (2007) are 100%/47%/31%/100% for D2/D3/D4/D6 scenarios. Using the proposed strategy herein, the corresponding success rates are 100%/78%/64%/100% for global identification, 100%/98%/89%/100% for T-Sub method and 96%/60%/69%/93% for F-Sub method. Recalling the basic damage scenarios from Table 6.4, the results herein show that using the enhanced identification method iSSRM with BFGS search, the global identification as well as substructural identification via F-Sub and T-Sub method can achieve

equally good identification success in single and multiple large damages, i.e., D2 and D6. More importantly, the results in this study are much better than that by Koh and Perry (2007) in the case of multiple damages with different magnitudes, i.e., D3 and D4, which include a small damage of only 4% in multiple damages.

The locations of maximum false change reported are mostly in the lower levels, i.e., levels 1, 2 and 3. Using 2 substructures for the 7-level frame, F-Sub method gives acceptable identification while global identification and T-Sub method performs even better. To have knowledge on the overall performance of the proposed methods, the average results of total 45 combinations are reported on the global identification and F-Sub method in Fig. 6.10 to Fig. 6.17, as these two methods produce a lower identification success than T-Sub method. The results are excellent and robust as both single change of small magnitude and multiple changes of different magnitudes can be accurately identified.

Incomplete measurement would compromise the identification accuracy as expected. To maintain a consistent investigation based on incomplete measurement, the accelerations are obtained from levels 1, 3, 5 and 7. The original results by Koh and Perry (2007) gave 100%/64%/27%/100% "1x" success for D2/D3/D4/D6 cases. Using the proposed strategy, the success rates decrease compared to complete measurement although still acceptable. The success rates are 100%/80%/60%/100% for global identification, 100%/73%/71%/100% for T-Sub method and 96%/44%/58%/87% for F-Sub method using 2 substructures. These results show that the decrease of the success rate is much larger in T-Sub and F-Sub than that in global identification, especially in D3 and D4 cases (Table 6.4) where the 4% small damage is involved in multiple damage cases. In addition, the maximum false damage is often associated with lower levels or the levels close to the damage. For strengthening cases, the maximum false events are also found in level 3, where a cut-induced damage was remained. As a conclusion, incomplete measurement has more influence on substructural method than global identification, as reducing equally the number of measurement will affect much less in richness of modal information

in a global level than in a substructural level.

6.5.2 Effect of Substructure Size

This section studies the effect of selection of substructure size. It is important because the dynamic characteristics captured by a substructure will be different to its size. As recommended by the previous research (Koh *et al.*, 2003b), PSI will be used in this study rather than substructure with/without overlap. To focus on the effect of substructure size, the identification herein is based on complete measurement. Two different sizes are studied since there are only 7 levels in the tested frame, which included 2 substructures with $S_1 = [4-7]$ and $S_2 = [1-7]$, as well as 4 substructures with $S_1 = [6-7]$; $S_2 = [4-7]$; $S_3 = [2-7]$; $S_4 = [1-7]$. The results are summarized in Table 6.10. In general, identification with 2 substructures achieves consistently better result than that by 4 substructures, regardless of using T-Sub or F-Sub method. This is reasonable as smaller substructures would be more difficult to identify unless the higher modes are picked up by the sensor arrays. In the case of 4 substructures, S_4 at the free end with only 2 elements is usually not well identified. In the next round to identify S_3, error propagates when S_4 is treated as known in PSI. Finally, the identification using 4 substructures would consistently degrade. Typically, the maximum false strengthening in Table 6.10 is as large as around 20% for all the strengthening case via T-Sub and F-Sub method.

6.6 Conclusions

This chapter has presented a comprehensive experimental study based on a 7-storey steel frame, incorporating baseline identification as well as detection of changes due to cut and welding. The study investigates the proposed uniformly sampled GA with gradient search, as well as its application into global identification and substructural identification

i.e., T-Sub and F-Sub method, by progressive substructuring (PSI).

Compared with the previous study by Perry (2006), the enhanced optimization strategy makes it possible to achieve similar accuracy using only 10% of evaluations in global identification and 4% of evaluations in T-Sub and F-Sub method. More importantly, the results on identification are consistently superior to the original work. Besides equally good performance in identifying large changes in stiffness, the proposed identification strategies are able to quantify multi-damage of different magnitudes and small damage/strengthening over false change.

Further experimental investigation on the effect due to incomplete measurement and substructure size yields engineering meaningful observations. In the case of incomplete measurement, the identification results are better than that by original SSRM with much less computer time. However, incomplete measurement brings more performance degradation in T-Sub and F-Sub than global identification. In addition, a suitable substructure size should be selected for substructural identification. For instance, the identification via 2 substructures produces consistently better results than via 4 substructures in the experimental study considered. This is observed in the substructural identification for both T-Sub and F-Sub methods.

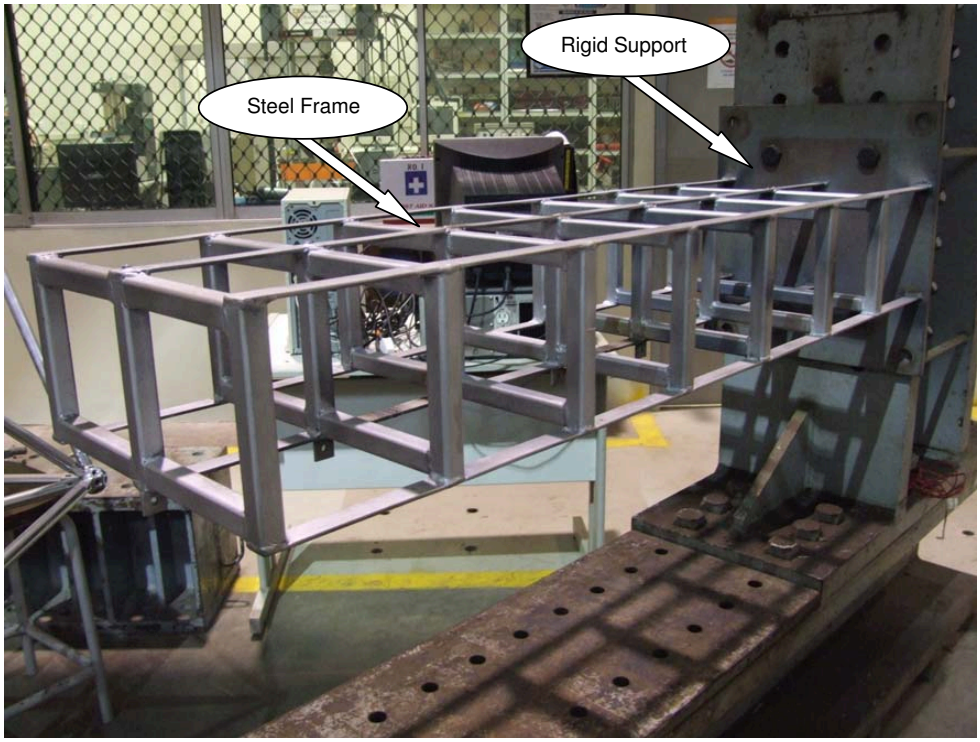

Figure 6.1: Experimental model of frame building

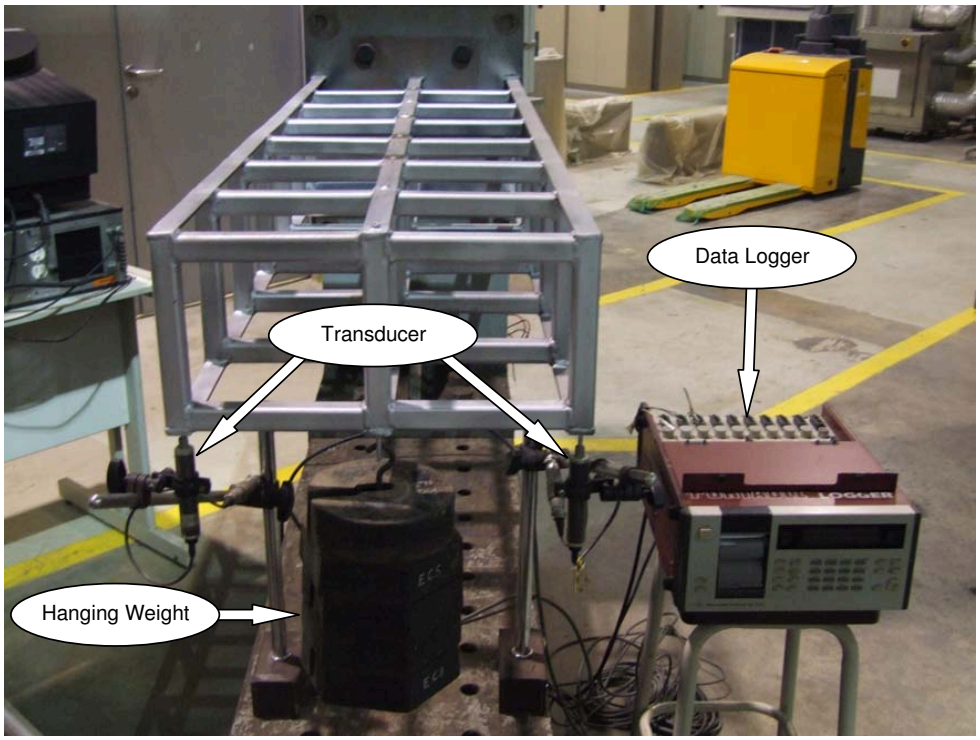

Figure 6.2: Static test set up

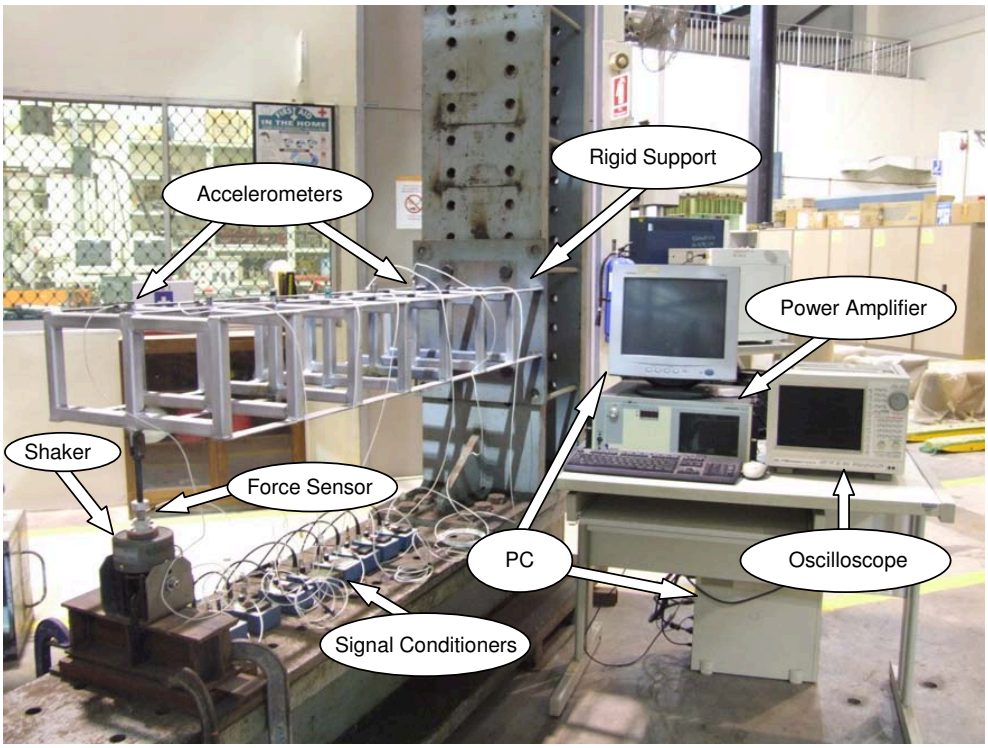

Figure 6.3: Dynamic test set up

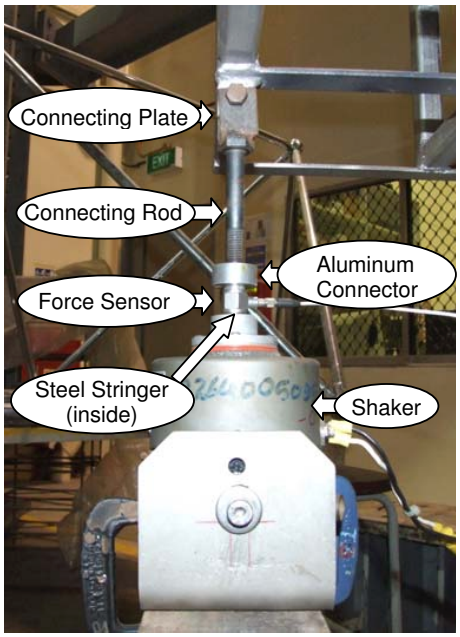

Figure 6.4: Shaker used to excite the frame model

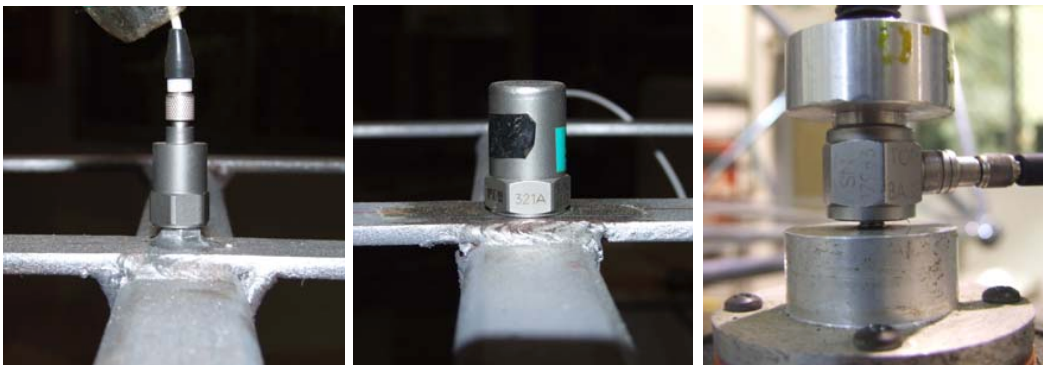

(a) Threaded (b) Double sided tape (c) Force sensor

Figure 6.5: Mounting of accelerometer and force sensor

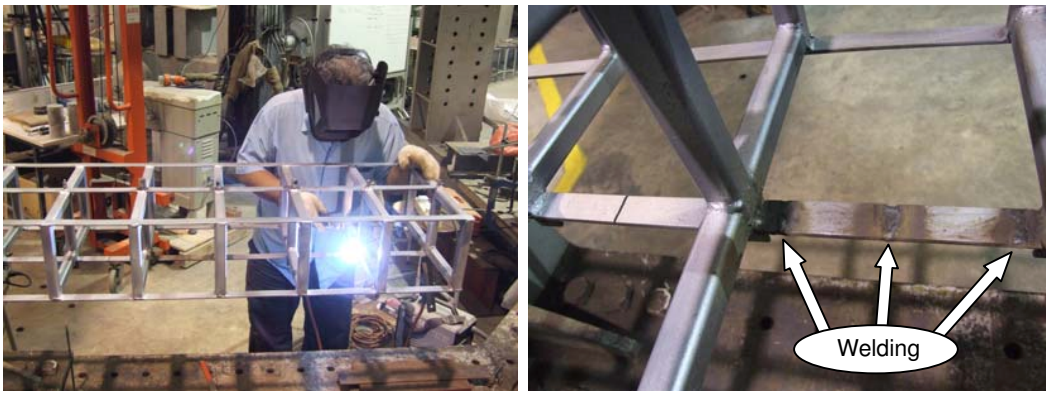

Figure 6.6: Welding at level 4, 6, and cut remained at level 3

Figure 6.7: Progressive strengthening at one level by welding: strengthening baseline (left), moderate strengthening (middle), large strengthening (right)

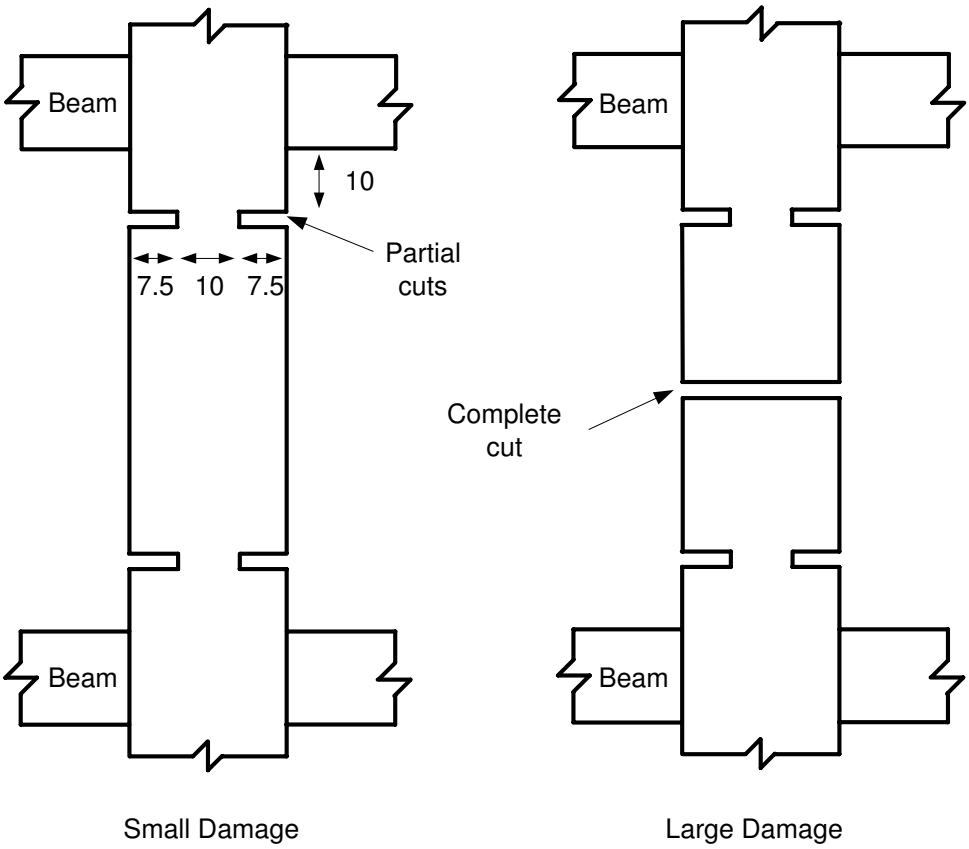

Figure 6.8: Damage induced by cutting

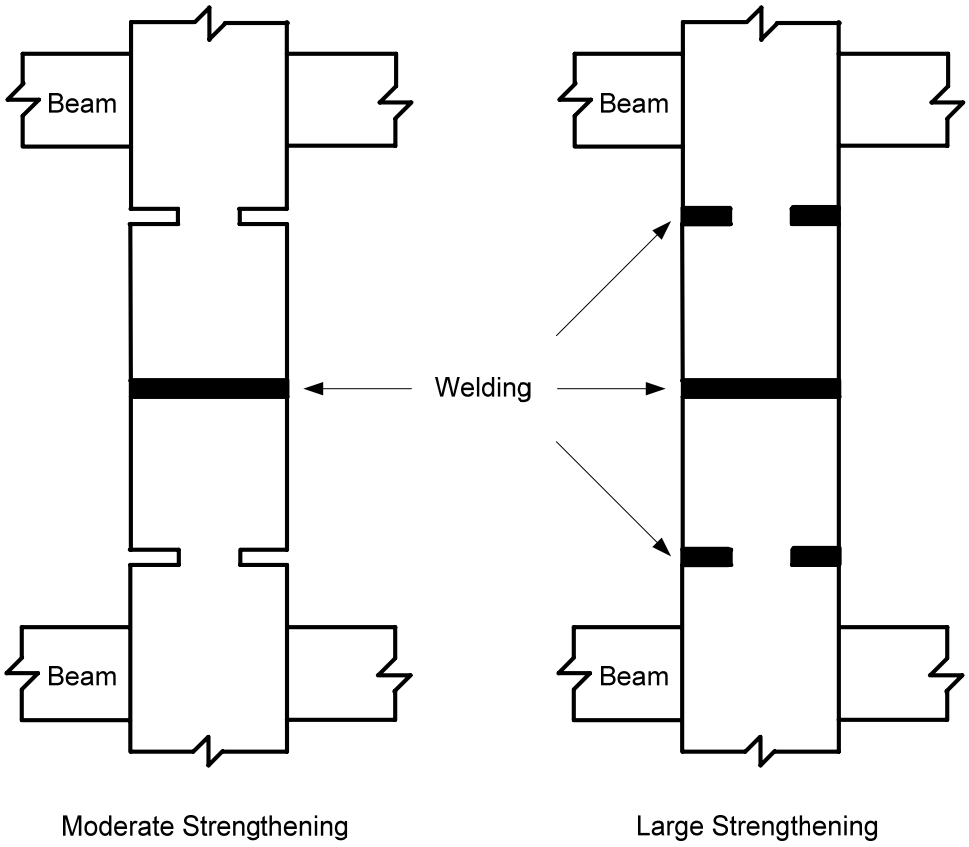

Figure 6.9: Strengthening by welding

(Small strengthening = Large strengthening - Moderate strengthening)

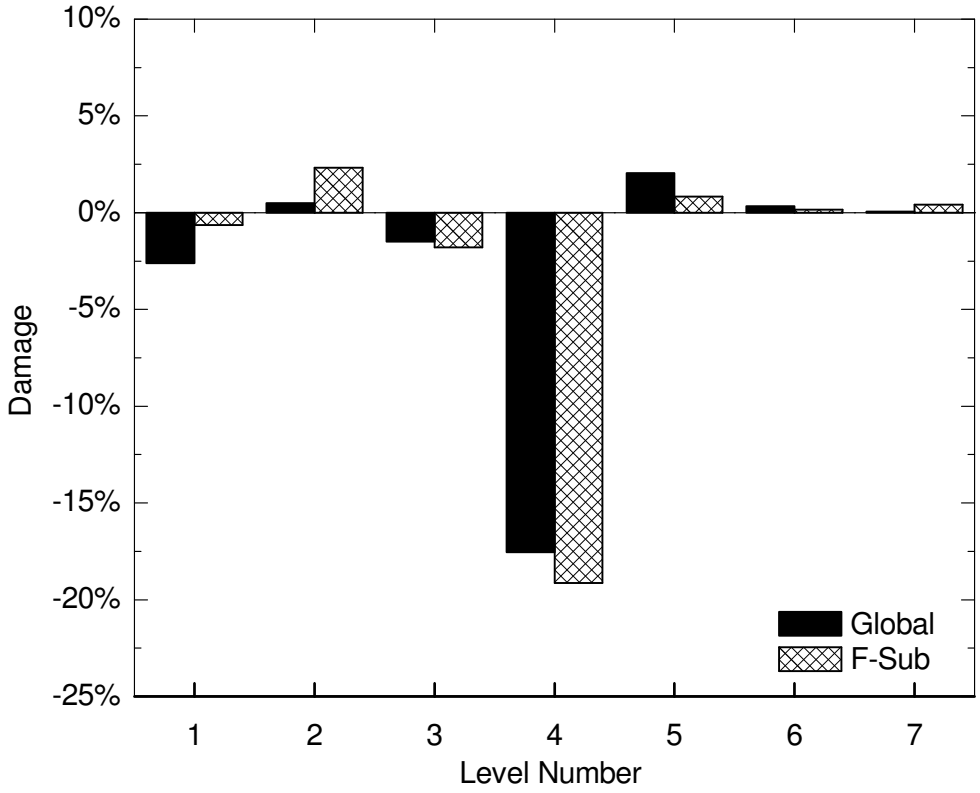

Figure 6.10: Damage case D2 (4L) with complete measurement: large damage (16.7%) at level 4

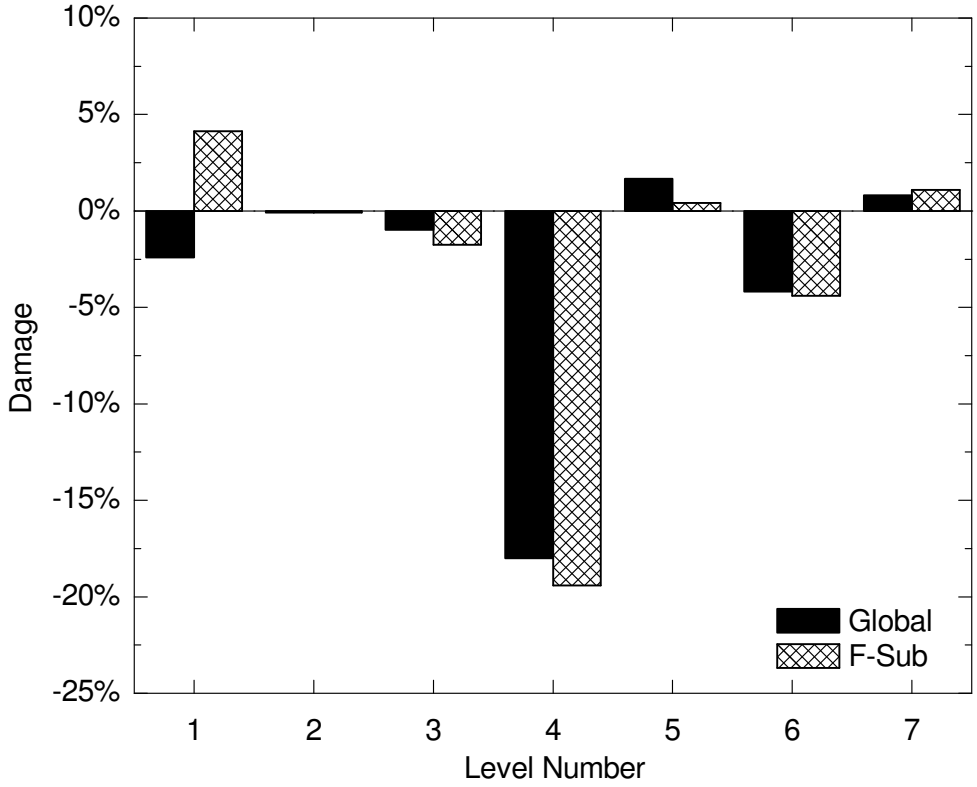

Figure 6.11: Damage case D3 (4L6S) with complete measurement: large damage (16.7%) at level 4 and small damage (4.1%) damage at level 6

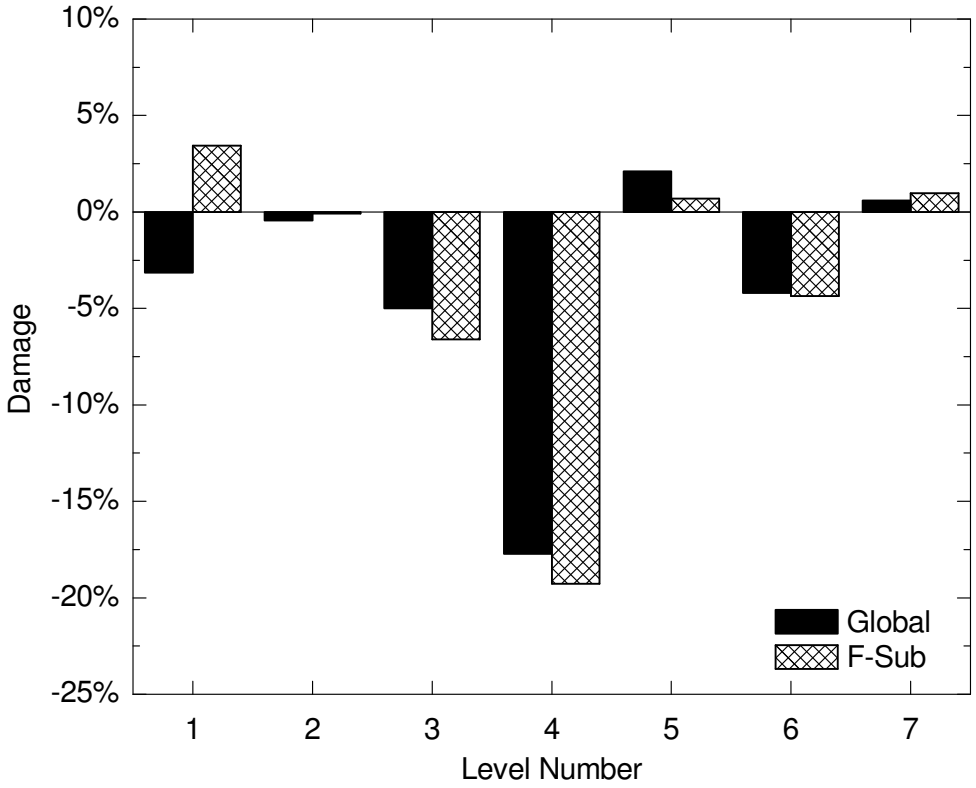

Figure 6.12: Damage case D4 (4L3S6S) with complete measurement: large damage (16.7%) at level 4 and small damage (4.1%) at levels 3 and 6

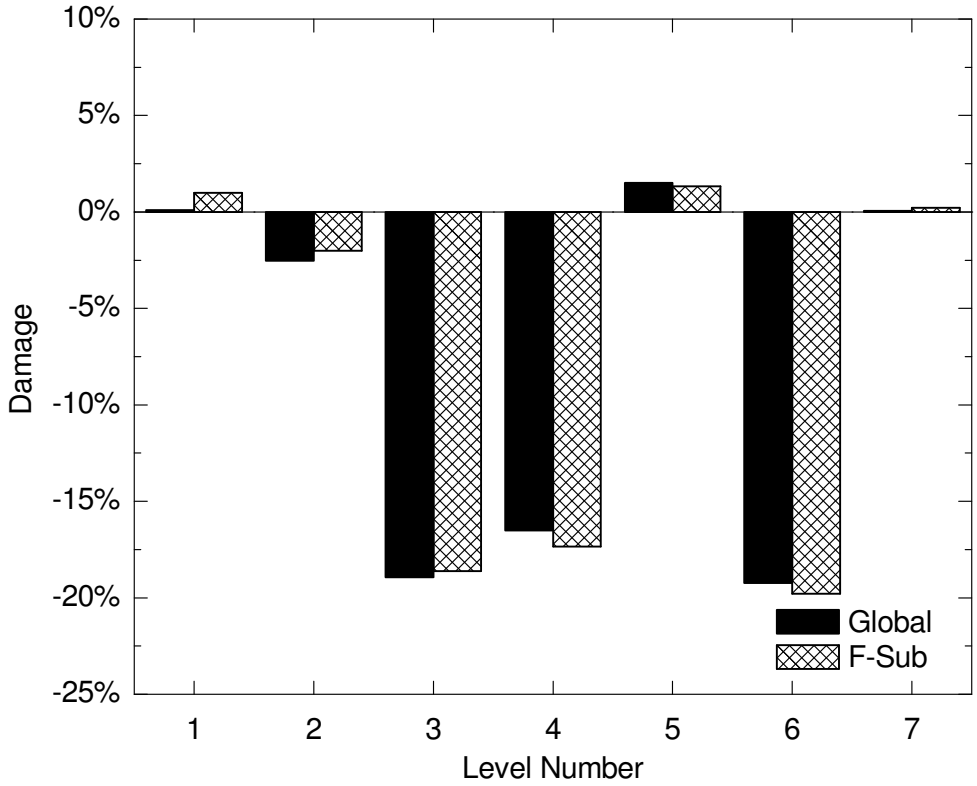

Figure 6.13: Damage case D6 (3L4L6L) with complete measurement: large damage (16.7%) at levels 3, 4 and 6

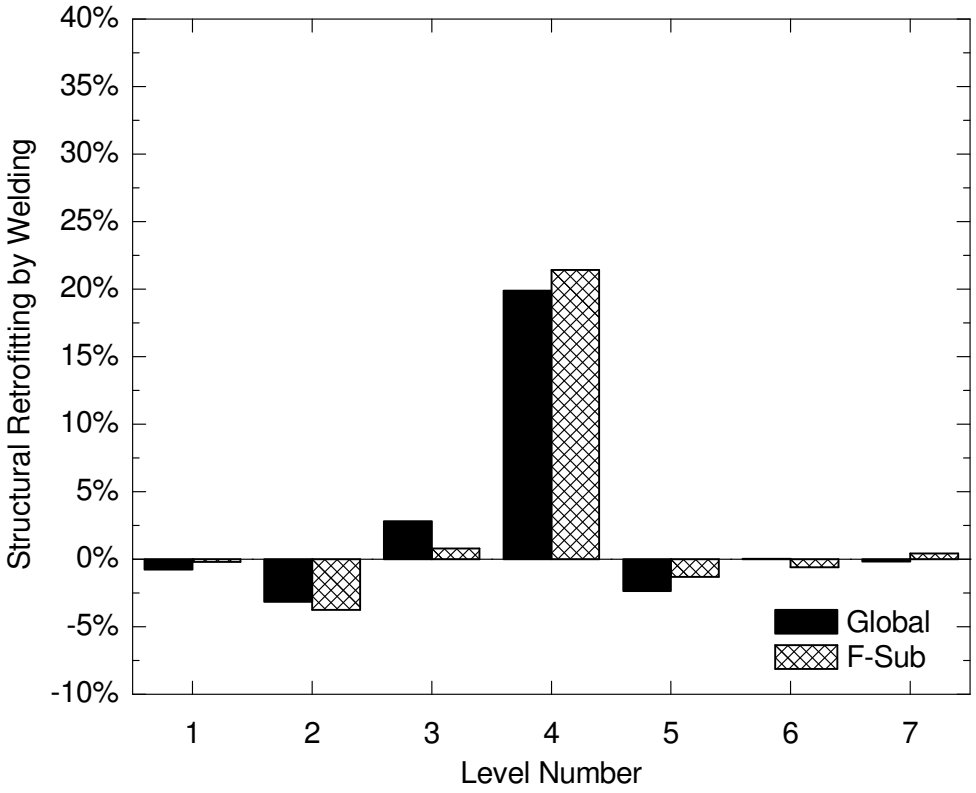

Figure 6.14: Strengthening case S1 (4M) with complete measurement: moderate strengthening at level 4

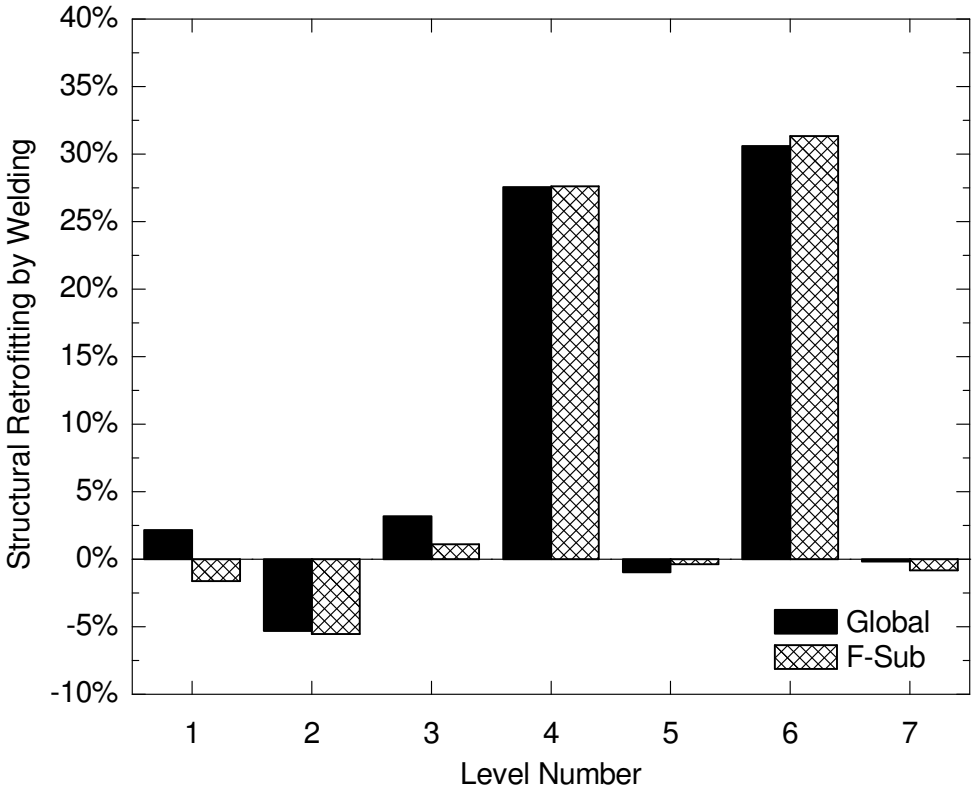

Figure 6.15: Strengthening case S4 (4L6L) with complete measurement: large strengthening at levels 4 and 6

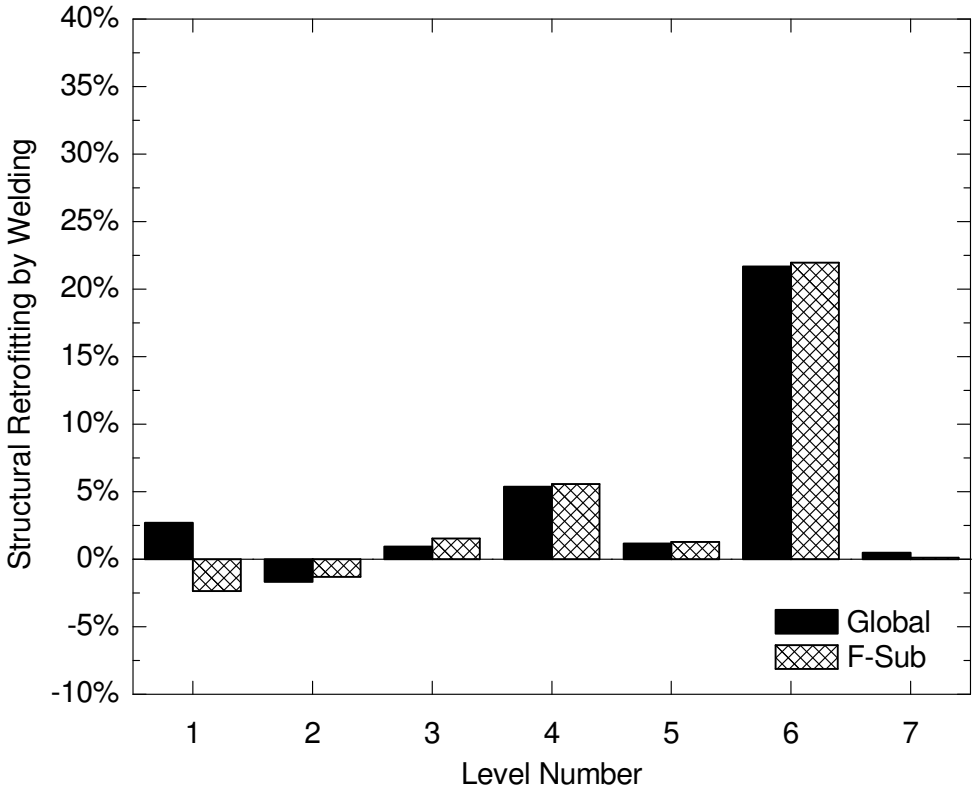

Figure 6.16: Strengthening case S5 (4S6M) with complete measurement: small strengthening at level 4 and moderate strengthening at level 6

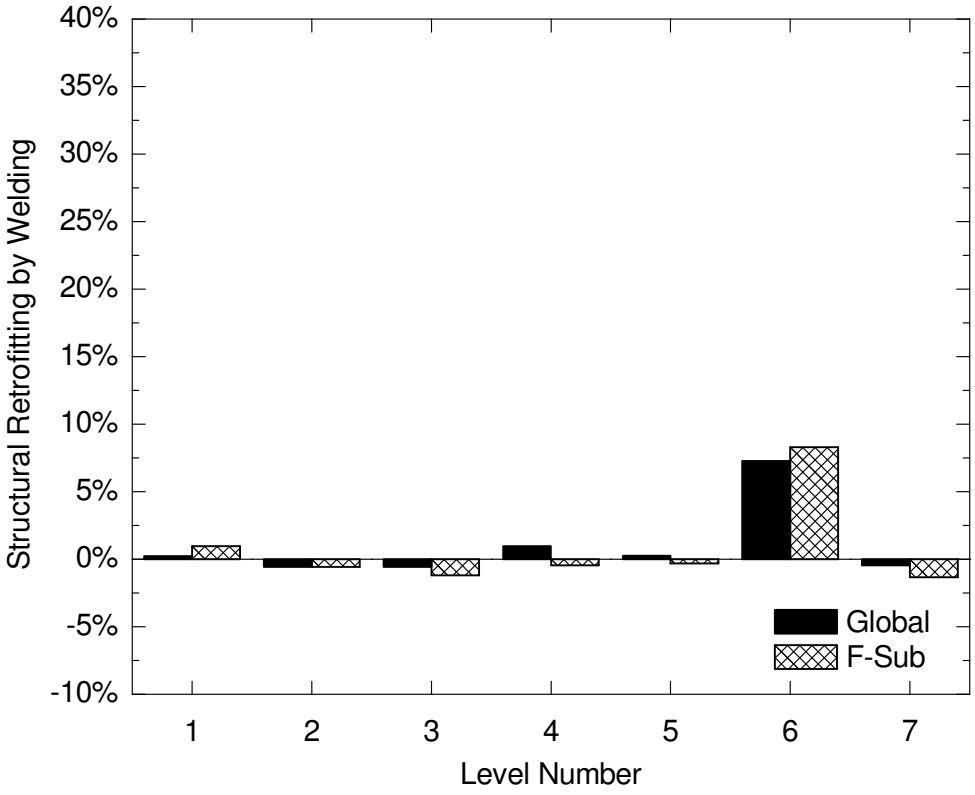

Figure 6.17: Strengthening case S7 (6S) with complete measurement: small strengthening at level 6

Table 6.1: Accelerometer specification

Level	Model	Serial no.	Range	Sensitivity	Frequency range
1	Kristler-8636C50	2028814	±50g	102.2mV/g	1-6000Hz
2	PCB-352C34	91468	±50g	98.7mV/g	1-10000Hz
3	PCB353B33	83737	±50g	99.1mV/g	1-4000Hz
4	PCB-321A	6532	±50g	92.6mV/g	1-2000Hz
5	PCB-321A	6533	±50g	88.6mV/g	1-2000Hz
6	Dytran-3055B2	4042	±50g	100.5mV/g	1-10000Hz
7	Dytran-3055B4	3878	±100g	51.7mV/g	1-10000Hz
Load cell	PCB-208C02	17983	-	113.7mV/g	0.001-36000Hz

Table 6.2: GA parameters for baseline identification

GA parameters	Global SI[a,b] via SSRM	Global SI[b] via iSSRM	Global SI[b] via iSSRM with BFGS	T-Sub (2S[c])	T-Sub (4S[c])
Total Evaluations	2,400,000	1,200,000	240,000	48,000	24,000
Population size	50×3	55×3	22×3	10×3	7×3
Generations	800	359	117	73	51
Sample size	-	720	2280	488	252
Number of runs	20	20	15	15	15
n_b value	5	5	5	5	5
Crossover rate	0.4	0.4	0.4	0.4	0.4
Mutation rate	0.2	0.2	0.2	0.2	0.2
Migration rate	0.05	0.05	0.05	0.05	0.05
Regeneration	3	3	3	3	3
Reintroduction	200	100	50	30	20
Window width	4.0	4.0	4.0	4.0	4.0
Data length	500	500	500	500	500
Time step (sec)	2.0×10^{-4}	2.0×10^{-4}	2.0×10^{-4}	2.0×10^{-4}	2.0×10^{-4}

[a] Results by Koh and Perry (2007)

[b] SI=system identification

[c] S=substructure

Table 6.3: GA parameters for identifying stiffness change due to cut and welding

GA parameters	Global SI[a,b] via SSRM	Global SI[b]	T-Sub (2S;4S[c])	F-Sub (2S;4S[c])
		via iSSRM with BFGS		
Total evaluations	108,000	10,800	1,080; 2,160	1,080; 2,160
Population size	20×3	5×3	4×3; 3×3	4×3; 3×3
Generations	120	23	5;3	5;3
Sample size	-	516	112; 60	112; 60
Number of runs	15	10	10	10
n_b value	5	5	5	5
Crossover rate	0.8	0.8	0.8	0.8
Mutation rate	0.2	0.2	0.2	0.2
Migration rate	0.05	0.05	0.05	0.05
Regeneration	3	2	2	2
Reintroduction	200	10	2	2
Window width	4.0	4.0	4.0	4.0
Data length	500	500	500	500
Time step (sec)	2.0×10^{-4}	2.0×10^{-4}	2.0×10^{-4}	2.0×10^{-4}

[a] Results by Koh and Perry (2007)

[b] SI=system identification

[c] S=substructure

Table 6.4: Basic damage scenarios

Scenarios	Small damage	Large damage
D0	-	-
D1	Level 4	-
D2	-	Level 4
D3	Level 6	Level 4
D4	Levels 3 and 6	Level 4
D5	Level 3	Levels 4 and 6
D6	-	Levels 3, 4 and 6

Table 6.5: Additional damage scenarios

Scenarios	Undamaged case	Damaged case	Resulting small damage
D7	D2	D3	Level 6
D8	D3	D4	Level 3
D9	D2	D4	Levels 3 and 6

Table 6.6: Basic strengthening scenarios with stiffness increase

Scenarios	Small increase	Moderate increase	Large increase
S0	-	-	-
S1	-	Level 4	-
S2	-	-	Level 4
S3	-	Level 6	Level 4
S4	-	-	level 4 and 6

Table 6.7: Additional strengthening scenarios

Scenarios	Small increase	Moderate increase	Resulting increase
S5	S1	S3	Level 4 small, and level 6 moderate
S6	S2	S3	Level 6 moderate
S7	S3	S4	Level 6 small

Table 6.8: Identification of damage due to cut

Cases	Global[a,b]	Global[a,c]			T-Sub[a,c] (2 substructures)			F-Sub[a,c] (2 substructures)		
	Success (1x)	Small/Large (S/L)	Max. false change	Success (1x)	Small/Large (S/L)	Max. false change	Success (1x)	Small/Large (S/L)	Max. false change	Success (1x)
Complete measurement										
D2 (4L)	**100%**	-17.56 (4L)	-3.35	**100%**	-18.97 (4L)	-2.16	**100%**	-19.08 (4L)	-5.87	**96%**
D3 (4L6S)	**47%**	-18.00 (4L) -4.17 (6S)	-2.88	**78%**	-19.31 (4L) -4.40(6S)	-2.28	**98%**	-19.33 (4L) -4.39 (6S)	-4.48	**60%**
D4 (4L3S6S)	**31%**	-5.00 (3S) -4.19 (6S) -17.72 (4L)	-3.15	**64%**	-5.03 (3S) -4.36(6S) -19.14 (4L)	-1.89	**89%**	-6.58 (3S) -4.35 (6S) -19.21 (4L)	-4.26	**69%**
D6 (3L4L6L)	**100%**	-18.93 (3L) -16.50 (4L) -19.22 (6L) (4L)	-2.76	**100%**	-18.31 (3L) -17.18 (4L) -19.65 (6L)	-2.80	**100%**	-18.57 (3L) -17.28 (4L) -19.77 (6L)	-4.99	**93%**
Incomplete measurement										
D2 (4L)	**100%**	-18.09 (4L)	-3.59	**100%**	-18.65 (4L)	-3.60	**100%**	-18.71 (4L)	-5.81	**96%**
D3 (4L6S)	**64%**	-18.17 (4L) -4.78 (6S)	-3.08	**80%**	-19.23 (4L) -3.92 (6S)	-3.30	**73%**	-19.35 (4L) -3.90 (6S)	-4.58	**44%**
D4 (4L3S6S)	**27%**	-5.03 (3S) -4.90 (6S) -17.49 (4L)	-4.04	**60%**	-5.11 (3S) -4.40(6S) -19.35 (4L)	-2.90	**71%**	-5.84 (3S) -4.34 (6S) -19.34 (4L)	-6.09	**58%**
D6 (3L4L6L)	**100%**	-19.04 (3L) -15.70 (4L) -19.66 (6L)	-2.95	**100%**	-19.37 (3L) -15.58 (4L) -20.80 (6L)	-4.61	**100%**	-18.54 (3L) -15.66 (4L) -20.80 (6L)	-9.62	**87%**

[a] Based on Table 6.3, total evaluations for Global[b], Global[c], T-Sub[c], and F-Sub[c] are 100%, 10%, 4%, and 4%, respectively.

[b] Results by Koh and Perry (2007)

[c] Results by the use of iSSRM with BFGS method

Table 6.9: Identification of strengthening due to welding

Cases	Global[a,b]			T-Sub[a,b] (2 substructures)			F-Sub[a,b] (2 substructures)		
	Small/Moderate/Large (S/M/L)	Max. false change	Success (1x)	Small/Moderate/Large (S/M/L)	Max. false change	Success (1x)	Small/Moderate/Large (S/M/L)	Max. false change	Success (1x)
Complete measurement									
S1 (4M)	19.93 (4M)	3.88	**100%**	21.71 (4M)	3.72	**100%**	21.49 (4M)	5.89	**100%**
S4 (4L6L)	27.61 (4L) 30.60 (6L)	8.39	**100%**	28.30 (4L) 31.11(6L)	6.19	**100%**	27.66 (4L) 31.38 (6L)	6.27	**96%**
S5 (4S6M)	5.38 (4S) 21.68 (6M)	5.89	**64%**	5.69 (4S) 21.76(6M)	6.18	**56%**	5.72 (4S) 21.98 (6M)	6.41	**69%**
S7 (6S)	7.33 (6S)	6.38	**71%**	8.48 (6S)	5.46	**78%**	8.34 (6S)	7.19	**73%**
Incomplete measurement									
S1 (4M)	18.06 (4M)	3.30	**100%**	21.57 (4M)	2.82	**100%**	20.88 (4M)	4.50	**98%**
S4 (4L6L)	26.20 (4L) 31.17 (6L)	7.08	**93%**	25.46 (4L) 33.69 (6L)	9.83	**82%**	24.88 (4L) 33.83 (6L)	9.22	**84%**
S5 (4S6M)	5.58 (4S) 22.24 (6M)	5.73	**62%**	4.42 (4S) 23.31(6M)	11.70	**31%**	4.79 (4S) 23.38 (6M)	7.34	**47%**
S7 (6S)	6.86 (6S)	7.46	**60%**	9.12 (6S)	7.90	**84%**	9.09 (6S)	13.60	**51%**

[a] Based on Table 6.3, total evaluations for Global[b], T-Sub[c], and F-Sub[c] are 100%, 40%, respectively.

[b] Results by the use of iSSRM with BFGS method

Table 6.10: Effect of substructure size

Cases	T-Sub[a,b] Small/Moderate/Large (S/M/L)	T-Sub[a,b] Max. false change	T-Sub[a,b] Success (1x)	F-Sub[a,b] Small/Moderate/Large (S/M/L)	F-Sub[a,b] Max. false change	F-Sub[a,b] Success (1x)
2 subsructures						
D2 (4L)	-18.97 (4L)	-2.16	**100%**	-19.08 (4L)	-5.87	**96%**
D3 (4L6S)	-19.31 (4L) -4.40 (6S)	-2.28	**98%**	-19.33 (4L) -4.39 (6S)	-4.48	**60%**
D4 (4L3S6S)	-19.14 (4L) -5.03 (3S) -4.36 (6S)	-1.89	**89%**	-19.21 (4L) -6.58 (4S) -4.35(6S)	-4.26	**69%**
D6 (3L4L6L)	-18.31 (3L) -17.18 (4L) -19.65 (4L)	-2.80	**100%**	-18.57 (3L) -17.28 (4L) -19.77 (6L)	-4.99	**93%**
S1 (4M)	21.71 (4M)	3.72	**100%**	21.49 (4M)	5.89	**100%**
S4 (4L6L)	28.30 (4L) 31.11 (6L)	6.19	**100%**	27.66 (4L) 31.38 (6L)	6.27	**96%**
S5 (4S6M)	5.69 (4S) 21.76 (6M)	6.18	**56%**	5.72 (4S) 21.98 (6M)	6.41	**69%**
S7 (6S)	8.48 (6S)	5.46	**78%**	8.34 (6S)	7.19	**73%**
4 substructures						
D2 (4L)	-19.15 (4L)	-6.87	**93%**	-19.12 (4L)	-6.63	**91%**
D3 (4L6S)	-19.09 (4L) -2.93 (6S)	-8.96	**16%**	-19.09 (4L) -3.09 (6S)	-8.40	**20%**
D4 (4L3S6S)	-19.12 (4L) -6.09 (3S) -3.27 (6S)	-6.21	**58%**	-18.97 (4L) -5.77 (3S) -3.53(6S)	-6.51	**53%**
D6 (3L4L6L)	-20.20 (3L) -17.08 (4L) -18.58 (6L)	-6.83	**93%**	-22.62 (3L) -15.52 (4L) -21.12 (6L)	-4.00	**93%**
S1 (4M)	22.78 (4M)	17.30	**62%**	22.73 (4M)	21.09	**62%**
S4 (4L6L)	30.46 (4L) 31.04 (6L)	22.86	**69%**	30.07 (4L) 30.40 (6L)	26.00	**67%**
S5 (4S6M)	4.16 (4S) 24.93 (6M)	17.19	**20%**	4.22 (4S) 24.74 (6M)	14.48	**27%**
S7 (6S)	5.34 (6S)	19.05	**31%**	4.95 (6S)	17.91	**36%**

[a] Based on Table 6.3, total evaluations for T-Sub[b] and F-Sub[b] are both 4% of those by Koh and Perry (2007).

[b] Results by the use of iSSRM with BFGS method

CHAPTER 7

Conclusions and Recommendations

The primary objective of this thesis is to develop a robust and efficient algorithm for structural identification. Through a series of numerical and experimental verification, as well as comparison with five recent research papers, the main contributions of the thesis are made in the following aspects and they are summarized in Table 7.1:

(1) Investigation of measurement noise induced peak-shifting which has formed the basis of the proposed identification strategy

(2) Formulation and implementation of a uniformly sampled genetic algorithm with gradient search, that has shown to improve the optimization process substantially

(3) Extension of F-Sub method to accommodate random excitation, that has achieved a impressive substructural efficiency (see Eq. (4.34)) as high as 0.96 based on the 50-DOF system (Tee *et al.*, 2005)

(4) Verification of T-Sub method with the proposed identification strategy, that has achieved a very good substructural efficiency of 0.89 based on the 50-DOF system (Tee *et al.*, 2005)

(5) Experimental verification of the proposed identification strategy in identifying small stiffness changes caused by cut and welding

7.1 Conclusions

The main findings for (1) to (5) above are highlighted in this section. The nature of system identification is firstly investigated from an optimization perspective, via fitness surface analysis of small scale systems. In the noise free case, it is observed that there is only one global peak within the search range, surrounded by several local optima. Increasing the noise level, the global peak decreases in the magnitude and shifts in location accordingly. However, no further local optima are introduced. In this study, this is referred to as "peak shifting". The investigation also reveals a finding consistent with Koh *et al.* (2003a) in that the lower-level stiffness of a lumped mass system is usually more difficult to identify.

Based on these findings, an efficient hybrid optimization strategy is proposed. This strategy comprises an improved SSRM method via sampling and gradient based local searcher. The former is to overcome the local optima far away from the global peak, and the latter is then to accomplish fine tuning for the global peak.

Firstly, the SSRM is improved by sampling test. Instead of reducing the search space via initial MGAMAS runs in the original SSRM, samples will be obtained in the solution domain to define the promising subdomains. Four sampling methods are tested on 10-DOF and 20-DOF systems, including random uniform distribution, Latin hypercube, orthogonal arrays (OA), and Hammersley sequence. Based on the comparison study, Hammersley sequence is recommended for iSSRM method. The reason is Hammersley sequence can generate uniform samples in a deterministic way, yielding more reliable results than random uniform distribution and Latin hypercube. Although equally good result is achieved by OA, the Hammersley sequence outperforms OA because it has no restrictive requirements on orthogonality and is thus more flexible to construct uniform

samples of arbitrary size. Furthermore, extensive parametric studies are carried out on selecting the generation size, population size, runs, and sample size. The purpose is to provide a reasonably balanced exploration and exploitation for identification at different scale .

Secondly, local searchers are investigated for fine tuning in the proposed strategy. Both gradient based methods, i.e., CG and BFGS, and non-gradient based method, i.e., SA, are considered. The presence of non-gradient local search is to provide a reference of identification and ensure that the gradient local search is not trapped in local optima. This is judged by comparing the mean absolute errors via the three local searchers. The BFGS method is recommended in the study because of the efficient backtracking line search.

Through the numerical studies, the "peak-shifting" is reflected in high dimensional identification although the observation is directly visualized in low dimensional fitness surface analysis. In Chapter 3, the gradient based BFGS and CG method have successfully identified the exact peak in the absence of measurement noise. The "peak-shifting" effect is partially validated by the CG local search. The global peak decreases and approaches a shape of parabolic function in the presence of noise. This change of global peak becomes more traceable by the Brent line search in CG, as parabolic interpolation is used in each step of line search. Therefore a significant time reduction is achieved for identification with measurement noise.

The application of the proposed strategy is investigated at a substructural level. The frequency domain substructural method, referred to as F-Sub method, is extended to random excitation. The key is to make the steady state formulation possible for non-periodic loading. To maintain the periodic requirement of discrete Fourier transform, exponential window is adopted to ensure a quiet ending in the response histories. With this improvement, traditional lengthy time histories due to zero padding can be replaced

by an arbitrary length of response. The reduction in time history in identification will significantly benefit in saving computational effort. The application of the proposed strategy is also examined in time domain substructural identification, i.e., T-Sub method.

The findings of this study are compared with five recent research works to show the impressive enhancement achieved herein. The numerical comparison includes identification algorithms in the backward analysis (Koh *et al.*, 2003a; Perry *et al.*, 2006) and the divide-and-conquer strategies in the forward analysis (Koh *et al.*, 2003b; Tee *et al.*, 2005). Besides, the experimental study are compared with Koh and Perry (2007). Typically, for the identification algorithm, the proposed iSSRM method achieves consistently better results, i.e., about 2% mean identification error under 10% noise, over SSRM (Perry *et al.*, 2006), but uses only 50% computer time for known mass case and less than 30% computer time in unknown mass case. The iSSRM with gradient search is able to reach the same level of accuracy, i.e., about 3% mean error under 10% noise, similar to that by Koh *et al.* (2003a), but uses only 8.6% computer time.

The efficiency of divide-and-conquer strategies is compared based on the platform of the proposed iSSRM with gradient search. By introducing a substructural efficiency, i.e., computer time by substructural method over global identification when approaching the same level of accuracy, the comparison suggests F-Sub is the best over T-Sub (Koh *et al.*, 2003b) and Sub-SOMI-RR (Tee *et al.*, 2005) in terms of efficiency. The substructural efficiency is an impressive 0.96 for F-Sub in identifying a 50-DOF system under 5% noise, and 0.89 for T-Sub, but it was -0.11 for Sub-SOMI-RR which means more computer time than the global identification. At the same time, the corresponding mean errors are 1.63%, 2.19%, and 11%. The substructural efficiency is expected to be even less in case of a system with a large number of DOFs. Besides, the T-Sub method is shown to have better performance in unknown mass case since F-Sub and Sub-SOMI-RR are not applicable in this case.

Eventually, the comparison with Koh and Perry (2007) shows good results with a time reduction of 90% by iSSRM with gradient search and a further 90% reduction by introducing divide-and-conquer strategies in the backward analysis. In addition to the efficiency of proposed identification strategy, the accuracy and robustness is also verified through experimental study. For example, when there is damage of 4% only in levels 3 and 4, and 17% damage in level 6, the identification success rate achieved by Koh and Perry (2007) is 31% while the results by this study are 64%/69%/89% for global identification, F-Sub and T-Sub method, respectively.

7.2 Recommendations for Further Study

It is the observation of "peak-shifting" that leads to the proposed iSSRM with gradient search in the study. The use of this method brings about a series of excellent results in terms of accuracy and efficiency, through both numerical simulation and experimental studies. To tap the full potential and versatility of GAs and divide-and-conquer methods in large-scale structural health monitoring, it is believed that this study has contributed to the advancement in GA based structural identification and more can be done to extend the work.

In short, the present study paves the way for further research on parallel computing to accelerate the uniformly sampled GA with gradient search, substructural identification of plates and shells, special problems in parameter identification of dynamic models, and uncertainty quantification of structural identification. Specifically, these potential topics could be extended as follows.

A promising advancement of the proposed methodology will be in the parallel computing. It should be noted that all the results achieved in the study are based on serial coding, which has already shown remarkable saving in computer time. By virtue of the parallel philosophy, computer time of the proposed identification strategy is expected to

have a further reduction.

With more advanced identification, it is then possible to investigate problems in large-scale structural health monitoring. In that case, divide-and-conquer strategies are suggested in the forward analysis. Possible issues then arise as the unknown rotational measurement for identifying plate and shell structures. Traditional ways to cope with this problem are to treat them as unknowns and solve for them through available measurement (Reich and Park, 2001; Koh and Shankar, 2003a), i.e., translational measurements. A trade-off to consider is the selection of substructure size and maintaining sufficient measurements within it.

Besides the applications in backward analysis and forward analysis, further study should also focus on the special problems associated with the mathematical model of structural dynamics, for example, identification with unknown initial conditions. This problem originates from the first/second-order mathematical model for structural dynamics. Some related publications are identification with unknown input (Wang and Haldar, 1994; Yang *et al.*, 2003b; Perry and Koh, 2008), and with unknown mass (Koh *et al.*, 2003b).

Another area to explore is research in identification uncertainties (Koh and See, 1994). The uncertainty may be attributed to the modeling error in the forward analysis and uncertainty associated with the identification strategy (Htun, 2004; Koh and Htun, 2004), or due to measurement noise and incomplete measurement (Beck and Katafygiotis, 1998). Further investigation will help to gain confidence in the success of identification.

Table 7.1: Main findings from the thesis

Studies	Methods	Comparison & examples	Accomplishment
Peak shifting: an observation of global peak movement induced by measurement noise			The nature of system identification is firstly investigated from an optimization perspective
Numerical studies on backward analysis (Chapter 2 and 3)	iSSRM	(Perry *et al.*, 2006): 10-DOF and 20-DOF system	(1) 50% computer time reduction in mass known case (2) More than 70% time reduction in mass unknown case
	iSSRM with gradient search (BFGS)	(Koh *et al.*, 2003a; Perry *et al.*, 2006): 10-DOF system	More than 90% reductions in computer time
Numerical studies on forward analysis (Chapter 4 and 5)	F-Sub	(Tee *et al.*, 2005): 12-DOF and 50-DOF system	(1) Applicable to random excitation (2) A further 96% reduction in computer time by merely F-Sub[a,b] (3) Significant improvement on accuracy, for example, the mean identification error is only 1.63% for the 50-DOF system under 5% noise while that was 11.0% in Tee *et al.* (2005).
	T-Sub	(Koh *et al.*, 2003b): 50-DOF system and Truss	(1) A further 89% reduction in computer time by merely T-Sub[a,b] (2) Much better identification accuracy, for example, identifying the 50-DOF system under 5% noise, the mean identification errors by PSI give 1.46%/1.34% for stiffness and mass in this study while those were 5.1%/5.0% in Koh *et al.* (2003b).
Experiment (Chapter 6)	Global, F-Sub, and T-Sub + iSSRM with gradient search (BFGS)	(Koh and Perry, 2007): 7-storey steel frame model	Better identification success in small damage, i.e., 4%, and multiple damages with different magnitudes

[a] Based on the 50-DOF system by (Tee *et al.*, 2005)

[b] Substructural efficiency by Eq. (4.34) is 0.96 for F-Sub, 0.89 for T-Sub, and -0.11 for Sub-SOMI-RR

References

Adeli, H. (2001). "Neural networks in civil engineering: 1989-2000," Computer-Aided Civil and Infrastructure Engineering, 16(2), 126-142.

Agbabian, M. S., Masri, S. F., Miller, R. K., and Caughey, T. K. (1991). "System identification approach to detection of structural changes," Journal of Engineering Mechanics, 117(2), 370-390.

Alvin, K. F., Peterson, L. D., and Park, K. C. (1995). "Method for determining minimum-order mass and stiffness matrices from modal test data," AIAA Journal, 33(1), 128-135.

Bathe, K. J. (1996). Finite Element Procedures, Prince Hall, New Jersey.

Beck, J. L. (1979). "Determining models of structures from earthquake records," EERL 91-03, Earthquake Engineering Research Laboratory, California Institute of Technology.

Beck, J. L., and Jennings, P. C. (1980). "Structural identification using linear models and earthquake records," Earthquake Engineering & Structural Dynamics, 8(2), 145-160.

Beck, J. L., and Katafygiotis, L. S. (1998). "Updating models and their uncertainties. I: Bayesian statistical framework," Journal of Engineering Mechanics, 124(4), 455-461.

Begambre, O., and Laier, J. E. (2009). "A hybrid Particle Swarm Optimization - Simplex algorithm (PSOS) for structural damage identification," Advances in Engineering Software, 40(9), 883-891.

Bekey, G. A. (1970). System identification-an introduction and a survey. Simulation, 15(4), 151-166.

Bernal, D. (2000). "Extracting flexibility matrices from state-space realizations," European COST F3 Conference on System Identification & Structural Health Monitoring, Madrid, Spain, 127-135.

Besterfield, D. H., Besterfield-Michna, C., Besterfield, G. H., and Besterfield-Sacre, M. (1995). Total Quality Management, Prentice Hall, Englewood Cliffs, NJ.

Bicanic, N., and Chen, H. P. (1997). "Damage identification in framed structures using natural frequencies," International Journal for Numerical Methods in Engineering, 40(23), 4451-4468.

Bishop, C. M. (1995). Neural Networks for Pattern Recognition, Oxford University Press, Oxford.

Bowles, R. L., and Straeter, T. A. (1972). "System identification computational considerations," In: System identification of vibrating structures: Mathematical models from test data; Proceedings of the Winter Annual Meeting, New York, N.Y., November 26-30, 1972. (A73-20426 07-32) New York, American Society of Mechanical Engineers, 23-43.

Box, G. E. P. (1957). "Evolutionary operation: a method for increasing industrial productivity," Journal of the Royal Statistical Society, Series C (Applied Statistics), 6(2), 81-101.

Brincker, R., Krenk, S., and Jensen, J. L. (1991). "Estimation of correlation functions by the Random Decrement Technique," The 9th International Modal Analysis Conference (IMAC), Florence, Italy, April 15-18, 610-615.

Broyden, C. G. (1970). "The convergence of a class of double-rank minimization algorithms," Journal of the Institute of Mathematics and Its Applications, 6(1), 76-90.

Caicedo, J. M., Dyke, S. J., and Johnson, E. A. (2004). "Natural excitation technique and eigensystem realization algorithm for phase I of the IASC-ASCE benchmark problem: Simulated data," Journal of Engineering Mechanics, 130(1), 49-60.

Cao, X., Sugiyama, Y., and Mitsui, Y. (1998). "Application of artificial neural networks to load identification," Computers & Structures, 69(1), 63-78.

Caravani, B., Watson, M. L., and Thomson, W. T. (1977). "Recursive least-squares time domain identification of structural parameters," Journal of Applied Mechanics, 44, 135-140.

Caughey, T. K. (1960). "Classical normal modes in damped linear dynamic systems," Journal of Applied Mechanics, 27, 269-271.

Chakraborty, A., Basu, B., and Mitra, M. (2006). "Identification of modal parameters of a mdof system by modified L-P wavelet packets," Journal of Sound and Vibration, 295(3-5), 827-837.

Chang, C. C., Chang, T. Y. P., Xu, Y. G., and Wang, M. L. (2000). "Structural damage detection using an iterative neural network," Journal of Intelligent Material Systems and Structures, 11(1), 32-42.

Chassiakos, A. G., and Masri, S. F. (1996). "Modeling unknown structural systems through the use of neural networks," Earthquake Engineering & Structural Dynamics, 25(2), 117-128.

Chen, H. P., and Bicanic, N. (2000). "Assessment of damage in continuum structures based on incomplete modal information," Computers & Structures, 74(5), 559-570.

Chen, S. Y., Ju, M. S., and Tsuei, Y. G. (1996). "Estimation of mass, stiffness and damping matrices from frequency response functions," Journal of Vibration and Acoustics, 118(1), 78-82.

Chiang, D. Y., and Lin, C. S. (2008). "Identification of modal parameters from nonstationary ambient vibration data using correlation technique," AIAA Journal, 46(11), 2752-2759.

Ching, J. Y., Beck, J. L., and Porter, K. A. (2006). "Bayesian state and parameter estimation of uncertain dynamical systems," Probabilistic Engineering Mechanics, 21(1), 81-96.

Chou, J. H., and Ghaboussi, J. (2001). "Genetic algorithm in structural damage detection," Computers & Structures, 79(14), 1335-1353.

Cole, H. A., Jr. (1973). "On-line failure detection and damping measurement of aerospace structures by random decrement signatures," NASA-CR-2205, NASA.

Corana, A., Marchesi, M., Martini, C., and Ridella, S. (1987). "Minimizing multimodal functions of continuous variables with the simulated annealing algorithm," ACM Transactions on Mathematical Software, 13(3), 262-280.

Corigliano, A., and Mariani, S. (2004). "Parameter identification in explicit structural dynamics: performance of the extended Kalman filter," Computer Methods in Applied Mechanics and Engineering, 193(36-38), 3807-3835.

Craig, R. R. Jr., and Bampton, M. C. C. (1968). "Coupling of substructures for dynamic analysis," AIAA Journal, 6(7), 1313-1319.

De Angelis, M., Lus, H., Betti, R., and Longman R. W. (2002). "Extracting physical parameters of mechanical models from identified state-space representations," Journal of Applied Mechanics, 69(5), 617-625.

De Callafon, R. A., Moaveni, B., Conte, J. P., He, X., and Udd, E. (2008). "General realization algorithm for modal identification of linear dynamic systems," Journal of Engineering Mechanics, 134(9), 712-722.

Dennis, J. E., and Schnabel, R. B. (1996). Numerical Methods for Unconstrained Optimization and Nonlinear Equations, SIAM Publications, Philadelphia.

Doyle, J. F. (1994). "A genetic algorithm for determining the location of structural impacts," Experimental Mechanics, 34(1), 37-44.

Doyle, J. F. (1997). "Wavelet deconvolution method for impact force identification," Experimental Mechanics, 37(4), 403-408.

Ewins, D. J. (2000). Modal Testing: Theory, Practice and Application, Research Studies Press, UK.

Eykhoff, P. (1974). System Identification: Parameter and State Estimation, John Wiley & Sons, New York.

Feng, M. Q., Kim, J. M., and Xue, H. (1998). "Identification of a dynamic system using ambient vibration measurements," Journal of Applied Mechanics, 65(4), 1010-1021.

Fletcher, R. (1970). "A new approach to variable metric algorithms," Computer Journal, 13(3), 317-322.

Flood, I., and Kartam, N. (1994a). "Neural Networks in civil engineering .1. Principles and understanding. Journal of Computing in Civil Engineering, 8(2), 131-148.

Flood, I., and Kartam, N. (1994b). "Neural Networks in civil engineering .2. Systems and application," Journal of Computing in Civil Engineering, 8(2), 149-162.

Flood, I. (2006). "Next generation artificial neural networks for civil engineering," Journal of Computing in Civil Engineering, 20(5), 305-307.

Fogel, L. J., Owens, A. J., and Walsh, M. J. (1966). Artificial Intelligence through Simulated Evolution, Wiley, New York.

Franco, G., Betti, R., and Lus, H. (2004). "Identification of structural systems using an evolutionary strategy," Journal of Engineering Mechanics, 130(10), 1125-1139.

Franco, G., Betti, R., and Longman, R. W. (2006). "On the uniqueness of solutions for the identification of linear structural systems," Journal of Applied Mechanics, 73, 153-162.

Friedman, G. J. (1959). "Digital simulation of an evolutionary process," General Systems Yearbook, 4, 171-184.

Fujino, Y., Abe, M., Shibuya, H., Yanagihara, M., Sato, M., Nakamura, S., and Sakamoto, Y. (2000). "Forced and ambient vibration tests and vibration monitoring of Hakucho suspension bridge," The 5th International Bridge Engineering Conference, Tampa, Florida, 57-63.

Garibaldi, L., Marchesiello, S., and Bonisoli, E. (2003). "Identification and up-dating over the Z24 benchmark," Mechanical Systems and Signal Processing, 17(1), 153-161.

Ghanem, R., and Shinozuka, M. (1995). "Structural system identification .1: Theory," Journal of Engineering Mechanics, 121(2), 255-264.

Goldberg, D. E. (1989). Genetic Algorithms in Search, Optimization, and Machine Learning, Addison-Wesley Professional, Boston, MA.

Goldfarb, D. (1970). "A family of variable metric updates derived by variational means," Mathematics of Computation, 24(109), 23-26.

Haddara, M. R., Wishahy, M., and Wu, X. (1994). "Assessment of ships transverse stability at sea," Ocean Engineering, 21(8), 781-800.

Hammersley, J. M. (1960). "Monte Carlo methods for solving multivariable problems," Annals of the New York Academy of Sciences 86, 844-874.

Harris, C. M., and Piersol, A. G. (2001). Harris' Shock and Vibration Handbook, McGraw-Hill, New York.

Haykin, S. (1994). Neural Networks: A Comprehensive Foundation, Prentice Hall, Upper Saddle, NJ.

He, R. S., and Hwang, S. F. (2006). "Damage detection by an adaptive real-parameter simulated annealing genetic algorithm," Computers & Structures, 84(31-32), 2231-2243.

He, X. F., Moaveni, B., Conte, J. P., Elgamal, A., and Masri, S. F. (2009). "System identification of Alfred Zampa Memorial Bridge using dynamic field test data," Journal of Structural Engineering, 135(1), 54-66.

Hedayat, A. S., Sloane, N. J. A., and Stufken, J. (1999). Orthogonal Arrays: Theory and Applications, Springer-Verlag, New York.

Hinton, E., and Owen, D. R. J. (1984). Finite Element Software for Plates and Shells, Pineridge Press, Swansea, UK.

Holland, J. H. (1975). Adaptation in Natural and Artificial Systems, University of Michigan Press, Ann Arbor.

Hoshiya, M., and Saito, E. (1984). "Structural identification by Extended Kalman Filter," Journal of Engineering Mechanics, 110(12), 1757-1770.

Htun, S. (2004). Uncertainty of parameters in structural identification by genetic algorithm. Master Thesis, Department of Civil Engineering, National University of Singapore, Singapore.

Huang, C. S., Yang, Y. B., Lu, L. Y., and Chen, C. H. (1999). "Dynamic testing and system identification of a multi-span highway bridge," Earthquake Engineering & Structural Dynamics, 28(8), 857-878.

Huang, C. S., and Lin, H. L. (2001). "Modal identification of structures from ambient vibration, free vibration, and seismic response data via subspace approach," Earthquake Engineering & Structural Dynamics, 30(12), 1857-1878.

Huang, C. S., Hung, S. L., Lin, C. I., and Su, W. C. (2005). "A wavelet-based approach to identifying structural modal parameters from seismic response and free vibration data," Computer-Aided Civil and Infrastructure Engineering, 20(6), 408-423.

Huang, N. E., Shen, Z., Long, S. R., Wu, M. C., Shih, H. H., Zheng, Q., Yen, N. C., Tung, C. C., and Liu, H. H. (1998). "The empirical mode decomposition and the Hilbert spectrum for nonlinear and non-stationary time series analysis," Proceedings of the Royal Society A: Mathematical, Physical and Engineering Sciences, 454(1971), 903-995.

Huang, N. E., and Shen, S. S. (2005). Hilbert-Huang Transform and Its Applications, World Scientific, London.

Humar, J. L. (1990). Dynamics of Structures, Prentice Hall, Englewood Cliffs, NJ.

Ibrahim, S. R., and Mikulcik, E. C. (1977). "A method for the direct identification of vibration parameters from the free response," The Shock and Vibration Bulletin, 47(4), 183-198.

James, G. H., Carne, T. G., and Lauffer, J. P. (1993). "The natural excitation technique (NExT) for modal parameter extraction from operating wind turbines," SAND92-1666, UC261, Sandia National Laboratories.

James, G. H., Carne, T. G., and Lauffer, J. P. (1995). "The natural excitation technique (NExT) for modal parameter extraction from operating structures," Modal Analysis-the International Journal of Analytical and Experimental Modal Analysis, 10(4), 260-277.

Jiang, R. J., Au, F. T. K., and Cheung, Y. K. (2003). "Identification of masses moving on multi-span beams based on a genetic algorithm," Computers & Structures, 81(22-23), 2137-2148.

Juang, J. N. (1993). Applied System Identification, Prentice Hall, Upper Saddle River, NJ, USA.

Juang, J. N., and Pappa, R. S. (1985). "An eigensystem realization algorithm for modal parameter identification and model reduction," Journal of Guidance Control and Dynamics, 8(5), 620-627.

Juang, J. N., and Pappa, R. S. (1986). "Effects of noise on modal parameters identified by the eigensystem realization algorithm," Journal of Guidance Control and Dynamics, 9(3), 294-303.

Juang, J. N., and Suzuki, H. (1988). "An eigensystem realization algorithm in frequency domain for modal parameter identification," Journal of Vibration Acoustics Stress and Reliability in Design, 110(1), 24-29.

Kausel, E., and Roesset, J. M. (1992). "Frequency domain analysis of undamped systems," Journal of Engineering Mechanics, 118(4), 721-734.

Kijewski-Correa, T., and Kareem, A. (2006). "Efficacy of Hilbert and wavelet transforms for time-frequency analysis," Journal of Engineering Mechanics, 132(10), 1037-1049.

Kim, H. S., and Melhem, H. (2004). "Damage detection of structures by wavelet analysis," Engineering Structures, 26(3), 347-362.

Kirkpatrick, S., Gelatt, C. D., and Vecchi, M. P. (1983). "Optimization by simulated annealing," Science, 220(4598), 671-680.

Kishore Kumar, R., Sandesh S., and Shankar, K. (2007). "Parametric identification of non-linear dynamic systems using Levenburg-Marquardt method and Genetic Algorithm," International Journal of Structural Stability and Dynamics, 7(4), 715-725.

Kitagawa, G. (1996). "Monte Carlo filter and smoother for non-Gaussian state space models," Journal of Computational and Graphical Statistics, 5(1), 1-25.

Ko, W. J., and Hung, C. F. (2002). "Extraction of structural system matrices from an identified state-space system using the combined measurements of DVA," Journal of Sound and Vibration, 249(5), 955-970.

Kocis, L., and Whiten, W. J. (1997). "Computational investigations of low-discrepancy sequences," ACM Transactions on Mathematical Software, 23(2), 266-294.

Koh, C. G., See, L. M., and Balendra, T. (1991). "Estimation of structural parameters in time domain - a substructure approach," Earthquake Engineering & Structural Dynamics, 20(8), 787-801.

Koh, C. G., and See, L. M. (1994). "Identification and uncertainty estimation of structural parameters," Journal of Engineering Mechanics, 120(6), 1219-1236.

Koh, C. G., Hong, B., and Liaw, C. Y. (2000). "Parameter identification of large structural systems in time domain," Journal of Structural Engineering, 126(8), 957-963.

Koh, C. G., Wu, L. P., and Liaw, C. Y. (2002). "Distributed computing strategy for structural monitoring and diagnostics," US-Korea Workshop on Smart Structural Systems, Busan, South Korea.

Koh, C. G., Chen, Y. F., and Liaw, C. Y. (2003a). "A hybrid computational strategy for identification of structural parameters," Computers & Structures, 81(2), 107-117.

Koh, C. G., Hong, B., and Liaw, C. Y. (2003b). "Substructural and progressive structural identification methods," Engineering Structures, 25(12), 1551-1563.

Koh, C. G., and Shankar, K. (2003). "Substructural identification method without interface measurement," Journal of Engineering Mechanics, 129(7), 769-776.

Koh, C. G., and Shankar, K. (2003). "Stiffness identification by a substructural approach in frequency domain," International Jounal of Structural Stability and Dynamics, 3(2), 267-281.

Koh, C. G., and Htun, S. (2004). "Adaptive search genetic algorithm for structural system identification," Proceedings of the Second International Workshop on Structural Health Monitoring of Innovative Civil Engineering Structures, ed. A Mufti and F Ansari: pp. 393-403. Winnipeg: ISI Canada Corporation. (Second International Workshop on Structural Health Monitoring of Innovative Civil Engineering Structures, 22-23 Sep 2004, Winnipeg, Canada.

Koh, C. G., and Perry, M. J. (2007). "Structural damage quantification by system identification," Journal of Earthquake and Tsunami, 1(3), 211-231.

Ku, C. J., Cermak, J. E., and Chou, L. S. (2007). "Biased modal estimates from random decrement signatures of forced acceleration responses," Journal of Structural Engineering, 133(8), 1180-1185.

Lee, J. W., Kim, J. D., Yun, C. B., Yi, J. H., and Shim, J. M. (2002). "Health-monitoring method for bridges under ordinary traffic loadings," Journal of Sound and Vibration, 257(2), 247-264.

Lee, J. (2009). "Identification of multiple cracks in a beam using natural frequencies," Journal of Sound and Vibration, 320(3), 482-490.

Lin, C. C., Wang, J. F., and Ueng, J. M. (2001). "Vibration control identification of seismically excited m.d.o.f. structure-PTMD systems," Journal of Sound and Vibration, 240(1), 87-115.

Lin, C. C., Hong, L. L., Ueng, J. M., Wu, K. C., and Wang, C. E. (2005). "Parametric identification of asymmetric buildings from earthquake response records," Smart Materials & Structures, 14(4), 850-861.

Liu, G. R., and Chen, S. C. (2002). "A novel technique for inverse identification of distributed stiffness factor in structures," Journal of Sound and Vibration, 254(5), 823-835.

Liu, D. C., and Nocedal, J. (1989). "On the limited memory BFGS method for large scale optimization," Mathematical Programming, 45(3), 503-528.

Ljung, L., and McKelvey, T. (1996). "A least squares interpretation of sub-space methods for system identification," Proceedings of the 35th IEEE Conference on Decision and Control, Kobe, Japan, 335-342.

Ljung, L. (1999). System Identification: Theory for The User, Prentice Hall, Upper Saddle River, NJ, USA.

Loh, C. H., and Tsaur, Y. H. (1988). "Time domain estimation of structural parameters," Engineering Structures, 10(2), 95-105.

Loh, C. H., Lin, C. Y., and Huang, C. C. (2000). "Time domain identification of frames under earthquake loadings," Journal of Engineering Mechanics, 126(7), 693-703.

Lus, H., Betti, R., and Longman, R. W. (1999). "Identification of linear structural systems using earthquake-induced vibration data," Earthquake Engineering & Structural Dynamics, 28(11), 1449-1467.

Lus, H., De Angelis, M., Betti, R., and Longman, R. W. (2003a). "Constructing second-order models of mechanical systems from identified state space realizations. Part I: Theoretical discussions," Journal of Engineering Mechanics, 129(5), 477-488.

Lus, H., De Angelis, M., Betti, R., and Longman, R. W. (2003b). "Constructing second-order models of mechanical systems from identified state space realizations. Part II: Numerical investigations," Journal of Engineering Mechanics, 129(5), 489-501.

Lus, H., Betti, R., Yu, J., and De Angelis, M. (2004). "Investigation of a system identification methodology in the context of the ASCE benchmark problem," Journal of Engineering Mechanics, 130(1), 71-84.

Maia, N. M. M., and Silva, J. M. M. (2001). Theoretical and Experimental Modal Analysis, Research Studies Press, Hertfordshire, England.

Majji, M., and Junkins, J. L. (2008). "Time varying Eigensystem Realization Algorithm with repeated experiments," AAS/AIAA 18th Space Flight Mechanics Meeting, Galveston, TX, 1069-1078.

Mallat, S. (1999). A Wavelet Tour of Signal Processing, Academic Press, San Diego.

Mares, C., and Surace, C. (1996). "An application of genetic algorithms to identify damage in elastic structures," Journal of Sound and Vibration, 195(2), 195-215.

McKay, M. D., Beckman, R. J., and Conover, W. J. (1979). "A comparison of three methods for selecting values of input variables in the analysis of output from a computer code," Technometrics, 21(2), 239-245.

Michalewicz, Z. (1992). Genetic Algorithms + Data Structures = Evolution Programs, Springer-Verlag, Berlin.

Mitchell, M. (1996). An Introduction to Genetic Algorithms, MIT Press Cambridge, MA, USA.

Mohanty, P., and Rixen, D. J. (2003). "Operational dynamic testing in the presence of harmonic excitation," The 2nd MIT Conference on Computational Fluid and Solid Mechanics, Cambridge, MA, 477-481.

Nayeri, R. D., Masri, S. F., and Chassiakos, A. G. (2007). "Application of structural health monitoring techniques to track structural changes in a retrofitted building based on ambient vibration," Journal of Engineering Mechanics, 133(12), 1311-1325.

Ndambi, J. M., Peeters, B., Maeck, J., De Visscher, J., Wahab, M., Vantomme, J., De Roeck, G., and De Wilde, W. (2000). "Comparison of techniques for modal analysis of concrete structures," Engineering Structures, 22(9), 1159-1166.

Nicholas, M., Arianna, W. R., Marshall, N. R., Augusta, H. T., and Edward, T. (1953). "Equation of state calculations by fast computing machines," Journal of Chemical Physics, 21(6), 1087-1092.

Nocedal, J., and Wright, S. J. (1999). Numerical Optimization, Springer-Verlag, New York.

Peeters, B., and De Roeck, G. (1999). "Reference-based stochastic subspace identification for output-only modal analysis," Mechanical Systems and Signal Processing, 13(6), 855-878.

Perry, M. J. (2006). Modified GA approach to system identification with structural and offshore application. Department of Civil Engineering, National University of Singapore, Singapore.

Perry, M. J., Koh, C. G., and Choo, Y. S. (2006). "Modified genetic algorithm strategy for structural identification," Computers & Structures, 84(8-9), 529-540.

Perry, M. J., and Koh, C. G. (2008). "Output-only structural identification in time domain: Numerical and experimental studies," Earthquake Engineering & Structural Dynamics, 37(4), 517-533.

Polak, E., and Ribire, G. (1969). "Note sur la convergence de mthodes de directions conjugues," Revue Francaise Informat. Reserche Oprationnelle, 16, 35-43.

Press, W. H., Flannery, B. P., Teukolsky, S. A., and Vetterling, W. T. (1992). Numerical Recipes in Fortran 77: The Art of Scientific Computing, Cambridge University Press, Cambridge, England.

Qian, J., Jia, X., and Xu, Y. L. (2007). "Two-stage damage diagnosis approach for steel braced space frame structures," Engineering Structures, 29(12), 3277-3292.

Qin, Q., Li, H. B., Qian, L. Z., and Lau C. K. (2001). "Modal identification of Tsing Ma bridge by using improved eigensystem realization algorithm," Journal of Sound and Vibration, 247(2), 325-341.

Reich, G. W., and Park, K. C. (2001). "A theory for strain-based structural system identification," Journal of Applied Mechanics, 68(4), 521-527.

Ren, W. X., Zhao, T., and Harik, I. E. (2004). "Experimental and analytical modal analysis of steel arch bridge," Journal of Structural Engineering, 130(7), 1022-1031.

Robinson, D. G., and Atcitty, C. (1999). "Comparison of quasi- and pseudo-Monte Carlo sampling for reliability and uncertainty analysis," Proceedings of the AIAA Probabilistic Methods Conference, St. Louis MO, AIAA99-1589.

Quek, S. T., Wang, Q., Zhang, L., and Ong, K. H. (2001). "Practical issues in the detection of damage in beams using wavelets," Smart Materials & Structures, 10(5), 1009-1017.

Quek, S. T., Tua, P. S., and Wang, Q. (2003). "Detecting anomalies in beams and plate based on the Hilbert-Huang transform of real signals," Smart Materials & Structures, 12(3), 447-460.

Rao, C. R. (1947). "Factorial experiments derivable from combinatorial arrangements of arrays," Journal of the Royal Statistical Society, Supplement 9, 128-139.

Rechenberg, I. (1965). "Cybernetic Solution Path of an Experimental Problem," Royal Aircraft Establishment, Translation No. 1122, Ministry of Aviation, Farnborough Hants, UK.

Reynders, E., De Roeck, G., Bakir, P. G., and Sauvage, C. (2007). "Damage identification on the Tilff bridge by vibration monitoring using optical fiber strain sensors," Journal of Engineering Mechanics, 133(2), 185-193.

Robertson, A. N., Park, K. C., and Alvin, K. F. (1998). "Identification of structural dynamics models using wavelet-generated impulse response data," Journal of Vibration and Acoustics, 120(1), 261-266.

Rodrigues, J. (2002). "Dynamic performance of a steel truss bridge under railway traffic," The 20th IMAC Conference on Structural Dynamics, Los Angeles, CA, 14-20.

Sato, T., and Qi, K. (1998). "Adaptive H-infinite filter: Its application to structural identification," Journal of Engineering Mechanics, 124(11), 1233-1240.

Sato, T., Kaji, K., and Honda, R. (2000). "Structural system identification using Monte Carlo filter," The 8th ASCE Joint EMD/SEI/GI/AD Specialty Conference on Probabilistic Mechanics and Structural Reliability (PMC2000), Notre Dame, Indiana.

Shanno, D. F. (1970). "Conditioning of Quasi-Newton methods for function minimization," Mathematics of Computation, 24(111), 647-656.

Shi, Z. Y., Law, S. S., and Li, H. N. (2007). "Subspace-based identification of linear time-varying system," AIAA Journal, 45(8), 2042-2050.

Siringoringo, D. M., and Fujino, Y. (2006). "Observed dynamic performance of the Yokohama-Bay Bridge from system identification using seismic records," Structural Control & Health Monitoring, 13(1), 226-244.

Siringoringo, D. M., and Fujino, Y. (2008). "System identification of suspension bridge from ambient vibration response," Engineering Structures, 30(2), 462-477.

Skolnik, D., Lei, Y., Yu, E. J., and Wallace, J. W. (2006). "Identification, model updating, and response prediction of an instrumented 15-story steel-frame building," Earthquake Spectra, 22(3), 781-802.

Sohn, H., and Law, K. H. (2000). "Bayesian probabilistic damage detection of a reinforced-concrete bridge column," Earthquake Engineering & Structural Dynamics, 29(8), 1131-1152.

Sone, A., Hata, H., and Masuda, A. (2004). "Identification of structural parameters using the wavelet transform of acceleration measurements," Journal of Pressure Vessel Technology, 126(1), 128-133.

Spanos, P. D., and Zeldin, B. A. (1998). "Generalized random decrement method for analysis of vibration data," Journal of Vibration and Acoustics, 120(3), 806-813.

Sun, Z., and Chang, C. C. (2004). "Statistical wavelet-based method for structural health monitoring," Journal of Structural Engineering, 130(7), 1055-1062.

Taguchi, G., Chowdhury, S., and Wu, Y. (2004). Taguchi's Quality Engineering Handbook, Wiley-Interscience.

Tamura, Y., Fujii, K., Ohtsuki, T., Wakahara T., and Kohsaka R. (1995). "Effectiveness of tuned liquid dampers under wind excitation," Engineering Structures, 17(9), 609-621.

Tanaka, Y., and Sato, T. (2004). "Efficient system identification algorithm using Monte Carlo Filter and its application," Conference on Health Monitoring and Smart Nondestructive Evaluation of Structural and Biological Systems III, San Diego, CA, 464-474.

Tang, H., Fukuda, M., and Xue, S. (2007). "Particle swarm optimization for structural system identification," The 6th International Workshop on Structural Health Monitoring, Stanford, CA, 483-492.

Tang, H. S., Xue, S. T., and Fan, C. X. (2008). "Differential evolution strategy for structural system identification," Computers & Structures, 86(21-22), 2004-2012.

Tee, K. F., Koh, C. G., and Quek, S. T. (2005). "Substructural first- and second-order model identification for structural damage assessment," Earthquake Engineering & Structural Dynamics, 34(15), 1755-1775.

Udwadia, F. E., and Sharma D. K. (1978). "Some uniqueness results related to building structural identification," SIAM Journal on Applied Mathematics, 34(1), 104-118.

Udwadia, F. E. (1985). "Some uniqueness results related to soil and building structural identification, " SIAM Journal on Applied Mathematics, 45(4), 674-685.

Ueng, J. M., Lin, C. C., and Lin, P. L. (2000). "System identification of torsionally coupled buildings," Computers & Structures, 74(6), 667-686.

Vanik, M. W., Beck, J. L., and Au, S. K. (2000). "Bayesian probabilistic approach to structural health monitoring," Journal of Engineering Mechanics, 126(7), 738-745.

Veletsos, A. S., and Ventura, C. E. (1984). "Efficient analysis of dynamic response of linear systems," Earthquake Engineering & Structural Dynamics, 12(4), 521-536.

Veletsos, A. S., and Ventura, C. E. (1985). "Dynamic analysis of structures by the DFT method," Journal of Structural Engineering, 111(12), 2625-2642.

Wang, D., and Haldar, A. (1994). "Element level system identification with unknown input," Journal of Engineering Mechanics, 120(1), 159-176.

Wang, D., and Haldar, A. (1997). "System identification with limited observations and without input," Journal of Engineering Mechanics, 123(5), 504-511.

Van Overschee, P., and De Moor, B. (1996). Subspace Identification for Linear Systems: Theory, Implementation, Applications, Kluwer Academic Publishers, Dordretch.

Vandiver, J. K., Dunwoody, A. B., Campbell, R. B., and Cook, M. F. (1982). "A mathematical basis for the random decrement vibration signature analysis technique," Journal of Mechanical Design, 104(2), 307-313.

Xia, Y., Hao, H., Brownjohn, J. M. W., and Xia, P. Q. (2002). "Damage identification of structures with uncertain frequency and mode shape data," Earthquake Engineering & Structural Dynamics, 31(5), 1053-1066.

Xu, B., Wu, Z. S., Chen, G. D., and Yokoyama, K. (2004). "Direct identification of structural parameters from dynamic responses with neural networks," Engineering Applications of Artificial Intelligence, 17(8), 931-943.

Yang, H. Z., Park, H. I., Li, H. J., and Choi, K. S. (2006). "Field experimental and numerical modal analyses of a jacket platform under ambient excitations," The 7th ISOPE Pacific/Asia Offshore Mechanics Symposium, Dalian, P. R. China, 30-34.

Yang, J. C. S., Dagalakis, N. G., Everstine, G. C., and Yang, Y.F. (1983). "Measurement of structural damping using the random decrement technique," The Shock and Vibration Bulletin, 53(4), 63-71.

Yang, J. N., Lei, Y., Pan, S. W., and Huang, N. (2003a). "System identification of linear structures based on Hilbert-Huang spectral analysis. Part 1: normal modes," Earthquake Engineering & Structural Dynamics, 32(9), 1443-1467.

Yang, J. N., Lei, Y., Pan, S. W., and Huang, N. (2003b). "System identification of linear structures based on Hilbert-Huang spectral analysis. Part 2: Complex modes," Earthquake Engineering & Structural Dynamics, 32(10), 1533-1554.

Yang, J. N., Lei, Y., Lin, S., and Huang, N. (2004). "Hilbert-Huang based approach for structural damage detection," Journal of Engineering Mechanics, 130(1), 85-95.

Yang, J. N., and Huang, H. (2007). "Sequential non-linear least-square estimation for damage identification of structures with unknown inputs and unknown outputs," International Journal of Non-Linear Mechanics, 42(5), 789-801.

Yang, J. N., Pan, S., and Huang, H. (2007a). "An adaptive extended Kalman filter for structural damage identifications II: unknown inputs," Structural Control & Health Monitoring, 14(3), 497-521.

Yao, L., Sethares, W. A., and Kammer, D. C. (1993). "Sensor placement for on-orbit modal identification via a genetic algorithm," AIAA Journal, 31(10), 1922-1928.

Yi, J. H., and Yun, C. B. (2004). "Comparative study on modal identification methods using output-only information," Structural Engineering and Mechanics, 17(3-4), 445-466.

Yoshida, I., and Sato, T. (2002). "Identification of damping ratio using monte carlo filter based on exclusive non-Gaussian process noise," The 15th ASCE Engineering Mechanics Conference, Columbia University, New York.

Yoshimoto, R., Mita, A., and Okada, K. (2005). "Damage detection of base-isolated buildings using multi-input multi-output subspace identification," Earthquake Engineering & Structural Dynamics, 34(3), 307-324.

Yuen, K. V., and Katafygiotis, L. S. (2001). "Bayesian time-domain approach for modal updating using ambient data," Probabilistic Engineering Mechanics, 16(3), 219-231.

Yuen, K. V., Au, S. K., and Beck, J. L. (2004). "Two-stage structural health monitoring approach for phase I benchmark studies," Journal of Engineering Mechanics, 130(1), 16-33.

Yuen, K. V., and Katafygiotis, L. S. (2006). "Substructure identification and health monitoring using noisy response measurements only," Computer-Aided Civil and Infrastructure Engineering, 21(4), 280-291.

Yun, H., Nayeri, R., Tasbihgoo, F., Wahbeh, M., Caffrey, J., Wolfe, R., Nigbor, R., Masri, S. F., Abdel-Ghaffar, A., and Sheng, L. H. (2008). "Monitoring the collision of a cargo ship with the Vincent Thomas Bridge," Structural Control & Health Monitoring, 15(2), 183-206.

Yun, C. B., and Shinozuka, M. (1980). "Identification of nonlinear structural dynamic system," Journal of Structural Mechanics, 8(2), 187-203.

Yun, C. B., and Bahng, E. Y. (2000). "Substructural identification using neural networks," Computers & Structures, 77(1), 41-52.

Zhang, Z., Koh, C. G., and Zhang, J. (2009). "System identification via orthogonal arrays sampled genetic algorithms," Proceedings of the 27th International Modal Analysis Conference, Orlando, Florida, US: No. 263.

Appendix A

Sampling Test and Parametric Study on iSSRM Method

The results listed here correspond to the content discussed in Chapter 2. Tables A.1 and A.2 show the comparison of sampling methods in order to recommend a suitable one for iSSRM. They are conducted on 10-DOF and 20-DOF lumped mass systems and are supplemental to Tables 2.3 and 2.4, respectively. Tables A.3 to A.6 demonstrate on the parametric study for known mass systems, including 5 DOFs, 10 DOFs, 20 DOFs, and 50 DOFs, in support of Section 2.6.1. Tables A.7 to A.9 show the parametric study for unknown mass systems, including 5 DOFs, 10 DOFs, and 20 DOFs, in support of Section 2.6.2.

Table A.1: Sampling method comparison via 10-DOF known mass system

Results	10-DOF lumped mass system					
	SGA	SSRM	SSRMRand[a]	SSRMLatin[a]	SSRMOA[a]	SSRMHam[a]
			0% Noise			
Perturbation	-	-	0	0	0	0
CPU time (h:m:s)	00:00:01	00:00:01	00:00:01	00:00:01	00:00:01	00:00:01
Mean error - k (%)	11.48	2.01	0.89	0.80	0.66	0.54
Max error - k (%)	32.94	5.31	2.21	2.58	1.88	1.44
			5% Noise			
Perturbation	-	-	0	0	0	0
CPU time (h:m:s)	00:00:01	00:00:01	00:00:01	00:00:01	00:00:01	00:00:01
Mean error - k (%)	12.19	2.68	1.86	1.76	1.57	1.51
Max error - k (%)	35.31	7.37	4.47	4.98	3.82	3.47
			10% Noise			
Perturbation	-	-	0	0	0	0
CPU time (h:m:s)	00:00:01	00:00:01	00:00:01	00:00:01	00:00:01	00:00:01
Mean error - k (%)	12.69	3.49	3.13	3.12	2.65	2.52
Max error - k (%)	30.48	9.38	8.07	7.96	5.84	6.26

[a] SSRMRand, SSRMLatin, SSRMOA, and SSRMHam are the iSSRM method sampled by random uniformly, Latin hypercube, orthogonal arrays, and Hammersley sequence, respectively.

Table A.2: Sampling method comparison via 20-DOF known mass system

Results	20-DOF lumped mass system					
	SGA	SSRM	SSRMRand[a]	SSRMLatin[a]	SSRMOA[a]	SSRMHam[a]
			0% Noise			
Perturbation	-	-	0	0	0	0
CPU time (h:m:s)	00:00:06	00:00:06	00:00:06	00:00:06	00:00:06	00:00:06
Mean error - k (%)	18.91	3.70	2.56	2.06	1.79	1.61
Max error - k (%)	56.81	12.49	9.96	7.09	7.13	6.87
			5% Noise			
Perturbation	-	-	0	0	0	0
CPU time (h:m:s)	00:00:06	00:00:06	00:00:06	00:00:06	00:00:06	00:00:06
Mean error - k (%)	20.65	3.94	3.49	2.59	2.61	2.07
Max error - k (%)	56.83	12.01	12.68	9.21	8.27	7.86
			10% Noise			
Perturbation	-	-	0	0	0	0
CPU time (h:m:s)	00:00:06	00:00:06	00:00:06	00:00:06	00:00:06	00:00:06
Mean error - k (%)	21.60	4.65	4.52	4.16	4.04	3.92
Max error - k (%)	64.41	15.11	14.51	14.54	15.20	12.48

[a] SSRMRand, SSRMLatin, SSRMOA, and SSRMHam are the iSSRM method sampled by random uniformly, Latin hypercube, orthogonal arrays, and Hammersley sequence, respectively.

Table A.3: Known mass system - Test on iSSRM method: 5-DOF

Test	Fitness			Stiffness Error (%)		CPU Time	Evaluations	Perturb-
	Mean	SD[a]	Median	Mean	SD[a]	(h:m:s)		ation
01AAA	843	(43)	906	0.67	(0.24)	00:00:00:777	5,004	0
02AAB	956	(27)	997	0.14	(0.04)	00:00:00:769	4,965	0
03AAC	960	(35)	1000	0.09	(0.05)	00:00:00:780	5,000	0
04ABA	960	(13)	988	0.22	(0.04)	00:00:00:795	5,022	0
05ABB	999	(0)	1000	0.02	(0.00)	00:00:00:784	4,995	0
06ABC	958	(38)	1000	0.24	(0.21)	00:00:00:795	5,040	0
07ACA	992	(2)	994	0.09	(0.01)	00:00:00:787	4,968	0
08ACB	993	(7)	1000	0.02	(0.01)	00:00:00:804	5,040	0
09ACC	979	(17)	1000	0.06	(0.02)	00:00:00:768	4,920	0
10BAA	866	(39)	955	0.38	(0.07)	00:00:00:778	4,977	0
11BAB	991	(4)	998	0.08	(0.02)	00:00:00:796	5,145	0
12BAC	999	(0)	1000	0.03	(0.01)	00:00:00:801	5,180	0
13BBA	970	(7)	980	0.19	(0.04)	00:00:00:780	4,914	0
14BBB	999	(0)	1000	0.02	(0.00)	00:00:00:775	5,040	0
15BBC	977	(22)	1000	0.03	(0.02)	00:00:00:794	5,040	0
16BCA	992	(2)	996	0.10	(0.01)	00:00:00:756	4,914	0
17BCB	1000	(0)	1000	0.01	(0.00)	00:00:00:780	5,040	0
18BCC	993	(5)	1000	0.04	(0.03)	00:00:00:781	5,040	0
19CAA	843	(45)	965	0.42	(0.09)	00:00:00:800	5,166	0
20CAB	946	(25)	989	0.21	(0.06)	00:00:00:751	4,830	0
21CAC	936	(34)	999	0.28	(0.15)	00:00:02:002	5,000	0
22CBA	975	(7)	993	0.14	(0.02)	00:00:00:773	5,022	0
23CBB	921	(53)	999	0.52	(0.33)	00:00:00:802	5,130	1
24CBC	992	(6)	1000	0.05	(0.02)	00:00:00:734	4,680	0
25CCA	984	(4)	992	0.12	(0.02)	00:00:00:786	5,130	0
26CCB	986	(13)	1000	0.06	(0.04)	00:00:00:731	4,770	0
27CCC	971	(19)	1000	0.11	(0.05)	00:00:00:804	4,920	0
Additional test on N_b								
4	922	(36)	1000	0.13	(0.06)	00:00:00:799	5040	0
7	981	(9)	998	0.10	(0.03)	00:00:00:791	5040	0
Additional test on sample size								
$S^b - 5N_U$	955	(25)	1000	0.08	(0.04)	00:00:00:801	5,145	0
$S^b - 2N_U$	986	(14)	1000	0.04	(0.02)	00:00:00:803	5,145	0
$S^b + 2N_U$	1000	(0)	1000	0.01	(0.00)	00:00:00:775	4,935	0
$S^b + 5N_U$	994	(6)	1000	0.05	(0.03)	00:00:00:768	4,935	0

[a] SD=standard deviation

[b] "S" represents the recommended sample size from the main test of Table 2.6.

Table A.4: Known mass system - Test on iSSRM method: 10-DOF

Test	Fitness			Stiffness Error (%)		CPU Time	Evaluations	Perturb-
	Mean	SD[a]	Median	Mean	SD[a]	(h:m:s)		ation
01AAA	941	(16)	965	0.33	(0.05)	0:00:03	9,990	0
02AAB	978	(15)	997	0.14	(0.03)	0:00:03	9,900	0
03AAC	987	(8)	1000	0.11	(0.03)	0:00:03	9,900	0
04ABA	956	(12)	975	0.32	(0.07)	0:00:03	10,044	0
05ABB	993	(7)	1000	0.09	(0.05)	0:00:03	9,990	0
06ABC	979	(11)	1000	0.15	(0.08)	0:00:03	10,020	0
07ACA	975	(7)	986	0.22	(0.02)	0:00:03	9,990	0
08ACB	993	(3)	1000	0.07	(0.02)	0:00:03	9,900	0
09ACC	895	(43)	994	0.54	(0.23)	0:00:03	9,900	0
10BAA	966	(5)	971	0.28	(0.03)	0:00:03	10,071	0
11BAB	992	(3)	997	0.10	(0.02)	0:00:03	9,900	0
12BAC	990	(7)	1000	0.05	(0.02)	0:00:03	9,960	0
13BBA	949	(24)	975	0.27	(0.03)	0:00:03	9,963	0
14BBB	969	(25)	1000	0.14	(0.06)	0:00:03	10,125	0
15BBC	922	(41)	1000	0.35	(0.21)	0:00:03	10,260	0
16BCA	975	(9)	990	0.27	(0.05)	0:00:03	10,044	0
17BCB	985	(10)	1000	0.09	(0.03)	0:00:03	9,855	0
18BCC	989	(4)	1000	0.06	(0.01)	0:00:03	9,900	0
19CAA	941	(7)	942	0.37	(0.04)	0:00:03	9,801	0
20CAB	995	(1)	997	0.10	(0.01)	0:00:03	10,215	0
21CAC	969	(30)	1000	0.11	(0.06)	0:00:03	9,540	0
22CBA	952	(8)	966	0.35	(0.05)	0:00:03	10,206	0
23CBB	957	(21)	998	0.21	(0.09)	0:00:03	10,125	0
24CBC	968	(13)	1000	0.16	(0.06)	0:00:03	10,440	0
25CCA	952	(20)	983	0.29	(0.06)	0:00:03	10,125	0
26CCB	939	(27)	999	0.22	(0.07)	0:00:03	9,990	0
27CCC	874	(56)	993	0.66	(0.27)	0:00:03	10,260	0
Additional test on N_b								
4	927	(30)	989	0.44	(0.14)	00:00:03	9,900	0
7	985	(3)	990	0.20	(0.03)	00:00:03	9,900	0
Additional test on sample size								
$S^b - 5N_U$	979	(20)	1000	0.11	(0.07)	00:00:03	9,900	0
$S^b - 2N_U$	987	(10)	1000	0.07	(0.03)	00:00:03	9,990	0
$S^b + 2N_U$	998	(1)	1000	0.06	(0.02)	00:00:03	10,035	0
$S^b + 5N_U$	958	(36)	1000	0.41	(0.32)	00:00:03	9,900	0

[a] SD=standard deviation

[b] "S" represents the recommended sample size from the main test of Table 2.6.

Table A.5: Known mass system - Test on iSSRM method: 20-DOF

Test	Fitness			Stiffness Error (%)		CPU Time	Evaluations	Perturb-
	Mean	SD[a]	Median	Mean	SD[a]	(h:m:s)		ation
01AAA	790	(34)	829	1.60	(0.26)	0:00:26	40,050	0
02AAB	924	(22)	949	0.87	(0.19)	0:00:26	40,200	0
03AAC	954	(28)	996	0.34	(0.09)	0:00:26	39,800	0
04ABA	880	(20)	905	0.96	(0.14)	0:00:26	40,014	0
05ABB	973	(6)	987	0.43	(0.07)	0:00:26	40,140	0
06ABC	996	(1)	999	0.18	(0.04)	0:00:26	39,720	0
07ACA	947	(12)	969	0.67	(0.09)	0:00:26	39,960	0
08ACB	997	(1)	998	0.15	(0.02)	0:00:26	40,050	0
09ACC	993	(7)	1000	0.10	(0.06)	0:00:26	40,200	0
10BAA	789	(33)	832	1.63	(0.27)	0:00:26	39,942	0
11BAB	940	(17)	984	0.69	(0.14)	0:00:26	40,065	0
12BAC	966	(12)	993	0.46	(0.13)	0:00:26	39,740	0
13BBA	886	(17)	907	0.84	(0.10)	0:00:26	39,987	0
14BBB	979	(6)	989	0.34	(0.05)	0:00:26	40,140	0
15BBC	986	(5)	998	0.23	(0.05)	0:00:26	39,840	0
16BCA	953	(8)	970	0.56	(0.08)	0:00:26	39,798	0
17BCB	997	(1)	998	0.13	(0.02)	0:00:26	39,825	0
18BCC	979	(14)	1000	0.16	(0.05)	0:00:27	40,560	0
19CAA	700	(40)	751	2.27	(0.37)	0:00:26	40,293	0
20CAB	897	(33)	957	1.11	(0.31)	0:00:27	40,425	0
21CAC	953	(18)	991	0.46	(0.13)	0:00:26	40,040	0
22CBA	841	(19)	869	1.31	(0.16)	0:00:26	40,095	0
23CBB	975	(4)	983	0.42	(0.05)	0:00:26	40,095	0
24CBC	970	(9)	990	0.34	(0.06)	0:00:26	39,600	0
25CCA	907	(18)	937	0.81	(0.11)	0:00:26	39,798	0
26CCB	959	(22)	996	0.30	(0.08)	0:00:29	39,600	0
27CCC	993	(5)	999	0.17	(0.07)	0:00:30	40,920	0
Additional test on N_b								
4	913	(163)	996	0.31	(0.36)	00:00:26	40,050	0
7	983	(56)	998	0.21	(0.50)	00:00:25	40,050	0
Additional test on sample size								
$S^b - 5N_U$	978	(15)	998	0.18	(0.03)	00:00:26	40,200	0
$S^b - 2N_U$	981	(16)	998	0.17	(0.03)	00:00:25	39,840	0
$S^b + 2N_U$	997	(1)	999	0.12	(0.02)	00:00:25	39,810	0
$S^b + 5N_U$	993	(4)	998	0.15	(0.03)	00:00:25	39,900	0

[a] SD=standard deviation

[b] "S" represents the recommended sample size from the main test of Table 2.6.

Table A.6: Known mass system - Test on iSSRM method: 50-DOF

Test	Fitness			Stiffness Error (%)		CPU Time	Evaluations	Perturb-
	Mean	SD[a]	Median	Mean	SD[a]	(h:m:s)		ation
01AAA	962	(6)	973	1.45	(0.12)	00:07:08	250,290	0
02AAB	979	(3)	982	1.08	(0.07)	00:13:15	249,720	0
03AAC	970	(13)	986	1.15	(0.16)	00:07:09	250,275	0
04ABA	967	(4)	978	1.46	(0.10)	00:13:12	249,525	0
05ABB	979	(4)	986	1.14	(0.13)	00:07:01	250,200	0
06ABC	958	(18)	988	1.10	(0.13)	00:07:02	250,875	0
07ACA	969	(5)	979	1.22	(0.12)	00:07:01	249,975	0
08ACB	986	(2)	988	0.87	(0.11)	00:06:59	249,300	0
09ACC	982	(5)	992	0.94	(0.12)	00:06:59	249,750	0
10BAA	955	(5)	961	1.69	(0.12)	00:07:01	250,290	0
11BAB	973	(3)	974	1.49	(0.10)	00:06:57	249,720	0
12BAC	978	(3)	984	1.23	(0.11)	00:06:56	248,400	0
13BBA	952	(10)	965	1.52	(0.12)	00:07:00	250,650	0
14BBB	980	(3)	982	1.20	(0.11)	00:07:00	250,200	0
15BBC	978	(6)	985	1.19	(0.15)	00:06:59	249,000	0
16BCA	958	(8)	976	1.61	(0.17)	00:07:03	251,100	0
17BCB	969	(8)	987	1.23	(0.16)	00:07:02	250,800	0
18BCC	969	(5)	982	1.36	(0.13)	00:07:00	249,750	0
19CAA	937	(9)	944	1.91	(0.15)	00:07:08	249,345	0
20CAB	959	(7)	969	1.72	(0.15)	00:07:03	247,800	0
21CAC	918	(24)	961	1.93	(0.19)	00:07:04	247,500	0
22CBA	936	(10)	949	1.97	(0.17)	00:07:03	251,235	0
23CBB	917	(21)	950	1.98	(0.20)	00:07:00	250,320	0
24CBC	939	(15)	961	1.78	(0.18)	00:07:01	250,650	0
25CCA	961	(6)	968	1.46	(0.12)	00:07:06	251,730	0
26CCB	931	(26)	972	1.57	(0.16)	00:07:02	250,980	0
27CCC	931	(13)	961	1.85	(0.19)	00:07:04	251,475	0
Additional test on N_b								
4	574	(67)	737	3.49	(0.30)	00:06:49	249,300	0
7	989	(2)	991	0.86	(0.11)	00:06:48	249,300	0
Additional test on sample size								
$S^b - 2N_U$	984	(2)	985	1.04	(0.10)	00:06:57	250,220	0
$S^b + 2N_U$	976	(6)	986	1.18	(0.13)	00:06:59	249,880	0

[a] SD=standard deviation

[b] "S" represents the recommended sample size from the main test of Table 2.6.

Table A.7: Unknown mass system - Test on iSSRM method: 5-DOF

Test	Fitness			Stiffness Error (%)		Mass Error (%)		CPU Time	Evalu-	Perturb-
	Mean	SD[a]	Median	Mean	SD[a]	Mean	SD[a]	(h:m:s)	ations	ation
01AAA	628	(58)	660	1.22	(0.24)	1.23	(0.28)	00:00:15	40,140	0
02AAB	746	(69)	931	0.95	(0.31)	0.98	(0.38)	00:00:15	39,720	2
03AAC	747	(66)	897	1.20	(0.46)	1.21	(0.41)	00:00:15	39,900	0
04ABA	845	(47)	962	0.61	(0.30)	0.48	(0.17)	00:00:14	40,050	0
05ABB	910	(35)	981	0.33	(0.11)	0.24	(0.07)	00:00:15	40,200	0
06ABC	745	(74)	920	1.39	(0.47)	1.26	(0.43)	00:00:14	39,750	1
07ACA	582	(76)	709	1.86	(0.52)	1.06	(0.22)	00:00:15	40,050	0
08ACB	541	(69)	506	1.90	(0.48)	1.17	(0.24)	00:00:15	40,200	0
09ACC	553	(65)	521	1.82	(0.36)	1.04	(0.16)	00:00:15	39,750	0
10BAA	600	(42)	690	1.14	(0.14)	1.09	(0.14)	00:00:15	40,140	0
11BAB	745	(60)	889	1.01	(0.28)	1.15	(0.39)	00:00:15	40,320	0
12BAC	657	(70)	765	1.11	(0.30)	1.39	(0.46)	00:00:14	39,900	0
13BBA	700	(72)	926	1.31	(0.50)	1.04	(0.29)	00:00:38	39,600	1
14BBB	741	(64)	847	0.82	(0.21)	0.83	(0.24)	00:00:15	39,600	0
15BBC	654	(69)	749	1.70	(0.58)	1.45	(0.52)	00:00:15	40,500	0
16BCA	703	(61)	796	1.00	(0.22)	0.69	(0.13)	00:00:15	39,600	0
17BCB	597	(74)	581	1.77	(0.41)	1.22	(0.28)	00:00:15	39,600	0
18BCC	470	(69)	464	2.11	(0.38)	1.64	(0.32)	00:00:38	40,500	0
19CAA	631	(51)	678	1.35	(0.50)	1.17	(0.39)	00:00:15	40,365	0
20CAB	568	(67)	599	2.19	(0.62)	2.47	(0.85)	00:00:15	39,960	0
21CAC	660	(73)	861	2.11	(0.93)	2.25	(1.01)	00:00:15	40,050	1
22CBA	695	(62)	776	1.60	(0.78)	1.20	(0.46)	00:00:14	39,555	0
23CBB	529	(74)	490	2.76	(0.71)	1.83	(0.49)	00:00:15	40,860	1
24CBC	625	(71)	724	2.07	(0.82)	1.65	(0.51)	00:00:15	41,175	1
25CCA	548	(72)	470	1.77	(0.39)	1.36	(0.28)	00:00:14	39,285	0
26CCB	461	(72)	376	2.25	(0.42)	1.72	(0.32)	00:00:15	40,500	0
27CCC	306	(67)	178	4.07	(0.68)	3.09	(0.51)	00:00:16	40,725	0
Additional test on N_b										
4	721	(68)	944	1.02	(0.32)	0.97	(0.28)	00:00:15	40,200	0
7	857	(52)	938	0.95	(0.53)	0.72	(0.38)	00:00:15	40,200	0
Additional test on sample size										
$S^b - 2N_U$	769	(59)	900	1.02	(0.34)	0.74	(0.24)	00:00:15	40,320	0
$S^b + 2N_U$	750	(56)	870	0.88	(0.25)	0.69	(0.21)	00:00:15	40,080	0

[a] SD=standard deviation

[b] "S" represents the recommended sample size from the main test of Table 2.8.

Table A.8: Unknown mass system - Test on iSSRM method: 10-DOF

Test	Fitness			Stiffness Error (%)		Mass Error (%)		CPU Time	Evalu-	Perturb-
	Mean	SD[a]	Median	Mean	SD[a]	Mean	SD[a]	(h:m:s)	ations	ation
01AAA	884	(34)	943	0.31	(0.09)	0.29	(0.07)	00:01:05	80,280	0
02AAB	935	(27)	988	0.18	(0.05)	0.17	(0.05)	00:01:06	80,160	0
03AAC	956	(24)	995	0.12	(0.03)	0.11	(0.03)	00:01:05	80,250	0
04ABA	840	(56)	982	0.33	(0.10)	0.33	(0.10)	00:01:05	79,830	0
05ABB	968	(23)	997	0.11	(0.04)	0.11	(0.04)	00:01:05	80,400	0
06ABC	954	(20)	999	0.13	(0.04)	0.13	(0.04)	00:01:05	79,500	0
07ACA	861	(43)	968	0.43	(0.13)	0.40	(0.12)	00:01:04	79,740	0
08ACB	871	(34)	946	0.40	(0.09)	0.38	(0.08)	00:01:05	80,280	0
09ACC	727	(67)	912	0.74	(0.20)	0.69	(0.18)	00:01:05	80,400	0
10BAA	786	(45)	895	0.38	(0.06)	0.36	(0.06)	00:01:05	80,280	0
11BAB	901	(35)	962	0.30	(0.06)	0.27	(0.05)	00:01:04	80,160	0
12BAC	830	(49)	945	0.34	(0.07)	0.34	(0.07)	00:01:03	79,200	0
13BBA	857	(43)	951	0.40	(0.09)	0.37	(0.09)	00:01:03	80,460	0
14BBB	925	(33)	990	0.27	(0.10)	0.23	(0.09)	00:01:04	80,400	0
15BBC	902	(43)	998	0.27	(0.09)	0.26	(0.09)	00:01:04	79,500	0
16BCA	839	(31)	892	0.45	(0.07)	0.44	(0.06)	00:01:04	80,370	0
17BCB	781	(54)	956	0.56	(0.13)	0.53	(0.12)	00:01:04	80,280	0
18BCC	482	(71)	360	1.67	(0.32)	1.59	(0.30)	00:01:04	79,350	0
19CAA	723	(48)	813	0.61	(0.13)	0.58	(0.12)	00:01:04	79,965	0
20CAB	768	(60)	941	0.49	(0.11)	0.47	(0.10)	00:01:05	81,240	0
21CAC	833	(51)	987	0.31	(0.08)	0.31	(0.08)	00:01:04	80,400	0
22CBA	813	(42)	890	0.50	(0.10)	0.48	(0.10)	00:01:04	79,695	0
23CBB	888	(36)	976	0.32	(0.08)	0.30	(0.07)	00:01:04	80,880	0
24CBC	737	(61)	881	0.72	(0.18)	0.71	(0.18)	00:01:05	79,950	0
25CCA	734	(45)	788	0.71	(0.12)	0.66	(0.11)	00:01:05	80,415	0
26CCB	429	(62)	482	2.31	(0.59)	2.16	(0.56)	00:01:03	79,020	0
27CCC	444	(55)	389	1.41	(0.17)	1.38	(0.17)	00:01:05	81,150	0
Additional test on N_b										
4	510	(65)	442	1.05	(0.22)	1.04	(0.22)	00:01:03	80,250	0
7	913	(38)	960	0.36	(0.18)	0.35	(0.17)	00:01:03	80,250	0
Additional test on sample size										
$S^b - 2N_U$	909	(37)	990	0.17	(0.04)	0.17	(0.04)	00:01:02	80,200	0
$S^b + 2N_U$	827	(59)	994	0.47	(0.24)	0.38	(0.18)	00:01:02	80,300	0

[a] SD=standard deviation

[b] "S" represents the recommended sample size from the main test of Table 2.8.

Table A.9: Unknown mass system - Test on iSSRM method: 20-DOF

Test	Fitness			Stiffness Error (%)		Mass Error (%)		CPU Time	Evalu-	Perturb-
	Mean	SD[a]	Median	Mean	SD[a]	Mean	SD[a]	(h:m:s)	ations	ation
01AAA	844	(25)	904	0.23	(0.02)	0.34	(0.05)	00:17:01	599,265	0
02AAB	921	(21)	969	0.14	(0.02)	0.18	(0.03)	00:17:13	600,120	0
03AAC	973	(15)	997	0.05	(0.01)	0.09	(0.03)	00:17:09	600,975	0
04ABA	884	(32)	922	0.21	(0.04)	0.26	(0.04)	00:17:03	599,805	0
05ABB	973	(9)	994	0.07	(0.01)	0.08	(0.01)	00:17:04	600,840	0
06ABC	952	(36)	999	0.08	(0.04)	0.09	(0.05)	00:16:33	598,950	0
07ACA	872	(37)	943	0.16	(0.02)	0.26	(0.04)	00:17:11	600,480	0
08ACB	949	(33)	995	0.07	(0.02)	0.10	(0.03)	00:17:40	599,400	0
09ACC	927	(42)	998	0.07	(0.03)	0.09	(0.03)	00:17:05	600,075	0
10BAA	808	(22)	815	0.27	(0.02)	0.36	(0.03)	00:17:13	600,390	0
11BAB	944	(15)	974	0.12	(0.02)	0.18	(0.03)	00:17:28	601,860	0
12BAC	933	(30)	995	0.10	(0.03)	0.18	(0.05)	00:16:54	602,175	0
13BBA	844	(39)	906	0.28	(0.08)	0.26	(0.04)	00:16:59	601,020	0
14BBB	914	(47)	990	0.15	(0.07)	0.16	(0.05)	00:16:51	598,080	0
15BBC	956	(34)	998	0.09	(0.06)	0.08	(0.04)	00:16:48	597,450	0
16BCA	859	(31)	921	0.19	(0.02)	0.27	(0.03)	00:16:02	600,075	0
17BCB	914	(35)	987	0.10	(0.02)	0.19	(0.05)	00:16:56	601,440	0
18BCC	922	(48)	998	0.09	(0.05)	0.12	(0.04)	00:17:15	601,650	0
19CAA	743	(28)	767	0.33	(0.02)	0.42	(0.05)	00:16:30	597,645	0
20CAB	872	(44)	933	0.24	(0.08)	0.34	(0.11)	00:17:15	603,360	0
21CAC	871	(47)	985	0.19	(0.07)	0.27	(0.11)	00:16:59	599,400	0
22CBA	849	(26)	890	0.24	(0.03)	0.25	(0.03)	00:16:41	599,400	0
23CBB	898	(39)	976	0.14	(0.03)	0.18	(0.03)	00:16:42	597,960	0
24CBC	846	(58)	992	0.18	(0.06)	0.22	(0.07)	00:16:39	602,325	0
25CCA	811	(37)	869	0.26	(0.04)	0.33	(0.04)	00:16:31	597,240	0
26CCB	888	(45)	973	0.19	(0.08)	0.22	(0.07)	00:16:40	602,820	0
27CCC	859	(59)	993	0.16	(0.06)	0.27	(0.13)	00:16:33	598,725	0
Additional test on N_b										
4	489	(68)	387	0.78	(0.20)	1.07	(0.25)	00:16:50	600,975	0
7	973	(4)	979	0.09	(0.01)	0.11	(0.01)	00:16:51	600,975	0
Additional test on sample size										
$S^b - 2N_U$	910	(43)	997	0.12	(0.05)	0.17	(0.07)	00:16:14	598,875	0
$S^b + 2N_U$	948	(36)	996	0.08	(0.03)	0.10	(0.04)	00:16:48	599,325	0

[a] SD=standard deviation

[b] "S" represents the recommended sample size from the main test of Table 2.8.

Appendix B

Identification of Structural Change via Experimental Data

The results listed here correspond to the content discussed in Chapter 6. In total, the identification of structural changes consist of four cut-induced damage cases, i.e., D2, D3, D4, and D6 from Tables 6.4 and 6.5, and four strengthening cases, i.e. S1, S4, S5, and S7 from Tables 6.6 and 6.7. The purpose is to verify experimentally the proposed identification strategies taking into considerations the effects of incomplete measurement and substructural size. The incomplete measurement cases use the measurement from levels 1, 3, 5, and 7. To identify these eight structural change cases, three strategies are considered, with GA parameters listed in Table 6.3, as follows.

(1) Global identification using iSSRM with BFGS. Tables B.1 to B.8 show the identifications via complete measurement while Tables B.9 to B.16 are based on incomplete measurement.

(2) F-Sub using iSSRM with BFGS. Tables B.17 to B.24 give the identifications via complete measurement with 2 substructures. Tables B.25 to B.32 are via incomplete measurement with 2 substructures. Tables B.33 to B.40 are based on complete measurement with 4 substructures.

(3) T-Sub using iSSRM with BFGS. Tables B.41 to B.48 demostrate the identifications via complete measurement with 2 substructures. Tables B.49 to B.56 are based on incomplete measurement with 2 substructures. Tables B.57 to B.64 are the basis of complete measurement with 4 substructures.

Some typical results of these 64 identifications are extracted and shown in Tables 6.8, 6.9, and 6.10.

Table B.1: D2-Global identification: 17% damage at level 4 via complete measurement

Force	Average damage (%)		Success[a]			Location of maximum false change						
	4^{th} floor	Max. false change	1x	2x	4x	1	2	3	4	5	6	7
A	-20.15	-1.32	9/9	9/9	9/9	1	0	8	0	0	0	0
B	-17.59	-3.21	9/9	9/9	9/9	7	0	2	0	0	0	0
C	-15.66	-5.33	9/9	9/9	1/9	9	0	0	0	0	0	0
D	-18.18	-3.63	9/9	9/9	9/9	9	0	0	0	0	0	0
E	-16.22	-3.25	9/9	9/9	7/9	1	0	7	0	0	1	0
	-17.56[b]	-3.35[b]	45/45	45/45	35/45							
	(1.77)[c]	(1.43)[c]	100%	100%	78%	60%	0%	38%	0%	0%	2%	0%

[a] Identification success is defined by "1x", "2x", and "4x" herein. For instance, if the identified damage is one times larger than the maximum false damage, then the success is marked as "2x".

[b] Mean value of the corresponding column

[c] Standard deviation of the corresponding column

Table B.2: D3-Global identification: 17% damage at level 4 and 4% damage at level 6 via complete measurement

Force	Average damage (%)			Success			Location of maximum false change						
	4^{th} floor	6^{th} floor	Max. false change	1x	2x	4x	1	2	3	4	5	6	7
A	-19.76	-3.14	-1.15	9/9	9/9	1/9	2	0	7	0	0	0	0
B	-17.03	-4.41	-3.06	9/9	0/9	0/9	6	0	3	0	0	0	0
C	-16.44	-3.75	-3.98	5/9	0/9	0/9	9	0	0	0	0	0	0
D	-18.34	-3.76	-4.06	3/9	0/9	0/9	9	0	0	0	0	0	0
E	-18.44	-5.76	-2.12	9/9	7/9	2/9	2	1	6	0	0	0	0
	-18.00	-4.17	-2.88	35/45	16/45	3/45							
	(1.30)	(1.00)	(1.25)	78%	36%	7%	62%	2%	36%	0%	0%	0%	0%

Table B.3: D4-Global identification: 17% damage at level 4 and 4% damage at levels 3 and 6 via complete measurement

Force	Average damage (%)				Success			Location of maximum false change						
	3^{th} floor	4^{th} floor	6^{th} floor	Max. false change	1x	2x	4x	1	2	3	4	5	6	7
A	-5.62	-20.21	-2.74	0.277	9/9	9/9	9/9	5	0	0	0	2	0	2
B	-6.57	-17.12	-4.46	-3.76	9/9	3/9	0/9	9	0	0	0	0	0	0
C	-2.22	-16.58	-4.39	-5.31	0/9	0/9	0/9	9	0	0	0	0	0	0
D	-4.17	-17.55	-3.94	-4.68	2/9	0/9	0/9	9	0	0	0	0	0	0
E	-6.40	-17.13	-5.42	-2.28	9/9	7/9	2/9	9	0	0	0	0	0	0
	-5.00	-17.72	-4.19	-3.15	29/45	19/45	11/45							
	(1.82)	(1.43)	(0.98)	(2.23)	64%	42%	24%	91%	0%	0%	0%	4%	0%	4%

Table B.4: D6-Global identification: 17% damage at levels 3, 4 and 6 via complete measurement

	Average damage (%)				Success			Location of maximum false change						
Force	3^{th} floor	4^{th} floor	6^{th} floor	Max. false change	1x	2x	4x	1	2	3	4	5	6	7
A	-20.18	-17.74	-19.90	-2.93	9/9	9/9	9/9	0	9	0	0	0	0	0
B	-20.14	-16.31	-19.89	-4.70	9/9	9/9	9/9	1	8	0	0	0	0	0
C	-16.24	-16.39	-18.28	-2.27	9/9	9/9	9/9	0	7	0	0	0	0	2
D	-16.82	-15.54	-18.91	-4.05	9/9	9/9	6/9	8	1	0	0	0	0	0
E	-21.29	-16.51	-19.13	0.16	9/9	9/9	9/9	0	3	0	0	5	0	1
	-18.93	-16.50	-19.22	-2.76	45/45	45/45	42/45							
	(2.25)	(0.79)	(0.69)	(1.88)	100%	100%	93%	20%	62%	0%	0%	11%	0%	7%

Table B.5: S1-Global identification: moderate strengthening at level 4 via complete measurement

Force	Average damage (%)		Success			Location of maximum false change						
	4^{th} floor	Max. false change	1x	2x	4x	1	2	3	4	5	6	7
A	16.37	5.62	9/9	6/9	6/9	9	0	0	0	0	0	0
B	20.48	3.82	9/9	9/9	6/9	0	0	8	0	0	1	0
C	20.89	3.50	9/9	9/9	9/9	0	0	9	0	0	0	0
D	20.31	1.32	9/9	9/9	9/9	3	0	3	0	0	0	3
E	21.62	5.12	9/9	9/9	6/9	0	0	9	0	0	0	0
	19.93	3.88	45/45	42/45	36/45							
	(2.06)	(1.68)	100%	93%	80%	27%	0%	64%	0%	0%	2%	7%

Table B.6: S4-Global identification: large strengthening at levels 4 and 6 via complete measurement

Force	Average damage (%)			Success			Location of maximum false change						
	4^{th} floor	6^{th} floor	Max. false change	1x	2x	4x	1	2	3	4	5	6	7
A	22.94	33.94	7.53	9/9	6/9	3/9	3	0	6	0	0	0	0
B	27.54	31.83	8.04	9/9	9/9	5/9	8	0	0	0	1	0	0
C	30.22	26.45	11.08	9/9	6/9	3/9	3	0	6	0	0	0	0
D	25.84	35.37	2.83	9/9	9/9	9/9	0	0	9	0	0	0	0
E	31.51	25.42	12.47	9/9	7/9	1/9	9	0	0	0	0	0	0
	27.61	30.60	8.39	45/45	37/45	21/45							
	(3.43)	(4.46)	(3.73)	100%	82%	47%	51%	0%	47%	0%	2%	0%	0%

Table B.7: S5-Global identification: small strengthening at level 4 and moderate strengthening at level 6 via complete measurement

Force	Average damage (%)			Success			Location of maximum false change						
	4^{th} floor	6^{th} floor	Max. false change	1x	2x	4x	1	2	3	4	5	6	7
A	5.38	20.10	3.50	9/9	4/9	0/9	0	0	6	0	3	0	0
B	3.98	18.28	14.79	0/9	0/9	0/9	9	0	0	0	0	0	0
C	8.82	21.99	3.29	9/9	9/9	0/9	0	0	9	0	0	0	0
D	2.15	28.77	5.03	4/9	1/9	0/9	3	0	2	0	4	0	0
E	6.59	19.24	2.84	7/9	6/9	5/9	4	0	5	0	0	0	0
	5.38	21.68	5.89	29/45	20/45	5/45							
	(2.53)	(4.19)	(5.04)	64%	44%	11%	36%	0%	49%	0%	16%	0%	0%

Table B.8: S7-Global identification: small strengthening at level 6 via complete measurement

Force	Average damage (%)		Success			Location of maximum false change						
	6^{th} floor	Max. false change	1x	2x	4x	1	2	3	4	5	6	7
A	11.48	6.12	7/9	6/9	0/9	0	0	5	0	4	0	0
B	9.92	5.68	7/9	4/9	2/9	0	3	0	4	0	0	2
C	4.56	10.30	6/9	6/9	6/9	3	0	4	2	0	0	0
D	6.07	3.05	6/9	6/9	3/9	0	0	4	5	0	0	0
E	4.63	6.75	6/9	2/9	0/9	7	0	0	2	0	0	0
	7.32	6.38	32/45	24/45	11/45							
	(3.18)	(2.60)	71%	53%	24%	22%	7%	29%	29%	9%	0%	4%

Table B.9: D2-Global identification: 17% damage at level 4 via incomplete measurement

Force	Average damage (%)		Success			Location of maximum false change						
	4^{th} floor	Max. false change	1x	2x	4x	1	2	3	4	5	6	7
A	-21.38	-1.49	9/9	9/9	9/9	0	0	6	0	0	0	3
B	-17.65	-4.33	9/9	9/9	4/9	9	0	0	0	0	0	0
C	-16.02	-5.55	9/9	7/9	2/9	9	0	0	0	0	0	0
D	-19.58	-2.37	9/9	9/9	9/9	9	0	0	0	0	0	0
E	-15.84	-4.20	9/9	9/9	3/9	1	0	6	0	0	2	0
	-18.09	-3.59	45/45	43/45	27/45							
	(2.38)	(1.63)	100%	96%	60%	62%	0%	27%	0%	0%	4%	7%

Table B.10: D3-Global identification: 17% damage at level 4 and 4% damage at level 6 via incomplete measurement

Force	Average damage (%)			Success			Location of maximum false change						
	4^{th} floor	6^{th} floor	Max. false change	1x	2x	4x	1	2	3	4	5	6	7
A	-21.06	-3.57	-1.43	9/9	7/9	1/9	0	0	8	0	0	0	1
B	-15.92	-5.07	-4.22	7/9	0/9	0/9	7	0	2	0	0	0	0
C	-16.94	-4.28	-4.17	3/9	0/9	0/9	9	0	0	0	0	0	0
D	-19.42	-4.70	-2.92	8/9	2/9	0/9	9	0	0	0	0	0	0
E	-17.48	-6.30	-2.68	9/9	3/9	3/9	2	1	6	0	0	0	0
	-18.17	-4.78	-3.08	36/45	12/45	4/45							
	(2.06)	(1.02)	(1.16)	80%	27%	9%	60%	2%	36%	0%	0%	0%	2%

Table B.11: D4-Global identification: 17% damage at level 4 and 4% damage at levels 3 and 6 via incomplete measurement

Force	Average damage (%)				Success			Location of maximum false change						
	3^{th} floor	4^{th} floor	6^{th} floor	Max. false change	1x	2x	4x	1	2	3	4	5	6	7
A	-5.72	-20.87	-3.62	-0.63	9	9	8	0	0	0	0	0	0	9
B	-6.35	-15.82	-5.41	-5.60	6	0	0	9	0	0	0	0	0	0
C	-2.61	-16.07	-4.44	-7.09	0	0	0	9	0	0	0	0	0	0
D	-3.42	-18.54	-5.18	-3.90	4	0	0	9	0	0	0	0	0	0
E	-7.07	-16.13	-5.84	-2.97	8	6	3	9	0	0	0	0	0	0
	-5.03	-17.49	-4.90	-4.04	27/45	15/45	11/45							
	(1.93)	(2.19)	(0.88)	(2.48)	60%	33%	24%	80%	0%	0%	0%	0%	0%	20%

Table B.12: D6-Global identification: 17% damage at levels 3, 4 and 6 via incomplete measurement

Force	Average damage (%)				Success			Location of maximum false change						
	3^{th} floor	4^{th} floor	6^{th} floor	Max. false change	1x	2x	4x	1	2	3	4	5	6	7
A	-20.91	-17.01	-21.13	-2.07	9/9	9/9	9/9	0	8	0	0	0	0	1
B	-20.20	-14.53	-20.63	-5.49	9/9	9/9	3/9	9	0	0	0	0	0	0
C	-16.58	-15.69	-17.92	-1.99	9/9	9/9	9/9	0	2	0	0	1	0	6
D	-16.23	-16.09	-19.69	-3.81	9/9	9/9	6/9	9	0	0	0	0	0	0
E	-21.32	-15.22	-18.95	-1.47	9/9	9/9	9/9	2	0	0	0	6	0	1
	-19.04	-15.70	-19.66	-2.95	45/45	45/45	36/45							
	(2.45)	(0.93)	(1.29)	(1.67)	100%	100%	80%	44%	22%	0%	0%	16%	0%	18%

Table B.13: S1-Global identification: moderate strengthening at level 4 via incomplete measurement

Force	Average damage (%)		Success			Location of maximum false change						
	4^{th} floor	Max. false change	1x	2x	4x	1	2	3	4	5	6	7
A	15.14	3.16	9/9	9/9	6/9	0	0	8	0	0	1	0
B	16.45	4.76	9/9	7/9	5/9	0	0	6	0	0	3	0
C	19.37	2.03	9/9	9/9	9/9	7	0	0	0	0	0	2
D	19.33	2.34	9/9	9/9	8/9	0	0	6	0	0	0	3
E	20.04	4.20	9/9	9/9	9/9	0	0	9	0	0	0	0
	18.06	3.30	45/45	43/45	37/45							
	(2.14)	(1.17)	100%	96%	82%	16%	0%	64%	0%	0%	9%	11%

Table B.14: S4-Global identification: large strengthening at levels 4 and 6 via incomplete measurement

Force	Average damage (%)			Success			Location of maximum false change						
	4^{th} floor	6^{th} floor	Max. false change	1x	2x	4x	1	2	3	4	5	6	7
A	22.55	36.69	6.73	9/9	6/9	3/9	0	0	9	0	0	0	0
B	24.45	29.68	9.45	9/9	6/9	3/9	7	0	2	0	0	0	0
C	27.03	27.11	12.86	6/9	6/9	6/9	3	0	6	0	0	0	0
D	26.07	37.04	2.15	9/9	9/9	9/9	0	0	9	0	0	0	0
E	30.91	25.35	4.21	9/9	9/9	7/9	2	0	6	0	0	0	1
	26.20	31.17	7.08	42/45	36/45	28/45							
	(3.14)	(5.42)	(4.23)	93%	80%	62%	27%	0%	71%	0%	0%	0%	2%

Table B.15: S5-Global identification: small strengthening at level 4 and moderate strengthening at level 6 via incomplete measurement

Force	Average damage (%)			Success			Location of maximum false change						
	4^{th} floor	6^{th} floor	Max. false change	1x	2x	4x	1	2	3	4	5	6	7
A	5.94	21.36	2.88	9/9	5/9	1/9	0	3	1	0	4	0	1
B	4.52	18.07	12.08	0/9	0/9	0/9	9	0	0	0	0	0	0
C	8.11	22.84	4.63	9/9	1/9	0/9	0	0	9	0	0	0	0
D	3.48	28.79	6.05	4/9	2/9	0/9	3	0	1	0	2	0	3
E	5.85	20.13	3.01	6/9	6/9	1/9	3	0	6	0	0	0	0
	5.58	22.24	5.73	28/45	14/45	2/45							
	(1.74)	(4.06)	(3.78)	62%	31%	4%	33%	7%	38%	0%	13%	0%	9%

Table B.16: S7-Global identification: small strengthening at level 6 via incomplete measurement

Force	Average damage (%)		Success			Location of maximum false change						
	6^{th} floor	Max. false change	1x	2x	4x	1	2	3	4	5	6	7
A	11.27	5.61	7/9	6/9	1/9	0	0	5	0	4	0	0
B	8.65	5.52	6/9	5/9	2/9	2	1	1	3	0	0	2
C	5.11	13.93	6/9	6/9	6/9	3	2	3	1	0	0	0
D	5.91	3.04	6/9	6/9	2/9	0	0	3	6	0	0	0
E	3.33	9.17	2/9	0/9	0/9	7	0	0	2	0	0	0
	6.86	7.46	27/45	2/45	1/45							
	(3.13)	(4.23)	60%	51%	24%	27%	7%	27%	27%	9%	0%	4%

Table B.17: D2-"F-Sub" identification: 17% damage at level 4 via complete measurement and 2 substructures

Force	Average damage (%)		Success			Location of maximum false change						
	4^{th} floor	Max. false change	1x	2x	4x	1	2	3	4	5	6	7
A	-19.79	-10.00	7/9	6/9	4/9	7	0	2	0	0	0	0
B	-15.70	-2.98	9/9	9/9	8/9	0	7	2	0	0	0	0
C	-19.91	-2.73	9/9	9/9	7/9	0	5	1	0	3	0	0
D	-21.26	-2.03	9/9	9/9	9/9	0	1	8	0	0	0	0
E	-18.75	-11.63	9/9	3/9	1/9	4	0	5	0	0	0	0
	-19.08	-5.87	43/45	36/45	29/45							
	(2.09)	(4.56)	96%	80%	64%	24%	29%	40%	0%	7%	0%	0%

Table B.18: D3-"F-Sub" identification: 17% damage at level 4 and 4% damage at level 6 via complete measurement and 2 substructures

Force	Average damage (%)			Success			Location of maximum false change						
	4^{th} floor	6^{th} floor	Max. false change	1x	2x	4x	1	2	3	4	5	6	7
A	-20.59	-3.57	-6.33	3/9	0/9	0/9	2	0	7	0	0	0	0
B	-14.71	-5.86	-3.95	7/9	4/9	0/9	1	4	4	0	0	0	0
C	-19.91	-3.72	-4.42	4/9	2/9	0/9	0	6	1	0	2	0	0
D	-21.38	-3.55	-1.88	8/9	4/9	1/9	0	2	7	0	0	0	0
E	-20.08	-5.24	-5.83	5/9	1/9	1/9	2	2	5	0	0	0	0
	-19.33	-4.39	-4.48	27/45	11/45	2/45							
	(2.65)	(1.09)	(1.75)	60%	24%	4%	11%	31%	53%	0%	4%	0%	0%

Table B.19: D4-"F-Sub" identification: 17% damage at level 4 and 4% damage at levels 3 and 6 via complete measurement and 2 substructures

Force	Average damage (%)				Success			Location of maximum false change						
	3^{th} floor	4^{th} floor	6^{th} floor	Max. false change	1x	2x	4x	1	2	3	4	5	6	7
A	-11.00	-20.47	-3.47	-6.64	7/9	6/9	2/9	3	4	0	0	2	0	0
B	-7.36	-15.40	-5.46	-2.02	8/9	7/9	4/9	4	3	0	0	0	0	2
C	-0.94	-19.77	-4.07	-3.94	2/9	2/9	1/9	0	7	0	0	2	0	0
D	-4.31	-21.14	-3.76	-1.48	9/9	7/9	4/9	0	4	0	0	5	0	0
E	-9.28	-19.24	-4.99	-7.23	5/9	3/9	2/9	6	2	0	0	1	0	0
	-6.58	-19.21	-4.350	-4.262	31/45	25/45	13/45							
	(4.01)	(2.25)	(0.84)	(2.61)	69%	56%	29%	29%	44%	0%	0%	22%	0%	4%

Table B.20: D6-"F-Sub" identification: 17% damage at levels 3, 4 and 6 via complete measurement and 2 substructures

	Average damage (%)				Success			Location of maximum false change						
Force	3^{th} floor	4^{th} floor	6^{th} floor	Max. false change	1x	2x	4x	1	2	3	4	5	6	7
A	-23.72	-19.64	-18.82	-4.45	9/9	8/9	7/9	3	6	0	0	0	0	0
B	-16.91	-13.59	-22.35	-6.66	6/9	6/9	4/9	0	9	0	0	0	0	0
C	-11.49	-17.52	-18.47	-5.81	9/9	3/9	2/9	0	9	0	0	0	0	0
D	-16.17	-19.66	-19.10	-2.35	9/9	9/9	8/9	1	4	0	0	4	0	0
E	-24.58	-15.97	-20.11	-5.69	9/9	8/9	5/9	6	2	0	0	1	0	0
	-18.57	-17.28	-19.77	-4.99	42/45	34/45	26/45							
	(5.51)	(2.58)	(1.57)	(1.68)	93%	76%	58%	22%	67%	0%	0%	11%	0%	0%

Table B.21: S1-"F-Sub" identification: moderate strengthening at level 4 via complete measurement and 2 substructures

Force	Average damage (%)		Success			Location of maximum false change						
	4^{th} floor	Max. false change	1x	2x	4x	1	2	3	4	5	6	7
A	19.77	10.25	9/9	3/9	0/9	9	0	0	0	0	0	0
B	22.09	5.88	9/9	8/9	5/9	1	0	6	0	1	0	1
C	22.71	2.38	9/9	9/9	9/9	0	0	6	0	0	0	3
D	20.99	3.66	9/9	9/9	6/9	6	0	0	0	1	0	2
E	21.89	7.29	9/9	6/9	5/9	9	0	0	0	0	0	0
	21.49	5.89	45/45	35/45	25/45							
	(1.141)	(3.09)	100%	78%	56%	56%	0%	27%	0%	4%	0%	13%

Table B.22: S4-"F-Sub" identification: large strengthening at levels 4 and 6 via complete measurement and 2 substructures

Force	Average damage (%)			Success			Location of maximum false change						
	4^{th} floor	6^{th} floor	Max. false change	1x	2x	4x	1	2	3	4	5	6	7
A	30.65	31.58	6.87	9/9	9/9	6/9	6	0	3	0	0	0	0
B	27.30	35.21	4.75	9/9	8/9	6/9	3	0	2	0	3	0	1
C	27.97	26.34	9.91	9/9	9/9	0/9	0	0	9	0	0	0	0
D	26.47	37.32	2.69	9/9	9/9	9/9	8	0	1	0	0	0	0
E	25.90	26.43	7.14	7/9	6/9	6/9	7	0	0	0	2	0	0
	27.66	31.38	6.27	43/45	41/45	27/45							
	(1.85)	(5.00)	(2.72)	96%	91%	60%	53%	0%	33%	0%	11%	0%	2%

Table B.23: S5-"F-Sub" identification: small strengthening at level 4 and moderate strengthening at level 6 via complete measurement and 2 substructures

Force	Average damage (%)			Success			Location of maximum false change						
	4^{th} floor	6^{th} floor	Max. false change	1x	2x	4x	1	2	3	4	5	6	7
A	6.74	20.75	4.07	6/9	4/9	4/9	1	0	2	0	6	0	0
B	4.42	19.95	11.88	3/9	3/9	0/9	7	0	2	0	0	0	0
C	5.21	21.88	2.61	9/9	4/9	0/9	0	0	6	0	3	0	0
D	4.88	25.38	10.46	4/9	0/9	0/9	2	0	3	0	4	0	0
E	7.34	21.92	3.04	9/9	6/9	3/9	0	0	9	0	0	0	0
	5.72	21.98	6.41	31/45	17/45	7/45							
	(1.26)	(2.07)	(4.41)	69%	38%	16%	22%	0%	49%	0%	29%	0%	0%

Table B.24: S7-"F-Sub" identification: small strengthening at level 6 via complete measurement and 2 substructures

Force	Average damage (%)		Success			Location of maximum false change						
	6^{th} floor	Max. false change	1x	2x	4x	1	2	3	4	5	6	7
A	9.62	6.11	7/9	4/9	0/9	2	0	4	3	0	0	0
B	11.94	9.01	8/9	1/9	0/9	4	2	1	2	0	0	0
C	5.30	5.68	6/9	0/9	0/9	0	0	9	0	0	0	0
D	9.48	8.55	6/9	6/9	4/9	5	1	3	0	0	0	0
E	5.38	6.58	6/9	4/9	0/9	6	3	0	0	0	0	0
	8.34	7.19	33/45	15/45	4/45							
	(2.91)	(1.50)	73%	33%	9%	38%	13%	38%	11%	0%	0%	0%

Table B.25: D2-"F-Sub" identification: 17% damage at level 4 via incomplete measurement and 2 substructures

Force	Average damage (%)		Success			Location of maximum false change						
	4^{th} floor	Max. false change	1x	2x	4x	1	2	3	4	5	6	7
A	-19.21	-10.98	7/9	6/9	4/9	7	0	2	0	0	0	0
B	-16.36	-3.09	9/9	9/9	8/9	1	0	3	0	0	2	3
C	-19.62	-2.58	9/9	9/9	8/9	1	2	0	0	5	1	0
D	-21.28	-3.22	9/9	9/9	8/9	1	0	7	0	0	1	0
E	-17.09	-9.15	9/9	5/9	0/9	6	0	1	0	2	0	0
	-18.71	-5.81	43/45	38/45	28/45							
	(1.99)	(3.95)	96%	84%	62%	36%	4%	29%	0%	16%	9%	7%

Table B.26: D3-"F-Sub" identification: 17% damage at level 4 and 4% damage at level 6 via incomplete measurement and 2 substructures

Force	Average damage (%)			Success			Location of maximum false change						
	4^{th} floor	6^{th} floor	Max. false change	1x	2x	4x	1	2	3	4	5	6	7
A	-20.62	-2.48	-7.39	1/9	0/9	0/9	2	0	6	0	0	0	1
B	-17.12	-3.73	-3.12	5/9	3/9	2/9	0	0	5	0	0	0	4
C	-19.99	-3.57	-3.76	5/9	1/9	0/9	1	5	0	0	3	0	0
D	-21.38	-3.49	-2.37	6/9	4/9	1/9	0	0	9	0	0	0	0
E	-17.65	-6.22	-6.27	3/9	1/9	0/9	1	0	6	0	2	0	0
	-19.35	-3.90	-4.58	20/45	9/45	3/45							
	(1.88)	(1.39)	(2.15)	44%	20%	7%	9%	11%	58%	0%	11%	0%	11%

Table B.27: D4-"F-Sub" identification: 17% damage at level 4 and 4% damage at levels 3 and 6 via incomplete measurement and 2 substructures

Force	Average damage (%)				Success			Location of maximum false change						
	3^{th} floor	4^{th} floor	6^{th} floor	Max. false change	1x	2x	4x	1	2	3	4	5	6	7
A	-10.70	-20.38	-2.60	-7.67	8/9	7/9	0/9	3	6	0	0	0	0	0
B	-7.29	-17.59	-5.66	-2.10	8/9	8/9	4/9	6	0	0	0	0	0	3
C	-0.59	-20.18	-4.22	-3.69	1/9	0/9	0/9	1	5	0	0	3	0	0
D	-4.91	-21.07	-3.92	-1.25	9/9	9/9	5/9	1	3	0	0	5	0	0
E	-5.69	-17.46	-5.30	-15.73	0/9	0/9	0/9	9	0	0	0	0	0	0
	-5.84	-19.34	-4.34	-6.09	26/45	24/45	9/45							
	(3.68)	(1.69)	(1.21)	(5.93)	58%	53%	20%	44%	31%	0%	0%	18%	0%	7%

Table B.28: D6-"F-Sub" identification: 17% damage at levels 3, 4 and 6 via incomplete measurement and 2 substructures

Force	Average damage (%)				Success			Location of maximum false change						
	3^{th} floor	4^{th} floor	6^{th} floor	Max. false change	1x	2x	4x	1	2	3	4	5	6	7
A	-22.59	-19.18	-18.92	-5.16	9/9	7/9	7/9	3	6	0	0	0	0	0
B	-23.59	-9.78	-25.07	-8.49	9/9	9/9	0/9	9	0	0	0	0	0	0
C	-11.17	-18.20	-18.94	-5.36	9/9	5/9	0/9	1	8	0	0	0	0	0
D	-14.50	-18.65	-19.60	-3.65	9/9	8/9	6/9	4	4	0	0	1	0	0
E	-20.91	-12.49	-21.47	-25.42	3/9	0/9	0/9	9	0	0	0	0	0	0
	-18.54	-15.66	-20.80	-9.62	39/45	29/45	13/45							
	(5.45)	(4.25)	(2.60)	(9.01)	87%	64%	29%	58%	40%	0%	0%	2%	0%	0%

Table B.29: S1-"F-Sub" identification: moderate strengthening at level 4 via incomplete measurement and 2 substructures

Force	Average damage (%)		Success			Location of maximum false change						
	4^{th} floor	Max. false change	1x	2x	4x	1	2	3	4	5	6	7
A	18.88	5.46	9/9	6/9	6/9	0	6	3	0	0	0	0
B	21.24	6.08	8/9	8/9	5/9	0	4	4	0	0	1	0
C	22.59	1.70	9/9	9/9	9/9	0	0	0	0	0	0	9
D	19.17	6.23	9/9	9/9	0/9	0	3	6	0	0	0	0
E	22.50	3.00	9/9	9/9	9/9	0	0	6	0	0	0	3
	20.88	4.50	44/45	41/45	29/45							
	(1.78)	(2.03)	98%	91%	64%	0%	29%	42%	0%	0%	2%	27%

Table B.30: S4-"F-Sub" identification: large strengthening at levels 4 and 6 via incomplete measurement and 2 substructures

Force	Average damage (%)			Success			Location of maximum false change						
	4^{th} floor	6^{th} floor	Max. false change	1x	2x	4x	1	2	3	4	5	6	7
A	29.96	31.12	8.19	9/9	7/9	6/9	0	6	0	0	3	0	0
B	25.09	38.61	8.50	8/9	5/9	4/9	5	0	0	0	2	0	2
C	27.93	26.02	5.03	9/9	9/9	6/9	0	0	3	0	0	0	6
D	18.27	47.94	21.03	3/9	0/9	0/9	0	0	9	0	0	0	0
E	23.25	25.46	3.37	9/9	9/9	6/9	3	6	0	0	0	0	0
	24.88	33.83	9.22	38/45	30/45	22/45							
	(4.52)	(9.49)	(6.94)	84%	67%	49%	18%	27%	27%	0%	11%	0%	18%

Table B.31: S5-"F-Sub" identification: small strengthening at level 4 and moderate strengthening at level 6 via incomplete measurement and 2 substructures

Force	Average damage (%)			Success			Location of maximum false change						
	4^{th} floor	6^{th} floor	Max. false change	1x	2x	4x	1	2	3	4	5	6	7
A	6.56	21.49	4.62	5/9	3/9	2/9	2	3	3	0	1	0	0
B	2.33	23.16	7.69	3/9	0/9	0/9	3	0	5	0	1	0	0
C	5.00	21.86	3.16	9/9	2/9	0/9	8	0	0	0	1	0	0
D	4.05	27.98	13.19	2/9	1/9	0/9	1	0	7	0	1	0	0
E	6.01	22.39	8.05	2/9	0/9	0/9	0	0	9	0	0	0	0
	4.79	23.38	7.34	21/45	6/45	2/45							
	(1.68)	(2.65)	(3.86)	47%	13%	4%	31%	7%	53%	0%	9%	0%	0%

Table B.32: S7-"F-Sub" identification: small strengthening at level 6 via incomplete measurement and 2 substructures

Force	Average damage (%)		Success			Location of maximum false change						
	6^{th} floor	Max. false change	1x	2x	4x	1	2	3	4	5	6	7
A	8.76	5.60	7/9	4/9	1/9	0	2	1	4	2	0	0
B	12.14	14.68	4/9	1/9	0/9	6	1	0	1	0	0	1
C	5.15	10.98	6/9	0/9	0/9	0	0	9	0	0	0	0
D	15.34	17.94	6/9	0/9	0/9	3	0	6	0	0	0	0
E	4.03	18.79	0/9	0/9	0/9	8	1	0	0	0	0	0
	9.09	13.60	23/45	5/45	1/45							
	(4.73)	(5.43)	51%	11%	2%	38%	9%	36%	11%	4%	0%	2%

Table B.33: D2-"F-Sub" identification: 17% damage at level 4 via complete measurement and 4 substructures

Force	Average damage (%)		Success			Location of maximum false change						
	4^{th} floor	Max. false change	1x	2x	4x	1	2	3	4	5	6	7
A	-20.18	-8.80	9/9	6/9	0/9	0	0	9	0	0	0	0
B	-18.15	-9.10	6/9	6/9	4/9	7	0	2	0	0	0	0
C	-18.95	-4.34	9/9	9/9	7/9	0	6	0	0	3	0	0
D	-20.67	-3.70	9/9	9/9	9/9	0	7	1	0	0	1	0
E	-17.64	-7.22	8/9	7/9	4/9	2	0	7	0	0	0	0
	-19.12	-6.63	41/45	37/45	24/45							
	(1.29)	(2.50)	91%	82%	53%	20%	29%	42%	0%	7%	2%	0%

Table B.34: D3-"F-Sub" identification: 17% damage at level 4 and 4% damage at level 6 via complete measurement and 4 substructures

Force	Average damage (%)			Success			Location of maximum false change						
	4^{th} floor	6^{th} floor	Max. false change	1x	2x	4x	1	2	3	4	5	6	7
A	-20.34	-6.18	-7.92	4/9	0/9	0/9	0	2	7	0	0	0	0
B	-16.75	-2.62	-15.88	0/9	0/9	0/9	9	0	0	0	0	0	0
C	-18.68	-2.85	-5.60	0/9	0/9	0/9	0	7	0	0	2	0	0
D	-19.66	-4.40	-3.95	5/9	1/9	0/9	0	9	0	0	0	0	0
E	-20.02	0.63	-8.65	0/9	0/9	0/9	0	0	5	0	4	0	0
	-19.09	-3.09	-8.40	9/45	1/45	0/45							
	(1.45)	(2.52)	(4.58)	20%	2%	0%	20%	40%	27%	0%	13%	0%	0%

Table B.35: D4-"F-Sub" identification: 17% damage at level 4 and 4% damage at levels 3 and 6 via complete measurement and 4 substructures

Force	Average damage (%)				Success			Location of maximum false change						
	3^{th} floor	4^{th} floor	6^{th} floor	Max. false change	1x	2x	4x	1	2	3	4	5	6	7
A	-10.62	-19.47	-5.50	-4.59	9/9	6/9	0/9	0	9	0	0	0	0	0
B	-2.50	-17.96	-3.27	-12.83	2/9	1/9	0/9	8	1	0	0	0	0	0
C	-1.89	-19.32	-3.57	-5.31	0/9	0/9	0/9	0	8	0	0	1	0	0
D	-4.24	-19.78	-4.00	-4.12	5/9	0/9	0/9	0	9	0	0	0	0	0
E	-9.62	-18.34	-1.31	-5.72	8/9	5/9	0/9	4	0	0	0	5	0	0
	-5.77	-18.97	-3.53	-6.51	24/45	12/45	0/45							
	4.08	0.78	1.51	3.58	53%	27%	0%	27%	60%	0%	0%	13%	0%	0%

Table B.36: D6-"F-Sub" identification: 17% damage at levels 3, 4 and 6 via complete measurement and 4 substructures

	Average damage (%)				Success			Location of maximum false change						
Force	3^{th} floor	4^{th} floor	6^{th} floor	Max. false change	1x	2x	4x	1	2	3	4	5	6	7
A	-20.66	-17.85	-20.32	-4.10	9/9	9/9	9/9	0	3	0	0	6	0	0
B	-16.61	-15.03	-18.29	-9.99	6/9	6/9	3/9	8	0	0	0	1	0	0
C	-26.79	-15.71	-24.26	-0.08	9/9	9/9	9/9	6	3	0	0	0	0	0
D	-21.26	-15.04	-20.69	-3.83	9/9	9/9	9/9	0	9	0	0	0	0	0
E	-27.76	-13.97	-22.07	-2.02	9/9	9/9	9/9	0	3	0	0	6	0	0
	-22.62	-15.52	-21.12	-4.00	42/45	42/45	39/45							
	(4.63)	(1.44)	(2.21)	(3.72)	93%	93%	87%	31%	40%	0%	0%	29%	0%	0%

Table B.37: S1-"F-Sub" identification: moderate strengthening at level 4 via complete measurement and 4 substructures

Force	Average damage (%)		Success			Location of maximum false change						
	4^{th} floor	Max. false change	1x	2x	4x	1	2	3	4	5	6	7
A	21.75	44.08	0/9	0/9	0/9	9	0	0	0	0	0	0
B	24.49	15.53	7/9	5/9	2/9	3	5	0	0	1	0	0
C	24.52	9.81	9/9	9/9	0/9	0	9	0	0	0	0	0
D	20.52	23.50	3/9	3/9	3/9	6	0	3	0	0	0	0
E	22.34	12.55	9/9	2/9	0/9	0	9	0	0	0	0	0
	22.73	21.09	28/45	19/45	5/45							
	(1.75)	(13.84)	62%	42%	11%	40%	51%	7%	0%	2%	0%	0%

Table B.38: S4-"F-Sub" identification: large strengthening at levels 4 and 6 via complete measurement and 4 substructures

Force	Average damage (%)			Success			Location of maximum false change						
	4^{th} floor	6^{th} floor	Max. false change	1x	2x	4x	1	2	3	4	5	6	7
A	33.02	30.65	35.64	6/9	3/9	0/9	9	0	0	0	0	0	0
B	35.19	34.60	16.67	9/9	4/9	3/9	6	2	0	0	1	0	0
C	28.88	30.99	19.79	9/9	0/9	0/9	0	6	3	0	0	0	0
D	31.49	31.61	39.85	0/9	0/9	0/9	9	0	0	0	0	0	0
E	21.78	24.14	18.05	6/9	0/9	0/9	0	6	3	0	0	0	0
	30.07	30.40	26.00	30/45	7/45	3/45							
	(5.18)	(3.83)	(10.88)	67%	16%	7%	53%	31%	13%	0%	2%	0%	0%

Table B.39: S5-"F-Sub" identification: small strengthening at level 4 and moderate strengthening at level 6 via complete measurement and 4 substructures

Force	Average damage (%)			Success			Location of maximum false change						
	4^{th} floor	6^{th} floor	Max. false change	1x	2x	4x	1	2	3	4	5	6	7
A	1.95	24.90	9.41	4/9	3/9	1/9	0	5	3	0	0	0	1
B	3.96	25.12	33.12	0/9	0/9	0/9	6	3	0	0	0	0	0
C	5.45	21.44	10.16	0/9	0/9	0/9	0	0	9	0	0	0	0
D	5.13	28.56	15.38	2/9	0/9	0/9	2	3	0	0	4	0	0
E	4.63	23.69	4.34	6/9	1/9	0/9	0	9	0	0	0	0	0
	4.23	24.74	14.48	12/45	4/45	1/45							
	(1.39)	(2.59)	(11.13)	27%	9%	2%	18%	44%	27%	0%	9%	0%	2%

Table B.40: S7-"F-Sub" identification: small strengthening at level 6 via complete measurement and 4 substructures

Force	Average damage (%)		Success			Location of maximum false change						
	6^{th} floor	Max. false change	1x	2x	4x	1	2	3	4	5	6	7
A	5.74	18.26	2/9	1/9	0/9	6	0	0	3	0	0	0
B	5.71	21.47	0/9	0/9	0/9	6	3	0	0	0	0	0
C	7.90	18.68	6/9	4/9	0/9	3	0	6	0	0	0	0
D	4.11	19.44	2/9	0/9	0/9	9	0	0	0	0	0	0
E	1.28	11.69	6/9	4/9	3/9	3	5	0	0	0	0	1
	4.95	17.91	16/45	9/45	3/45							
	(2.46)	(3.69)	36%	20%	7%	60%	18%	13%	7%	0%	0%	2%

Table B.41: D2-"T-Sub" identification: 17% damage at level 4 via complete measurement and 2 substructures

Force	Average damage (%)		Success			Location of maximum false change						
	4^{th} floor	Max. false change	1x	2x	4x	1	2	3	4	5	6	7
A	-19.82	-1.32	9/9	9/9	9/9	0	0	3	0	6	0	0
B	-15.09	-4.41	9/9	9/9	2/9	7	0	2	0	0	0	0
C	-19.97	-1.25	9/9	9/9	9/9	0	4	0	0	5	0	0
D	-21.30	-2.02	9/9	9/9	9/9	0	0	9	0	0	0	0
E	-18.67	-1.80	9/9	9/9	9/9	0	0	6	0	0	3	0
	-18.97	-2.16	45/45	45/45	38/45							
	(2.36)	(1.30)	100%	100%	84%	16%	9%	44%	0%	24%	7%	0%

Table B.42: D3-"T-Sub" identification: 17% damage at level 4 and 4% damage at level 6 via complete measurement and 2 substructures

Force	Average damage (%)			Success			Location of maximum false change						
	4^{th} floor	6^{th} floor	Max. false change	1x	2x	4x	1	2	3	4	5	6	7
A	-20.68	-3.53	-1.29	9/9	9/9	1/9	0	0	5	0	4	0	0
B	-14.28	-6.14	-4.72	8/9	0/9	0/9	4	0	5	0	0	0	0
C	-19.99	-3.65	-2.16	9/9	3/9	0/9	0	6	0	0	3	0	0
D	-21.49	-3.48	-1.86	9/9	4/9	0/9	0	0	9	0	0	0	0
E	-20.10	-5.22	-1.42	9/9	9/9	4/9	0	2	6	0	1	0	0
	-19.31	-4.40	-2.28	44/45	25/45	5/45							
	(2.87)	(1.21)	(1.40)	98%	56%	11%	9%	18%	56%	0%	18%	0%	0%

Table B.43: D4-"T-Sub" identification: 17% damage at level 4 and 4% damage at levels 3 and 6 via complete measurement and 2 substructures

	Average damage (%)				Success			Location of maximum false change						
Force	3^{th} floor	4^{th} floor	6^{th} floor	Max. false change	1x	2x	4x	1	2	3	4	5	6	7
A	-5.33	-20.57	-3.48	-0.69	9/9	9/9	6/9	3	0	0	0	6	0	0
B	-7.38	-15.01	-5.67	-4.65	9/9	2/9	0/9	9	0	0	0	0	0	0
C	-2.05	-19.72	-3.99	-2.78	4/9	0/9	0/9	0	9	0	0	0	0	0
D	-5.85	-21.24	-3.70	-0.69	9/9	9/9	9/9	0	0	0	0	9	0	0
E	-4.53	-19.15	-4.94	-0.66	9/9	9/9	6/9	0	9	0	0	0	0	0
	-5.03	-19.14	-4.36	-1.89	40/45	29/45	21/45							
	(1.96)	(2.44)	(0.92)	(1.79)	89%	64%	47%	27%	40%	0%	0%	33%	0%	0%

Table B.44: D6-"T-Sub" identification: 17% damage at levels 3, 4 and 6 via complete measurement and 2 substructures

Force	Average damage (%)				Success			Location of maximum false change						
	3^{th} floor	4^{th} floor	6^{th} floor	Max. false change	1x	2x	4x	1	2	3	4	5	6	7
A	-19.64	-19.69	-18.83	-0.68	9/9	9/9	9/9	0	0	0	0	6	0	3
B	-20.65	-12.72	-22.77	-6.66	9/9	9/9	0/9	9	0	0	0	0	0	0
C	-13.83	-17.71	-18.35	-3.64	9/9	9/9	3/9	0	9	0	0	0	0	0
D	-17.20	-19.84	-18.35	-2.50	9/9	9/9	6/9	0	7	0	0	2	0	0
E	-20.25	-15.91	-19.94	-0.56	9/9	9/9	9/9	3	2	0	0	4	0	0
	-18.31	-17.18	-19.65	-2.80	45/45	45/45	27/45							
	(2.84)	(2.97)	(1.86)	(2.51)	100%	100%	60%	27%	40%	0%	0%	27%	0%	7%

Table B.45: S1-"T-Sub" identification: moderate strengthening at level 4 via complete measurement and 2 substructures

Force	Average damage (%)		Success			Location of maximum false change						
	4^{th} floor	Max. false change	1x	2x	4x	1	2	3	4	5	6	7
A	20.73	5.09	9/9	9/9	5/9	6	3	0	0	0	0	0
B	21.34	3.63	9/9	7/9	6/9	0	0	4	0	3	2	0
C	22.94	3.10	9/9	9/9	9/9	0	0	9	0	0	0	0
D	21.37	1.40	9/9	9/9	9/9	0	2	6	0	0	0	1
E	22.16	5.37	9/9	9/9	3/9	9	0	0	0	0	0	0
	21.71	3.72	45/45	43/45	32/45							
	(0.86)	(1.61)	100%	96%	71%	33%	11%	42%	0%	7%	4%	2%

Table B.46: S4-"T-Sub" identification: large strengthening at levels 4 and 6 via complete measurement and 2 substructures

Force	Average damage (%)			Success			Location of maximum false change						
	4^{th} floor	6^{th} floor	Max. false change	1x	2x	4x	1	2	3	4	5	6	7
A	31.63	30.88	6.98	9	9	6	3	0	6	0	0	0	0
B	27.21	34.91	3.13	9	9	8	4	0	1	0	3	0	1
C	28.43	26.51	8.16	9	9	3	0	0	6	0	0	0	3
D	26.75	36.73	6.63	9	9	6	0	0	9	0	0	0	0
E	27.49	26.50	6.09	9	7	6	0	0	9	0	0	0	0
	28.30	31.11	6.19	45	43	29							
	(1.96)	(4.70)	(1.87)	100%	96%	64%	16%	0%	69%	0%	7%	0%	9%

Table B.47: S5-"T-Sub" identification: small strengthening at level 4 and moderate strengthening at level 6 via complete measurement and 2 substructures

Force	Average damage (%)			Success			Location of maximum false change						
	4^{th} floor	6^{th} floor	Max. false change	1x	2x	4x	1	2	3	4	5	6	7
A	6.77	20.03	5.88	4/9	4/9	4/9	2	2	5	0	0	0	0
B	3.83	19.92	11.62	2/9	0/9	0/9	9	0	0	0	0	0	0
C	5.18	21.93	5.09	5/9	0/9	0/9	0	0	9	0	0	0	0
D	5.04	24.84	6.16	5/9	0/9	0/9	3	0	2	0	4	0	0
E	7.60	22.06	2.13	9/9	9/9	3/9	3	0	6	0	0	0	0
	5.69	21.76	6.18	25/45	13/45	7/45							
	(1.50)	(2.00)	(3.44)	56%	29%	16%	38%	4%	49%	0%	9%	0%	0%

Table B.48: S7-"T-Sub" identification: small strengthening at level 6 via complete measurement and 2 substructures

Force	Average damage (%)		Success			Location of maximum false change						
	6^{th} floor	Max. false change	1x	2x	4x	1	2	3	4	5	6	7
A	9.88	7.25	6/9	3/9	0/9	1	2	4	2	0	0	0
B	11.88	5.63	8/9	4/9	3/9	2	3	0	4	0	0	0
C	5.31	7.93	6/9	6/9	4/9	3	0	6	0	0	0	0
D	9.83	3.90	9/9	7/9	0/9	0	0	6	0	3	0	0
E	5.52	2.61	6/9	6/9	3/9	0	0	3	6	0	0	0
	8.48	5.46	35/45	26/45	10/45							
	(2.92)	(2.23)	78%	58%	22%	13%	11%	42%	27%	7%	0%	0%

Table B.49: D2-"T-Sub" identification: 17% damage at level 4 via incomplete measurement and 2 substructures

Force	Average damage (%)		Success			Location of maximum false change						
	4^{th} floor	Max. false change	1x	2x	4x	1	2	3	4	5	6	7
A	-19.33	-2.00	9/9	9/9	9/9	0	0	3	0	1	0	5
B	-15.74	-6.10	9/9	6/9	0/9	4	0	5	0	0	0	0
C	-19.63	-2.02	9/9	9/9	9/9	0	3	0	0	6	0	0
D	-21.36	-1.23	9/9	9/9	9/9	1	0	7	0	0	1	0
E	-17.16	-6.67	9/9	9/9	0/9	1	2	0	0	6	0	0
	-18.65	-3.60	45/45	42/45	27/45							
	(2.21)	(2.57)	100%	93%	60%	13%	11%	33%	0%	29%	2%	11%

Table B.50: D3-"T-Sub" identification: 17% damage at level 4 and 4% damage at level 6 via incomplete measurement and 2 substructures

Force	Average damage (%)			Success			Location of maximum false change						
	4^{th} floor	6^{th} floor	Max. false change	1x	2x	4x	1	2	3	4	5	6	7
A	-20.76	-2.52	-2.12	6/9	1/9	0/9	0	0	5	0	1	0	3
B	-16.17	-4.17	-4.21	6/9	0/9	0/9	6	0	2	0	0	0	1
C	-19.92	-3.51	-2.82	7/9	1/9	0/9	0	5	0	0	4	0	0
D	-21.51	-3.47	-1.09	9/9	7/9	3/9	0	0	6	0	2	0	1
E	-17.79	-5.95	-6.24	5/9	0/9	0/9	3	0	0	0	6	0	0
	-19.23	-3.92	-3.30	33/45	9/45	3/45							
	(2.20)	(1.27)	(2.00)	73%	20%	7%	20%	11%	29%	0%	29%	0%	11%

Table B.51: D4-"T-Sub" identification: 17% damage at level 4 and 4% damage at levels 3 and 6 via incomplete measurement and 2 substructures

Force	Average damage (%)				Success			Location of maximum false change						
	3^{th} floor	4^{th} floor	6^{th} floor	Max. false change	1x	2x	4x	1	2	3	4	5	6	7
A	-5.94	-20.49	-2.63	-1.35	9/9	8/9	5/9	0	0	0	0	2	0	7
B	-7.89	-17.40	-6.19	-3.25	8/9	5/9	2/9	8	1	0	0	0	0	0
C	-1.63	-20.11	-4.17	-3.06	0/9	0/9	0/9	0	7	0	0	2	0	0
D	-4.96	-21.18	-3.92	-0.46	9/9	9/9	9/9	1	0	0	0	8	0	0
E	-5.12	-17.57	-5.08	-6.40	6/9	0/9	0/9	3	0	0	0	6	0	0
	-5.11	-19.35	-4.40	-2.90	32/45	22/45	16/45							
	(2.27)	(1.75)	(1.33)	(2.28)	71%	49%	36%	27%	18%	0%	0%	40%	0%	16%

Table B.52: D6-"T-Sub" identification: 17% damage at levels 3, 4 and 6 via incomplete measurement and 2 substructures

Force	Average damage (%)				Success			Location of maximum false change						
	3^{th} floor	4^{th} floor	6^{th} floor	Max. false change	1x	2x	4x	1	2	3	4	5	6	7
A	-21.13	-19.11	-18.91	-1.94	9/9	9/9	9/9	0	0	0	0	0	0	9
B	-22.47	-9.59	-25.37	-10.76	9/9	6/9	0/9	9	0	0	0	0	0	0
C	-12.93	-18.23	-18.76	-3.98	9/9	9/9	1/9	0	9	0	0	0	0	0
D	-17.27	-18.69	-19.66	-1.66	9/9	9/9	9/9	0	6	0	0	3	0	0
E	-23.06	-12.28	-21.28	-4.69	9/9	9/9	6/9	3	0	0	0	6	0	0
	-19.37	-15.58	-20.80	-4.61	45/45	42/45	25/45							
	(4.25)	(4.36)	(2.75)	(3.68)	100%	93%	56%	27%	33%	0%	0%	20%	0%	20%

Table B.53: S1-"T-Sub" identification: moderate strengthening at level 4 via incomplete measurement and 2 substructures

Force	Average damage (%)		Success			Location of maximum false change						
	4^{th} floor	Max. false change	1x	2x	4x	1	2	3	4	5	6	7
A	19.96	1.39	9/9	9/9	9/9	6	0	0	0	0	0	3
B	20.83	4.63	9/9	7/9	5/9	0	0	2	0	3	3	1
C	22.64	2.40	9/9	9/9	9/9	6	0	0	0	0	0	3
D	20.84	3.35	9/9	9/9	7/9	0	3	1	0	0	5	0
E	23.55	2.33	9/9	9/9	9/9	0	0	9	0	0	0	0
	21.57	2.82	45/45	43/45	39/45							
	(1.48)	(1.23)	100%	96%	87%	27%	7%	27%	0%	7%	18%	16%

Table B.54: S4-"T-Sub" identification: large strengthening at levels 4 and 6 via incomplete measurement and 2 substructures

Force	Average damage (%)			Success			Location of maximum false change						
	4^{th} floor	6^{th} floor	Max. false change	1x	2x	4x	1	2	3	4	5	6	7
A	30.81	30.14	4.28	9/9	9/9	8/9	0	0	6	0	3	0	0
B	26.93	36.81	4.78	9/9	9/9	6/9	1	0	2	0	2	0	4
C	28.17	25.96	12.07	9/9	3/9	3/9	0	0	6	0	0	0	3
D	16.20	49.93	17.78	3/9	0/9	0/9	0	0	9	0	0	0	0
E	25.17	25.61	10.22	7/9	6/9	2/9	0	0	9	0	0	0	0
	25.46	33.69	9.83	37/45	27/45	19/45							
	(5.57)	(10.14)	(5.58)	82%	60%	42%	2%	0%	71%	0%	11%	0%	16%

Table B.55: S5-"T-Sub" identification: small strengthening at level 4 and moderate strengthening at level 6 via incomplete measurement and 2 substructures

Force	Average damage (%)			Success			Location of maximum false change						
	4^{th} floor	6^{th} floor	Max. false change	1x	2x	4x	1	2	3	4	5	6	7
A	6.32	21.07	6.91	6/9	4/9	2/9	3	3	3	0	0	0	0
B	2.52	23.25	11.50	1/9	0/9	0/9	5	0	4	0	0	0	0
C	5.01	21.89	21.34	0/9	0/9	0/9	0	0	9	0	0	0	0
D	2.48	27.97	14.64	0/9	0/9	0/9	3	4	2	0	0	0	0
E	5.75	22.38	4.09	7/9	1/9	0/9	0	0	9	0	0	0	0
	4.42	23.31	11.70	14/45	5/45	2/45							
	(1.81)	(2.72)	(6.76)	31%	11%	4%	24%	16%	60%	0%	0%	0%	0%

Table B.56: S7-"T-Sub" identification: small strengthening at level 6 via incomplete measurement and 2 substructures

Force	Average damage (%)		Success			Location of maximum false change						
	6^{th} floor	Max. false change	1x	2x	4x	1	2	3	4	5	6	7
A	8.93	4.61	9/9	4/9	1/9	0	0	2	3	4	0	0
B	10.76	6.07	8/9	4/9	0/9	2	1	0	4	1	0	1
C	5.12	12.40	6/9	6/9	6/9	3	0	6	0	0	0	0
D	16.59	12.78	9/9	1/9	0/9	0	3	6	0	0	0	0
E	4.22	3.61	6/9	6/9	6/9	0	0	7	2	0	0	0
	9.12	7.90	38/45	21/45	13/45							
	(4.96)	(4.38)	84%	47%	29%	11%	9%	47%	20%	11%	0%	2%

Table B.57: D2-"T-Sub" identification: 17% damage at level 4 via complete measurement and 4 substructures

Force	Average damage (%)		Success			Location of maximum false change						
	4^{th} floor	Max. false change	1x	2x	4x	1	2	3	4	5	6	7
A	-20.150	-9.057	9/9	6/9	0/9	0	0	9	0	0	0	0
B	-18.205	-11.680	6/9	6/9	2/9	6	0	3	0	0	0	0
C	-18.930	-4.473	9/9	9/9	7/9	0	6	0	0	3	0	0
D	-20.820	-4.313	9/9	9/9	7/9	0	7	1	0	0	1	0
E	-17.650	-4.845	9/9	9/9	5/9	1	0	8	0	0	0	0
	-19.151	-6.874	42/45	39/45	21/45							
	(1.321)	(3.328)	93%	87%	47%	16%	29%	47%	0%	7%	2%	0%

Table B.58: D3-"T-Sub" identification: 17% damage at level 4 and 4% damage at level 6 via complete measurement and 4 substructures

Force	Average damage (%)			Success			Location of maximum false change						
	4^{th} floor	6^{th} floor	Max. false change	1x	2x	4x	1	2	3	4	5	6	7
A	-20.42	-5.74	-8.19	3/9	0/9	0/9	0	2	7	0	0	0	0
B	-16.41	-2.70	-17.11	0/9	0/9	0/9	9	0	0	0	0	0	0
C	-18.78	-2.86	-5.89	0/9	0/9	0/9	0	8	0	0	1	0	0
D	-19.79	-4.25	-4.34	4/9	1/9	0/9	0	9	0	0	0	0	0
E	-20.07	0.913	-9.29	0/9	0/9	0/9	0	0	6	0	3	0	0
	-19.09	-2.93	-8.96	7/45	1/45	0/45							
	(1.62)	(2.47)	(4.95)	16%	2%	0%	20%	42%	29%	0%	9%	0%	0%

Table B.59: D4-"T-Sub" identification: 17% damage at level 4 and 4% damage at levels 3 and 6 via complete measurement and 4 substructures

Force	Average damage (%)				Success			Location of maximum false change						
	3^{th} floor	4^{th} floor	6^{th} floor	Max. false change	1x	2x	4x	1	2	3	4	5	6	7
A	-10.83	-19.49 -5.46	-4.53	9/9	6/9	0/9	0	9	0	0	0	0	0	
B	-2.81	-18.32	-2.57	-12.11	3/9	1/9	0/9	8	1	0	0	0	0	0
C	-1.88	-19.50	-3.60	-5.54	0/9	0/9	0/9	0	8	0	0	1	0	0
D	-4.86	-19.98	-3.77	-4.70	5/9	0/9	0/9	0	9	0	0	0	0	0
E	-10.08	-18.34	-0.94	-4.16	9/9	8/9	0/9	0	0	0	0	9	0	0
	-6.09	-19.12	-3.27	-6.21	26/45	15/45	0/45							
	(4.13)	(0.75)	(1.67)	(3.34)	58%	33%	0%	18%	60%	0%	0%	22%	0%	0%

Table B.60: D6-"T-Sub" identification: 17% damage at levels 3, 4 and 6 via complete measurement and 4 substructures

	Average damage (%)				Success			Location of maximum false change					
Force	3^{th} floor	4^{th} floor	6^{th} floor	Max. false change	1x	2x	4x	1	2	3	4	5	6	7
A	-20.26	-17.47	-19.76	-3.95	9/9	9/9	9/9	0	3	0	0	6	0	0
B	-17.36	-17.13	-18.44	-10.47	6/9	4/9	3/9	8	1	0	0	0	0	0
C	-14.01	-18.79	-18.72	-5.63	9/9	7/9	1/9	0	7	0	0	2	0	0
D	-26.49	-17.69	-18.84	-8.40	9/9	9/9	1/9	0	9	0	0	0	0	0
E	-22.88	-14.30	-17.14	-5.70	9/9	9/9	5/9	4	0	0	0	5	0	0
	-20.20	-17.08	-18.58	-6.83	42/45	38/45	19/45							
	(4.83)	(1.67)	(0.95)	(2.58)	93%	84%	42%	27%	44%	0%	0%	29%	0%	0%

Table B.61: S1-"T-Sub" identification: moderate strengthening at level 4 via complete measurement and 4 substructures

Force	Average damage (%)		Success			Location of maximum false change						
	4^{th} floor	Max. false change	1x	2x	4x	1	2	3	4	5	6	7
A	22.09	30.14	0/9	0/9	0/9	9	0	0	0	0	0	0
B	24.19	14.90	7/9	5/9	3/9	2	5	0	0	2	0	0
C	24.47	8.97	9/9	9/9	0/9	0	9	0	0	0	0	0
D	20.26	19.58	3/9	3/9	1/9	6	0	3	0	0	0	0
E	22.89	12.93	9/9	3/9	0/9	0	9	0	0	0	0	0
	22.78	17.30	28/45	20/45	4/45							
	(1.71)	(8.13)	62%	44%	9%	38%	51%	7%	0%	4%	0%	0%

Table B.62: S4-"T-Sub" identification: large strengthening at levels 4 and 6 via complete measurement and 4 substructures

Force	Average damage (%)			Success			Location of maximum false change						
	4^{th} floor	6^{th} floor	Max. false change	1x	2x	4x	1	2	3	4	5	6	7
A	32.96	31.35	22.51	8/9	3/9	3/9	9	0	0	0	0	0	0
B	35.26	35.03	17.09	7/9	4/9	4/9	5	2	0	0	1	0	1
C	29.21	31.72	19.04	9/9	0/9	0/9	0	6	3	0	0	0	0
D	31.53	31.87	37.38	0/9	0/9	0/9	9	0	0	0	0	0	0
E	23.37	25.23	18.26	7/9	0/9	0/9	0	6	3	0	0	0	0
	30.46	31.04	22.86	31/45	7/45	7/45							
	(4.54)	(3.57)	(8.37)	69%	16%	16%	51%	31%	13%	0%	2%	0%	2%

Table B.63: S5-"T-Sub" identification: small strengthening at level 4 and moderate strengthening at level 6 via complete measurement and 4 substructures

Force	Average damage (%)			Success			Location of maximum false change						
	4^{th} floor	6^{th} floor	Max. false change	1x	2x	4x	1	2	3	4	5	6	7
A	1.56	24.89	10.80	3/9	1/9	0/9	0	6	3	0	0	0	0
B	3.84	25.27	40.87	0/9	0/9	0/9	6	3	0	0	0	0	0
C	5.42	21.87	11.09	0/9	0/9	0/9	0	0	9	0	0	0	0
D	5.30	29.12	18.69	0/9	0/9	0/9	3	2	0	0	4	0	0
E	4.68	23.50	4.50	6/9	0/9	0/9	0	9	0	0	0	0	0
	4.16	24.93	17.19	9/45	1/45	0/45							
	(1.59)	(2.70)	(14.16)	20%	2%	0%	20%	44%	27%	0%	9%	0%	0%

Table B.64: S7-"T-Sub" identification: small strengthening at level 6 via complete measurement and 4 substructures

Force	Average damage (%)		Success			Location of maximum false change						
	6^{th} floor	Max. false change	1x	2x	4x	1	2	3	4	5	6	7
A	5.97	14.30	1/9	0/9	0/9	6	0	0	3	0	0	0
B	6.08	18.75	0/9	0/9	0/9	6	3	0	0	0	0	0
C	8.20	24.58	6/9	5/9	0/9	3	0	6	0	0	0	0
D	4.27	21.23	1/9	0/9	0/9	9	0	0	0	0	0	0
E	2.17	16.38	6/9	2/9	1/9	5	4	0	0	0	0	0
	5.34	19.05	14/45	7/45	1/45							
	(2.26)	(4.03)	31%	16%	2%	64%	16%	13%	7%	0%	0%	0%